Aus der Klinik und Poliklinik für Neurologie

Der Technischen Universität München

Direktor: Univ.-Prof. Dr. med. Bernhard Hemmer

Multimodale zerebrale Bildgebung bei Dystonien

Zusammenstellung wissenschaftlicher Veröffentlichungen

zur Erlangung der Lehrbefähigung für das Fach Neurologie

an der Fakultät für Medizin der Technischen Universität München

vorgelegt von Dr. med. Tobias Alexander Mantel

München, den 05.11.2023

Fachmentorat:

Prof. Dr. med. Bernhard Hemmer (Vorsitzender)

Prof. Dr. med. Helge Topka

Priv.-Doz. Dr. med. Christian Sorg

Inhaltsverzeichnis

Abkürzungsverzeichnis

ABV	atlasbasierte Volumetrie
ADLD	adductor-type laryngeal dystonia, Laryngeale Dystonie vom Adduktor-Typ
AI	Asymmetrie-Index
AOFD	adult-onset focal dystonia, fokale Dystonie mit Beginn im Erwachsenenalter
BOLD	blood oxygen level-dependent, Blutsauerstoffgehalts-abhängig
BoNT-A	Botulinum-Neurotoxin Typ A
CON(TR)	healthy controls, gesunde Kontrollen/Probanden
DTCT	dentato-thalamo-cortikale Trajektorie
ED	Embouchure-Dystonie, Ansatzdystonie
FA	fraktionelle Anisotropie
FC	functional connectivity, funktionelle Konnektivität
fMRT	funktionelle zerebrale Magnetresonanztomographie
GM	grey matter, graue Substanz
L(H)	linke Hemisphäre
M1	primärer motorischer Kortex
MNI	Montreal Neurological Institute
MR-	magnetresonanztomographisch
MuCON	healthy (brass) musician controls, gesunde professionelle (Blas-)Musiker-Kontrollen/Probanden
MRT	Magnetresonanztomographie
PAT	Dystoniepatienten
PET-	positronenemissionstomographisch
PTCT	pallido-thalamo-cortikale Trajektorie
R(H)	rechte Hemisphäre
s.	siehe
S1	primärer somatosensorischer Kortex
SMA	supplementär-motorisches Areal

sMRT	strukturelle zerebrale Magnetresonanztomographie
SPL	superiorer Parietallappen
VBM	voxelbasierte Morphometrie

Abbildungsverzeichnis

1. Fokale Dystonie als Netzwerkerkrankung – die Rolle der Bildgebung

Dystonie bezeichnet eine Bewegungsstörung, die sich durch unwillkürliche, anhaltend oder intermittierend auftretende Muskelkontraktionen auszeichnet. Dies führt zu abnormen, oftmals repetitiven Bewegungen und/oder Fehlhaltungen betroffener Körperregionen [1-3]. Das Krankheitsbild der Dystonie ist klinisch wie ätiologisch heterogen. Klinisch lassen sich hierbei neben Differenzen im Manifestationsalter (frühes Kindes- bis Erwachsenenalter) und in der topographischen Verteilung (fokal bis generalisiert) Unterschiede in Bezug auf die Entwicklung über die Zeit sowie auf das begleitende Vorliegen anderer neurologischer Symptome beobachten. Ätiologisch werden Manifestationen, die mit Pathologien des zentralen Nervensystems oder einer spezifischen hereditären (gesicherten genetischen) bzw. erworbenen Ursache (z.B. struktureller Hirndefekten, Toxin-/Medikamentenwirkung) assoziiert sind, von idiopathischen Formen unterschieden [1]. Dystonien als eigenständige und isolierte Krankheitsentität sind dabei insgesamt selten. Die größte Gruppe stellen die isolierten fokalen Dystonien mit Beginn im Erwachsenenalter (adult-onset focal dystonias, AOFD) dar, die in der Ätiologie überwiegend idiopathisch sind. Auf Basis von Krankendaten wird eine mittlere Prävalenz von mindestens 15/100.000 für fokale/segmentale Dystonien angenommen [4], wobei populationsbasierte Analysen auf eine relevante Dunkelziffer hinweisen [4,5]. Die nicht aufgaben- bzw. aktionsspezifisch auftretenden AOFD, mit zervikaler Dystonie und Blepharospasmus als überwiegende Manifestationen, stellen die häufigsten Formen dar (geschätzte krankheitsdatenbasierte mittlere Prävalenzen um 4-5/100.000) [4]. Die nur im Rahmen bestimmter feinmotorischer Tätigkeiten auftretenden Manifestationen (sog. aufgaben- bzw. aktionsspezifische AOFD) sind seltener (geschätzte krankheitsdatenbasierte mittlere Prävalenzen um 1-2/100.000), wobei die – bezogen auf die Gesamtbevölkerung – sehr seltenen Formen wie die Musikerdystonien eine relevante kollektivspezifische Prävalenz aufweisen [4]. Neurophysiologisch lassen sich bei den AOFD auf Gruppenebene regelmäßig Korrelate einer gestörten Inhibition und maladaptiven Plastizität im zentralen sensomotorischen System, sowie eine Störung der sensomotorischen Integration am ehesten auf Basis abnormer sensorischer Reizverarbeitung nachweisen [6,7]. Die in den letzten Jahrzehnten im Rahmen von Läsionsstudien, bildgebenden und elektrophysiologischen Untersuchungen hereditärer wie idiopathischer Dystonien, neurochirurgischen

Fallserien, sowie Tiermodellen gesammelte Evidenz hat dabei zunehmend Limitationen der zuvor vorherrschenden Sicht auf Dystonien als reine Basalganglienerkrankungen aufgezeigt. Dies hat zur alternativen Konzeption fokaler Dystonien als Netzwerkerkrankungen geführt [8,9]. Im Rahmen eines solchen hypothetischen „Netzwerkmodells" wird das Auftreten dystoner Symptomatik als Resultat einer Störung innerhalb eines Netzwerkes direkt oder indirekt kommunizierender Hirnregionen angenommen. Neben den Basalganglien werden dabei eine Rolle des Kleinhirns, des Thalamus, kortikaler sensomotorischer Areale sowie von Hirnstammkernen diskutiert [6,8,9]. Dabei bleibt bislang ungeklärt, ob das Auftreten der dystonen Symptomatik aus der Dysfunktion eines oder mehrerer Knotenpunkte, oder aus der Störung ihrer Kommunikation bzw. Interaktion resultiert. Ebenso ist offen, inwieweit phänotypassoziierte Unterschiede (mit differierender oder gemeinsamer Endstrecke) innerhalb dieses Netzwerkmodells bei AOFDs bestehen könnten [7-10]. Insgesamt stellen die AOFD somit ein ätiologisch heterogenes Krankheitsbild mit letztlich weiterhin unzureichend geklärter Pathogenese dar. Nachdem bis zum heutigen Tag keine spezifischen histopathologischen zerebralen Auffälligkeiten bei idiopathischen Dystonien nachweisbar sind [11,12], kommt der nichtinvasiven zerebralen Bildgebung („Neuroimaging") eine wesentliche Rolle beim Sammeln von Information hinsichtlich des Charakters zerebraler Netzwerkveränderungen im Menschen bei den verschiedenen Dystonieausprägungen zu [13]. Hierzu wurden in der Vergangenheit positronenemissions- (PET-) und magnetresonanztomographische (MR-) bildgebende Verfahren eingesetzt [9,14,15]. Letztere bieten vielfältige Möglichkeiten, statische (strukturelle bzw. anatomische) sowie – basierend auf Blutsauerstoffgehalts-abhängigen (sog. BOLD, blood oxygen level-dependent) Untersuchungstechniken – dynamische (funktionelle), räumlich verteilte zerebrale Veränderungen strahlungsfrei zu erfassen (z.B. [16-22]). Der kombinierte Einsatz solcher MR-basierter Verfahren (multimodale Bildgebung) kann hierbei über die Assoziation verschiedener struktureller und/oder funktioneller Veränderungen ein umfassenderes Verständnis potentieller Pathomechanismen ermöglichen. Initial stand bei Dystonien vor allem die Identifikation von Mustern abnormer sensomotorischer Aktivierung mittels aufgaben- bzw. ereignisgekoppelter funktioneller zerebraler Magnetresonanztomographie (fMRT) und kortikaler Struktur mittels hochaufgelöster struktureller zerebraler MRT (sMRT) im Vordergrund [14,15]. Hierdurch konnte ein entsprechender Beitrag zur Netzwerkhypothese geleistet werden [8,9]. In den letzten Jahren rückt nun die Identifikation von

Veränderungen in den Verbindungsmustern beteiligter Hirnregionen in den Fokus. Frühe Arbeiten bei hereditären Dystonieformen konnten u.a. durch bildgebende Untersuchungen der Hirnfunktion im (nichtschlafenden) Ruhezustand sowie der anatomischen Konnektivität und Mikrostruktur zerebraler Faserbahnen das Verständnis von Regelkreisveränderungen bei diesen Erkrankungsformen erweitern. Insbesondere fanden sich bei hereditären Dystonien Hinweise auf eine besondere Rolle zerebello-thalamischer Regelkreise, sowie auf manifestations- und phänotypassoziierte Aspekte zerebraler Netzwerkveränderungen [23,24]. Bei idiopathischen Formen waren die Charakteristika von Konnektivitätsveränderungen jedoch bislang kaum evaluiert.

In den in dieser Habilitationsschrift zusammengefassten Arbeiten wurden verschiedene fokale Dystonien mit Fokus auf aufgabenspezifische kraniale Formen hinsichtlich magnetresonanztomographisch nachweisbarer Korrelate funktioneller und/oder struktureller Veränderungen sowie deren Beziehung näher untersucht. Hierbei wurde schwerpunktmäßig der Frage nach Veränderungen im Verbindungsmuster sensomotorischer Hirnregionen über die Evaluation intrinsischer, funktioneller Konnektivität und/oder der Eigenschaften rekonstruierter zentraler Fasertrajektorien nachgegangen.

2. Synopsis eigener Forschungsarbeiten

2.1. Aspekte funktioneller Konnektivität und Aktivität bei aufgabenspezifischen fokalen Dystonien

Hirnregionen zeigen auch in Abwesenheit spezieller experimenteller Interventionen (experimenteller Ruhezustand, sog. ‚resting state') spontane Aktivität, die mittels fMRT als niederfrequente Schwankung des zerebralen BOLD-Signals messbar ist [18,25]. Das Konzept der funktionellen Konnektivität (functional connnectivity, FC) im Ruhezustand beschreibt die in diesem Rahmen zu beobachtende zeitliche Kohärenz solcher Ruheaktivität innerhalb und zwischen Hirnregionen. Dies ermöglicht die Beschreibung sog. intrinsischer (funktioneller) Konnektivitätsnetzwerke von Hirnregionen mit zeitlich kohärenten niederfrequenten Signalfluktuationen [18,25,26]. Diese zeigen – hinweisend auf eine gemeinsame Funktionalität – eine ähnliche räumliche Topographie wie aufgabenassoziierte Hirnaktivität, und das Konnektivitätsmuster solcher Netzwerke wird als Grundlage der durch externe Einflüsse (z.B. Aufgaben, Stimuli) induzierten Veränderungen von Hirnaktivität diskutiert [18,27-29]. Hierdurch eröffnet sich die Möglichkeit, zerebrale Netzwerkveränderungen bei AOFD unter Vermeidung von Störfaktoren (z.B. nicht primär dystone motorische Aktivität) zu charakterisieren. Bei aufgabenspezifischer Dystonie war dies zunächst nur spärlich untersucht worden [30,31]. In den ersten beiden hier vorgestellten Arbeiten hatten wir daher Aspekte der sensomotorischen funktionellen Konnektivität im Ruhezustand bei den zwei häufigsten Formen fokaler aufgabenspezifischer Dystonien bei Nichtmusikern näher betrachtet und in Bezug auf Veränderungen in anderen, parallel erhobenen Neuroimaging-Ansätzen eingeordnet.

2.1.1. Konnektivitätsprofile intrinsischer sensomotorischer Netzwerke und ihre Relation zu Veränderungen der grauen Substanz bei Schreibkrampf

Mantel, T., Meindl, T., Li, Y., Jochim, A., Gora-Stahlberg, G., Kräenbring, J., Berndt, M., Dresel, C., Haslinger, B. (2017). Network-specific resting-state connectivity changes in the premotor-parietal axis in writer's cramp. *NeuroImage. Clinical*, *17*, 137–144. https://doi.org/10.1016/j.nicl.2017.10.001

Bei der häufigsten aufgabenspezifischen Dystonie der Extremitäten, dem meist zwischen dem dritten und fünften Lebensjahrzehnt manifestierenden Schreibkrampf [32], hatten frühere MRT-Studien strukturelle Auffälligkeiten und aufgabenassoziierte Aktivitätsveränderungen vor allem in primären sensomotorischen, prä- bzw. supplementär-motorischen Hirnarealen, im Kleinhirn sowie in den Basalganglien beschrieben [9,33]. Allerdings war in solchen Arbeiten die Ausrichtung der Aktivierungsveränderungen mit teilweiser Über- und Unteraktivität in veränderten Hirnregionen heterogen. Auch die wenigen verfügbaren Untersuchungen der FC im Ruhezustand konnten mit kleinen Gruppengrößen und variierenden methodischen Ansätzen kein einheitliches Bild der Veränderungen im sensomotorischen System herstellen [30,34]. Mit dem Ziel einer Einordnung und Erweiterung solcher funktioneller Konnektivitätsänderungen einschließlich ihrer Relation zu möglichen strukturellen Veränderungen der grauen Substanz führten wir daher eine multimodale bildgebende Folgestudie bei einer größeren Gruppe Schreibkrampfpatienten mit einem sensitiven, robusten, und hypothesenfreien Analyseansatz durch.

Methoden und Ergebnisse

Hierzu wurden von 26 Schreibkrampfpatienten und 27 gesunden Probanden jeweils eine fMRT-Messung im experimentellen Ruhezustand (sog. Ruhe-fMRT) sowie ein hochaufgelöster (T_1-gewichteter) sMRT-Scan erhoben.

Veränderungen der Ruhezustands-FC wurden über eine sog. Unabhängigkeitsanalyse (auch Independent Component Analysis) untersucht. Hierbei wurden die bewegungs- und

schichtaufnahmezeitkorrigierten, in den Referenzkoordinatenraum des Montreal Neurological Institute (MNI) registrierten sowie geglätteten Ruhe-fMRT-Aufnahmen der jeweiligen Gruppenteilnehmer in einen vierdimensionalen (räumlich-zeitlichen) Datensatz zusammengefasst. Nach einer initialen schrittweisen Dimensionsreduktion wurden dann räumlich maximal unabhängige Netzwerke funktionell verbundener (= zeitlich kohärent signalaktiver) Hirnregionen unter Anwendung des *InfoMax*-Algorithmus extrahiert. Zur Detektion möglicher relevanter Veränderungen bei Schreibkrampf wurden unter den so extrahierten, stabilen intrinsischen funktionellen Konnektivitätsnetzwerken solche mit mutmaßlicher sensomotorischer Funktionalität [35-37] über multiple Regression mit räumlichen Koaktivierungskarten aus einer Metaanalyse von aufgaben- bzw. ereignisbezogenen fMRT-Studien zur weiteren Auswertung identifiziert [38]: ein prämotorisch-parietales Netzwerk, ein dorsales und ventrales sensomotorisches Netzwerk, ein Basalganglien-Thalamus-Netzwerk, sowie ein Kleinhirn-Netzwerk. Das primär visuelle Netzwerk diente als Kontrollnetzwerk. Nach direkter Rückrekonstruktion (*GICA1*-Algorithmus) der Netzwerkraumkarten auf die Einzeldatensätze der Studienteilnehmer wurden diese zum einen hinsichtlich Zwischengruppenveränderungen der FC innerhalb der untersuchten Netzwerke in alters-, geschlechts- und Kopfbewegungsparameter-adjustierten sowie für multiple Netzwerkanalysen korrigierten t-Tests untersucht. Zum anderen erfolgte eine Evaluation von Veränderungen der FC zwischen diesen Netzwerken über Zwischengruppenvergleich der Pearson-Korrelationen ihrer durchschnittlichen (für Trends, Signalspitzen, Hochfrequenzrauschen und Kopfbewegungseffekte bereinigten bzw. adjustieren) Signalverläufe in alters- und geschlechtsadjustierten, für multiple Zwischennetzwerkvergleiche korrigierten Kovarianzanalysen.

Im *prämotorisch-parietalen Netzwerk* zeigten Schreibkrampfpatienten linkshemisphärisch vermehrte FC des primären sensomotorischen Kortex sowie der lateroventralen prämotorischen Kortizes. Reduzierte FC bestand dagegen für den rechtshemisphärischen primären sensomotorischen Kortex, sowie weiterhin linkshemisphärisch betont für den bilateralen posterioren parietalen Kortex und den bilateralen inferioren frontalen Sulcus (s. Abbildung 1). In den untersuchten *sensomotorischen Netzwerken* zeigte sich bei Schreibkrampfpatienten im dorsalen sensomotorischen Netzwerk eine bilateral reduzierte FC der mediodorsalen prämotorischen und supplementär-motorischen Kortizes,

sowie weiterhin des linkshemisphärischen ventromedialen präfrontalen Kortex (s. Abbildung 1). Im ventralen sensomotorischen Netzwerk ergab sich lediglich vermehrte FC bei Patienten im Bereich des temporo-okzipitalen Übergangs.

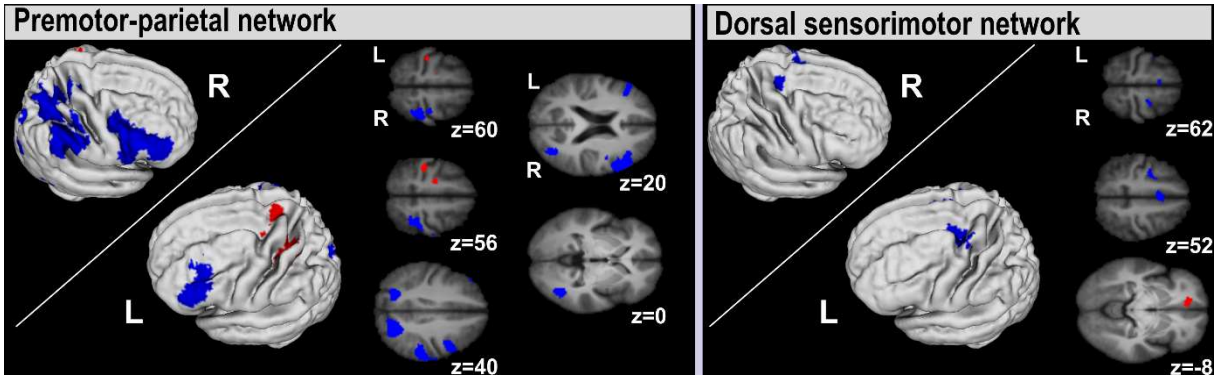

Abbildung 1. Zwischengruppenunterschiede der FC innerhalb des prämotorisch-parietalen, sowie des dorsalen sensomotorischen Netzwerks bei Schreibkrampf.

Areale signifikant vermehrter bzw. verminderter FC in der Patientengruppe im Vergleich zu gesunden Kontrollen sind in Rot bzw. Blau auf den axialen Schichten und 3D-Rekonstruktionen der gemittelten Gehirne aller Studieneilnehmer dargestellt. Raumkoordinaten beschreiben die Schichtposition im MNI-Referenzraum.

Abkürzungen: L, linke Hemisphäre; R, rechte Hemisphäre.

Im *Basalganglien-Thalamus-Netzwerk* wurde bei Patienten bilateral vermehrte FC ventraler und dorsaler prämotorischer Kortizes, hinterer Kleinhirnanteile und der sekundären somatosensorischen Kortizes gesehen. Weiterhin bestand erhöhte FC im linkshemisphärischen primären sensomotorischen Kortex und Zingulum, sowie in rechtshemisphärischen posterioren parietalen Kortizes (supramarginaler Gyrus, superiorer parietaler Kortex). Reduzierte FC bei Patienten zeigte sich vor allem für den Ncl. caudatus und Thalamus bilateral, sowie rechtshemisphärisch für Pallidum und Hippocampus (s. Abbildung 2). Im *Kleinhirn-Netzwerk* zeigte sich bilateral erhöhte FC bei Patienten für das hintere Kleinhirn und den kaudalen ventralen prämotorischen Kortex. Der linkshemisphärische superiore parietale Kortex wies reduzierte FC auf (s. Abbildung 2).

Die zusätzliche Analyse der Ruhezustands-FC zwischen den untersuchten Netzwerken ergab einen signifikanten Konnektivitätsverlust zwischen dem Kleinhirn-Netzwerk und Basalganglien-Thalamus-Netzwerk, sowie dem Kleinhirn-Netzwerk und dem primären visuellen Netzwerk bei Schreibkrampfpatienten gegenüber dem gesunden Kontrollkollektiv.

Das Vorliegen parallel zu den funktionellen Konnektivitätsänderungen bestehender struktureller Veränderungen der grauen Substanz (grey matter, GM) wurde mittels voxelbasierter Morphometrie (VBM) evaluiert. Der Vergleich der segmentierten, in den MNI-Referenzkoordinatenraum registrierten, modulierten und geglätteten grauen Substanz der anatomische MRT-Aufnahmen (alters-, geschlechts- und für intrakranielles Gesamtvolumen adjustierter t-Test) ergab in der Patientengruppe ein signifikant reduziertes Volumen der grauen Substanz im rechten hinteren Kleinhirn, bei einem entsprechenden Trend für die linke Kleinhirnhemisphäre (s. Abbildung 2).

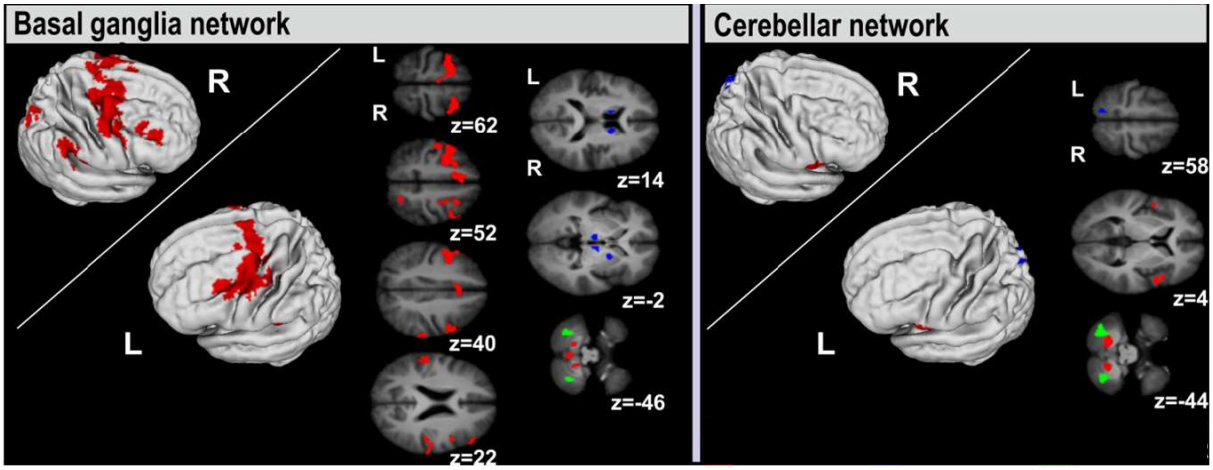

Abbildung 2. Zwischengruppenunterschiede der FC innerhalb des Basalganglien-Thalamus- und des Kleinhirn-Netzwerks, und ihre topographische Relation zu strukturellen Veränderungen bei Schreibkrampf.

Areale signifikant vermehrter bzw. verminderter FC in der Patientengruppe im Vergleich zu Kontrollen sind in Rot bzw. Blau auf den axialen Schichten und 3D-Rekonstruktionen der gemittelten Gehirne aller Studieneilnehmer dargestellt. Areale erhöhten GM-Volumens in der Patientengruppe sind einschließlich Trends zur Signifikanz in Grün aufgetragen. Raumkoordinaten beschreiben die Schichtposition im MNI-Referenzraum.

Abkürzungen: L, linke Hemisphäre; R, rechte Hemisphäre.

Die multiple Regression mit klinischen Parametern ergab eine signifikante Korrelation zwischen der krankheitsbedingten Einschränkung der Schreibfähigkeit (nach Writer's Cramp Rating Scale[39]) und dem Volumen der grauen Substanz im sekundären somatosensorischen Kortex bei Schreibkrampfpatienten, aber keine signifikanten Assoziationen mit den funktionellen Konnektivitätsmaßen.

2.1.2. Aktivitätsprofile unter somatosensorischer Reizverarbeitung und ihre Relation zu Konnektivitätsveränderungen im Ruhezustand bei laryngealer Dystonie

Mantel, T., Dresel, C., Welte, M., Meindl, T., Jochim, A., Zimmer, C., Haslinger, B. (2020). Altered sensory system activity and connectivity patterns in adductor spasmodic dysphonia. *Scientific reports*, *10*(1), 10179. https://doi.org/10.1038/s41598-020-67295-w

Die aufgabenspezifische laryngeale Dystonie führt bei Betroffenen zu einer Störung der Stimmbildung [10,40]. Der mit Abstand häufigste Phänotyp, der Adduktor-Typ (adductor-type laryngeal dystonia, ADLD), präsentiert sich mit einer gepressten und brüchigen Sprechstimme [40]. Regelmäßige Injektionen mit Botulinum-Neurotoxin Typ A (BoNT-A) in die Stimmfalten führen durch Abschwächung der symptominduzierenden Muskelspasmen zu einer jeweils vorübergehenden Beschwerdebesserung. Frühere Bildgebungsstudien hatten bereits verschiedene strukturelle Veränderungen der grauen und weißen Substanz, und/oder funktionelle Veränderungen von Aktivität oder Konnektivität innerhalb von Arealen des phonationsassoziierten Hirnnerzwerkes zeigen können [41], die insbesondere in primären und übergeordneten sensomotorischen Kortizes, sowie im Bereich von Putamen, Thalamus sowie Kleinhirn zu beobachten waren [42-47]. Angesichts der technischen Limitationen in Bezug auf die direkte Stimulierbarkeit des Larynx [48] blieb jedoch bislang offen, ob bei laryngealer Dystonie kongruent zu anderen Formen aufgabenspezifischer fokaler Dystonien auch eine Veränderung zentralen Verarbeitung somatosensibler Stimuli vorliegt, und in welchem Bezug diese zu dysfunktionaler Ruhezustands-FC bei der Erkrankung stehen. Weiter war ungeklärt, ob elektrophysiologische Hinweise auf einen möglichen zentralen Effekt des zur symptomatischen Therapie eingesetzten BoNT-A [49] einem von phonationsassoziierter Muskelaktivität unabhängigen Modulationsprozess der somatosensorischen Reizverarbeitung entsprechen, oder sekundär auf die BoNT-A-assoziierte Modulation motorischer Aktivität während Phonation zurückzuführen sind.

Methoden und Ergebnisse

Zur Klärung dieser Fragestellungen wurden 14 Patienten mit phoniatrisch gesicherter idiopathischer ADLD und 15 gesunde Probanden MR-bildgebend untersucht. Zur Evaluation möglicher BoNT-A-Effekte wurde eine Untergruppe von zwölf regelmäßig mit gutem Effekt mit BoNT-A-Injektionen behandelten Patienten zweimalig in pseudorandomisierter Reihenfolge untersucht: wenn der klinische Effekt vergangen war (kurz vor der nächsten Injektionsbehandlung), sowie wenn klinische Effekt am besten war (4-6 Wochen nach Injektionsbehandlung).

Zur Evaluation von Veränderungen der zentralen somatosensorischen Reizverarbeitung wurde ein bereits bei anderen AOFD angewandtes taktiles Stimulationsexperiment während funktioneller MRT durchgeführt [50-52]. Angesichts der bislang unzureichend gelösten technischen Anforderungen für eine sensitive und reproduzierbare direkten Stimulation des Larynx [48] wurde stellvertretend, dem in Studien bei anderen fokalen Dystonien nahegelegten Konzept einer gestörten somatosensibler Reizverarbeitung als endophänotypes Merkmal dieser Erkrankungen folgend [53], die somatosensorische Reizverarbeitung primär über die Stimulation besser zugänglicher nicht-dystoner kutaner Surrogatareale untersucht. Mittels eines MRT-kompatiblen Stimulationsgerätes wurden hierfür über von Frey-Monofilamente kurze Folgen punktueller taktiler Stimuli in pseudorandomisierter Reihenfolge und regionsadaptierter Intensität an Stirn, Oberlippe und Hand jeder Körperseite während drei funktioneller MRT-Sessions appliziert [50-52]. Die Vorverarbeitung erfolgte in Analogie zu vorherigen Studien die dieses Stimulationsparadigma angewendet hatten [50]. Die resultierenden teilnehmerindividuellen statistischen t-Kontrast-Bilder der kopfbewegungskorrigierten, stimulationsinduzierten zerebralen Aktivität in den sechs untersuchten Körperregionen wurden anschließend in einem für multiple Stimulationsbedingungen (stimulierte Körperregionen) korrigierten Random-Effects-Modell mit flexiblem faktoriellem Design zwischen den Gruppen verglichen. Zur Evaluation möglicher BoNT-A-Effekte wurden *post hoc* Längsschnittkontraste der Patientensubgruppen ohne vs. mit vorhandener klinischer BoNT-A-Wirkung im Falle signifikanter Ergebnisse im Vergleich von Patienten- und gesunder Kontrollgruppe berechnet.

In dieser Analyse ließ sich bei ADLD-Patienten unter linksseitiger wie rechtsseitiger Hand-, und linksseitiger Gesichtsstimulation, signifikant vermehrte Aktivität im jeweils kontralateralen primären somatosensorischen Kortex (S1) nachweisen (s. Abbildung 3). Weiterhin bestand unter rechtsseitiger Gesichtsstimulation vermehrte Aktivität im kontralateralen sekundären somatosensorischen Kortex. Zusätzlich fanden sich in der Patientengruppe Aktivitätssteigerungen in kontralateralen parietalen Assoziationskortizes (intraparietaler Sulcus, supramarginaler Gyrus, und/oder oberer Parietallappen). Insulär fand sich vermehrte kontralaterale Aktivität unter Stimulation links- wie rechtsseitiger Gesichtsareale. Unter Stimulation der rechten Gesichtsregion fand sich zudem linkshemisphärisch gesteigerte Aktivität im oberen temporalen Gyrus, welche im oberen Gesichtsbereich mit der krankheitsbedingten Phonationseinschränkung (nach Voice Handicap Index[54]) assoziiert war. Aktivitätssteigerungen in frontalen (insb. ventralen (prä)motorischen) Arealen waren lediglich bei linkshemisphärischer Gesichtsstimulation zu beobachten. Die *post hoc* Evaluation möglicher BoNT-A-Effekte auf diese Veränderungen ergab keine signifikanten Auffälligkeiten.

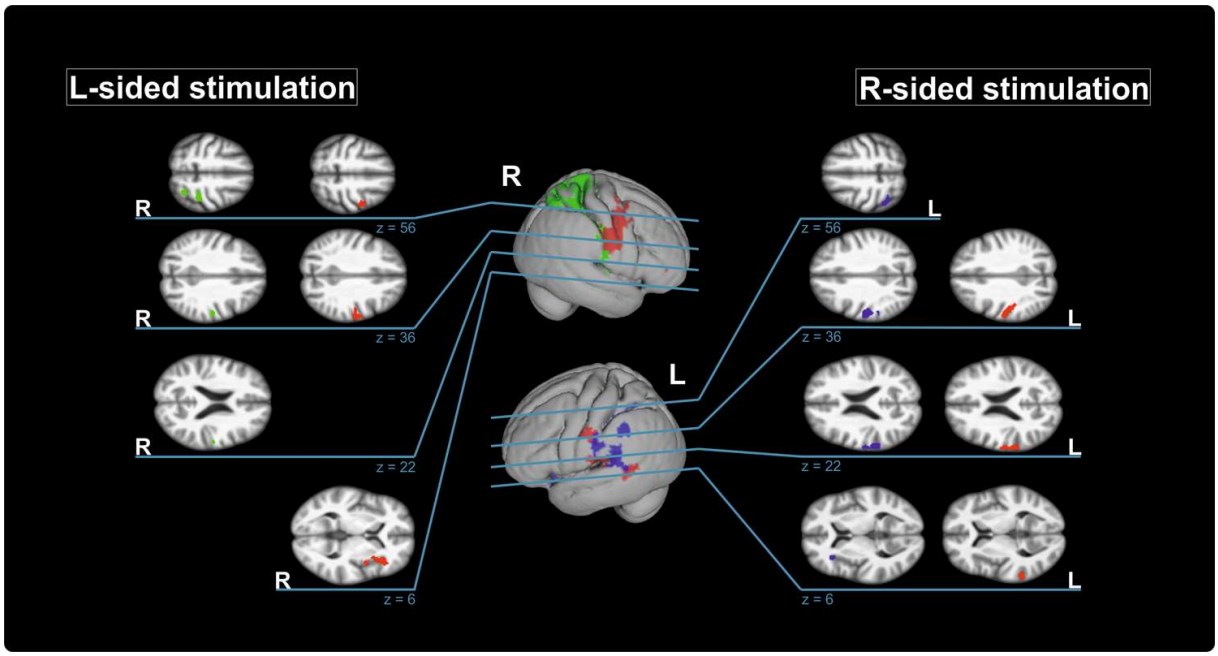

Abbildung 3. Hirnregionen vermehrter stimulationsassoziierter funktioneller Aktivität bei ADLD-Patienten (ohne klinische BoNT-A-Wirkung).

Areale signifikant vermehrter Aktivität im Vergleich zu Kontrollen sind farbkodiert für die stimulierte Körperregion (Stirn in Blau; Oberlippe in Rot; Handrücken, in Grün) auf den gemittelten Gehirnen aller Studienteilnehmer dargestellt. Die mittlere Spalte zeigt die Projektion auf die 3D-rekonstruierte kontralaterale Hemisphäre, die seitlichen Spalten jene auf die axialen Schichten in ausgewählten Hirnbereichen (von oben nach unten: S1/oberer Parietallappen; sekundärer somatosensorischer Kortex; insulärer/temporaler Kortex). Raumkoordinaten beschreiben die Schichtposition im MNI-Referenzraum.

Abkürzungen: L, linke Hemisphäre; R, rechte Hemisphäre.

Zur Evaluation der räumlichen Beziehung von Veränderungen somatosensibler Reizverarbeitung zu möglichen Veränderungen der funktionellen Konnektivität im Ruhezustand erfolgte eine Ruhe-fMRT-Messung. Die Ruhe-fMRT Daten wurden nach Vorverarbeitung (s. Kapitel 2.1.1.) inkl. Korrektur für Trends, Signalspitzen und Bewegungsartefakte hinsichtlich Auffälligkeiten der funktionellen Konnektivität (i) mit fernen (netzwerkbezogene/„long-range“ FC) sowie (ii) nahen Hirnbereichen („regional“ FC) untersucht.

Die Beurteilung der (i) long-range FC erfolgte analog zum in Kapitel 2.1.1. beschriebenen Vorgehen über eine Independent Component Analysis des geglätteten vierdimensionalen (räumlich-zeitlichen) Ruhe-fMRT-Datensatzes aller Studienteilnehmer. Entsprechend der Studienhypothese wurden, orientiert am stimulationsevozierten topographischen zerebralen Aktivitätsmuster, drei kortikale Ruhenetzwerke zur weiteren Analyse ausgewählt: das sensomotorische Netzwerk, das auditorische Netzwerk sowie das zentrale Exekutivnetzwerk (auch sog. aufgabenpositives Netzwerk). Zur Evaluation der (ii) regional FC wurde eine regionale Homogenitätsanalyse durchgeführt. In dieser wurde die zeitliche Kohärenz der (zusätzlich Bandpassgefilterten und für Störsignal aus Liquor/weißer Substanz bereinigten) spontanen BOLD-Signal-Fluktuation zerebraler Voxel mit ihren Nachbarvoxeln über den Kendallschen Konkordanzkoeffizienten berechnet.

Der kongruent zur Stimulationsanalyse in einem Random-Effects-Modell mit flexiblem faktoriellem Design durchgeführte Zwischengruppenvergleich ergab nach Korrektur für die Analyse multipler Netzwerke innerhalb des *sensomotorischen Netzwerkes* eine signifikant gesteigerte FC des rechten medialen prämotorischen Kortex bei Patienten. Weiterhin ergab sich bei Patienten innerhalb des *auditorischen Netzwerkes* eine signifikant stärkere FC des linken primären auditorischen Kortex. Hinsichtlich regionaler Konnektivitätsänderungen war eine signifikant reduzierte regionale FC im Bereich der rechten temporo-parietalen Übergangs bei Patienten (mit einem entsprechenden Trend in der linken Hemisphäre, der nicht Signifikanzniveau erreichte) zu beobachten (s. Abbildung 4). Wiederum fanden sich im longitudinalen *post hoc* Vergleich keine signifikanten BoNT-A-Effekte.

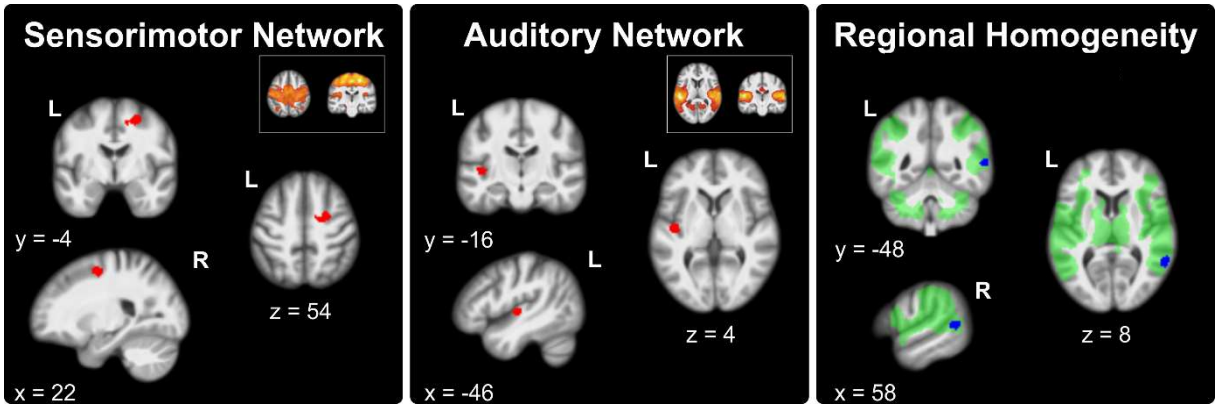

Abbildung 4. Veränderungen der Ruhezustands-FC bei ADLD-Patienten (ohne klinische BoNT-A-Wirkung).

Signifikante FC-Erhöhungen innerhalb intrinsischer Konnektivitätsnetzwerke sind rot dargestellt, Reduktionen der regionalen FC in Bereichen robuster taktil-stimulationsinduzierter zerebraler Aktivität (grün unterlegt) sind blau dargestellt. Raumkoordinaten beschreiben die Schichtposition im MNI-Referenzraum.

Abkürzungen: L, linke Hemisphäre; R, rechte Hemisphäre.

2.2. Charakterisierung struktureller zerebraler Veränderungen bei aufgabenspezifischer orofazialer Musikerdystonie (Ansatzdystonie)

Ansatzdystonie (auch Embouchure-Dystonie, ED) stellt die zweite wesentliche Manifestationsform der Musikerdystonie neben jener der oberen Extremitäten dar [55]. Sie zeichnet sich klinisch durch unwillkürliche Aktivität der Muskulatur des Mund-Gesicht-Bereichs (insbesondere der mimischen Muskeln, Zungen- und/oder Kaumuskeln) während des Spielens eines Blasinstrumentes aus. Überwiegend sind Blechbläser betroffen [56,57]. Die resultierende Störung der hochtrainierten willkürmotorischen Kontrolle der Ansatzregion führt bei den Erkrankten – in der Regel professionell tätigen Musikern – zur Einschränkung der Spielfähigkeit. Dies bedeutet im hochkompetitiven Feld der professionellen Musik oftmals das Ende der beruflichen Karriere [55,57]. Bislang waren bei Ansatzdystonie bildgebend hauptsächlich funktionelle (überwiegend MR-bildgebende) Untersuchungen zur Identifikation veränderter Aktivitätsmuster von Hirnregionen durchgeführt worden. Diese konnten unter anderem während symptomatischen wie asymptomatischen Bewegungsaufgaben der orofazialen Ansatzmuskulatur oder während somatosensibler Reizverarbeitung aus betroffenen fazialen wie nicht betroffenen Körperregionen Korrelate vermehrter zerebraler Aktivität bei Erkrankten zeigen [50,58]. Weiter

wurde abnorme FC im Ruhezustand innerhalb sensomotorischer, auditorischer Netzwerke, sowie mit dem zerebellären Netzwerk beschrieben [59].

2.2.1. Veränderungen der grauen Substanz bei Ansatzdystonie

Mantel, T., Altenmüller, E., Li, Y., Meindl, T., Jochim, A., Lee, A., Zimmer, C., Dresel, C., Haslinger, B. (2019). Abnormalities in grey matter structure in embouchure dystonia. *Parkinsonism & related disorders*, *65*, 111–116. https://doi.org/10.1016/j.parkreldis.2019.05.008

Zerebrale funktionelle Aktivitätsveränderungen waren bei ED während motorischer und somatosensorischer Informationsverarbeitung vor allem im Bereich der primären, aber auch in übergeordneten (parietalen, prämotorischen) sensomotorischen Hirnarealen, im Bereich subkortikaler Kerne und im Kleinhirn beschrieben worden [50,58]. Während strukturelle MR-bildgebende Untersuchungen bei anderen idiopathischen fokalen Dystonien (insb. von Hals und Hand) Auffälligkeiten der grauen Substanz solcher Regionen gezeigt hatten [9], waren Vorliegen, Art, und Lokalisation struktureller zerebraler Veränderungen bei der aufgabenspezifischen kranialen Ansatzdystonie bislang ungeklärt. Zudem war bekannt, dass gesunde Musiker ebenfalls Veränderungen in Struktur und Symmetrie der grauen Substanz zeigen. Diese werden als die Professionalisierung begünstigendes endophänotypes Merkmal oder als Korrelat plastischer Veränderungen im Rahmen kontinuierlicher motorischer Übung diskutiert [60-62]. Jedoch war – neben Wissenslücken über die Art solcher Veränderungen in der Subpopulation der Blasmusiker – bislang unzureichend untersucht, wie sich solche Veränderungen in gesunden professionellen Musikern zu jenen der an Dystonie erkrankten Musiker verhalten.

Methoden und Ergebnisse

Zur Klärung dieser Fragestellungen wurden Unterschiede in Volumen und hemisphärischer Symmetrie der grauen Substanz in hochauflösenden (T_1-gewichteten) zerebralen sMRT-Aufnahmen

einer Gruppe professioneller Blechbläser mit Ansatzdystonie, einer Gruppe professioneller gesunder Blechbläser, sowie eines Kollektivs gesunder Nichtmusiker untersucht.

Zur Detektion von Volumenunterschieden der grauen Substanz wurden die vorverarbeiteten, in den MNI-Referenzkoordinatenraum registrierten und modulierten Segmentierungen der grauen Substanz der Studienteilnehmer in zwei komplementären Ansätzen evaluiert: zum einen wurden die geglätteten Segmentierungen der grauen Substanz der Teilnehmer mittels VBM auf voxelweise Auffälligkeiten hypothesenfrei über das gesamte Gehirn hinweg untersucht. Zum anderen das mittlere Volumen der grauen Substanz hypothesengesteuert innerhalb gezielt ausgewählter Hirnareale (präzentraler und postzentraler Gyrus, Pallidum und Putamen) evaluiert (atlasbasierte Volumetrie, ABV). Diese analysierten Areale waren zuvor auf Basis einer „Activation Likelihood Estimation"-Metaanalyse geeigneter früherer morphometrischer Studien bei anderen idiopathischen AOFD identifiziert worden. Die Zwischengruppenvergleiche erfolgten jeweils in einem für Geschlecht, Alter und intrakranielles Gesamtvolumen adjustierten Random-Effects-Modell mit flexiblem faktoriellem Design (VBM-Analyse) bzw. in einfaktoriellen Varianzanalysen (ABV-Analyse).

Im Vergleich von erkrankten und gesunden Blechbläsern ergab sich dabei im voxelbasierten Analyseverfahren bei Erkrankten ein signifikant erhöhtes Volumen der grauen Substanz im Bereich des rechts- und linkshemisphärischen präzentralen Gyrus, sowie im Bereich des linkshemisphärischen postzentralen Gyrus. Im Vergleich der erkrankten Blechbläser mit gesunden Nichtmusikern erreichten lediglich rechtshemisphärische Volumenerhöhungen im präzentralen und postzentralen Gyrus Signifikanz (s. Abbildung 5). Im atlasbasierten volumetrischen Ansatz ergab sich bei signifikantem Gruppeneffekt für den prä- und postzentralen Gyrus beider Hemisphären in den Folgenanalysen kongruent ein signifikant erhöhtes mittleres Volumen der grauen Substanz im prämotorischen Gyrus bei erkrankten Blechbläsern

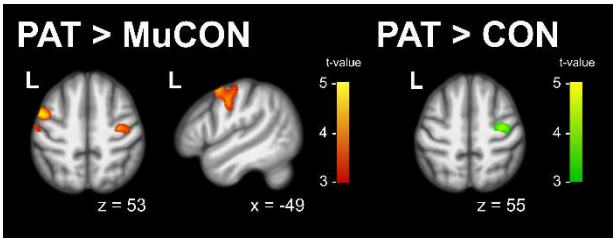

Abbildung 5. Areale mit erhöhten GM-Volumina bei ED-Patienten.

Signifikante Volumensteigerungen im Vergleich zu gesunden Blechbläsern (in Rot) und Nichtmusikern (in Grün) sind auf den gemittelten anatomischen Scan aller Studienteilnehmer dargestellt. Raumkoordinaten beschreiben die Schichtposition im MNI-Referenzraum.

Abkürzungen: CON, gesunde Nichtmusiker-Kontrollen; MuCON, gesunde professionelle Blasmusiker-Kontrollen; L, linke Hemisphäre; PAT, Patienten mit ED.

im Vergleich sowohl mit gesunden Blechbläsern als auch mit gesunden Nichtmusikern. Im rechtshemisphärischen postzentralen Gyrus zeigte sich ein signifikant erhöhtes Volumen der grauen Substanz lediglich im Vergleich mit Nichtmusikern.

Zur Evaluation interhemisphärischer Symmetrieveränderungen in der Verteilung der zerebralen grauen Substanz wurde ein von Kurth und Kollegen beschriebenes Verfahren der voxelbasierten zerebralen Asymmetrieanalyse angewendet [63]. Hierfür wurde die segmentierte graue Substanz der Studienteilnehmer in normaler und gespiegelter Orientierung auf eine eigens hierfür aus dem Datensatz des „Information eXtraction from Images"/IXI-Projektes [64] generierte symmetrische Vorlage zur Berechnung eines voxelweisen Asymmetrie-Index ($AI = \frac{normale - gespiegelte\ Orientierung}{0{,}5 \times (normale + gespiegelte\ Orientierung)}$) registriert, und die geglätteten zerebralen Asymmetriekarten dann in einem geschlechts- und altersadjustierten Random-Effects-Modell mit vollfaktoriellem Design untersucht. Hier ergab sich eine signifikante Veränderung der hemisphärischen Symmetrie der grauen Substanz sowohl bei erkrankten als auch gesunden Blasmusikern im Vergleich zu Nichtmusikern. Betrafen die Veränderungen bei gesunden Musikern vor allem den Thalamus, erstreckten sie sich bei erkrankten Blasmusikern nach lateral bis auf das Putamen und die Inselregion. Explorative Folgeanalysen der mittleren Asymmetrie-Indizes und Volumina der grauen Substanz in den signifikanten Clustern legten eine vermehrte Symmetrie dieser Strukturen bei erkrankten wie bei gesunden Musikern verglichen mit gesunden Nichtmusikern nahe. Dies war am ehesten auf die Abnahme einer bei Letzteren bestehenden Asymmetrie zugunsten der linken Hemisphäre zurückzuführen. Bei erkrankten Blasmusikern war dies im Gegensatz zu den gesunden Blasmusikern jedoch nicht nur durch die Zunahme des rechtshemisphärischen Volumens, sondern auch durch eine Abnahme von linkshemisphärischem Volumen der grauen Substanz in der betroffenen Region getrieben. Regressionsanalysen mit klinischen Parametern ergaben dabei weiter, dass letztere Beobachtung im Bereich des Putamens und lateralen Pallidums signifikant mit der Krankheitsdauer assoziiert war (s. Abbildung 6).

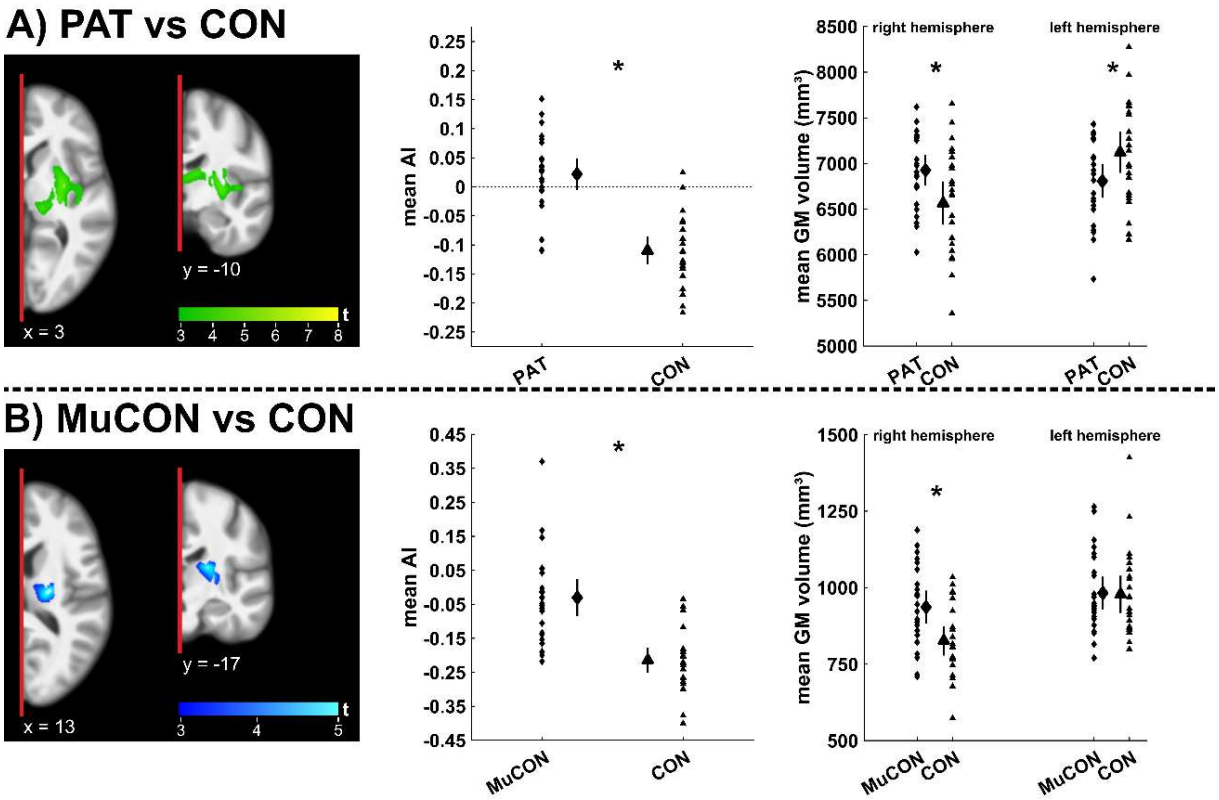

Abbildung 6. Hirnregionen mit signifikant höheren Asymmetrie Indizes bei ED-Patienten (A) und gesunden Blechbläsern (B) gegenüber Nichtmusikern.

Clusterdarstellung in Projektion auf die rechte Hemisphäre der gemittelten anatomischen Scans aller Studienteilnehmer. Die nebenstehenden Punktdiagramme zeigen die clusterspezifischen mittleren AIs sowie GM-Volumina für die rechte und linke Hemisphäre jeder Gruppe. Raumkoordinaten beschreiben die Schichtposition im MNI-Referenzraum. Fehlerbalken zeigen den doppelten Standardfehler des Mittelwerts.

Abkürzungen: AI, Asymmetrie-Index; CON, gesunde Nichtmusiker-Kontrollen; MuCON, gesunde professionelle Blasmusiker-Kontrollen; PAT, Patienten mit ED.

2.2.2. Veränderungen von Schlüsseltrajektorien in der weißen Substanz bei Ansatzdystonie

Mantel, T., Altenmüller, E., Li, Y., Lee, A., Meindl, T., Jochim, A., Zimmer, C., Haslinger, B. (2020). Structure-function abnormalities in cortical sensory projections in embouchure dystonia. *NeuroImage. Clinical*, *28*, 102410. https://doi.org/10.1016/j.nicl.2020.102410

Dysfunktionale Integration sensomotorischer Information wird als ein zentraler Aspekt bei der Ausbildung dystoner Fehlhaltungen angenommen [7]. Bisherige Beobachtungen bei Ansatzdystonie

legten nahe, dass diese sowohl die primäre als auch die übergeordneten kortikalen Ebenen einbeziehen könnte [58,59]. Insbesondere wurden eine betonte dysfunktionale Rolle der Sensorik [50,65-67] sowie von Regelkreisen mit striataler Beteiligung bei Musikerdystonien vermutet [58,68]. Neben den in Kapitel 2.2.1. beschriebenen strukturellen Veränderungen der grauen Substanz war auch das Vorliegen von Veränderungen der strukturellen Integrität von Faserbahnen einschließlich ihrer Relation zu funktionellen Konnektivitätsveränderungen zwischen vermutlich beteiligten Hirnregionen bislang unzureichend erforscht. Wir erstellten daher anhand bestehender Vorarbeiten bei Musikerdystonien ein literaturbasiertes vereinfachtes sensomotorisches Netzwerkmodell von *a priori* wahrscheinlich betroffenen zerebralen Trajektorien, um die als subtil angenommenen strukturo-funktionellen Verbindungsveränderungen bei ED möglichst sensitiv zu untersuchen.

Methoden und Ergebnisse

Zur Beantwortung der Fragestellung wurde ein vereinfachtes Netzwerk aus Hirnregionen entworfen, die über mehrere MR-bildgebende Vorstudien und Neuroimaging-Verfahren hinweg bei Musikerdystonien wiederholt Auffälligkeiten gezeigt hatten [50,58,59,68-70]: fazialer Repräsentationsbereich von primär motorischem ($M1_{GESICHT}$) und primär somatosensorischem Kortex ($S1_{GESICHT}$), supplementär-motorisches Areal (SMA), superiorer Parietallappen (SPL), sowie Putamen. Die wesentlichen neuroanatomischen Verbindungsbahnen zwischen diesen Hirnregionen wurden in einem Kollektiv von 16 professionellen Blechbläsern mit Ansatzdystonie und 16 gesunden professionellen Blechbläsern näher betrachtet. Diese wurden hierzu multimodal mittels hochaufgelöster (T_1-gewichteter) sMRT, herzschlaggetriggerter Diffusionsbildgebung mit insgesamt 64 Gradientenrichtungen sowie Ruhe-fMRT untersucht.

Zur Evaluation der (mikro)strukturellen Integrität der Trajektorien zwischen den genannten Hirnarealen wurden die für bewegungs-/wirbelstrom- und suszeptibilitätsinduzierte Distorsionen korrigierten [71,72], qualitätskontrollierten Diffusions-MRT-Aufnahmen mit probabilistischer Traktographie untersucht. Basierend auf einem Tensormodell mit zwei berechneten Faserverlaufs(richtungen) pro Voxel wurde in einem Anatomie- und Anisotropie-geführten

Rekonstruktionsverfahren mit zwei Rekonstruktionsdurchgängen [73] der wahrscheinliche Verlauf der Faserverbindungen zwischen SPL und SMA im medialen superioren longitudinalen Faszikel, zwischen $M1_{GESICHT}$ und $S1_{GESICHT}$ in U-Fasern bzw. im lateralen superioren longitudinalen Faszikel [74-76], sowie den genannten kortikalen Arealen und dem Putamen rekonstruiert [77].

Für die Mehrheit der Trajektorien gelangen die Rekonstruktionen bei allen (Kortizes → Putamen, $S1_{GESICHT}$ ↔ $M1_{GESICHT}$) bzw. bei über 90 % (SMA ↔ SPL) der Studienteilnehmer. Lediglich die Trajektorie zwischen SMA und $M1_{GESICHT}$ wies eine geringere Rekonstruktionsrate auf, deren Ursache außerhalb möglicher technischer Limitationen (infolge der regionalen Fülle kreuzender Fasern) ungeklärt blieb. Sensomotorische kortio-kortikale Trajektorien verliefen dabei in den medialen Anteilen des superioren longitudinalen Faszikels (SMA-SPL), oder seinen lateralen Anteilen bzw. U-Fasern ($S1_{GESICHT}$-$M1_{GESICHT}$; s. Abbildung 7). Die kortikalen Trakte zum Putamen folgten der publizierten anatomischen Verbindungstopographie dieses Kerngebietes [78].

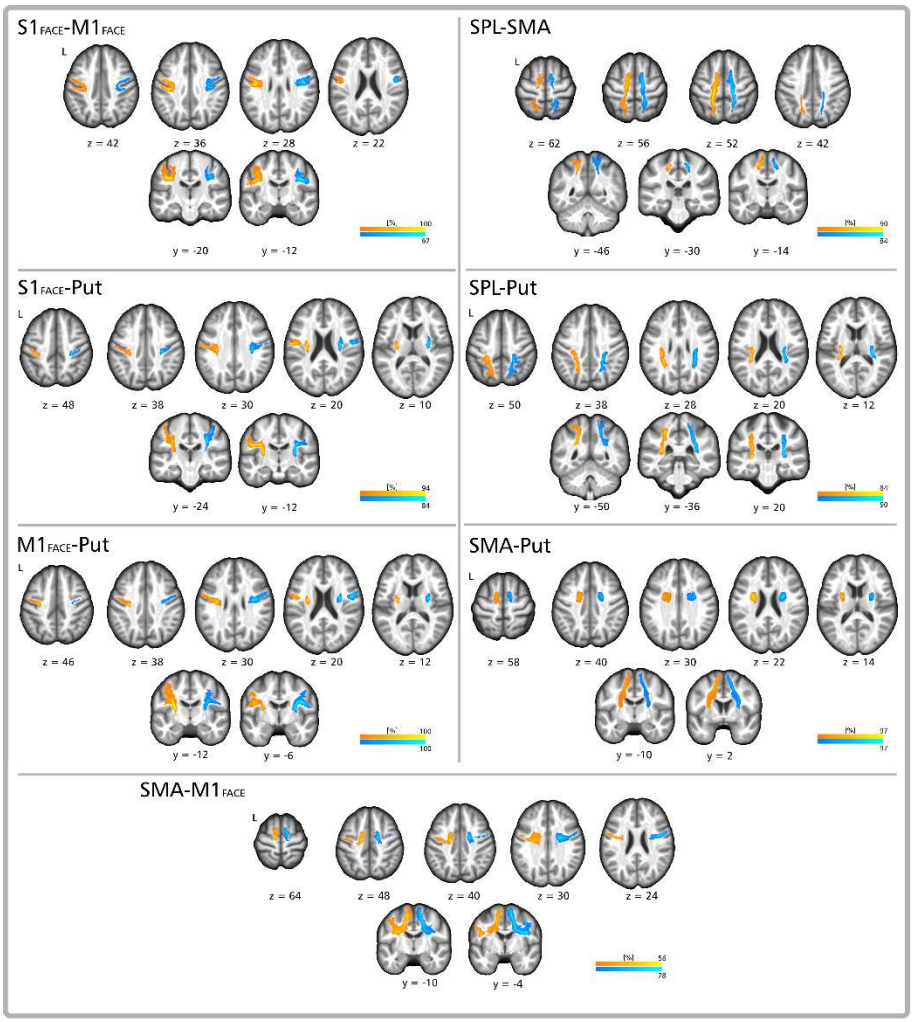

Abbildung 7. Wahrscheinlichkeitsbasierte Faserverläufe der untersuchten sensomotorischen Trajektorien.

Die Farbintensität gibt die prozentuale Überlagerung zwischen den Teilnehmern wieder (warme/kalte Farbskala für die linke/rechte Hemisphäre; Wahrscheinlichkeitsschwelle 5%). Raumkoordinaten beschreiben die Schichtposition im MNI-Referenzraum.

Abkürzungen: L, linke Hemisphäre; $M1_{FACE\ (GESICHT)}$, Gesichtsrepräsentation im primären motorischen Kortex; Put, Putamen; $S1_{FACE\ (GESICHT)}$, Gesichtsrepräsentation im primären somatosensorischen Kortex; SMA, supplementär-motorisches Areal; SPL, superiorer Parietallappen.

Zur Beschreibung der Traktintegrität wurden für jeden Teilnehmer die Mittelwerte verschiedener Diffusionsparameter (fraktionelle Anisotropie (FA), (orthogonaler) Modus der Anisotropie, axiale und radiale Diffusivität) über mehrere gebräuchliche Verbindungswahrscheinlichkeitsschwellenwerte hinweg aus den einzelnen Traktvolumina extrahiert. Zwischengruppenunterschiede wurden in zweiseitigen, alters- und geschlechtsadjustierten Permutationstests nach der Methode von Freedman-Lane, korrigiert für multiple Traktanalysen, untersucht [79,80]. Hierbei zeigte sich eine signifikant reduzierte axiale Diffusivität in den Trajektorien zwischen $S1_{GESICHT}$ und dem Putamen bei

Ansatzdystoniepatienten. In den Trajektorien zwischen SPL und SMA war die axiale Diffusivität dagegen erhöht, linkshemisphärisch kongruent begleitet von einem signifikant erhöhten Modus der Anisotropie. Weiterhin zeigte sich der Modus der Anisotropie in der linkshemisphärischen Trajektorie zwischen SMA und $M1_{GESCICHT}$ signifikant erhöht.

Zur Evaluation begleitender funktioneller Konnektivitätsveränderungen erfolgte eine Analyse der funktionellen Konnektivität im Ruhezustand für die acht untersuchten kortikalen Areale entsprechend der zuvor evaluierten strukturellen Trajektorien. Die Ruhe-fMRT-Aufnahmen wurden zunächst bewegungs- sowie schichtaufnahmezeitkorrigiert, in den MNI-Referenzkoordinatenraum registriert, für Trends und Rauschen (Signalkomponenten aus weißer Substanz/Liquor, Kopfbewegungsparameter) bereinigt, bandbreitengefiltert und geglättet. Das bereinigte mittlere zeitliche Signal aus jedem untersuchten Hirnareal wurde anschließend mit den Voxeln der grauen Substanz der anderen untersuchten Hirnareale Pearson-korreliert und die entsprechenden Korrelationskarten, korrigiert für multiple analysierte Verbindungen, zwischen den Gruppen verglichen (alters- und geschlechtsadjustierte Permutationstests nach der Methode von Freedman-Lane). Dabei zeigte sich linkshemisphärisch eine signifikant reduzierte funktionelle Konnektivität zwischen $S1_{GESICHT}$ und dem Putamen links mit entsprechender Clusterlokalisation im Eintrittsbereich der rekonstruierten Faserverbindung mit $S1_{GESICHT}$ in das Putamen (s. Abbildung 8A).

Zur weiteren Einordnung der gemeinsamen strukturellen und funktionellen Veränderungen in der untersuchten Trajektorie erfolgten geplante atlasbasierte volumetrische Analysen der aus den anatomischen MRT-Aufnahmen segmentierten grauen Substanz in den beteiligten Hirnregionen ($S1_{GESICHT}$, Putamen) *post hoc* analog zum in Kapitel 2.2.1. beschriebenen Vorgehen. Dies ergab eine signifikante Reduktion des Volumens der grauen Substanz in $S1_{GESICHT}$ linkshemisphärisch, nicht aber im Putamen (alters-, geschlechts-, und für intrakranielles Gesamtvolumen adjustierte Permutationstest nach Freedman-Lane). P*ost hoc* Regressionsanalysen ergaben eine signifikante positive Assoziation zwischen der Reduktion der mittleren funktionellen Konnektivität und der Reduktion mittleren axialen

Diffusivität in der Patientengruppe, aber keine Assoziation mit der Volumenerhöhung der grauen Substanz in S1GESICHT in dieser Trajektorie (s. Abbildung 8B-C).

Kontrollanalysen der Traktintegrität, Ruhezustands-FC und Volumina der grauen Substanz im somatotopen Repräsentationsbereich klinisch nicht von dystoner Symptomatik betroffener Körperregionen im medialen primären somatosensorischen Kortex ergaben dagegen keine signifikanten Auffälligkeiten.

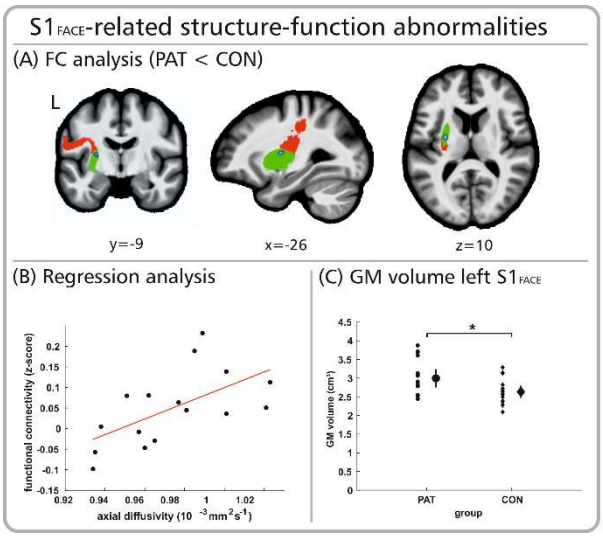

Abbildung 8. Signifikante Veränderungen von Struktur und Funktion der Projektion zwischen S1GESICHT und Putamen bei ED.

(A) Reduzierte Ruhezustands-FC (in Blau) im Putamen (grün hervorgehoben) in Ansatzdystoniepatienten verglichen mit gesunden Kontrollen, bei (B) positiver Assoziation mit der im Gruppenvergleich reduzierten axialen Diffusivität in der entsprechenden strukturellen Trajektorie. (C) Begleitende Unterschiede im GM-Volumen in S1GESICHT. Raumkoordinaten beschreiben die Schichtposition im MNI-Referenzraum. Fehlerbalken zeigen den doppelten Standardfehler des Mittelwerts.

Abkürzungen: CON, gesunde Kontrollen; FC, funktionelle Konnektivität (functional connectivity); GM, graue Substanz (grey matter); L, linke Hemisphäre; PAT, Patienten mit Ansatzdystonie; S1FACE (GESICHT), Gesichtsrepräsentation im primären somatosensorischen Kortex.

2.3. Der Thalamus als Knotenpunkt - strukturelle Konnektivitätsprofile bei Blepharospasmus/Meige-Syndrom

Mantel, T., Jochim, A., Meindl, T., Deppe, J., Zimmer, C., Li, Y., Haslinger, B. (2022). Thalamic structural connectivity profiles in blepharospam/Meige's syndrome. *NeuroImage. Clinical*, *34*, 103013. https://doi.org/10.1016/j.nicl.2022.103013

In den bisher vorgestellten Arbeiten hatten wir uns mit der multimodalen Beschreibung von sensomotorischen zerebralen Netzwerkveränderungen bei aufgabenspezifischen Dystonien beschäftigt.

Insbesondere strukturelle Netzwerkveränderungen waren jedoch auch bei nicht aufgabenspezifischen Dystonien bisher unzureichend charakterisiert. In dieser abschließend präsentierten Arbeit hatten wir uns daher zum Ziel gesetzt, strukturelle Netzwerkveränderungen bei einer der häufigsten dieser Dystonieformen – dem Blepharospasmus – näher zu beschreiben. Die für die Erkrankung charakteristische dystone Symptomatik mit ungewolltem Blinzeln und Lidschlussspasmen schränkt den Alltag stark ein (in schweren Fällen bis hin zur funktionellen Blindheit) [81], und breitet sich in der Hälfte der Fälle im Krankheitsverslauf auch auf die untere Kopf- bzw. Halsregion aus (sog. Meige-Syndrom) [82,83]. Im Fokus unseres Interesses stand dabei die Evaluation einer möglichen Rolle des Thalamus im Rahmen des Netzwerkkonzeptes, welche zu diesem Zeitpunkt kaum näher von struktureller Seite beleuchtet worden war. Der Thalamus verlinkt als wichtiger zerebraler neuroanatomischer Knotenpunkt jene Regelkreise zwischen Kleinhirn, Basalganglien, Hirnstammkernen und Kortex, für die eine zentrale Rolle in der Pathophysiologie der AOFD angenommen wird [8,84] und welche bei Blepharospasmus bildgebend abnorme funktionelle Konnektivitätsprofile zeigen [85]. In publizierten Fällen läsionsassoziierter (erworbener) Blepharospasmus-Manifestationen stellt der Thalamus zudem einen der am häufigsten berichteten symptomatisch gewerteten Läsionsorte dar [85,86]. Wir gingen daher der Frage nach, ob sich bei Blepharospasmus Veränderungen thalamischer Konnektivitätsprofile finden, und ob solche Auffälligkeiten von Zeichen veränderter Integrität der über den Thalamus verlinkten aufsteigenden Faserbahnen von Basalganglien und Kleinhirn begleitet werden.

Methoden und Ergebnisse

Hierzu wurden 17 Patienten mit Blepharospasmus (fünf davon mit milder dystoner Beteiligung des unteren Gesichts im Sinne eines Meige-Syndroms) und 17 gesunde Probanden mittels (T1-gewichteter) sMRT, und herzschlaggetriggerter Diffusions-MRT mit insgesamt 64 Gradientenrichtungen untersucht. Für jeden Teilnehmer wurde mittels probabilistischer Traktographie ein strukturelles Konnektivitätsprofil von sechs, auf Basis der thalamischen Verbindungsanatomie definierten, Hirnregionen und dem Thalamus erstellt[87-89]: dem (1) Motorisch/Prämotorischen Kortex, (2) (Somato)Sensorischen Kortex, (3) Posterior-Parietalen Kortex, (4) Okzipitalen Kortex, (5) Temporalen Kortex, sowie dem (6) Präfrontalen Kortex (s. Abbildung 9). Hierfür wurde zunächst die

graue Substanz der mit den vorverarbeiteten (s. Kapitel 2.2.2.) Diffusionsaufnahmen co-registrierten anatomischen Bildgebung segmentiert, und dann anhand eines konnektivitätsbasiert-generiertem Hirnatlasses (sog. „Brainnetome"-Atlas [90]) den oben genannten sechs kortikalen Regionen zugeordnet. Im Anschluss wurde mittels eines anatomisch geführten probabilistischen Traktographieansatzes, ausgehend der Grenzfläche mit der weißen Substanz, ein voxelbasiertes normalisiertes wahrscheinlichkeitsbasiertes (probabilistisches) intrathalamisches Konnektivitätsprofil für die jeweiligen Hirnregionen berechnet (s. Abbildung 9). Dabei repräsentiert jeder Voxel die relative Wahrscheinlichkeit einer vorliegenden Verbindung zwischen der jeweiligen Hirnregion und Thalamus getrennt für jede Hemisphäre.

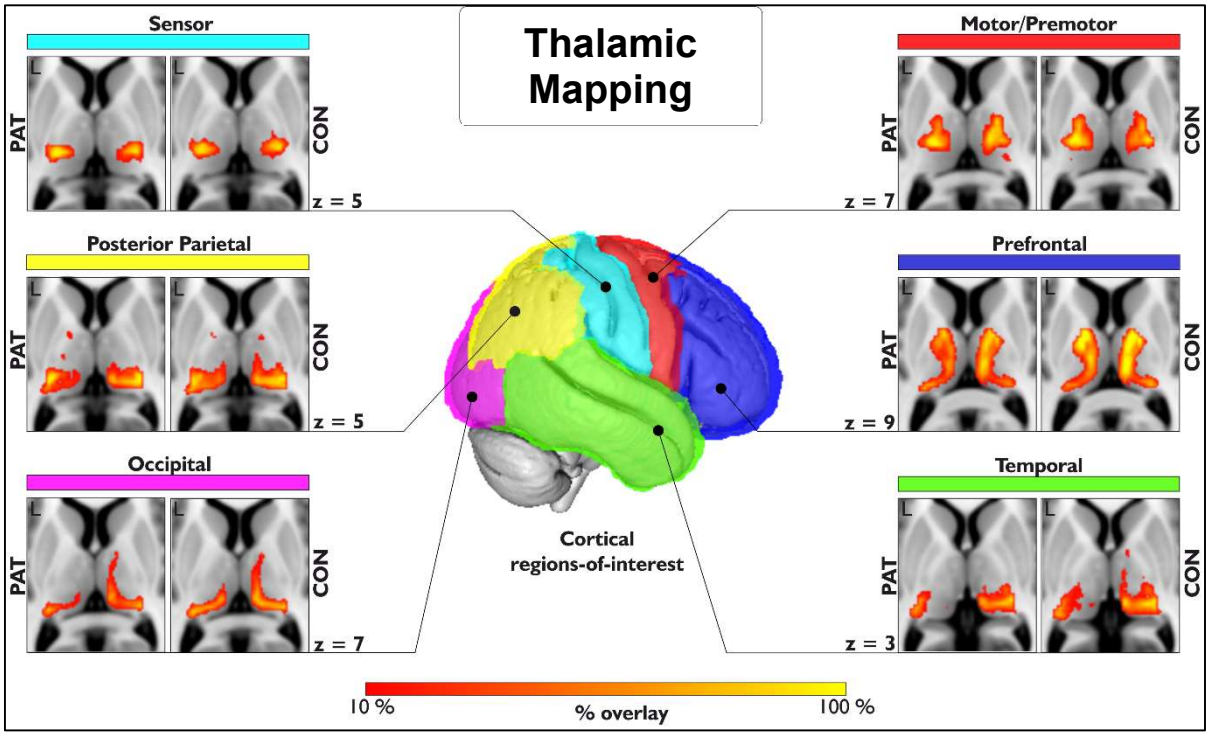

Abbildung 9. Thalamische strukturelle Konnektivitätskarten bei Patienten mit Blepharospasmus/Meige-Syndrom und Kontrollen.

Farbskala: Überlagerung (in Prozent) der strukturellen Konnektivitätsverteilungen der Teilnehmer innerhalb jeder Gruppe bei einer bei eine mittleren relativen Verbindungswahrscheinlichkeitsschwelle von 10% für die sechs untersuchten kortikalen Regionen. Raumkoordinaten beschreiben die Schichtposition im MNI-Referenzraum.

Abkürzungen: CON, gesunde Kontrollen; L, linke Hemisphäre; PAT, Patienten mit Blepharospasmus/Meige-Syndrom; R, rechte Hemisphäre.

Anschließend wurden Zwischengruppenunterschiede des relativen thalamischen Konnektivitätsausmaßes in für multiple Analysen korrigierten voxelweisen nichtparametrischen Permutationstests nach der Methode von Freedman-Lane untersucht [79,80,91]. Diese Analyse der relativen

strukturellen Konnektivitätsstärken ergab eine signifikant reduzierte links okzipital-thalamische strukturelle Konnektivität, sowie reduzierte rechts motorisch/prämotorisch-thalamische strukturelle Konnektivität (s. Abbildung 10). In Spearman-Korrelationsanalysen mit klinischen Parametern ergab sich hierbei zudem eine signifikante inverse Beziehung zwischen der krankheitsbedingten motorischen Beeinträchtigung (gemäß Jankovic Rating Scale [92]) und niedrigerer okzipitaler thalamischer struktureller Konnektivität in der Gruppe der Patienten.

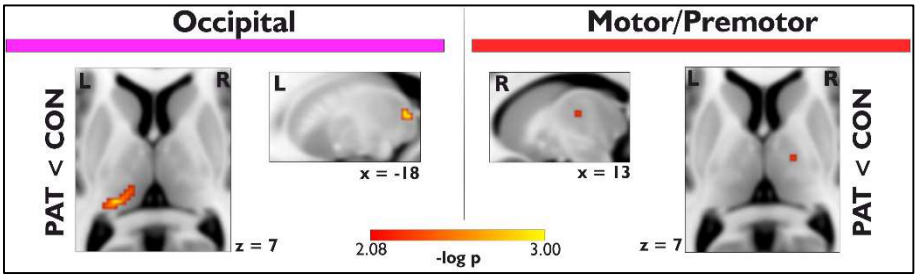

Abbildung 10. Zwischengruppenunterschiede der strukturellen Konnektivität.

Signifikante Reduktionen der strukturellen Konnektivität in den motorisch/ prämotorischen und okzipitalen thalamischen Konnektivitätsverteilungen bei Patienten mit Blepharospasmus/ Meige-Syndrom und Kontrollen. Raumkoordinaten beschreiben die Schichtposition im MNI-Referenzraum.

Abkürzungen: CON, gesunde Kontrollen; L, linke Hemisphäre; PAT, Patienten mit Blepharospasmus/Meige-Syndrom; R, rechte Hemisphäre.

Kontrollanalysen des Konnektivitätsprofils signifikanter Voxel mit dem zerebralen Kortex über alle Studienteilnehmer hinweg ergaben, dass die Voxel des okzipitalen Clusters insbesondere mit dem Cuneus, dem lateralen, und dem superioren okzipitalen Kortex sowie dem parieto-okzipitalen Sulcus verbunden waren. Die Voxel des motorischen/prämotorischen Clusters zeigten insbesondere strukturelle Konnektivität mit dem Cingulum, dem prämotorischen, und dem supplementär-motorischen Kortex.

Neben quantitativen Konnektivitätsunterschieden wurde die Topographie des thalamischen Konnektivitätsprofils der einzelnen Kortizes näher betrachtet. Hierzu wurde die Schwerpunktkoordinate der einzelnen dreidimensionalen voxelweisen strukturellen Konnektivitätsprofile als robuster Surrogatparameter berechnet und in zweifaktoriellen, für multiple untersuchte SC-Profile korrigierten, Varianzanalysen (Faktoren: Gruppe, Koordinate) evaluiert. Diese Analyse des topographischen Profils

zeigte eine signifikante medio-superiore Schwerpunktverschiebung des links okzipital-thalamischen Konnektivitätsmusters (s. Abbildung 11). Eine Kontrollanalyse der mittleren okzipitalen thalamischen strukturellen Konnektivität schloss diesen Shift als Treiber der fokalen thalamischen Konnektivitäts-veränderungen in der voxelbasierten Analyse aus.

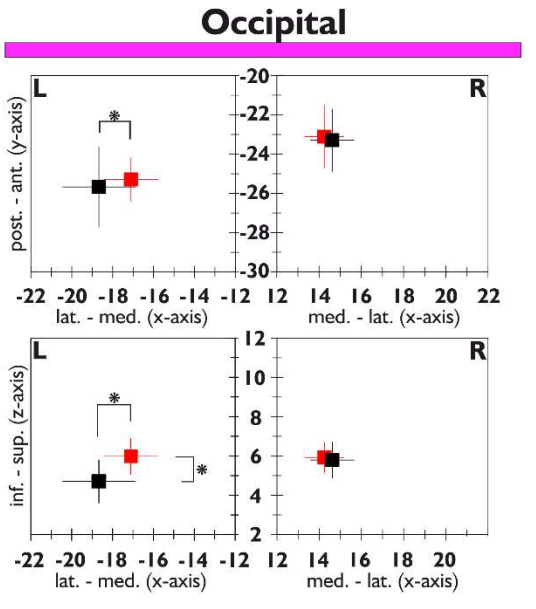

Abbildung 11. Topographischer Shift der okzipital-thalamischen Verteilung der strukturellen Konnektivität mit dem Schwerpunkt als Surrogatmarker.

Patienten sind in Rot, Kontrollen sind in Schwarz markiert. Raumkoordinaten beschreiben die Schichtposition im MNI-Referenzraum.

Abkürzungen: L, linke Hemisphäre; R, rechte Hemisphäre.

Zur näheren Einordnung der Rolle striato- und zerebellokortikaler Regelkreise in Bezug auf die thalamischen Konnektivitätsauffälligkeiten erfolgte sekundär eine Evaluation des aufsteigenden Segments dieser Regelschleifen mit jenen Hirnarealen, die in der oben beschriebenen Primäranalyse Auffälligkeiten thalamischer struktureller Konnektivität gezeigt hatten. Nach Rekonstruktion der pallido- bzw. dentato-thalamo-kortikalen Trajektorie (PTCT bzw. DTCT) in einem analog zum Vorgehen in Kapitel 2.2.2. angewandten, anatomisch geführten Traktographieansatz wurde die fraktionelle Anisotropie als reliables Maß für die Integrität der weißen Substanz eines repräsentativen präthalamischen Segments näher betrachtet. In dieser explorativen Zwischengruppenanalyse (Wilcoxon-Mann-Whitney-Test) zeigte sich eine signifikant reduzierte fraktionelle Anisotropie in den präthalamischen Anteilen der denato-thalamo-kortikalen Trajektorie zum rechtshemisphärischen motorisch/prämotorischen und linkshemisphärischen okzipitalen Kortex, nicht aber im präthalamischen Segment der pallido-thalamo-kortikalen Trajektorie (s. Abbildung 12).

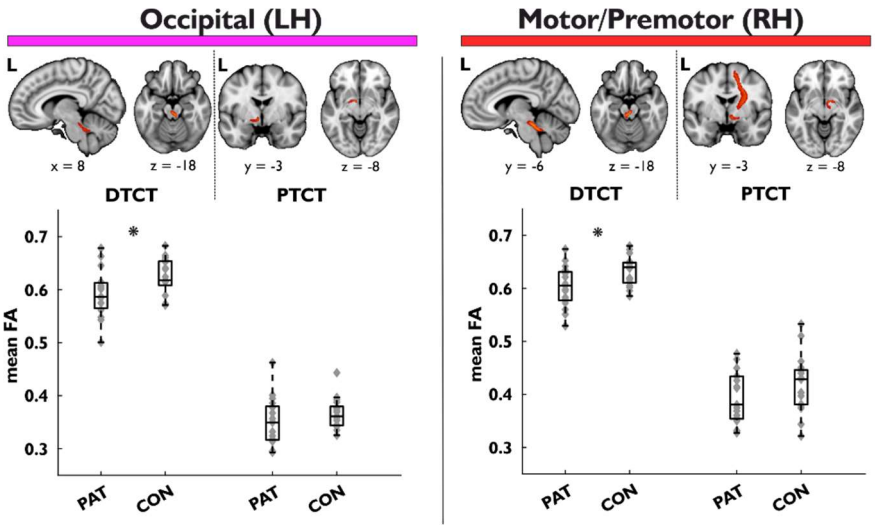

Abbildung 12. Zwischengruppenunterschiede der Integrität der weißen Substanz in präthalamischen Abschnitten des DTCT bei Blepharospasmus/Meige-Syndrom.

Dargestellt sind signifikante Veränderungen der FA im Vergleich zu Kontrollen in den zum rechten motorisch/prämotorischen bzw. linkshemisphärischen okzipitalen Kortex verlaufenden, rekonstruierten Anteilen des DTCT. Raumkoordinaten beschreiben die Schichtposition im MNI-Referenzraum.

Abkürzungen: CON, gesunde Kontrollen; DTCT, dentato-thalamo-cortikale Trajektorie; FA, fraktionelle Anisotropie; LH, linke Hemisphäre; PAT, Patienten mit Blepharospasmus/Meige-Syndrom; PTCT, pallido-thalamo-corticale Trajektorie; RH, rechte Hemisphäre.

3. Diskussion

Fokale Dystonien werden heute als sensomotorische Netzwerkerkrankungen konzeptualisiert. Frühe bildgebende Arbeiten konnten zur Bildung dieser Hypothese durch Beschreibung der Topographie von Veränderungen zerebraler Aktivität und Struktur der grauen Substanz wesentlich beitragen [8,9]; diese waren regelmäßig nicht nur in den Basalganglien, sondern auch im Bereich des Kleinhirns, des Thalamus, sensomotorischer Kortizes und im Hirnstamm zu beobachten [8,9,14,15]. Für die weitergehende Charakterisierung funktioneller Veränderungen innerhalb des Konzepts eines abnormen zerebralen sensomotorischen Netzwerks bei Dystonien waren die initial durchgeführten aufgaben- bzw. ereignisbezogenen fMRT-Untersuchungen durch ihre situations- bzw. kontextgebundene Interpretierbarkeit limitiert. So blieb unter anderem die Signifikanz der heterogenen Ausrichtung beobachteter funktioneller Aktivitätsänderungen mit teils vermehrter, teils verminderter sensomotorischer zerebraler Aktivität außerhalb technischer Aspekte (in Bezug auf experimentelles Setting oder Bildgebungsparameter) offen. Nachdem PET-bildgebende Untersuchungen im experimentellen Ruhezustand Veränderungen metabolischer Ruheaktivitätsmuster bei Trägern etablierter Dystonie-Genmutationen mit vom klinischen Manifestationsstatus und Phänotyp abhängigen Zügen nachweisen konnten [23,24], rückte daher auch bei AOFD zunehmend die funktionelle zerebrale Konnektivität im Ruhezustand mit dem Ziel der Identifikation grundlegenderer funktioneller Veränderungen in den Fokus. In ersten, zunächst bei Schreibkrampfpatienten durchgeführten, begrenzten Evaluationen konnten sensomotorische Veränderung der Ruhezustands-FC nachgewiesen werden [30,31,34], welche jedoch wie auch frühere aktivitätsbezogene Untersuchungen weiterhin ein heterogenes Veränderungsmuster aufwiesen. Unsere in einer großen Gruppe von Schreibkrampfpatienten durchgeführte breite Evaluation der sensomotorischen Ruhezustands-FC konnte multiple, und dabei für verschiedene untersuchte intrinsische Konnektivitätsnetzwerke differierende, Konnektivitätsveränderungen betont in prämotorischen und parietalen Kortizes im Ruhezustand aufzeigen, die – außerhalb methodisch-technischer Aspekte - ein mögliches Erklärungsmodell der variablen Beobachtungen u.a. in aufgabenbezogenen fMRT-Aktivierungsstudien bieten können. Beobachtete Konnektivitätsveränderungen innerhalb und zwischen Kleinhirn- und Basalganglien-zentrierten Netzwerken mit begleitenden strukturellen Veränderungen im Kleinhirn

stützen zudem die Annahme einer dysfunktionalen Interaktion dieser Strukturen bzw. der mit ihnen assoziierten Regelkreise als einen zentralen Aspekt der Netzwerkveränderungen bei AOFD. Über die Basalganglien als auch über das Kleinhirn verlaufende Regelkreise modulierenden in der Endstrecke die motorkortikale synaptische Plastizität und Erregbarkeit, deren Dysfunktion bei Dystonien als pathophysiologische Korrelate zu beobachten sind [93-98]. Eine Dysbalance in der Interaktion von Basalganglien und Kleinhirn wird daher als ein wesentlicher Faktor innerhalb der Netzwerkhypothese mit Blick auf die klinische Manifestation dystoner Symptomatik diskutiert. Der Charakter (kausale oder (dys)funktional kompensatorische Rolle einer, beider Strukturen oder ihrer Kommunikation) und die Ebene der gestörten Interaktion (subcortikale (disynaptisch), oder kortikale Ebene des sensomotorischen Systems) bleibt dabei aktuell offen [99-101]. Der deskriptive bzw. korrelative Charakter fMRT-basierter Evidenz lässt hierauf limitierend keine Rückschlüsse zu. Funktionelle Veränderungen in primären und/oder übergeordneten sensomotorischen Kortizes, wie sie in dieser und (in variierender Ausprägung) in früheren funktionellen MR- oder PET-bildgebenden-Studien bei (aufgabenspezifischen) AOFD zu beobachten waren, werden als Korrelate gestörter sensomotorischer Integrationsprozesse angesehen [9,14,15]. Im Rahmen eines solchen gestörten Prozesses wird eine Veränderung der zentralen somatosensorischen Reizverarbeitung als weiteres pathophysiologisches Charakteristikum fokaler Dystonien angenommen [6,7]; neben „sensorischen Tricks“ lässt sich bei Betroffenen auf Gruppenebene eine Veränderung somatosensorischer Reizdiskriminationsschwellen oder propriozeptiver afferenter Verarbeitung in der Körperperipherie als mögliches Korrelat beobachten [6,102]. Für die laryngeale Dystonie konnten wir hier eine Evidenzlücke durch Nachweis von Korrelaten einer gestörten zentralen somatosensiblen Reizverarbeitung in primären und übergeordneten somatosensorischen Hirnarealen schließen, auch wenn hier limitierend nur nicht dystone Surrogatareale evaluiert werden konnten. Die Abwesenheit eines direkten räumlichen Überlappens von Veränderungen stimulationsinduzierter Aktivität mit jenen der Ruhezustands-FC in mit Somatosensorik bzw. Sensomotorik assoziierten intrinsischen Konnektivitätsnetzwerken unterstreicht dabei den Wert der Untersuchung im multimodalen bildgebenden Setting angesichts möglicher kontextbezogener Dynamik funktioneller Veränderungen. Die zudem beobachtete räumliche Konzentration diverser funktioneller Veränderungen (regionale und netzwerkbezogene Ruhezustands-FC, Aktivität unter somatosensibler Reizverarbeitung)

im temporoparietalen Assoziationskortex könnte hierbei auf eine gestörte multisensorische Integration hindeuten, für die sich auch bei anderen AOFDs klinische bzw. funktionell-bildgebende Hinweise ergeben [59,103-106]; dies weiter einzuordnen bleibt zukünftigen Untersuchungen vorbehalten.

Neben solch funktionellen Untersuchungen könnten strukturelle Analysen dazu beitragen, kontextinvariable Auffälligkeiten bei AOFD zu identifizieren. Primäre Untersuchungen struktureller Veränderungen der grauen Substanz in entsprechenden Bildgebungsstudien ergaben hierbei über die AOFD hinweg betrachtet Auffälligkeiten in vergleichbaren Hirnarealen wie in funktionellen MR- bzw. PET-bildgebenden Untersuchungen[14,15]. Meist wurden Zunahmen von Volumen bzw. Dichte in der grauen Substanz von Basalganglien, Kleinhirn, sensomotorischen Kortizes oder seltener des Thalamus, teils aber auch Reduktionen dieser Maße mit studienbezogener Variabilität beobachtet [8,14]. Abgeleitet von Untersuchungen motorischer Trainingsparadigmen gesunder Probanden und in Tiermodellen [107,108] werden solche Strukturveränderungen der grauen Substanz bei Dystonien als Korrelat dysplastischer Veränderungen interpretiert, auch wenn die mit solchen bildgebenden Veränderungen assoziierten Mechanismen auf Zellebene bislang nicht eindeutig geklärt sind [109-111]. Unter Berücksichtigung der prinzipiellen methodische Beschränkung von Neuroimaging-Ansätzen auf ihren deskriptiven Charakter liefern auch speziell bei Dystonien Assoziationsdaten mit Krankheitsdauer und -schweremaßen sowie (allerdings spärliche) longitudinale bildgebende Verlaufsdaten korrelative Evidenz für einen wahrscheinlich mindestens in Teilen kompensatorischen oder adaptiven Charakter solcher Veränderungen (u.a. auch im Basalganglienbereich) [112-115].

Angesichts der motorischen Trainingseinflüsse auf Veränderungen der grauen Substanz mit nachweisbaren Veränderungen auch im Gesunden stellen Musikerdystonien Modellpopulationen zur besseren relativen Einordnung solch plastischer Veränderungen dar [60]. Unsere detaillierte Untersuchung von Ansatzdystoniepatienten konnte in diesem Zusammenhang den Nachweis von Strukturveränderungen der grauen Substanz in den primär sensomotorischen Kortizes über Trainingseffekte hinaus erbringen. Diese zeigten dabei eine zu früher beschriebenen funktionellen Aktivierungsänderungen bei diesem Krankheitsbild kongruente Somatotopie [50,58,59]. Neben diesen

krankheitsformbezogenen Auffälligkeiten konnten wir mit konkordanten Ergebnissen parallel durchgeführter hypothesenfreier und eines metaanalysebasierter Verfahren Evidenz für die Eignung letzteren Ansatzes zur sensitiveren Identifizierung geteilter Veränderungsmuster bei diesen seltenen Erkrankungen mit oft kleinen Studienpopulationen sammeln. Erstmals gelang der Nachweis subkortikaler zerebraler Symmetrieveränderungen sowohl bei gesunden und erkrankten (Blech)Blasmusikern. Waren diese bei gesunden Musikern als mögliches Korrelat adaptiver Veränderungen infolge bilateralen Trainings auf den Thalamus begrenzt, erstreckten sie sich bei Erkrankten zusätzlich bis in den Basalganglienbereich. Eine Assoziation mit der Krankheitsdauer stützte hier die Möglichkeit dort ablaufender sekundärer (z.B. mal-/adaptiver) Prozesse nach Manifestation der Erkrankung bei aufgabenspezifischen AOFD [113].

Neben Veränderungen der grauen Substanz konnten wir über den Nachweis subtiler Zeichen abnormer Integrität der weißen Substanz in vermutlich zentralen Faserverbindungen eines abnormen sensomotorischen Netzwerkes bei der Ansatzdystonie die Charakterisierung struktureller Veränderungen bei dieser Dystonieform auf die weiße Substanz erweitern. Hierbei ließ sich erstmals die kombinierte strukturo-funktionellen Störung einer primär somatosensorischen kortiko-putaminalen Trajektorie als möglicher Hinweis auf eine Beeinträchtigung afferenten somatosensorischen Inputs zum Putamen beobachten. Weiterhin waren Auffälligkeiten im oberen Längsfaszikel nachweisbar, welches in Zusammenschau mit funktionellen Bildgebungsdaten [31,116-118] bei anderen aufgabenspezifischen Dystonien ein Korrelat von Veränderungen der Moderationsprozesse übergeordneter sensomotorischer (prämotorisch-parietaler) Kortizes darstellen könnte. Insgesamt betonen diese Ergebnisse eine mögliche Schlüsselrolle dysfunktionaler sensorischer Informationsverarbeitung, fielen allerdings nur subtil aus, was limitierend methodisch-technischen Aspekten in Bezug auf Gruppengröße oder Analyseansatz angesichts der spezialisierten aufgabenabhängigen Symptomatik geschuldet sein könnte. Auch andere idiopathische Dystonieformen waren in den letzten Jahren mit der zunehmenden Etablierung der Diffusionstensorbildgebung hinsichtlich Strukturveränderungen der weißen Substanz untersucht worden. Studien mit Anwendung aktueller robusterer traktbasierter Verfahren lagen aber bislang spärlich vor. In diesen konnten innerhalb der idiopathischen aufgabenspezifischen AOFD teilweise Veränderungen im Traktverlauf zwischen prä- bzw. primär sensomotorischen Arealen und

subkortikalen Strukturen bei Schreibkrampf [119,120], und Auffälligkeiten im wahrscheinlichen Verlaufsbereich auf- bzw. absteigender kortikaler, sowie zerebellärer Faserbahnen bei laryngealer Dystonie beobachtet werden [47,121]. Im Bereich der nicht aufgabenspezifischen Dystonien waren traktographisch bei zervikaler Dystonie Auffälligkeiten in thalamusbezogenen (kortikalen bzw. zerebellären) Projektionsbahnen gesehen worden [122-124], während bei Blepharospasmus bisher keine Auffälligkeiten klassischer Diffusionsmaße nachweisbar gewesen waren [125]. Hier konnten wir in unserem regelkreisfokussierten Analyseansatz des Thalamus eine strukturelle Dyskonnektivität thalamo-kortikaler visuo-motorischer Leitungssegmente nachweisen, und dabei begleitend erstmals Hinweise auf topographische Konnektivitätsänderungen in sensorischen Hirnarealen außerhalb der somatosensiblen Domäne aufzeigen. Dies stellt eine mögliche Rolle der thalamo-kortikalen Endstrecke heraus, die Teil verschiedener potentiell zentraler Regelkreise im Rahmen der Netzwerkhypothese einnimmt. Veränderungen der funktionellen Konnektivitätsprofile solcher Regelkreise konnten bereits gezeigt werden [103]. In diesem Zusammenhang lieferte diese Arbeit über den erstmaligen Nachweis von mikrostrukturellen Veränderungen der über den Ncl. dentatus vom Kleinhirn aufsteigenden, durch den thalamischen Netzwerkknoten verlaufenden zerebellären Bahnen Evidenz für einen Einfluss zerebellärer Regelkreise bei dieser AOFD.

Unsere aktuellen und die bisher erfolgten Untersuchungen zeigen auch, dass - neben dem Verständnis der funktionellen Abläufe - insbesondere in der Charakterisierung struktureller Konnektivitäts- bzw. Netzwerkauffälligkeiten noch relevante Wissenslücken bei den fokalen Dystonieformen bestehen, die in zukünftigen Forschungsarbeiten gefüllt werden müssen. Die kontinuierlichen technischen Fortschritte in diesem Bereich bieten dabei Potential zur Überwindung bisheriger analytischer Limitationen struktureller Bildgebungsansätze [126,127], wenn auch prävalenzbedingt meist geringen Kollektivgrößen sowie die Heterogenität von Bildgebungssequenzen auch in der Zukunft Herausforderungen darstellen werden.

4. Zusammenfassung und Ausblick

Zusammenfassend konnten wir in unseren Untersuchungen zum einen das Wissen zu Aspekten funktioneller sensomotorischer Veränderungen bei Formen der aufgabenspezifischen fokalen Dystonie erweitern. Weiterhin gelang es erstmals, strukturelle zerebrale Veränderungen bei Ansatzdystonie zu charakterisieren und die Rolle des Thalamus als möglichen Knotenpunkt im Rahmen der Hypothese eines dysfunktionalen zerebralen sensomotorischen Netzwerkes bei Blepharospasmus strukturell näher zu beschreiben. Insgesamt liefern diese Daten wichtige Ansatzpunkte für weitere Forschungsarbeiten zu Netzwerkveränderungen bei Dystonien, deren besseres Verständnis sowohl für die Entwicklung diagnostischer Tools für die bisher lediglich klinisch basierte Diagnosestellung, als auch für die Entwicklung optimierter therapeutischer Ansätze in der Zukunft essentiell sein könnte.

5. Referenzen

1. Albanese A, Bhatia K, Bressman SB, et al. Phenomenology and classification of dystonia: a consensus update. *Mov Disord*. Jun 15 2013;28(7):863-73. doi:10.1002/mds.25475
2. Fahn S. The varied clinical expressions of dystonia. *Neurol Clin*. Aug 1984;2(3):541-54.
3. Fahn S. Concept and classification of dystonia. *Adv Neurol*. 1988;50:1-8.
4. Steeves TD, Day L, Dykeman J, Jette N, Pringsheim T. The prevalence of primary dystonia: a systematic review and meta-analysis. *Mov Disord*. Dec 2012;27(14):1789-96. doi:10.1002/mds.25244
5. Defazio G, Abbruzzese G, Livrea P, Berardelli A. Epidemiology of primary dystonia. *Lancet Neurol*. Nov 2004;3(11):673-8. doi:10.1016/S1474-4422(04)00907-X
6. Conte A, Defazio G, Hallett M, Fabbrini G, Berardelli A. The role of sensory information in the pathophysiology of focal dystonias. *Nat Rev Neurol*. Apr 2019;15(4):224-233. doi:10.1038/s41582-019-0137-9
7. Quartarone A, Hallett M. Emerging concepts in the physiological basis of dystonia. *Mov Disord*. Jun 15 2013;28(7):958-67. doi:10.1002/mds.25532
8. Jinnah HA, Neychev V, Hess EJ. The Anatomical Basis for Dystonia: The Motor Network Model. *Tremor Other Hyperkinet Mov (N Y)*. 2017;7:506. doi:10.7916/D8V69X3S
9. Neychev VK, Gross RE, Lehericy S, Hess EJ, Jinnah HA. The functional neuroanatomy of dystonia. *Neurobiol Dis*. May 2011;42(2):185-201. doi:10.1016/j.nbd.2011.01.026
10. Jinnah HA, Berardelli A, Comella C, et al. The focal dystonias: current views and challenges for future research. *Mov Disord*. Jun 15 2013;28(7):926-43. doi:10.1002/mds.25567
11. Paudel R, Hardy J, Revesz T, Holton JL, Houlden H. Review: genetics and neuropathology of primary pure dystonia. *Neuropathol Appl Neurobiol*. Oct 2012;38(6):520-34. doi:10.1111/j.1365-2990.2012.01298.x
12. Sharma N. Neuropathology of Dystonia. *Tremor Other Hyperkinet Mov (N Y)*. 2019;9:569. doi:10.7916/d8-j6sx-b156

13. Asanuma K, Carbon-Correll M, Eidelberg D. Neuroimaging in human dystonia. *J Med Invest*. Nov 2005;52 Suppl:272-9. doi:10.2152/jmi.52.272

14. Lehericy S, Tijssen MA, Vidailhet M, Kaji R, Meunier S. The anatomical basis of dystonia: current view using neuroimaging. *Mov Disord*. Jun 15 2013;28(7):944-57. doi:10.1002/mds.25527

15. Zoons E, Booij J, Nederveen AJ, Dijk JM, Tijssen MA. Structural, functional and molecular imaging of the brain in primary focal dystonia--a review. *Neuroimage*. Jun 1 2011;56(3):1011-20. doi:10.1016/j.neuroimage.2011.02.045

16. Lindquist MA. The Statistical Analysis of fMRI Data. *Statistical Science*. 2008;23(4):439-464, 26.

17. Lee MH, Smyser CD, Shimony JS. Resting-state fMRI: a review of methods and clinical applications. *AJNR American journal of neuroradiology*. Oct 2013;34(10):1866-72. doi:10.3174/ajnr.A3263

18. Fox MD, Raichle ME. Spontaneous fluctuations in brain activity observed with functional magnetic resonance imaging. Research Support, N.I.H., Extramural Review. *Nat Rev Neurosci*. Sep 2007;8(9):700-11. doi:10.1038/nrn2201

19. Ashburner J, Friston KJ. Voxel-based morphometry--the methods. *Neuroimage*. Jun 2000;11(6 Pt 1):805-21. doi:10.1006/nimg.2000.0582

20. Mechelli A, Price C, Friston K, Ashburner J. Voxel-Based Morphometry of the Human Brain: Methods and Applications. *Current Medical Imaging Reviews - CURR MED IMAGING REV*. 06/01 2005;1doi:10.2174/1573405054038726

21. Le Bihan D, Mangin JF, Poupon C, et al. Diffusion tensor imaging: concepts and applications. *J Magn Reson Imaging*. Apr 2001;13(4):534-46. doi:10.1002/jmri.1076

22. Jones DK, Leemans A. Diffusion tensor imaging. *Methods Mol Biol*. 2011;711:127-44. doi:10.1007/978-1-61737-992-5_6

23. Niethammer M, Carbon M, Argyelan M, Eidelberg D. Hereditary dystonia as a neurodevelopmental circuit disorder: Evidence from neuroimaging. *Neurobiol Dis*. May 2011;42(2):202-9. doi:10.1016/j.nbd.2010.10.010

24. Carbon M, Eidelberg D. Abnormal structure-function relationships in hereditary dystonia. *Neuroscience*. Nov 24 2009;164(1):220-9. doi:10.1016/j.neuroscience.2008.12.041

25. Biswal BB, Van Kylen J, Hyde JS. Simultaneous assessment of flow and BOLD signals in resting-state functional connectivity maps. Research Support, Non-U.S. Gov't Research Support, U.S. Gov't, P.H.S. *NMR Biomed*. Jun-Aug 1997;10(4-5):165-70.

26. Cordes D, Haughton VM, Arfanakis K, et al. Frequencies contributing to functional connectivity in the cerebral cortex in "resting-state" data. *AJNR American journal of neuroradiology*. Aug 2001;22(7):1326-33.

27. Cole MW, Ito T, Bassett DS, Schultz DH. Activity flow over resting-state networks shapes cognitive task activations. *Nat Neurosci*. Dec 2016;19(12):1718-1726. doi:10.1038/nn.4406

28. Tavor I, Parker Jones O, Mars RB, Smith SM, Behrens TE, Jbabdi S. Task-free MRI predicts individual differences in brain activity during task performance. *Science*. Apr 8 2016;352(6282):216-20. doi:10.1126/science.aad8127

29. Cole MW, Bassett DS, Power JD, Braver TS, Petersen SE. Intrinsic and task-evoked network architectures of the human brain. *Neuron*. Jul 2 2014;83(1):238-51. doi:10.1016/j.neuron.2014.05.014

30. Mohammadi B, Kollewe K, Samii A, Beckmann CF, Dengler R, Munte TF. Changes in resting-state brain networks in writer's cramp. Research Support, Non-U.S. Gov't. *Hum Brain Mapp*. Apr 2012;33(4):840-8. doi:10.1002/hbm.21250

31. Delnooz CC, Helmich RC, Toni I, van de Warrenburg BP. Reduced parietal connectivity with a premotor writing area in writer's cramp. *Mov Disord*. Sep 15 2012;27(11):1425-31. doi:10.1002/mds.25029

32. Sheehy MP, Marsden CD. Writers' cramp-a focal dystonia. *Brain*. Sep 1982;105 (Pt 3):461-80.

33. Hallett M. Pathophysiology of writer's cramp. Review. *Human movement science*. Oct 2006;25(4-5):454-63. doi:10.1016/j.humov.2006.05.004

34. Dresel C, Li Y, Wilzeck V, Castrop F, Zimmer C, Haslinger B. Multiple changes of functional connectivity between sensorimotor areas in focal hand dystonia. Research

Support, Non-U.S. Gov't. *J Neurol Neurosurg Psychiatry*. Nov 2014;85(11):1245-52. doi:10.1136/jnnp-2013-307127

35. Allen EA, Erhardt EB, Damaraju E, et al. A baseline for the multivariate comparison of resting-state networks. *Frontiers in systems neuroscience*. 2011;5:2. doi:10.3389/fnsys.2011.00002

36. Smith SM, Fox PT, Miller KL, et al. Correspondence of the brain's functional architecture during activation and rest. Research Support, N.I.H., Extramural Research Support, Non-U.S. Gov't. *Proc Natl Acad Sci U S A*. Aug 04 2009;106(31):13040-5. doi:10.1073/pnas.0905267106

37. Beckmann CF, DeLuca M, Devlin JT, Smith SM. Investigations into resting-state connectivity using independent component analysis. Comparative Study Research Support, Non-U.S. Gov't. *Philosophical transactions of the Royal Society of London Series B, Biological sciences*. May 29 2005;360(1457):1001-13. doi:10.1098/rstb.2005.1634

38. Laird AR, Fox PM, Eickhoff SB, et al. Behavioral interpretations of intrinsic connectivity networks. Research Support, N.I.H., Extramural Research Support, Non-U.S. Gov't. *Journal of cognitive neuroscience*. Dec 2011;23(12):4022-37. doi:10.1162/jocn_a_00077

39. Wissel J, Kabus C, Wenzel R, et al. Botulinum toxin in writer's cramp: objective response evaluation in 31 patients. *J Neurol Neurosurg Psychiatry*. Aug 1996;61(2):172-5. doi:10.1136/jnnp.61.2.172

40. Ludlow CL. Spasmodic dysphonia: a laryngeal control disorder specific to speech. *J Neurosci*. Jan 19 2011;31(3):793-7. doi:10.1523/JNEUROSCI.2758-10.2011

41. Brown S, Laird AR, Pfordresher PQ, Thelen SM, Turkeltaub P, Liotti M. The somatotopy of speech: phonation and articulation in the human motor cortex. *Brain Cogn*. Jun 2009;70(1):31-41. doi:10.1016/j.bandc.2008.12.006

42. Simonyan K, Ludlow CL. Abnormal activation of the primary somatosensory cortex in spasmodic dysphonia: an fMRI study. *Cereb Cortex*. Nov 2010;20(11):2749-59. doi:10.1093/cercor/bhq023

43. Ali SO, Thomassen M, Schulz GM, et al. Alterations in CNS activity induced by botulinum toxin treatment in spasmodic dysphonia: an H215O PET study. *J Speech Lang Hear Res*. Oct 2006;49(5):1127-46. doi:10.1044/1092-4388(2006/081)

44. Haslinger B, Erhard P, Dresel C, Castrop F, Roettinger M, Ceballos-Baumann AO. "Silent event-related" fMRI reveals reduced sensorimotor activation in laryngeal dystonia. *Neurology*. Nov 22 2005;65(10):1562-9. doi:10.1212/01.wnl.0000184478.59063.db

45. Simonyan K, Ludlow CL. Abnormal structure-function relationship in spasmodic dysphonia. *Cereb Cortex*. Feb 2012;22(2):417-25. doi:10.1093/cercor/bhr120

46. Battistella G, Fuertinger S, Fleysher L, Ozelius LJ, Simonyan K. Cortical sensorimotor alterations classify clinical phenotype and putative genotype of spasmodic dysphonia. *Eur J Neurol*. Oct 2016;23(10):1517-27. doi:10.1111/ene.13067

47. Simonyan K, Tovar-Moll F, Ostuni J, et al. Focal white matter changes in spasmodic dysphonia: a combined diffusion tensor imaging and neuropathological study. *Brain*. Feb 2008;131(Pt 2):447-59. doi:10.1093/brain/awm303

48. Miyaji H, Hironaga N, Umezaki T, et al. Neuromagnetic detection of the laryngeal area: Sensory-evoked fields to air-puff stimulation. *Neuroimage*. Mar 2014;88:162-9. doi:10.1016/j.neuroimage.2013.11.008

49. Weise D, Weise CM, Naumann M. Central Effects of Botulinum Neurotoxin-Evidence from Human Studies. *Toxins (Basel)*. Jan 6 2019;11(1)doi:10.3390/toxins11010021

50. Mantel T, Dresel C, Altenmuller E, Zimmer C, Noe J, Haslinger B. Activity and topographic changes in the somatosensory system in embouchure dystonia. *Mov Disord*. Nov 2016;31(11):1640-1648. doi:10.1002/mds.26664

51. Dresel C, Bayer F, Castrop F, Rimpau C, Zimmer C, Haslinger B. Botulinum toxin modulates basal ganglia but not deficient somatosensory activation in orofacial dystonia. *Mov Disord*. Jul 2011;26(8):1496-502. doi:10.1002/mds.23497

52. Dresel C, Parzinger A, Rimpau C, Zimmer C, Ceballos-Baumann AO, Haslinger B. A new device for tactile stimulation during fMRI. *Neuroimage*. Feb 1 2008;39(3):1094-103. doi:10.1016/j.neuroimage.2007.09.033

53. Meunier S, Garnero L, Ducorps A, et al. Human brain mapping in dystonia reveals both endophenotypic traits and adaptive reorganization. Research Support, Non-U.S. Gov't. *Ann Neurol*. Oct 2001;50(4):521-7.

54. Jacobson BH, Johnson A, Grywalski C, et al. The Voice Handicap Index (VHI). *American Journal of Speech-Language Pathology*. 1997;6(3):66-70. doi:doi:10.1044/1058-0360.0603.66

55. Altenmüller E, Lee A, Jabusch HC. Musikerdystonien. Musicians' dystonia. *Nervenheilkunde*. // 04.10.2018 2018;37(10):667-678.

56. Frucht SJ, Fahn S, Greene PE, et al. The natural history of embouchure dystonia. Case Reports Research Support, Non-U.S. Gov't. *Mov Disord*. Sep 2001;16(5):899-906.

57. Frucht SJ. Embouchure dystonia--Portrait of a task-specific cranial dystonia. *Mov Disord*. Sep 15 2009;24(12):1752-62. doi:10.1002/mds.22550

58. Haslinger B, Altenmuller E, Castrop F, Zimmer C, Dresel C. Sensorimotor overactivity as a pathophysiologic trait of embouchure dystonia. *Neurology*. Jun 1 2010;74(22):1790-7. doi:10.1212/WNL.0b013e3181e0f784

59. Haslinger B, Noe J, Altenmuller E, et al. Changes in resting-state connectivity in musicians with embouchure dystonia. *Mov Disord*. Mar 2017;32(3):450-458. doi:10.1002/mds.26893

60. Schlaug G. Musicians and music making as a model for the study of brain plasticity. Research Support, N.I.H., Extramural Review. *Progress in brain research*. 2015;217:37-55. doi:10.1016/bs.pbr.2014.11.020

61. Luders E, Gaser C, Jancke L, Schlaug G. A voxel-based approach to gray matter asymmetries. Research Support, Non-U.S. Gov't Research Support, U.S. Gov't, Non-P.H.S. *Neuroimage*. Jun 2004;22(2):656-64. doi:10.1016/j.neuroimage.2004.01.032

62. Herholz SC, Zatorre RJ. Musical training as a framework for brain plasticity: behavior, function, and structure. Research Support, Non-U.S. Gov't Review. *Neuron*. Nov 8 2012;76(3):486-502. doi:10.1016/j.neuron.2012.10.011

63. Kurth F, Gaser C, Luders E. A 12-step user guide for analyzing voxel-wise gray matter asymmetries in statistical parametric mapping (SPM). Research Support, Non-U.S. Gov't. *Nature protocols*. Feb 2015;10(2):293-304. doi:10.1038/nprot.2015.014

64. IXI Dataset. Biomedical Image Analysis Group. Accessed 01.02.2023, https://brain-development.org/ixi-dataset/

65. Lim VK, Bradshaw JL, Nicholls ME, Altenmuller E. Perceptual differences in sequential stimuli across patients with musician's and writer's cramp. *Mov Disord*. Nov 2003;18(11):1286-93. doi:10.1002/mds.10528

66. Rosenkranz K, Williamon A, Butler K, Cordivari C, Lees AJ, Rothwell JC. Pathophysiological differences between musician's dystonia and writer's cramp. *Brain*. Apr 2005;128(Pt 4):918-31. doi:10.1093/brain/awh402

67. Uehara K, Furuya S, Numazawa H, Kita K, Sakamoto T, Hanakawa T. Distinct roles of brain activity and somatotopic representation in pathophysiology of focal dystonia. *Hum Brain Mapp*. Apr 15 2019;40(6):1738-1749. doi:10.1002/hbm.24486

68. Granert O, Peller M, Jabusch HC, Altenmuller E, Siebner HR. Sensorimotor skills and focal dystonia are linked to putaminal grey-matter volume in pianists. *J Neurol Neurosurg Psychiatry*. Nov 2011;82(11):1225-31. doi:10.1136/jnnp.2011.245811

69. Kita K, Rokicki J, Furuya S, Sakamoto T, Hanakawa T. Resting-state basal ganglia network codes a motor musical skill and its disruption From dystonia. *Mov Disord*. Sep 2018;33(9):1472-1480. doi:10.1002/mds.27448

70. Mantel T, Altenmuller E, Li Y, et al. Abnormalities in grey matter structure in embouchure dystonia. *Parkinsonism Relat Disord*. Aug 2019;65:111-116. doi:10.1016/j.parkreldis.2019.05.008

71. Leemans A, Jones DK. The B-matrix must be rotated when correcting for subject motion in DTI data. *Magn Reson Med*. Jun 2009;61(6):1336-49. doi:10.1002/mrm.21890

72. Irfanoglu MO, Walker L, Sarlls J, Marenco S, Pierpaoli C. Effects of image distortions originating from susceptibility variations and concomitant fields on diffusion MRI

tractography results. *Neuroimage*. May 15 2012;61(1):275-88. doi:10.1016/j.neuroimage.2012.02.054

73. Schulz R, Koch P, Zimerman M, et al. Parietofrontal motor pathways and their association with motor function after stroke. *Brain*. Jul 2015;138(Pt 7):1949-60. doi:10.1093/brain/awv100

74. Bozkurt B, Yagmurlu K, Middlebrooks EH, et al. Fiber Connections of the Supplementary Motor Area Revisited: Methodology of Fiber Dissection, DTI, and Three Dimensional Documentation. *J Vis Exp*. May 23 2017;(123)doi:10.3791/55681

75. Makris N, Kennedy DN, McInerney S, et al. Segmentation of subcomponents within the superior longitudinal fascicle in humans: a quantitative, in vivo, DT-MRI study. *Cereb Cortex*. Jun 2005;15(6):854-69. doi:10.1093/cercor/bhh186

76. Kamali A, Flanders AE, Brody J, Hunter JV, Hasan KM. Tracing superior longitudinal fasciculus connectivity in the human brain using high resolution diffusion tensor tractography. *Brain Struct Funct*. Jan 2014;219(1):269-81. doi:10.1007/s00429-012-0498-y

77. Lehericy S, Ducros M, Van de Moortele PF, et al. Diffusion tensor fiber tracking shows distinct corticostriatal circuits in humans. *Ann Neurol*. Apr 2004;55(4):522-9. doi:10.1002/ana.20030

78. Tziortzi AC, Haber SN, Searle GE, et al. Connectivity-based functional analysis of dopamine release in the striatum using diffusion-weighted MRI and positron emission tomography. *Cereb Cortex*. May 2014;24(5):1165-77. doi:10.1093/cercor/bhs397

79. Winkler AM, Ridgway GR, Douaud G, Nichols TE, Smith SM. Faster permutation inference in brain imaging. *Neuroimage*. Nov 1 2016;141:502-516. doi:10.1016/j.neuroimage.2016.05.068

80. Winkler AM, Ridgway GR, Webster MA, Smith SM, Nichols TE. Permutation inference for the general linear model. *Neuroimage*. May 15 2014;92:381-97. doi:10.1016/j.neuroimage.2014.01.060

81. Valls-Sole J, Defazio G. Blepharospasm: Update on Epidemiology, Clinical Aspects, and Pathophysiology. *Front Neurol*. 2016;7:45. doi:10.3389/fneur.2016.00045

82. Berman BD, Groth CL, Sillau SH, et al. Risk of spread in adult-onset isolated focal dystonia: a prospective international cohort study. *J Neurol Neurosurg Psychiatry*. Mar 2020;91(3):314-320. doi:10.1136/jnnp-2019-321794

83. Pandey S, Sharma S. Meige's syndrome: History, epidemiology, clinical features, pathogenesis and treatment. *J Neurol Sci*. Jan 15 2017;372:162-170. doi:10.1016/j.jns.2016.11.053

84. Conte A, Defazio G, Mascia M, Belvisi D, Pantano P, Berardelli A. Advances in the pathophysiology of adult-onset focal dystonias: recent neurophysiological and neuroimaging evidence. *F1000Res*. 2020;9doi:10.12688/f1000research.21029.2

85. Mascia MM, Dagostino S, Defazio G. Does the network model fits neurophysiological abnormalities in blepharospasm? *Neurol Sci*. Aug 2020;41(8):2067-2079. doi:10.1007/s10072-020-04347-z

86. Khooshnoodi MA, Factor SA, Jinnah HA. Secondary blepharospasm associated with structural lesions of the brain. *J Neurol Sci*. Aug 15 2013;331(1-2):98-101. doi:10.1016/j.jns.2013.05.022

87. Jones EG. *The Thalamus*. University Press; 2007.

88. Zhang D, Snyder AZ, Shimony JS, Fox MD, Raichle ME. Noninvasive functional and structural connectivity mapping of the human thalamocortical system. *Cereb Cortex*. May 2010;20(5):1187-94. doi:10.1093/cercor/bhp182

89. Nair A, Treiber JM, Shukla DK, Shih P, Muller RA. Impaired thalamocortical connectivity in autism spectrum disorder: a study of functional and anatomical connectivity. *Brain*. Jun 2013;136(Pt 6):1942-55. doi:10.1093/brain/awt079

90. Fan L, Li H, Zhuo J, et al. The Human Brainnetome Atlas: A New Brain Atlas Based on Connectional Architecture. *Cereb Cortex*. Aug 2016;26(8):3508-26. doi:10.1093/cercor/bhw157

91. Smith SM, Nichols TE. Threshold-free cluster enhancement: addressing problems of smoothing, threshold dependence and localisation in cluster inference. *Neuroimage*. Jan 1 2009;44(1):83-98. doi:10.1016/j.neuroimage.2008.03.061

92. Jankovic J, Orman J. Botulinum A toxin for cranial-cervical dystonia: a double-blind, placebo-controlled study. *Neurology*. Apr 1987;37(4):616-23. doi:10.1212/wnl.37.4.616

93. Hamada M, Strigaro G, Murase N, et al. Cerebellar modulation of human associative plasticity. *J Physiol*. May 15 2012;590(10):2365-74. doi:10.1113/jphysiol.2012.230540

94. Koch G, Porcacchia P, Ponzo V, et al. Effects of two weeks of cerebellar theta burst stimulation in cervical dystonia patients. *Brain Stimul*. Jul-Aug 2014;7(4):564-72. doi:10.1016/j.brs.2014.05.002

95. Brighina F, Romano M, Giglia G, et al. Effects of cerebellar TMS on motor cortex of patients with focal dystonia: a preliminary report. *Experimental brain research*. Feb 2009;192(4):651-6. doi:10.1007/s00221-008-1572-9

96. Hallett M. Neurophysiology of dystonia: The role of inhibition. *Neurobiol Dis*. May 2011;42(2):177-84. doi:10.1016/j.nbd.2010.08.025

97. Silberstein P, Kuhn AA, Kupsch A, et al. Patterning of globus pallidus local field potentials differs between Parkinson's disease and dystonia. *Brain*. Dec 2003;126(Pt 12):2597-608. doi:10.1093/brain/awg267

98. Chen CC, Kuhn AA, Trottenberg T, Kupsch A, Schneider GH, Brown P. Neuronal activity in globus pallidus interna can be synchronized to local field potential activity over 3-12 Hz in patients with dystonia. *Exp Neurol*. Dec 2006;202(2):480-6. doi:10.1016/j.expneurol.2006.07.011

99. Sadnicka A, Hoffland BS, Bhatia KP, van de Warrenburg BP, Edwards MJ. The cerebellum in dystonia - help or hindrance? Research Support, Non-U.S. Gov't Review. *Clinical neurophysiology : official journal of the International Federation of Clinical Neurophysiology*. Jan 2012;123(1):65-70. doi:10.1016/j.clinph.2011.04.027

100. Shakkottai VG, Batla A, Bhatia K, et al. Current Opinions and Areas of Consensus on the Role of the Cerebellum in Dystonia. *Cerebellum*. Apr 2017;16(2):577-594. doi:10.1007/s12311-016-0825-6

101. Bostan AC, Dum RP, Strick PL. Cerebellar networks with the cerebral cortex and basal ganglia. *Trends Cogn Sci*. May 2013;17(5):241-54. doi:10.1016/j.tics.2013.03.003

102. Stamelou M, Edwards MJ, Hallett M, Bhatia KP. The non-motor syndrome of primary dystonia: clinical and pathophysiological implications. *Brain*. Jun 2012;135(Pt 6):1668-81. doi:10.1093/brain/awr224

103. Jochim A, Li Y, Gora-Stahlberg G, et al. Altered functional connectivity in blepharospasm/orofacial dystonia. *Brain Behav*. Jan 2018;8(1):e00894. doi:10.1002/brb3.894

104. Nguyen P, Kelly D, Glickman A, et al. Abnormal Neural Responses During Reflexive Blinking in Blepharospasm: An Event-Related Functional MRI Study. *Mov Disord*. Jul 2020;35(7):1173-1180. doi:10.1002/mds.28042

105. Putzki N, Stude P, Konczak J, Graf K, Diener HC, Maschke M. Kinesthesia is impaired in focal dystonia. *Mov Disord*. Jun 2006;21(6):754-60. doi:10.1002/mds.20799

106. Chillemi G, Calamuneri A, Morgante F, et al. Spatial and Temporal High Processing of Visual and Auditory Stimuli in Cervical Dystonia. *Front Neurol*. 2017;8:66. doi:10.3389/fneur.2017.00066

107. Draganski B, May A. Training-induced structural changes in the adult human brain. Review. *Behavioural brain research*. Sep 1 2008;192(1):137-42. doi:10.1016/j.bbr.2008.02.015

108. Draganski B, Gaser C, Busch V, Schuierer G, Bogdahn U, May A. Neuroplasticity: changes in grey matter induced by training. *Nature*. Jan 22 2004;427(6972):311-2. doi:10.1038/427311a

109. Keifer OP, Jr., Hurt RC, Gutman DA, Keilholz SD, Gourley SL, Ressler KJ. Voxel-based morphometry predicts shifts in dendritic spine density and morphology with auditory fear conditioning. *Nat Commun*. Jul 7 2015;6:7582. doi:10.1038/ncomms8582

110. Bandettini PA. What's new in neuroimaging methods? *Ann N Y Acad Sci*. Mar 2009;1156:260-93. doi:10.1111/j.1749-6632.2009.04420.x

111. Asan L, Falfan-Melgoza C, Beretta CA, et al. Cellular correlates of gray matter volume changes in magnetic resonance morphometry identified by two-photon microscopy. *Sci Rep*. Feb 19 2021;11(1):4234. doi:10.1038/s41598-021-83491-8

112. Draganski B, Schneider SA, Fiorio M, et al. Genotype-phenotype interactions in primary dystonias revealed by differential changes in brain structure. Research Support, Non-U.S. Gov't. *Neuroimage*. Oct 1 2009;47(4):1141-7. doi:10.1016/j.neuroimage.2009.03.057

113. Zeuner KE, Knutzen A, Granert O, et al. Increased volume and impaired function: the role of the basal ganglia in writer's cramp. Research Support, Non-U.S. Gov't. *Brain Behav*. Feb 2015;5(2):e00301. doi:10.1002/brb3.301

114. Martino D, Di Giorgio A, D'Ambrosio E, et al. Cortical gray matter changes in primary blepharospasm: a voxel-based morphometry study. *Mov Disord*. Aug 15 2011;26(10):1907-12. doi:10.1002/mds.23724

115. Pantano P, Totaro P, Fabbrini G, et al. A transverse and longitudinal MR imaging voxel-based morphometry study in patients with primary cervical dystonia. *AJNR American journal of neuroradiology*. Jan 2011;32(1):81-4. doi:10.3174/ajnr.A2242

116. Battistella G, Simonyan K. Top-down alteration of functional connectivity within the sensorimotor network in focal dystonia. *Neurology*. Apr 16 2019;92(16):e1843-e1851. doi:10.1212/WNL.0000000000007317

117. Merchant SHI, Frangos E, Parker J, et al. The role of the inferior parietal lobule in writer's cramp. *Brain*. Jun 1 2020;143(6):1766-1779. doi:10.1093/brain/awaa138

118. Mantel T, Meindl T, Li Y, et al. Network-specific resting-state connectivity changes in the premotor-parietal axis in writer's cramp. *Neuroimage Clin*. 2018;17:137-144. doi:10.1016/j.nicl.2017.10.001

119. Berndt M, Li Y, Gora-Stahlberg G, Jochim A, Haslinger B. Impaired white matter integrity between premotor cortex and basal ganglia in writer's cramp. *Brain Behav*. Oct 2018;8(10):e01111. doi:10.1002/brb3.1111

120. Delmaire C, Vidailhet M, Wassermann D, et al. Diffusion abnormalities in the primary sensorimotor pathways in writer's cramp. *Arch Neurol*. Apr 2009;66(4):502-8. doi:10.1001/archneurol.2009.8

121. Kostic VS, Agosta F, Sarro L, et al. Brain structural changes in spasmodic dysphonia: A multimodal magnetic resonance imaging study. *Parkinsonism Relat Disord*. Apr 2016;25:78-84. doi:10.1016/j.parkreldis.2016.02.003

122. Bonilha L, de Vries PM, Hurd MW, et al. Disrupted thalamic prefrontal pathways in patients with idiopathic dystonia. *Parkinsonism Relat Disord*. Jan 2009;15(1):64-7. doi:10.1016/j.parkreldis.2008.01.018

123. Bonilha L, de Vries PM, Vincent DJ, et al. Structural white matter abnormalities in patients with idiopathic dystonia. *Mov Disord*. Jun 15 2007;22(8):1110-6. doi:10.1002/mds.21295

124. Sondergaard RE, Rockel CP, Cortese F, et al. Microstructural Abnormalities of the Dentatorubrothalamic Tract in Cervical Dystonia. *Mov Disord*. Sep 2021;36(9):2192-2198. doi:10.1002/mds.28649

125. Horovitz SG, Ford A, Najee-Ullah MA, Ostuni JL, Hallett M. Anatomical correlates of blepharospasm. *Transl Neurodegener*. 2012;1(1):12. doi:10.1186/2047-9158-1-12

126. Weiskopf N, Edwards LJ, Helms G, Mohammadi S, Kirilina E. Quantitative magnetic resonance imaging of brain anatomy and in vivo histology. *Nature Reviews Physics*. 2021/08/01 2021;3(8):570-588. doi:10.1038/s42254-021-00326-1

127. Martinez-Heras E, Grussu F, Prados F, Solana E, Llufriu S. Diffusion-Weighted Imaging: Recent Advances and Applications. *Semin Ultrasound CT MR*. Oct 2021;42(5):490-506. doi:10.1053/j.sult.2021.07.006

6.2. Publikationsliste

6.2.1. Originalarbeiten als Erstautor

1. **Mantel T**, Dresel C, Altenmüller E, Zimmer C, Noe J, Haslinger B. Activity and topographic changes in the somatosensory system in embouchure dystonia. Mov Disord. 2016 Nov;31(11):1640-1648. doi: 10.1002/mds.26664.
2. **Mantel T**, Meindl T, Li Y, Jochim A, Gora-Stahlberg G, Kräenbring J, Berndt M, Dresel C, Haslinger B. Network-specific resting-state connectivity changes in the premotor-parietal axis in writer's cramp. Neuroimage Clin. 2017 Oct 14; 17:137-144. doi: 10.1016/j.nicl.2017.10.001.
3. **Mantel T**, Altenmüller E, Li Y, Meindl T, Jochim A, Lee A, Zimmer C, Dresel C, Haslinger B. Abnormalities in grey matter structure in embouchure dystonia. Parkinsonism Relat Disord. 2019 Aug; 65:111-116. doi: 0.1016/j.parkreldis.2019.05.008.
4. **Mantel T**, Dresel C, Welte M, Meindl T, Jochim A, Zimmer C, Haslinger B. Altered sensory system activity and connectivity patterns in adductor spasmodic dysphonia. Sci Rep. 2020 Jun 23; 10(1):10179. doi: 10.1038/s41598-020-67295-w.
5. **Mantel T**, Altenmüller E, Li Y, Lee A, Meindl T, Jochim A, Zimmer C, Haslinger B. Structure-function abnormalities in cortical sensory projections in embouchure dystonia. Neuroimage Clin. 2020; 28:102410. doi: 10.1016/j.nicl.2020.102410.
6. **Mantel T**, Jochim A, Meindl T, Deppe J, Zimmer C, Li Y, Haslinger B. Thalamic structural connectivity profiles in blepharospam/Meige's syndrome. Neuroimage Clin. 2022; 34:103013. doi: 10.1016/j.nicl.2022.103013.
7. **Mantel T**, Lee A, Furuya S, Morise M, Altenmüller E, Haslinger B. Reliability and Validity of the Embouchure Dystonia Severity Rating Scale. J Mov Disord. 2023 May;16(2):191-195. doi: 10.14802/jmd.22213.

6.2.2. Originalarbeiten als Koautor

1. Haslinger B, Noé J, Altenmüller E, Riedl V, Zimmer C, **Mantel T**, Dresel C. Changes in resting-state connectivity in musicians with embouchure dystonia. Mov Disord. 2017 Mar;32(3):450-458. doi: 10.1002/mds.26893.
2. Zech M, Jech R, Wagner M, **Mantel T**, Boesch S, Nocker M, Jochim A, Berutti R, Havránková P, Fečíková A, Kemlink D, Roth J, Strom TM, Poewe W, Růžička E, Haslinger B, Winkelmann J. Molecular diversity of combined and complex dystonia: insights from diagnostic exome sequencing. Neurogenetics. 2017 Dec;18(4):195-205. doi: 10.1007/s10048-017-0521-9.
3. Jochim A, Li Y, Gora-Stahlberg G, **Mantel T**, Berndt M, Castrop F, Dresel C, Haslinger B. Altered functional connectivity in blepharospasm/orofacial dystonia. Brain Behav. 2017 Dec 18;8(1):e00894. doi: 10.1002/brb3.894.
4. Jochim A, Meindl T, **Mantel T**, Zwirner S, Zech M, Castrop F, Haslinger B. Treatment of cervical dystonia with abo- and onabotulinumtoxinA: long-term safety and efficacy in daily clinical practice. J Neurol. 2019 Aug;266(8):1879-1886. doi: 10.1007/s00415-019- 09349-2.
5. Jochim A, Meindl T, Huber C, **Mantel T**, Zwirner S, Castrop F, Haslinger B. Treatment of blepharospasm and Meige's syndrome with abo- and onabotulinumtoxinA: long-term safety and efficacy in daily clinical practice. J Neurol. 2020 Jan;267(1):267-275. doi: 10.1007/s00415-019-09581-w.
6. Zech M, Jech R, Boesch S, Škorvánek M, Weber S, Wagner M, Zhao C, Jochim A, Necpál J, Dincer Y, Vill K, Distelmaier F, Stoklosa M, Krenn M, Grunwald S, Bock-Bierbaum T, Fečíková A, Havránková P, Roth J, Příhodová I, Adamovičová M, Ulmanová O, Bechyně K, Danhofer P, Veselý B, Haň V, Pavelekova P, Gdovinová Z, **Mantel T**, Meindl T, Sitzberger A, Schröder S, Blaschek A, Roser T, Bonfert MV, Haberlandt E, Plecko B, Leineweber B, Berweck S, Herberhold T, Langguth B, Švantnerová J, Minár M, RamosRivera GA, Wojcik MH, Pajusalu S, Õunap K, Schatz UA, Pölsler L, Milenkovic I, Laccone F, Pilshofer V, Colombo R, Patzer S, Iuso A, Vera J, Troncoso M, Fang F, Prokisch H, Wilbert F, Eckenweiler M, Graf E, Westphal DS, Riedhammer KM, Brunet T, Alhaddad B, Berutti R, Strom TM, Hecht M, Baumann M, Wolf M, Telegrafi A, Person RE, Zamora FM, Henderson LB, Weise D, Musacchio T,

Volkmann J, Szuto A, Becker J, Cremer K, Sycha T, Zimprich F, Kraus V, Makowski C, Gonzalez-Alegre P, Bardakjian TM, Ozelius LJ, Vetro A, Guerrini R, Maier E, Borggraefe I, Kuster A, Wortmann SB, Hackenberg A, Steinfeld R, Assmann B, Staufner C, Opladen T, Růžička E, Cohn RD, Dyment D, Chung WK, Engels H, Ceballos-Baumann A, Ploski R, Daumke O, Haslinger B, Mall V, Oexle K, Winkelmann J. Monogenic variants in dystonia: an exome-wide sequencing study. Lancet Neurol. 2020 Nov; 19(11):908-918. doi: 10.1016/S1474-4422(20)30312-4.

6.2.3. Buchkapitel

1. Doll-Lee J, Lee A, **Mantel T**, Haslinger B, Altenmüller E. Embouchure Dystonia as a Network Disease. In: Shaikh A, Sadnicka A, eds. *Basic and Translational Applications of the Network Theory for Dystonia*. Springer International Publishing; 2023:45-59.

6.3. Danksagung

Mein großer Dank gilt Herrn Prof. Dr. Bernhard Hemmer für seine kontinuierliche Unterstützung im Rahmen meiner klinischen und wissenschaftlichen Entwicklung und die Ermöglichung dieser Habilitation.

Ganz besonders möchte ich Herrn Prof. Dr. Bernhard Haslinger danken, der mich in meinem wissenschaftlichen Werdegang entscheidend unterstützt und geprägt hat. Mein Dank gilt auch den weiteren aktuellen und ehemaligen Mitarbeitern der Forschungsgruppe, insbesondere Frau PD Dr. Angela Jochim, Herrn Dr. Yong Li sowie Herrn Dr. Tobias Meindl, für die ergiebige und lehrreiche Zusammenarbeit bei zahlreichen Projekten.

Weiter danke ich den wissenschaftlichen Beiräten meiner Habilitation, Herrn Prof. Dr. Helge Topka und Herrn Priv.-Doz. Dr. Christian Sorg, herzlich für Ihre Unterstützung und Betreuung im Rahmen des Habilitationsverfahrens und der Erstellung dieser Arbeit.

Mein tiefer Dank gebührt ebenfalls meiner Familie. Meinen Eltern danke ich dabei für die stetige Motivation und Hilfestellung im Rahmen meiner Ausbildung. Ganz besonders danken möchte ich meiner Partnerin Dr. Mira Ganslmeier – für Ihre Geduld, Anteilnahme, und kontinuierliche Unterstützung im Rahmen meiner wissenschaftlichen Arbeit und des Habilitationsprozesses.

7. Originalarbeiten

Im Folgenden sind die in dieser Habilitationsschrift verwendeten Originalpublikationen in chronologischer Abfolge angehängt

NeuroImage: Clinical 17 (2018) 137–144

Contents lists available at ScienceDirect

NeuroImage: Clinical

journal homepage: www.elsevier.com/locate/ynicl

Network-specific resting-state connectivity changes in the premotor-parietal axis in writer's cramp

Tobias Mantel[a], Tobias Meindl[a], Yong Li[a], Angela Jochim[a], Gina Gora-Stahlberg[a], Jona Kräenbring[a,b], Maria Berndt[c], Christian Dresel[a,d], Bernhard Haslinger[a,*]

[a] Department of Neurology, Klinikum rechts der Isar, Technische Universität München, Ismaningerstrasse 22, Munich, Germany
[b] Department of Psychiatry, Isar-Amper-Klinikum München-Ost, Vockestrasse 72, Haar, Germany
[c] Department of Neuroradiology, Klinikum rechts der Isar, Technische Universität München, Ismaningerstrasse 22, Munich, Germany
[d] Department of Neurology, Johannes Gutenberg University, School of Medicine, Langenbeckstrasse 1, Mainz, Germany

ARTICLE INFO

Keywords:
Resting state
Functional connectivity
Dystonia
Premotor cortex
Cerebellum

ABSTRACT

Background: Writer's cramp is a task-specific dystonia impairing writing and sometimes other fine motor tasks. Neuroimaging studies using manifold designs have shown varying results regarding the nature of changes in the disease.

Objective: To clarify and extend the knowledge of underlying changes by investigating functional connectivity (FC) in intrinsic connectivity networks with putative sensorimotor function at rest in an increased number of study subjects.

Methods: Resting-state functional magnetic resonance imaging with independent component analysis was performed in 26/27 writer's cramp patients/healthy controls, and FC within and between resting state networks with putative sensorimotor function was compared. Additionally, voxel-based morphometry was carried out on the subjects' structural images.

Results: Patients displayed increased left- and reduced right-hemispheric primary sensorimotor FC in the premotor-parietal network. Mostly bilaterally altered dorsal/ventral premotor FC, as well as altered parietal FC were observed within multiple sensorimotor networks and showed differing network-dependent directionality. Beyond within-network FC changes and reduced right cerebellar grey matter volume in the structural analysis, the positive between-network FC of the cerebellar network and the basal ganglia network was reduced.

Conclusions: Abnormal resting-state FC in multiple networks with putative sensorimotor function may act as basis of preexisting observations made during task-related neuroimaging. Further, altered connectivity between the cerebellar and basal ganglia network underlines the important role of these structures in the disease.

1. Introduction

Writer's cramp (WC) is a task-specific focal hand dystonia (FHD) with a peak incidence between the 3rd and 5th decade causing abnormal and disabling postures through uncoordinated overflowing muscle activity solely during writing (simple WC) or also during fine motor tasks (dystonic WC) (Sheehy and Marsden, 1982). In the past, a number of neuroimaging studies have been conducted to further elucidate the yet not fully clear mechanisms of this disease, and both functional and structural changes in the primary sensorimotor and the premotor/supplementary motor cortex, the cerebellum and basal ganglia have been described (Hallett, 2006; Neychev et al., 2011). During the last years, the concept of resting state functional connectivity (FC) networks has gained much attention. It refers to the observation that networks of brain regions temporally correlate by low frequency fluctuations of the blood oxygen level dependent (BOLD) signal in the absence of experimental tasks (Biswal et al., 1997; Cordes et al., 2001; Fox and Raichle, 2007). Interestingly, those spatial

Abbreviations: ADDS, arm dystonia disability scale; BGN, basal ganglia network; BOLD, blood oxygen level-dependent; CN, cerebellar network; CONTR, healthy controls; FC, functional connectivity; FHD, focal hand dystonia; FWHM, full width at half maximum; FoV, field of view; GM, grey matter; IC, independent component; ICA, independent component analysis; ICN, intrinsic connectivity network; IPS, intraparietal sulcus; M1, primary motor cortex; PAT, writer's cramp patients; PCA, principal component analysis; PPN, premotor parietal network; PMd/v, dorsal/ventral premotor cortex; S1, primary somatosensory cortex; ROI, region of interest; rsfMRI, resting state functional magnetic resonance imaging; S2, secondary somatosensory cortex; SM1, primary sensorimotor cortex; SMA, supplementary motor area; SMG, supramarginal gyrus; v/dSMN, ventral/dorsal sensorimotor network; SPC, superior parietal cortex; TIV, total intracranial volume; WC, writer's cramp; WCRS, writer's cramp rating scale

* Corresponding author at: Klinik und Poliklinik für Neurologie, Klinikum rechts der Isar, Technische Universität München, Ismaninger Strasse 22, D - 81675 München, Germany.
E-mail address: bernhard.haslinger@tum.de (B. Haslinger).

http://dx.doi.org/10.1016/j.nicl.2017.10.001
Received 11 July 2017; Received in revised form 12 September 2017; Accepted 2 October 2017
Available online 14 October 2017

networks of temporally correlated brain areas have a distribution similar to what is observed in task activation studies, hinting at a common functionality. The correlation between the hubs in such networks has further been shown to increase in the presence of adequate tasks suggesting that task-related activity may constitute a superposition of spontaneous BOLD activity at rest (Fox and Raichle, 2007). In WC, task-based neuroimaging studies have promoted the identification of brain areas involved in this disease but, using various different experimental paradigms, yielded ambiguous results regarding the nature of changes. As an example, in FHD either reduced (Ibanez et al., 1999; Langbour et al., 2017; Nelson et al., 2009; Oga et al., 2002), increased (Lerner et al., 2004; Odergren et al., 1998) or opposed (Ceballos-Baumann et al., 1997) primary sensory (S1) and/or motor (M1) activity have been shown during sensory (Langbour et al., 2017; Nelson et al., 2009) or dystonic (Ceballos-Baumann et al., 1997; Lerner et al., 2004; Odergren et al., 1998) and asymptomatic (Ibanez et al., 1999; Oga et al., 2002) motor tasks. Studying the connectivity between brain regions in the absence of tasks might thus seem suitable to identify underlying changes in this disease. Still, earlier findings in resting state fMRI (rsfMRI) were not unequivocal. While one early rsfMRI study reported reduced left primary sensorimotor connectivity when investigating one sensorimotor network (Mohammadi et al., 2012), a seed-based approach reported increased connectivity between left S1 and M1 (Dresel et al., 2014) and had the constraint of a required prior spatial definition of regions of interest (ROIs). In this study, we aimed at further clarifying and possibly extending the knowledge of underlying changes in this disease by investigating cortical and subcortical intrinsic connectivity networks with attributed sensorimotor functionality applying an independent component based approach that avoids a possible bias induced by the choice of seed regions using an increased number of study subjects compared to previous trials. Additionally, a voxel-based morphometry analysis was performed to detect underlying grey matter changes as a possible cause of FC changes.

2. Methods

2.1. Participants

We investigated 26 WC patients (PAT; age 46.8 ± 13.7 years, m/f 15/11) and 27 healthy subjects (CONTR; age 49.3 ± 13.9 years, m/f 14/13) < 70 years of age with no neuro(psychiatric)/major internal disease, no neuroleptic or anticholinergic medication and a normal structural MRI, whose functional scans fulfilled the criteria of a composite (translation and rotation (Power et al., 2014)) head displacement of less than the voxel size in maximum and half the voxel size on average. No patient had received botulinum toxin therapy within the last three months prior to the study. The functional motor impairment of the hand was assessed with the arm dystonia disability scale (ADDS) for fine motor tasks, and specifically for writing using the writer's cramp rating scale (WCRS). The university ethics board approved the study. All participants gave their written informed consent according to the Declaration of Helsinki.

2.2. Data acquisition and preprocessing

For rsfMRI, 303 T2* echo-planar whole-brain functional MR images were acquired for each participant on a Philips Achieva 3.0 T scanner with an 8-channel head coil (TR/TE 2200/30 ms, field of view (FoV) 216 × 216 mm^2, 36 slices, voxel size 3 × 3 × 3 mm^3, scan time 11 min). The participants were instructed to keep their eyes closed during the whole experiment. To minimize the risk of motion artifacts, the head was fixed with foam pads. After rsfMRI, a high-resolution 3D T1-weighted structural image was acquired for anatomical reference (TR/TE/TI 59/4/780 ms, FoV 240 × 240 mm^2, 170 slices, voxel size 1 × 1 × 1 mm^3, scan time 6 min).

Preprocessing of functional data was performed in SPM12 (http://www.fil.ion.ucl.uk/spm) and Matlab2013a (The MathWorks, Natick, Massachusetts), and involved realignment for head motion correction, slice timing correction, coregistration with the anatomical reference image and normalization to the Montreal Neurological Institute (MNI) space with resampling to 2 × 2 × 2 mm^3 voxels. The data were spatially smoothed with an isotropic Gaussian kernel of 8 mm full width at half maximum (FWHM). The first five scans of the rsfMRI run were discarded to ensure longitudinal magnetization equilibrium. The average framewise displacement (Power et al., 2014) (translation and rotation) was 0.10 ± 0.03 mm in PAT and 0.10 ± 0.03 mm in CONTR ($F_{1,51}$ = 0, p = 1.0), the composite maximum head displacement 1.32 ± 0.71 mm in PAT and 1.15 ± 0.53 mm in CONTR ($F_{1,51}$ = 0.90, p = 0.35) and the total intracranial volume (TIV) 1612.1 ± 191.4 mm^3 in PAT and 1544.1 ± 164.9 mm^3 in CONTR ($F_{1,51}$ = 1.96, p = 0.17).

2.3. Group independent component analysis

Group spatial independent component analysis (ICA) on the rsfMRI data of each patients and healthy controls was performed as implemented in the GIFT v3.0 software (http://mialab.mrn.org). ICA estimates spatially maximally independent sources from the linearly mixed signals contained in a spatiotemporal fMRI dataset, providing spatial maps of temporally coherent brain regions (functional spatial networks) (Calhoun et al., 2001). This approach has been shown to effectively identify and remove various sources of motion and non-motion-related noise in fMRI data (Griffanti et al., 2014). Further, its suggested property of being sensitive to the detection of subtle changes (Koch et al., 2012) is desirable when investigating task-specific dystonia. The calculated spatially independent components (ICs) represent either meaningful (i.e. intrinsic connectivity networks (ICNs)) or spurious (e.g. noise) information.

In a first step, the number of components in the whole dataset was determined by a dimensionality estimation using the minimum description length algorithm resulting in an estimate of a maximum of 52 and a mean number of 33 ICs. Based on these estimates, a stepwise dimensionality reduction was performed in each group using principal component analysis (PCA) (Celone et al., 2006; Wu et al., 2011), retaining 52 components at the subject- and 33 components at the group-level. This was followed by IC separation using the InfoMax algorithm (Bell and Sejnowski, 1995). Reliability testing was performed using the ICASSO toolbox (Himberg et al., 2004): ICA was repeated 40 times, the components were clustered, and their quality quantified using the index I_q (range 0 to 1) which mirrors the difference between intra- and extra-cluster similarity. Back-reconstruction of subject-specific spatial maps was performed from the aggregate spatiotemporal data set using a method based on PCA compression and projection robust for low model orders (GICA I) (Calhoun et al., 2001). To identify components of likely functional relevance in WC for further analysis, the spatial IC maps were correlated with publicly available maps of ICNs identified in a meta-analysis of task fMRI studies performed by Laird and colleagues (Laird et al., 2011) using multiple regression. The non-noise IC with the best fit (highest coefficient of determination) was selected. ICs representing noise were identified by standardized visual inspection of their spatial (activation pattern and tissue overlap with grey matter (GM)) and temporal characteristics (e.g. presence of saw tooth and high frequency patterns or spikes) as previously described (Kelly et al., 2010). Those identified components with attributed sensorimotor function in the meta-analysis (Laird et al., 2011) were then selected for further analysis (see Fig. A.1): a basal ganglia-thalamus network (BGN, ~Laird's ICN3), a cerebellar network (CN, ~Laird's ICN14), a premotor-parietal network (PPN, ~Laird's ICN7), a dorsal sensorimotor network (dSMN, ~Laird's ICN8/9) and a ventral sensorimotor network (vSMN, ~Laird's ICN17). The primary visual network (VN, ~Laird's ICN12) was chosen as a control. All investigated components were highly stable ($I_q \geq 0.95$). All selected networks have been previously

described at rest (Allen et al., 2011; Beckmann et al., 2005; Smith et al., 2009). Other identified ICNs reported by Laird et al. not chosen for analysis are visualized in Fig. A.2.

2.3.1. Analysis of within-network FC

The corresponding single-subject spatial IC maps of each selected network were entered into within- and between-group *t*-tests in SPM12 to draw population-based inferences on the composition and FC of these RSNs. In addition to sex and age, the maximum composite total head displacement and the average framewise head displacement were included as regressors in the second-level model to control for possible residual head motion not accounted for by ICA. To correct for multiple voxel-wise comparisons, we applied a Bonferroni-corrected peak-level threshold of $p(FDR) < 0.0083$ ($p(FDR) < 0.05/6$ for six investigated ICNs) in addition to a cluster-level threshold of $p(FWE) < 0.05$. A combined binary mask from the within-group analyses was created to ensure that only highly connected regions of each network were analyzed.

2.3.2. Analysis of between-network FC

We calculated an estimate for the FC between the investigated ICNs by correlating the time courses of these ICNs in each subject. Processing of time courses involved the removal of linear, cubic and quadratic trends, despiking, filtering at a standard high-frequency cut-off of 15 Hz and regression of realignment parameters. The individual's Fisher's z-transformed Pearson correlation coefficients z_r were then compared between groups in an analysis of covariance including the covariates age and sex. The significance level was set at $p < 0.01$ ($p = 0.05/5$ for five comparisons/network).

2.4. Morphometric analysis

Voxel-based morphometry was performed using an optimized procedure as implemented in the CAT12 toolbox (http://www.neuro.uni-jena.de/cat/). Structural scans were skull-stripped, tissue segmented using the implemented adaptive maximum a posterior approach (Rajapakse et al., 1997) and normalized to MNI space using DARTEL (diffeomorphic anatomical registration using exponentiated lie algebra). Jacobian modulation was performed on the resulting GM segments that were smoothed with an 8 mm FWHM isotropic Gaussian kernel. The significance level of the age, sex and TIV-adjusted between-group *t*-test was set at a peak-level threshold of $p < 0.001$ (uncorrected) with an additional cluster level-threshold at $p(FWE) < 0.05$. Trends are reported for a cluster-level threshold of $p(FDR) < 0.05$.

2.5. Post hoc correlation with clinical characteristics

Given a significant result in the above-described between-group analyses, separate post hoc multiple regression analyses with the clinical parameters disease duration, ADDS and WCRS were set up for the PAT group. Inclusion of nuisance regressors and correction for multiple comparisons was performed as in the respective between-group analyses.

3. Results

Statistical analysis revealed no significant between-group difference in age ($F_{1,51} = 0.41$, $p = 0.53$) or sex ($F_{1,51} = 0.18$, $p = 0.68$). The mean disease duration in PAT was 13.2 ± 10.8 years, the ADDS was rated 60.8 ± 20.1% and the WCRS 11.7 ± 5.4 points.

3.1. Analysis of within-network FC

The between-group analysis of the six ICNs revealed significant FC changes in all networks except the VN (Fig. 1, Tables 1, 2). The networks and their spatial extent in each group are illustrated in Fig. A.1.

3.1.1. PPN

Increased FC in PAT was seen for the left lateral dorsal premotor cortex (PMd) and the left primary sensorimotor cortex (SM1, GM of the central sulcus). Reduced FC was observed for the right M1 and S1, supramarginal gyrus (SMG) and posterior superior parietal cortex (SPC) as well as for the medial intraparietal sulcus area (IPS) bilaterally. Further, we found reduced FC for the right caudal and rostral ventral premotor cortex (PMv) and bilateral inferior frontal sulcus area.

3.1.2. SMNs

Within the dSMN, PAT showed increased FC for the left ventromedial prefrontal cortex and reduced FC for the PMd and the supplementary motor area (SMA) bilaterally. Within the vSMN, there was increased FC in PAT for the temporo-occipital junction and there were no areas of significantly reduced FC.

3.1.3. CN

Increased FC in PAT was found for the posterior cerebellum and the caudal PMv bilaterally and reduced FC was observed for the left posterior SPC.

3.1.4. BGN

Increased FC in PAT was found for the PMd, PMv (with findings for the left PMd extending to the preSMA), posterior cerebellum and secondary somatosensory cortex (S2) bilaterally. Further, FC was increased for the left SM1, cingulate cortices and the right SMG and posterior SPC. Reduced FC in PAT was found for the caudate and thalamus bilaterally, as well as for the right pallidum and hippocampus.

3.2. Analysis of between-network FC

The analysis of inter-network FC revealed a significant reduction of positive FC between the CN and BGN ($F_{1,49} = 16.4$, $p = 0.0002$, $r = 0.51$) as well as the CN and VN ($F_{1,49} = 4.14$, $p = 0.003$, $r = 0.41$) in PAT (Figs. 2, A.3; Table 3).

3.3. Analysis of structural changes

Voxel-based morphometry revealed significantly reduced GM volume in PAT in the right posterior cerebellum ($x|y|z = 28|-64|-40$, $t = 4.31$, $k = 2478$) and a trend for reduced GM volume in the left posterior cerebellum ($x|y|z = -34|-74|-40$, $t = 4.42$, $k = 2159$; Fig. 1).

3.4. Correlation with clinical characteristics

Multiple regression did not reveal any significant correlation between disease duration, ADDS and WCRS with within- or between-network FC values in PAT. Multiple regression with voxel-wise GM values revealed a significant positive correlation between the score on the WCRS and GM volume in the left S2 ($x|y|z = -58|-22|32$, $t = 6.59$, $k = 1952$).

4. Discussion

WC patients displayed altered within-network FC at rest mainly in the dSMN, PPN, BGN and CN, involving various FC changes of primary sensorimotor, premotor and parietal cortices as well as of thalamus, basal ganglia and cerebellum. These encompassed in their entirety a web of regions previously identified as being active during the task of writing (Rijntjes et al., 1999). Parallel to this, for the cerebellum also structural changes of GM volume were shown.

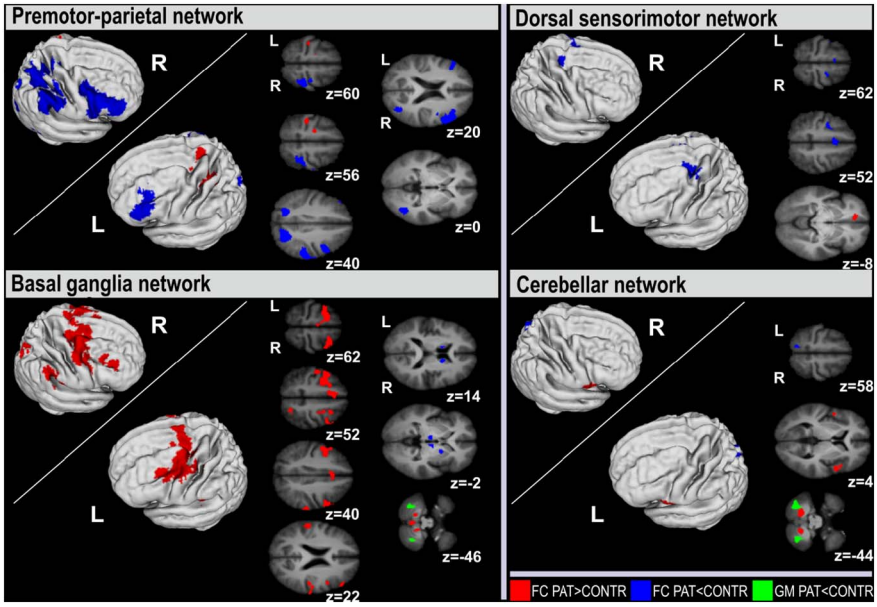

Fig. 1. Significant between-group differences of functional connectivity (FC) within the premotor-parietal, dorsal sensorimotor, basal ganglia and cerebellar network. Significant FC changes ($p_{(FDR)} < 0.0083$, $p_{cluster(FWE)} < 0.05$) are overlaid onto the axial slices/3D reconstructions of the participants' averaged, skull-stripped T1 images. For the cerebellum, additionally structural changes including trends at $p_{cluster(FDR)} < 0.05$ are displayed. Slice positions in Montreal Neurological Institute space in mm are given relative to the anterior commissure (z above/below [+]/[−]). CONTR, healthy controls; PAT, writer's cramp patients; L/R, left/right hemisphere.

4.1. Primary sensorimotor cortices

We observed abnormal FC of the primary sensorimotor cortex hand area(s) in patients within the PPN, showing increased left-hemispheric SM1 FC and a reduced right-hemispheric S1 and M1 FC. Additionally, there was increased left-hemispheric SM1 FC within the BGN. A previous ICA-based study investigating 16 WC patients described reduced left SM1 FC in the sensorimotor network (Mohammadi et al., 2012) in which we did not observe altered SM1 FC. The increased FC in the hemisphere contralateral to the dystonic hand is in line with the observation of increased S1-to-M1 FC in a recent seed-based rsfMRI study (Dresel et al., 2014). During task-related fMRI primary sensorimotor overactivity was seen when a dystonic task was involved (Preibisch et al., 2001), while the opposite was mainly observed in context of nondystonic interventions (simple motor tasks/sensory stimulation) (Langbour et al., 2017; Nelson et al., 2009; Oga et al., 2002). For S1, also altered functional topography of dystonic/non-dystonic body parts in task-induced FHDs has been shown (Meunier et al., 2001; Nelson et al., 2009). In analogy to the findings of task activation studies in FHD, our finding of increased FC of the dystonic hands' left-hemispheric SM1 representation may represent a correlate of defective intracortical inhibition and/or malfunctional plasticity that have been shown for FHD both in the left S1 and M1 (Quartarone and Hallett, 2013). Beyond intracortical changes, there is evidence for abnormal interhemispheric inhibition in FHD (Nelson et al., 2010; Niehaus et al., 2001). We observed increased left- and reduced right-hemispheric FC within the PPN. In healthy subjects unilateral motor tasks/tactile stimulation of the hand during fMRI lead to a contralateral increase and an ipsilateral reduction in M1/S1 BOLD activity which is assumed to mirror interhemispheric interactions (Eickhoff et al., 2008; Hamzei et al., 2002). Neurophysiologic studies in FHD reported reduced interhemispheric inhibition (right to left) of the right dystonic hand's M1 representation at rest (Nelson et al., 2010), and increased interhemispheric inhibition (left to right) of the unaffected left hand's M1 representation during muscle contraction (Niehaus et al., 2001). Congruently, transcranial dual current stimulation during bimanual mirrored finger movements reduced dystonic symptoms in musician's dystonia of the right hand when reducing the excitability of the left and increasing the excitability of the right M1 (Furuya et al., 2014). Thus, our observations within the PPN may provide some correlate for an abnormal interhemispheric interaction.

4.2. Premotor and parietal dysconnectivity

We observed multiple FC changes of the premotor cortex (PMC) affecting mostly the SMA, PMd and PMv. First, reduced bilateral SMA FC was seen within the dSMN, a network that has been linked to tasks involving hand action (Laird et al., 2011). Consistently, activity of the SMA was found reduced in most (Ceballos-Baumann et al., 1997; Ibanez et al., 1999; Lerner et al., 2004; Oga et al., 2002) task-based WC fMRI studies and contingent negative variation (attributed to a thalamo-SMA circuit (Nagai et al., 2004)) is reduced in WC (Hamano et al., 1999).

Second, we observed FC changes of the PMd within various ICNs. FC increases were seen in patients within the BGN bilaterally and the PPN (a mainly cortical network functionally associated with visuomotor task performance (Laird et al., 2011)) in the left hemisphere, and a FC reduction in patients was observed bilaterally within the dSMN. The PMd is found active during visuomotor tasks of the upper extremity and assumed to integrate multisensory information to compose task-adequate motor programs; it may further be involved in their subsequent execution (Hoshi and Tanji, 2007). Transcranial magnetic stimulation over the left-hemispheric PMd in healthy subjects interferes with hand motor sequences during visuomotor tasks (Schluter et al., 1998), the latter being dysfunctional in task-specific FHD (Granert et al., 2011). Motor task-related fMRI studies in WC reported both increased (Ceballos-Baumann et al., 1997; Lerner et al., 2004; Odergren et al., 1998) and reduced (Ibanez et al., 1999; Langbour et al., 2017) dorsal premotor activity.

Third, patients showed altered FC predominantly for caudal PMv domains (Brodmann's area 6). Increased FC was observed bilaterally within the CN and BGN and reduced FC was found within the PPN. In the latter, findings had right-hemispheric emphasis and also encompassed rostral PMv domains. Though the rostral PMv has classically been linked to speech, it has reliably been demonstrated to be also active during hand action (Rizzolatti et al., 2002). PMv areas are involved in the matching of multisensory input (esp. visuospatial information) to ongoing motor performance, thus enabling grip precision (Hoshi and Tanji, 2007; Rizzolatti et al., 2002) which has been shown to be impaired in FHD (Nowak et al., 2005).

Integrated multisensory information reaches the PMCs via the posterior parietal cortex (PPC). Its upper domain, the SPC, is suggested to provide integrated somatosensory and visual inputs to the PMd (Scheperjans et al., 2008). In the present study FC in patients was increased for the right SPC within the BGN, and reduced within the CN in

Table 1
Differences of functional connectivity in sensorimotor networks with predominantly cortical extent.

Area	x	y	z	*t* value	Cluster volume
Premotor-parietal network					
PAT > CONTR					
L lateral dorsal premotor, caudal (BA6)	− 18	− 12	56	5.17	48
L primary sensorimotor (BA3/4)	− 34	− 26	56	5.37	121
PAT < CONTR					
R supramarginal gyrus (BA40)	50	− 34	36	6.34	1551
R superior parietal, caudal (BA7)	30	− 42	50	5.50	
R primary somatosensory (BA2/5)	38	− 36	62	5.21	
R primary motor (BA4)	34	− 22	64	4.78	
R intraparietal sulcus (BA7)	22	− 64	34	7.14	1102
L intraparietal sulcus (BA7)	− 20	− 62	38	5.65	339
R inferior frontal sulcus (BA46)	52	36	8	7.26	1581
R ventral premotor, rostral (BA9/46)	56	24	24	7.14	
R ventral premotor, rostral (BA44/45)	56	14	18	6.87	
R ventral premotor, caudal (BA6)	44	2	34	5.56	
R inferior frontal sulcus (BA46)	50	30	16	4.90	
L inferior frontal sulcus (BA46)	− 46	− 30	16	4.45	409
R temporo-occipital junction (BA19/37)	42	− 64	− 2	5.82	410
Dorsal sensorimotor network					
PAT > CONTR					
L ventral medial prefrontal (BA11/32)	− 12	44	− 8	6.33	45
PAT < CONTR					
R supplementary motor (BA6)	2	8	54	6.29	164
L supplementary motor (BA6)	− 2	4	58	5.36	
R lateral dorsal premotor, caudal (BA6)	24	− 10	60	5.55	23
L lateral dorsal premotor, caudal (BA6)	− 28	− 6	52	5.15	76
Ventral sensorimotor network					
PAT > CONTR					
R temporo-occipital junction (BA19/37)	50	− 74	2	5.92	91
PAT < CONTR					
–	–				

Coordinates (in mm) in the Montreal Neurological Institute space. All FC differences are significant at $p < 0.0083$ (FDR) and $p < 0.05$ cluster at the cluster-level. PAT, writer's cramp patients; CONTR, healthy controls; R, right; L, left; ant., anterior (rostral), post., posterior (caudal). The term sensorimotor cortex describes maxima located in the central sulcus of the anatomical mean image that were not unequivocally assignable to the primary sensory or motor area.

Table 2
Differences of functional connectivity changes in sensorimotor networks with predominantly subcortical/cerebellar extent.

Area	x	y	z	*t* value	Cluster volume
Cerebellar network					
PAT > CONTR					
L cerebellum, post. (VIII)	− 14	− 60	− 42	7.66	124
R cerebellum, post. (VIII)	14	− 62	− 42	6.45	78
R ventral premotor, caudal (BA44)	54	8	6	5.90	118
L ventral premotor, caudal (BA44)	− 46	2	2	4.87	39
PAT < CONTR					
L superior parietal, caudal (BA7)	− 10	− 60	58	4.83	39
Basal ganglia network					
PAT > CONTR					
L cerebellum, post (VIII)	− 14	− 67	− 46	6.09	375
R cerebellum, post (IX)	12	− 50	− 44	4.75	93
L cingulum, posterior (BA32)	− 6	− 14	46	5.26	399
R cingulum, anterior (BA32)	8	20	38	4.27	
L cingulum, anterior (BA32)	− 2	16	42	4.16	
L lateral dorsal premotor, rostral (BA44)	− 46	6	4	7.62	1778
L pre-supplementary motor (BA6)	− 22	10	52	6.86	
L lateral dorsal premotor/frontal eye field (BA6)	− 34	2	60	6.73	
L inferior frontal junction (BA9)	− 48	16	34	5.81	
L primary sensorimotor (BA3/4)	− 46	− 14	50	5.04	
R ventral premotor, caudal (BA6)	54	6	44	5.47	1006
R lateral dorsal premotor, rostral (BA6)	26	10	62	6.83	
R lateral dorsal premotor, caudal (BA6)	28	− 10	54	4.55	
L secondary somatosensory (BA40)	− 58	− 28	16	7.08	113
R supramarginal gyrus (BA40)	64	− 28	40	5.98	102
R secondary somatosensory (BA40)	48	− 26	22	4.50	81
R superior parietal, caudal (BA7)	24	− 60	54	4.39	77
PAT < CONTR					
L thalamus, ventral	− 6	− 16	− 6	5.67	59
R thalamus, ventral	8	− 14	− 6	6.19	70
L caudate, corpus	− 12	14	6	6.92	109
R caudate, corpus	14	6	14	6.49	192
R pallidum	18	4	0	5.47	
R hippocampus	22	2	− 16	6.45	122

Coordinates (in mm) in the Montreal Neurological Institute space. All FC differences are significant at $p < 0.0083$ (FDR) and $p < 0.05$ cluster at the cluster-level. PAT, writer's cramp patients; CONTR, healthy controls; R, right; L, left; ant., anterior (rostral), post., posterior (caudal). The term sensorimotor cortex describes maxima located in the central sulcus of the anatomical mean image that were not unequivocally assignable to the primary sensory or motor area.

the left, and the PPN in the right hemisphere. Its lower domain, the inferior parietal cortex, is linked to the PMv. Here, we found the FC for the right SMG to be reduced within the dSMN and increased in the BGN. Further, the FC of GM encompassing the medial IPS area was reduced bilaterally within the PPN. The IPS area has been suggested to serve as an integration interface between perceptive systems and the PMv, with its medial parts assumed to play an important role in visuomotor coordination of hand motion (Grefkes and Fink, 2005; Hoshi and Tanji, 2007). Together with above-described premotor changes, these findings in the PPN fit well with the observation of reduced PMv-PPC connectivity during writing (Gallea et al., 2016) and in a seed-based approach at rest (Delnooz et al., 2012). The significance of the greater right-hemispheric extent of findings in the parietal cortex and the PMv remains unclear. One may hypothesize if they could be the result of a right-hemisphere emphasis of the activity of the frontoparietal mirror neuron system. Recently fMRI provided evidence for an emphasized activation of this system in the hemisphere ipsilateral to the visual hemifield in which a certain object-oriented action is performed (Aziz-Zadeh et al., 2006). Thus, our observation may reflect the main occurrence of writing in right-handers in the right visual hemifield.

An abnormal processing of (multi)sensory input is another key pathophysiologic concept in dystonia. It is suggested to lead to impaired sensorimotor integration in the disease, resulting in dystonic posture through loss of coordinated muscle activity (Quartarone and Hallett, 2013). Dysfunctional sensory processing in dystonia becomes evident in altered tactile spatiotemporal detection thresholds, vibration sense and mental rotation (Stamelou et al., 2012), with especially the latter pointing to an involvement of higher parietal areas. Abnormal integration at the premotor-parietal level has been discussed as foundation of task-specificity in WC (Hallett, 2006). Neuroimaging studies reporting parietal activity changes mostly reported reduced activity in the disease (Ceballos-Baumann et al., 1997; Langbour et al., 2017; Moore et al., 2012). Sensory tricks can improve dystonic symptoms (Stamelou et al., 2012), and amelioration of reduced PPC activity has been shown during sensory tricks in cervical dystonia (Naumann et al., 2000).

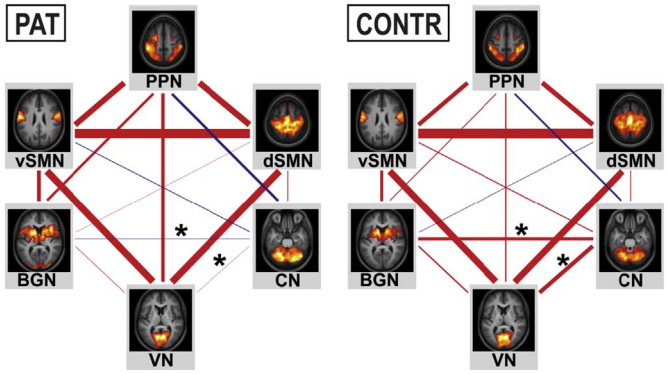

Fig. 2. Visualization of between-network functional connectivity in writer's cramp patients and healthy controls. The line thickness is proportional to the strength of positive (red) or negative (blue) time course correlation. Asterisks mark significant ($p < 0.01$) between-group differences. CONTR, healthy controls; PAT, writer's cramp patients; PPN, premotor parietal network; dSMN, dorsal sensorimotor network; vSMN ventral sensorimotor network; CN, cerebellar network; BGN, basal ganglia network; VN, medial visual network. (For interpretation of the references to color in this figure legend, the reader is referred to the web version of this article.)

Table 3
Matrix of between-network functional connectivity.

ICN	PMN	dSMN	vSMN	BGN	CN	VN
PAT						
PMN	1	0.3591	0.3355	0.1496	− 0.1503	0.1984
dSMN	0.3591	1	0.5438	0.0170	0.0453	0.4085
vSMN	0.3355	0.5438	1	0.2231	− 0.0445	0.4127
BGN	0.1496	0.0170	0.2231	1	**− 0.0207**	0.0272
CN	− 0.1503	0.0453	− 0.0445	**− 0.0207**	1	**− 0.0105**
VN	0.1984	0.4085	0.4127	0.0272	**− 0.0105**	1
CONTR						
PMN	1	0.2813	0.2478	0.0496	− 0.1051	0.0736
dSMN	0.2813	1	0.5739	− 0.0302	0.0457	0.3852
vSMN	0.2478	0.5739	1	0.1713	0.0586	0.3920
BGN	0.0496	− 0.0302	0.1713	1	**0.1923**	0.0801
CN	− 0.1051	0.0457	0.0586	**0.1923**	1	**0.2416**
VN	0.0736	0.3852	0.3920	0.0801	**0.2416**	1

Pairwise correlations between the ICN's time courses were Fisher z-transformed, averaged across the subjects in each group and subsequently inverse z-transformed for display. Significant results ($p < 0.01$) are highlighted in bold.

4.3. Cerebellar and basal ganglia circuits

Growing evidence suggests a role not only of the basal ganglia, but also the cerebellum in dystonia (Neychev et al., 2011; Shakkottai et al., 2017). Lesions of both basal ganglia and (rarely) cerebellum can cause dystonia (LeDoux and Brady, 2003), and both structures have been found to modulate cortical sensorimotor excitability (Restuccia et al., 2001; Tamburin et al., 2004). While some have argued for a mostly compensatory role of a dysfunctional basal ganglia-cerebellar interaction, alternative suggestions of primary defect have been made (Neychev et al., 2011; Shakkottai et al., 2017).

In the BGN, FC changes at the cortical level were focused on an increase in the dorsal > ventral PMC and in executive anterior cingulate areas. Additionally, FC changes in the left SM1 and bilateral S2, a relay for sensorimotor integration, were seen. In the latter, a lower left-hemispheric GM volume was associated with lower scores (= less impairment) on the WCRS. The basal ganglia enable learning of skilled movements and precise selection of movements in motor sequences (Mink, 1996). Dysfunctional surround inhibition resulting in impaired gating of (motor-related) sensory and motor information in the basal ganglia in FHD has been suggested as the cause of dystonic muscle co-activation (Quartarone and Hallett, 2013). Increased FC of the PMCs and bilaterally reduced FC of the corpus of the caudate nucleus and thalamus within the BGN might hence reflect reduced inhibitory basal ganglia influence. Earlier neuroimaging has shown both reduced and increased activity in the thalamus (Ceballos-Baumann et al., 1997; Odergren et al., 1998) and basal ganglia (Gallea et al., 2016; Peller et al., 2006) as well as altered motor putaminal functional topography (Delmaire et al., 2005) in FHD. Seed-based studies observed reduced connectivity of putaminal or pallidal ROIs to primary sensory (motor) cortices during a non-dystonic finger tapping, dystonic writing (Gallea et al., 2016; Moore et al., 2012) and at rest (Dresel et al., 2014). FC changes within the CN at the cortical level were focused on the left SPC and the bilateral PMv, both areas with an emphasis on multisensory integration. The cerebellum processes considerable sensory input. Within the concept of internal forward models, it is thought to quickly provide information about the expected sensory consequences of motor commands enabling appropriate selection and rapid adaption of motor programs (Baumann et al., 2015). Altered FC of the PMv and SPC within the CN, but also between the CN and VN (similarly observed previously in embouchure dystonia (Haslinger et al., 2016)) hints at a disruption of cerebellar sensory integration in dystonia. Dresel et al. recently observed increased anticorrelation of cerebellar ROIs to multiple cortical areas (Dresel et al., 2014). The concept of disturbed cerebello-cortical interaction in WC is supported by Hubsch and colleagues, who reported a loss of cerebellar capacity to modulate motor cortical plasticity in the presence of sensory input (Hubsch et al., 2013). At the cerebellar level, we found increased FC of the posterior sensorimotor cerebellum in the CN and BGN. Increased cerebellar activity has been frequently reported during dystonic writing (Ceballos-Baumann et al., 1997; Odergren et al., 1998). Studies in patients with structural cerebellar disease suggest that cerebellar output modulates primary sensory/motor cortical excitability (Restuccia et al., 2001; Tamburin et al., 2004). Structurally, this study confirmed previous observations by Delmaire and colleagues of reduced cerebellar GM density (Delmaire et al., 2007). The present study did not observe a direct spatial overlap of FC and structural changes, whose potential relationship thus remains unclear.

In a mouse model, increased cerebellar and reduced basal ganglia function led to dystonia (Neychev et al., 2008), though results from mouse studies have to be interpreted carefully. In this respect, the present study further made the interesting finding of a loss of between-network CN-to-BGN FC at rest, while the between-network FC of the CN to the PPN and v/dSMN was unchanged. Recent task-based studies suggested a disruption of striatal and cerebellar interaction during motor learning in FHD (Shakkottai et al., 2017), and Neumann et al. observed inverse correlation of pallido-cerebellar coupling and dystonic symptom severity in primary dystonia when investigating local field potentials that have been shown to correlate with the fMRI BOLD response (Magri et al., 2012; Neumann et al., 2015). All this supports the notion of a dysfunctional cerebellar-basal ganglia interaction in dystonia.

Significant correlations of FC values and measures of disease duration and severity were not observed in our sample. In the past, some functional neuroimaging studies have observed such correlations (Dresel et al., 2014; Peller et al., 2006) while others did not (Haslinger et al., 2016; Langbour et al., 2017). Besides methodological differences between studies, the reason for these mixed findings remains yet unclear.

5. Conclusion

The present study observed multiple and network-specific FC changes in primary and especially higher-order sensory and motor networks at rest. The involvement of multiple sensorimotor networks primarily or secondarily affected by the disease may act as basis of the preexisting observations in task-related fMRI studies. Further, we found supportive evidence for a disrupted interaction between the cerebellar and basal ganglia network at rest. Our findings underpin the concept of

dystonia as a network disorder centered around possible basal ganglia and/or cerebellar dysfunction. At the end, functional imaging as applied in this study does not ultimately allow discriminating if the results are an endophenotype or at least in part secondary or compensatory for dystonia. Further study is needed to better understand the underlying structural correlates of the observed neuronal network changes in this disease.

Acknowledgements

We cordially thank all subjects who took part in this study.

Ethics approval

The study has been approved by the local ethics review board and written informed consent was obtained from all subjects.

Funding

This work was supported by the Deutsche Forschungsgemeinschaft (DFG HA3370/5-1), Bonn, Germany.

Disclosures concerning the present manuscript

T.M. has received research support from the KKF (Klinikum rechts der Isar, Muenchen) (E03-15). C.D. has received research support from the German Research Foundation (DFG) (DFG HA3370/3-1) and the KKF (Klinikum rechts der Isar, Muenchen). B.H. receives research support from the German Research Foundation (DFG) (DFG HA3370/5-1) and Ipsen. The other authors report no disclosures.

Full financial disclosures for the previous 12 months

T. Mantel has received travel grants by Merz Pharmaceuticals GmbH, AbbVie Deutschland GmbH and Bayer Vital GmbH. T. Meindl has received travel grants from Merz Pharmaceuticals GmbH, Ipsen Pharma GmbH and Pharm-Allergan GmbH. B.H. receives research support from Ipsen Pharma GmbH and DFG, has received speaker honoraria from Pharm-Allergan GmbH, Bayer Health Care Pharmaceuticals and Ipsen Pharma GmbH and has received travel grants from Ipsen Pharma GmbH and Merz Pharmaceuticals GmbH. He has received royalties for book chapters from Cambridge University Press and Springer Medizin. The other authors report no disclosures.

Appendix A. Supplementary data

Supplementary data to this article can be found online at https://doi.org/10.1016/j.nicl.2017.10.001.

References

Allen, E.A., Erhardt, E.B., Damaraju, E., Gruner, W., Segall, J.M., Silva, R.F., Havlicek, M., Rachakonda, S., Fries, J., Kalyanam, R., Michael, A.M., Caprihan, A., Turner, J.A., Eichele, T., Adelsheim, S., Bryan, A.D., Bustillo, J., Clark, V.P., Feldstein Ewing, S.W., Filbey, F., Ford, C.C., Hutchison, K., Jung, R.E., Kiehl, K.A., Kodituwakku, P., Komesu, Y.M., Mayer, A.R., Pearlson, G.D., Phillips, J.P., Sadek, J.R., Stevens, M., Teuscher, U., Thoma, R.J., Calhoun, V.D., 2011. A baseline for the multivariate comparison of resting-state networks. Front. Syst. Neurosci. 5, 2.

Aziz-Zadeh, L., Koski, L., Zaidel, E., Mazziotta, J., Iacoboni, M., 2006. Lateralization of the human mirror neuron system. J. Neurosci. 26, 2964–2970.

Baumann, O., Borra, R.J., Bower, J.M., Cullen, K.E., Habas, C., Ivry, R.B., Leggio, M., Mattingley, J.B., Molinari, M., Moulton, E.A., Paulin, M.G., Pavlova, M.A., Schmahmann, J.D., Sokolov, A.A., 2015. Consensus paper: the role of the cerebellum in perceptual processes. Cerebellum 14, 197–220.

Beckmann, C.F., DeLuca, M., Devlin, J.T., Smith, S.M., 2005. Investigations into resting-state connectivity using independent component analysis. Philos. Trans. R. Soc. Lond. Ser. B Biol. Sci. 360, 1001–1013.

Bell, A.J., Sejnowski, T.J., 1995. An information-maximization approach to blind separation and blind deconvolution. Neural Comput. 7, 1129–1159.

Biswal, B.B., Van Kylen, J., Hyde, J.S., 1997. Simultaneous assessment of flow and BOLD signals in resting-state functional connectivity maps. NMR Biomed. 10, 165–170.

Calhoun, V.D., Adali, T., Pearlson, G.D., Pekar, J.J., 2001. A method for making group inferences from functional MRI data using independent component analysis. Hum. Brain Mapp. 14, 140–151.

Ceballos-Baumann, A.O., Sheean, G., Passingham, R.E., Marsden, C.D., Brooks, D.J., 1997. Botulinum toxin does not reverse the cortical dysfunction associated with writer's cramp. A PET study. Brain 120 (Pt 4), 571–582.

Celone, K.A., Calhoun, V.D., Dickerson, B.C., Atri, A., Chua, E.F., Miller, S.L., DePeau, K., Rentz, D.M., Selkoe, D.J., Blacker, D., Albert, M.S., Sperling, R.A., 2006. Alterations in memory networks in mild cognitive impairment and Alzheimer's disease: an independent component analysis. J. Neurosci. 26, 10222–10231.

Cordes, D., Haughton, V.M., Arfanakis, K., Carew, J.D., Turski, P.A., Moritz, C.H., Quigley, M.A., Meyerand, M.E., 2001. Frequencies contributing to functional connectivity in the cerebral cortex in "resting-state" data. AJNR Am. J. Neuroradiol. 22, 1326–1333.

Delmaire, C., Krainik, A., Tezenas du Montcel, S., Gerardin, E., Meunier, S., Mangin, J.F., Sangla, S., Garnero, L., Vidailhet, M., Lehericy, S., 2005. Disorganized somatotopy in the putamen of patients with focal hand dystonia. Neurology 64, 1391–1396.

Delmaire, C., Vidailhet, M., Elbaz, A., Bourdain, F., Bleton, J.P., Sangla, S., Meunier, S., Terrier, A., Lehericy, S., 2007. Structural abnormalities in the cerebellum and sensorimotor circuit in writer's cramp. Neurology 69, 376–380.

Delnooz, C.C., Helmich, R.C., Toni, I., van de Warrenburg, B.P., 2012. Reduced parietal connectivity with a premotor writing area in writer's cramp. Mov. Disord. 27, 1425–1431.

Dresel, C., Li, Y., Wilzeck, V., Castrop, F., Zimmer, C., Haslinger, B., 2014. Multiple changes of functional connectivity between sensorimotor areas in focal hand dystonia. J. Neurol. Neurosurg. Psychiatry 85, 1245–1252.

Eickhoff, S.B., Grefkes, C., Fink, G.R., Zilles, K., 2008. Functional lateralization of face, hand, and trunk representation in anatomically defined human somatosensory areas. Cereb. Cortex 18, 2820–2830.

Fox, M.D., Raichle, M.E., 2007. Spontaneous fluctuations in brain activity observed with functional magnetic resonance imaging. Nat. Rev. Neurosci. 8, 700–711.

Furuya, S., Nitsche, M.A., Paulus, W., Altenmuller, E., 2014. Surmounting retraining limits in musicians' dystonia by transcranial stimulation. Ann. Neurol. 75, 700–707.

Gallea, C., Horovitz, S.G., Ali Najee-Ullah, M., Hallett, M., 2016. Impairment of a parieto-premotor network specialized for handwriting in writer's cramp. Hum. Brain Mapp. 37, 4363–4375.

Granert, O., Peller, M., Jabusch, H.C., Altenmuller, E., Siebner, H.R., 2011. Sensorimotor skills and focal dystonia are linked to putaminal grey-matter volume in pianists. J. Neurol. Neurosurg. Psychiatry 82, 1225–1231.

Grefkes, C., Fink, G.R., 2005. The functional organization of the intraparietal sulcus in humans and monkeys. J. Anat. 207, 3–17.

Griffanti, L., Salimi-Khorshidi, G., Beckmann, C.F., Auerbach, E.J., Douaud, G., Sexton, C.E., Zsoldos, E., Ebmeier, K.P., Filippini, N., Mackay, C.E., Moeller, S., Xu, J., Yacoub, E., Baselli, G., Ugurbil, K., Miller, K.L., Smith, S.M., 2014. ICA-based artefact removal and accelerated fMRI acquisition for improved resting state network imaging. NeuroImage 95, 232–247.

Hallett, M., 2006. Pathophysiology of writer's cramp. Hum. Mov. Sci. 25, 454–463.

Hamano, T., Kaji, R., Katayama, M., Kubori, T., Ikeda, A., Shibasaki, H., Kimura, J., 1999. Abnormal contingent negative variation in writer's cramp. Clin. Neurophysiol. 110, 508–515.

Hamzei, F., Dettmers, C., Rzanny, R., Liepert, J., Buchel, C., Weiller, C., 2002. Reduction of excitability ("inhibition") in the ipsilateral primary motor cortex is mirrored by fMRI signal decreases. NeuroImage 17, 490–496.

Haslinger, B., Noe, J., Altenmuller, E., Riedl, V., Zimmer, C., Mantel, T., Dresel, C., 2016. Changes in Resting-State Connectivity in Musicians with Embouchure Dystonia. (Mov Disord).

Himberg, J., Hyvarinen, A., Esposito, F., 2004. Validating the independent components of neuroimaging time series via clustering and visualization. NeuroImage 22, 1214–1222.

Hoshi, E., Tanji, J., 2007. Distinctions between dorsal and ventral premotor areas: anatomical connectivity and functional properties. Curr. Opin. Neurobiol. 17, 234–242.

Hubsch, C., Roze, E., Popa, T., Russo, M., Balachandran, A., Pradeep, S., Mueller, F., Brochard, V., Quartarone, A., Degos, B., Vidailhet, M., Kishore, A., Meunier, S., 2013. Defective cerebellar control of cortical plasticity in writer's cramp. Brain 136, 2050–2062.

Ibanez, V., Sadato, N., Karp, B., Deiber, M.P., Hallett, M., 1999. Deficient activation of the motor cortical network in patients with writer's cramp. Neurology 53, 96–105.

Kelly Jr., R.E., Alexopoulos, G.S., Wang, Z., Gunning, F.M., Murphy, C.F., Morimoto, S.S., Kanellopoulos, D., Jia, Z., Lim, K.O., Hoptman, M.J., 2010. Visual inspection of independent components: defining a procedure for artifact removal from fMRI data. J. Neurosci. Methods 189, 233–245.

Koch, W., Teipel, S., Mueller, S., Benninghoff, J., Wagner, M., Bokde, A.L., Hampel, H., Coates, U., Reiser, M., Meindl, T., 2012. Diagnostic power of default mode network resting state fMRI in the detection of Alzheimer's disease. Neurobiol. Aging 33, 466–478.

Laird, A.R., Fox, P.M., Eickhoff, S.B., Turner, J.A., Ray, K.L., McKay, D.R., Glahn, D.C., Beckmann, C.F., Smith, S.M., Fox, P.T., 2011. Behavioral interpretations of intrinsic connectivity networks. J. Cogn. Neurosci. 23, 4022–4037.

Langbour, N., Michel, V., Dilharreguy, B., Guehl, D., Allard, M., Burbaud, P., 2017. The cortical processing of sensorimotor sequences is disrupted in writer's cramp. Cereb. Cortex 27, 2544–2559.

LeDoux, M.S., Brady, K.A., 2003. Secondary cervical dystonia associated with structural lesions of the central nervous system. Mov. Disord. 18, 60–69.

Lerner, A., Shill, H., Hanakawa, T., Bushara, K., Goldfine, A., Hallett, M., 2004. Regional cerebral blood flow correlates of the severity of writer's cramp symptoms.

NeuroImage 21, 904–913.
Magri, C., Schridde, U., Murayama, Y., Panzeri, S., Logothetis, N.K., 2012. The amplitude and timing of the BOLD signal reflects the relationship between local field potential power at different frequencies. J. Neurosci. 32, 1395–1407.
Meunier, S., Garnero, L., Ducorps, A., Mazieres, L., Lehericy, S., du Montcel, S.T., Renault, B., Vidailhet, M., 2001. Human brain mapping in dystonia reveals both endophenotypic traits and adaptive reorganization. Ann. Neurol. 50, 521–527.
Mink, J.W., 1996. The basal ganglia: focused selection and inhibition of competing motor programs. Prog. Neurobiol. 50, 381–425.
Mohammadi, B., Kollewe, K., Samii, A., Beckmann, C.F., Dengler, R., Munte, T.F., 2012. Changes in resting-state brain networks in writer's cramp. Hum. Brain Mapp. 33, 840–848.
Moore, R.D., Gallea, C., Horovitz, S.G., Hallett, M., 2012. Individuated finger control in focal hand dystonia: an fMRI study. NeuroImage 61, 823–831.
Nagai, Y., Critchley, H.D., Featherstone, E., Fenwick, P.B., Trimble, M.R., Dolan, R.J., 2004. Brain activity relating to the contingent negative variation: an fMRI investigation. NeuroImage 21, 1232–1241.
Naumann, M., Magyar-Lehmann, S., Reiners, K., Erbguth, F., Leenders, K.L., 2000. Sensory tricks in cervical dystonia: perceptual dysbalance of parietal cortex modulates frontal motor programming. Ann. Neurol. 47, 322–328.
Nelson, A.J., Blake, D.T., Chen, R., 2009. Digit-specific aberrations in the primary somatosensory cortex in writer's cramp. Ann. Neurol. 66, 146–154.
Nelson, A.J., Hoque, T., Gunraj, C., Ni, Z., Chen, R., 2010. Impaired interhemispheric inhibition in writer's cramp. Neurology 75, 441–447.
Neumann, W.J., Jha, A., Bock, A., Huebl, J., Horn, A., Schneider, G.H., Sander, T.H., Litvak, V., Kuhn, A.A., 2015. Cortico-pallidal oscillatory connectivity in patients with dystonia. Brain 138, 1894–1906.
Neychev, V.K., Fan, X., Mitev, V.I., Hess, E.J., Jinnah, H.A., 2008. The basal ganglia and cerebellum interact in the expression of dystonic movement. Brain 131, 2499–2509.
Neychev, V.K., Gross, R.E., Lehericy, S., Hess, E.J., Jinnah, H.A., 2011. The functional neuroanatomy of dystonia. Neurobiol. Dis. 42, 185–201.
Niehaus, L., von Alt-Stutterheim, K., Roricht, S., Meyer, B.U., 2001. Abnormal post-excitatory and interhemispheric motor cortex inhibition in writer's cramp. J. Neurol. 248, 51–56.
Nowak, D.A., Rosenkranz, K., Topka, H., Rothwell, J., 2005. Disturbances of grip force behaviour in focal hand dystonia: evidence for a generalised impairment of sensory-motor integration? J. Neurol. Neurosurg. Psychiatry 76, 953–959.
Odergren, T., Stone-Elander, S., Ingvar, M., 1998. Cerebral and cerebellar activation in correlation to the action-induced dystonia in writer's cramp. Mov. Disord. 13, 497–508.
Oga, T., Honda, M., Toma, K., Murase, N., Okada, T., Hanakawa, T., Sawamoto, N., Nagamine, T., Konishi, J., Fukuyama, H., Kaji, R., Shibasaki, H., 2002. Abnormal cortical mechanisms of voluntary muscle relaxation in patients with writer's cramp: an fMRI study. Brain 125, 895–903.
Peller, M., Zeuner, K.E., Munchau, A., Quartarone, A., Weiss, M., Knutzen, A., Hallett, M., Deuschl, G., Siebner, H.R., 2006. The basal ganglia are hyperactive during the discrimination of tactile stimuli in writer's cramp. Brain 129, 2697–2708.
Power, J.D., Mitra, A., Laumann, T.O., Snyder, A.Z., Schlaggar, B.L., Petersen, S.E., 2014. Methods to detect, characterize, and remove motion artifact in resting state fMRI. NeuroImage 84, 320–341.
Preibisch, C., Berg, D., Hofmann, E., Solymosi, L., Naumann, M., 2001. Cerebral activation patterns in patients with writer's cramp: a functional magnetic resonance imaging study. J. Neurol. 248, 10–17.
Quartarone, A., Hallett, M., 2013. Emerging concepts in the physiological basis of dystonia. Mov. Disord. 28, 958–967.
Rajapakse, J.C., Giedd, J.N., Rapoport, J.L., 1997. Statistical approach to segmentation of single-channel cerebral MR images. IEEE Trans. Med. Imaging 16, 176–186.
Restuccia, D., Valeriani, M., Barba, C., Le Pera, D., Capecci, M., Filippini, V., Molinari, M., 2001. Functional changes of the primary somatosensory cortex in patients with unilateral cerebellar lesions. Brain 124, 757–768.
Rijntjes, M., Dettmers, C., Buchel, C., Kiebel, S., Frackowiak, R.S., Weiller, C., 1999. A blueprint for movement: functional and anatomical representations in the human motor system. J. Neurosci. 19, 8043–8048.
Rizzolatti, G., Fogassi, L., Gallese, V., 2002. Motor and cognitive functions of the ventral premotor cortex. Curr. Opin. Neurobiol. 12, 149–154.
Scheperjans, F., Eickhoff, S.B., Homke, L., Mohlberg, H., Hermann, K., Amunts, K., Zilles, K., 2008. Probabilistic maps, morphometry, and variability of cytoarchitectonic areas in the human superior parietal cortex. Cereb. Cortex 18, 2141–2157.
Schluter, N.D., Rushworth, M.F., Passingham, R.E., Mills, K.R., 1998. Temporary interference in human lateral premotor cortex suggests dominance for the selection of movements. A study using transcranial magnetic stimulation. Brain 121 (Pt 5), 785–799.
Shakkottai, V.G., Batla, A., Bhatia, K., Dauer, W.T., Dresel, C., Niethammer, M., Eidelberg, D., Raike, R.S., Smith, Y., Jinnah, H.A., Hess, E.J., Meunier, S., Hallett, M., Fremont, R., Khodakhah, K., LeDoux, M.S., Popa, T., Gallea, C., Lehericy, S., Bostan, A.C., Strick, P.L., 2017. Current opinions and areas of consensus on the role of the cerebellum in dystonia. Cerebellum 16, 577–594.
Sheehy, M.P., Marsden, C.D., 1982. Writers' cramp-a focal dystonia. Brain 105 (Pt 3), 461–480.
Smith, S.M., Fox, P.T., Miller, K.L., Glahn, D.C., Fox, P.M., Mackay, C.E., Filippini, N., Watkins, K.E., Toro, R., Laird, A.R., Beckmann, C.F., 2009. Correspondence of the brain's functional architecture during activation and rest. Proc. Natl. Acad. Sci. U. S. A. 106, 13040–13045.
Stamelou, M., Edwards, M.J., Hallett, M., Bhatia, K.P., 2012. The non-motor syndrome of primary dystonia: clinical and pathophysiological implications. Brain 135, 1668–1681.
Tamburin, S., Fiaschi, A., Marani, S., Andreoli, A., Manganotti, P., Zanette, G., 2004. Enhanced intracortical inhibition in cerebellar patients. J. Neurol. Sci. 217, 205–210.
Wu, X., Li, R., Fleisher, A.S., Reiman, E.M., Guan, X., Zhang, Y., Chen, K., Yao, L., 2011. Altered default mode network connectivity in Alzheimer's disease—a resting functional MRI and Bayesian network study. Hum. Brain Mapp. 32, 1868–1881.

Table A.1: Demographic and clinical characteristics of patients with writer's cramp and healthy controls

PAT							CONTR		
	sex	**age**	**phenotype**	**disease duration, y**	**ADDS, %**	**WCRS**		**sex**	**age**
P1	f	45	dystonic	19	25	15	**C1**	m	58
P2	m	63	simple	20	65	6	**C2**	f	60
P3	m	22	simple	2	75	4	**C3**	f	67
P4	m	39	dystonic	5	55	5	**C4**	m	55
P5	f	47	simple	4	80	4	**C5**	m	49
P6	f	29	dystonic	2	58	18	**C6**	m	59
P7	m	54	dystonic	38	25	20	**C7**	f	50
P8	f	64	dystonic	22	80	9	**C8**	m	67
P9	f	60	simple	27	75	11	**C9**	m	32
P10	m	35	dystonic	13	70	9	**C10**	f	66
P11	f	55	simple	7	75	11	**C11**	f	47
P12	f	44	simple	2	65	10	**C12**	f	36
P13	m	60	dystonic	24	0	22	**C13**	m	55
P14	f	32	dystonic	15	69	22	**C14**	m	50
P15	m	25	simple	2	80	12	**C15**	f	61
P16	f	67	simple	30	66	14	**C16**	m	43
P17	m	49	simple	27	55	6	**C17**	f	59
P18	m	48	dystonic	17	40	8	**C18**	m	35
P19	m	53	dystonic	27	50	12	**C19**	f	68
P20	m	52	simple	11	80	9	**C20**	m	24
P21	f	60	simple	6	77	3	**C21**	f	24
P22	f	23	simple	9	80	14	**C22**	m	62
P23	m	41	simple	3	65	13	**C23**	m	44
P24	m	56	dystonic	7	45	14	**C24**	f	43
P25	m	63	dystonic	2	60	14	**C25**	f	28
P26	m	32	simple	2	65	18	**C26**	m	59
—	—	—	—	—	—	—	**C27**	f	29
Mean (SD)	NA	46.8 (13.7)	NA	13.2 (10.8)	60.8 (20.1)	11.7 (5.4)	**Mean (SD)**	NA	49.3 (13.9)

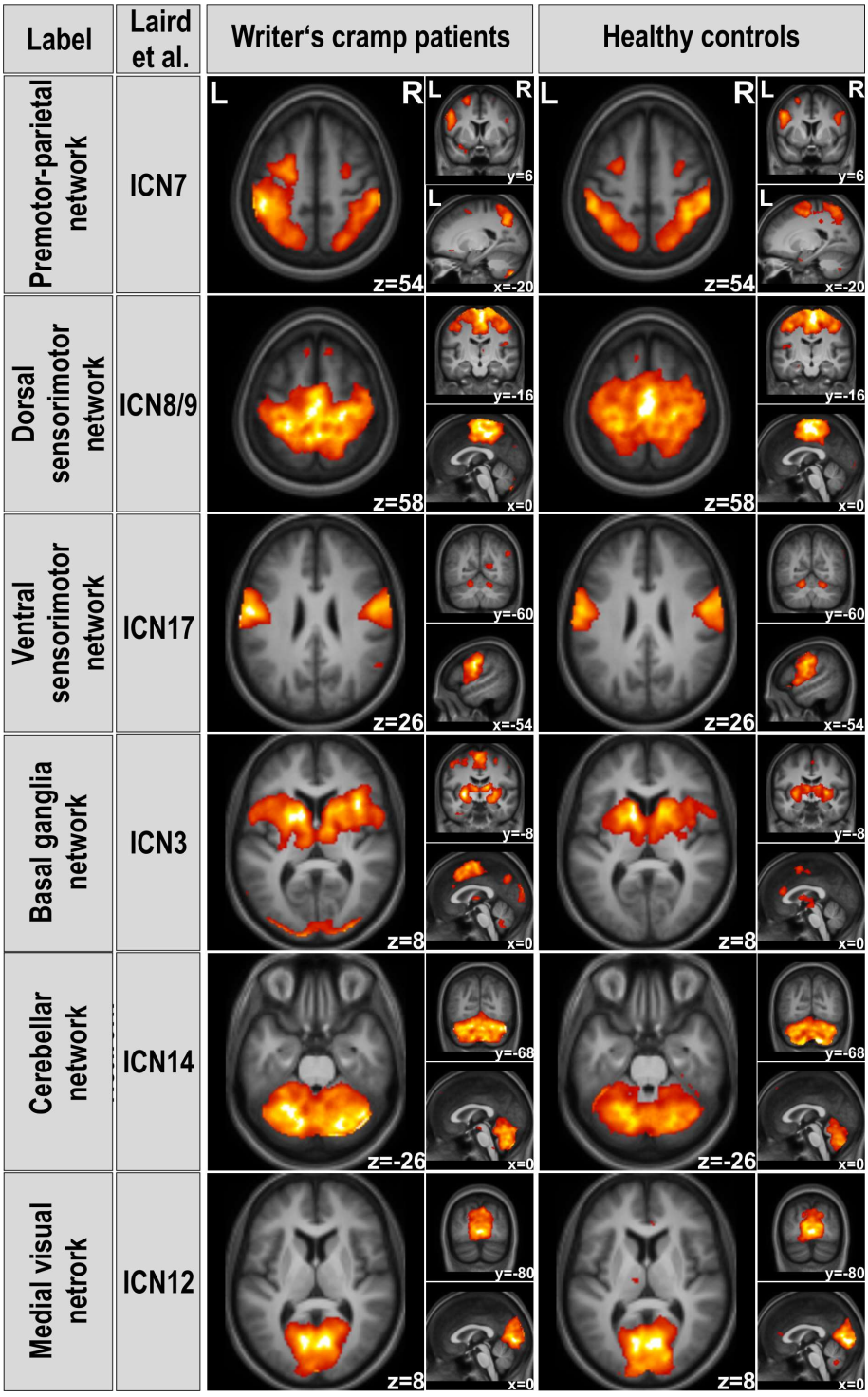

Figure A.1. Composition of the six intrinsic connectivity networks selected for analysis in both groups. Areas with significant functional connectivity at p(FDR)<.0083, $p_{cluster}$(FWE)<.05 are overlaid onto axial, coronal and sagittal slices of the participants' averaged normalized T1 images. The middle column identifies the corresponding network in Laird et al., 2011; Laird's ICNs 8 and 9 were not split in the present study, as also seen in earlier reports (Smith et al., 2009). The slice position in MNI space in mm is given relative to the anterior commissure (z: above/below [+]/[-]-; y: rostral/caudal [+]/[-], x: right/left [+]/[-]). L/R, left/right hemisphere; ICN, intrinsic connectivity network.

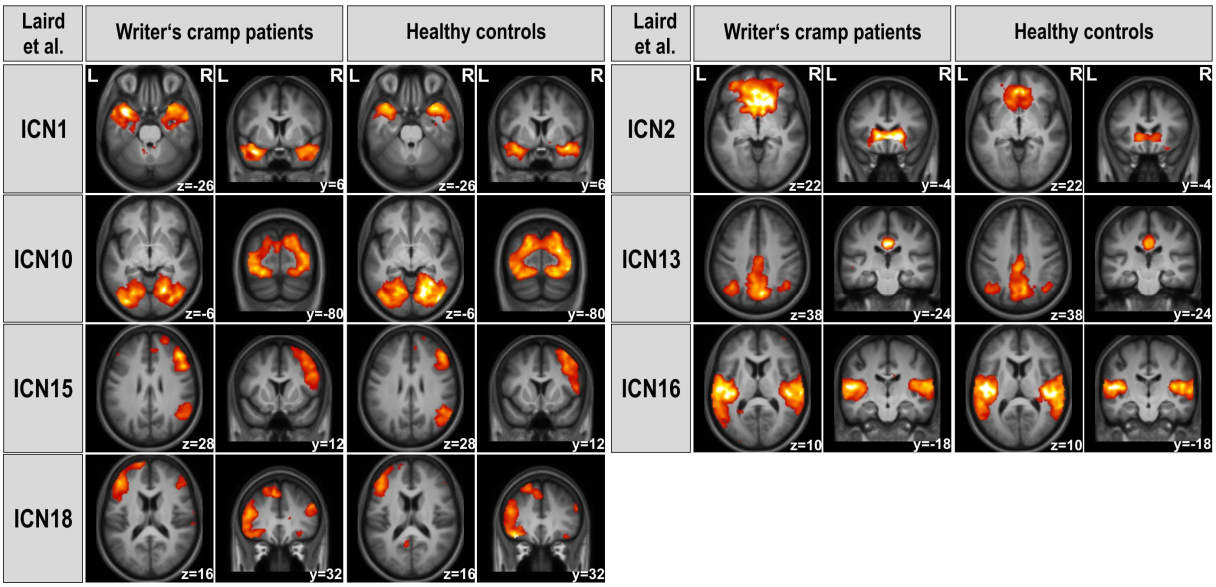

Figure A.2. Overview of other identified networks not selected for analysis. Areas with significant functional connectivity at p(FDR)<.0083, $p_{cluster}$(FWE)<.05 are overlaid onto axial and coronal slices of the participants' averaged normalized T1 images. The annotation identifies the corresponding network in Laird et al., 2011. The slice position in MNI space in mm is given relative to the anterior commissure (z: above/below [+]/[-], y: rostral/caudal [+]/[-],). L/R, left/right hemisphere; ICN, intrinsic connectivity network.

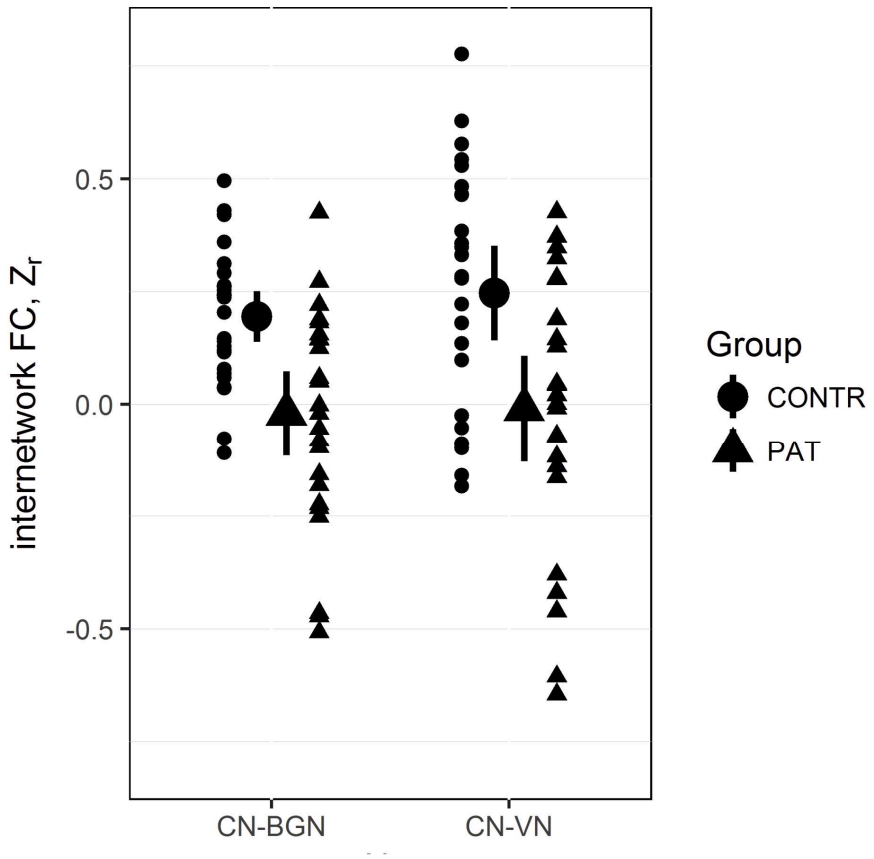

Figure A.3. Dot plot of the inter-network FC between the cerebellar network and the basal ganglia network (left)/medial visual network (right). Dots represent the Fisher's z-transformed Pearson correlation coefficients (z_r) of the motion-regressed, detrended, despiked and filtered time courses. Error bars depict the double standard error of mean. PAT, writer's cramp patients; CONTR, healthy controls; BGN, basal ganglia network; CN, cerebellar network; VN, medial visual network.

Parkinsonism and Related Disorders xxx (xxxx) xxx–xxx

Contents lists available at ScienceDirect

Parkinsonism and Related Disorders

journal homepage: www.elsevier.com/locate/parkreldis

Abnormalities in grey matter structure in embouchure dystonia

Tobias Mantel[a], Eckart Altenmüller[b], Yong Li[a], Tobias Meindl[a], Angela Jochim[a], André Lee[a], Claus Zimmer[c], Christian Dresel[a,d], Bernhard Haslinger[a,*]

[a] Department of Neurology, Klinikum rechts der Isar, Technische Universität München, Ismaningerstrasse 22, Munich, Germany
[b] Hochschule für Musik, Theater und Medien Hannover, Emmichplatz 1, Hanover, Germany
[c] Department of Neuroradiology, Klinikum rechts der Isar, Technische Universität München, Ismaningerstrasse 22, Munich, Germany
[d] Department of Neurology, Johannes Gutenberg University, Langenbeckstrasse 1, Mainz, Germany

ARTICLE INFO

Keywords:
Musician's dystonia
Sensorimotor cortex
MRI
Plasticity
Neuronal

ABSTRACT

Introduction: Embouchure dystonia (ED) is a debilitating movement disorder in professional brass players leading to involuntary muscle contractions/spasms during play. To date, activity changes in sensorimotor cortices during motor tasks and tactile processing, as well as connectivity changes at rest in sensorimotor and auditory brain networks have been described in the disease.
Objective: To characterize differences in grey matter volume and asymmetry between brass musicians suffering from ED, healthy brass musicians and healthy nonmusicians.
Methods: High-resolution structural magnetic resonance imaging was obtained from 24 brass musicians with ED, 23 healthy brass musicians and 24 healthy nonmusicians. Whole-brain voxel-wise morphometry and asymmetry analyses, as well as region-of-interest-based volumetry analysis were performed on the subjects' images and compared between groups. Further, correlations with clinical parameters were investigated.
Results: ED patients showed increased grey matter volume in the primary sensorimotor cortex in relation to both healthy brass players and nonmusicians. Both healthy and diseased musicians showed increased thalamic symmetry in relation to nonmusicians; diseased brass musicians additionally showed increased basal ganglia symmetry compared to nonmusicians. There was an inverse correlation of disease duration with both mean putaminal volume and the extent of basal ganglia asymmetry.
Conclusion: This work provides first evidence for structural abnormalities in task-specific orofacial (musician's) dystonia. Somatotopy-related structural primary sensorimotor cortex changes underlying previously observed functional abnormalities underscore the role of maladaptive plasticity in the disease. The study further shows subcortical brain (a)symmetry changes in healthy brass players and hints at a possible role of such changes in focal dystonia.

1. Introduction

Focal dystonia (FD) is characterized by involuntary activity of agonist and antagonist muscles in the affected body region, leading to loss of fine motor control. In embouchure dystonia (ED), those involuntary movements affect the orofacial muscles of professional brass musicians specifically during play (task-specific focal dystonia, TSFD), most often marking the end of their professional career [1]. Functional neuroimaging in ED showed increased activity in primary and higher-order sensorimotor cortices, cerebellum and/or basal ganglia (BG), either during dystonic/nondystonic motor tasks or tactile stimulation of dystonic/nondystonic body parts [2,3]. Further, abnormal resting-state functional connectivity within sensoriomotor, cerebellar and auditory networks was seen [4]. While grey matter (GM) structure has mostly been investigated for FD of hand and neck describing abnormality in sensorimotor cortices, BG and cerebellum, it has not yet been characterized in TSFD of the orofacial muscles [5]. Furthermore, healthy professional musicians themselves also display both structural and functional changes in the sensorimotor and cerebellar cortices [6] including changes in brain symmetry [7]. Besides possible

Abbreviations: ADDS, arm dystonia disability scale; AI, asymmetry index; BG, basal ganglia; CON, healthy nonmusicians; ED, embouchure dystonia; FD, focal dystonia; FWHM, full width at half maximum; GM, grey matter; GMV, grey matter volume; MuCON, healthy professional brass players; PAT, brass players with embouchure dystonia; ROI, region of interest; TIV, total intracranial volume; TSFD, task-specific focal dystonia

* Corresponding author. Klinik und Poliklinik für Neurologie, Klinikum rechts der Isar, Technische Universität München, Ismaninger Strasse 22, D - 81675, München, Germany.
E-mail address: bernhard.haslinger@tum.de (B. Haslinger).

https://doi.org/10.1016/j.parkreldis.2019.05.008
Received 30 November 2018; Received in revised form 19 March 2019; Accepted 5 May 2019
1353-8020/

endophenotypic traits advantageous for acquisition of highly-skilled movements, these changes are largely assumed to occur in response to intensive instrumental practice, and possible instrument-specific characteristics have been proposed [8]. Yet, neuroimaging literature is sparse regarding wind instruments in healthy subjects [9]. This study hence aimed at characterizing the abnormalities in GM structure and (a)symmetry between professional brass players suffering from the task-specific orofacial ED, healthy brass playing professionals and healthy nonmusicians.

2. Methods

2.1. Participants

We compared 24 professional brass players with ED (PAT; m/f = 21/3, age = 43.5 ± 11.2 years) recruited from the institute for music physiology and musicians medicine in Hanover with 23 professional healthy brass musicians (MuCON; m/f = 22/1, age = 42.4 ± 11.2 years) from local professional orchestras/conservatories and 24 healthy nonmusician controls (CON; m/f = 18/6, age = 42.7 ± 11.9 years; inclusion criteria see supplement). The university ethics board approved the study and all participants gave their informed consent according to the Declaration of Helsinki. For clinical rating of dystonia severity, all healthy/diseased brass musicians performed a videotaped standardized play as performed in previous studies [2–4]. As sensitive and established scales for rating of ED are yet lacking (i.e. ratings such as the Burke-Fahn-Marsden/Tubiana-Chamagne score are not sensitive for ED-specific symptoms such as deterioration of sound, attack of the tongue etc.) [10], the play was blindly rated by an expert in ED (E.A.) according to an ordinal scale specifically tailored for ED (Table 1) as previously performed [2–4]. To take possible coincidence of writer's cramp in ED into account, we screened PAT with the arm dystonia disability scale (ADDS). Between-group differences in age, sex, total intracranial volume (TIV) as well as (for musicians) age at start of play, duration of active period, daily musical practice at time of the study, and ED score were tested for using parametric/nonparametric tests in SPSS25 wherever appropriate.

2.2. Data acquisition

Anatomic high-resolution MRI scans were acquired on one Philips Achieva 3.0 T scanner (Philips, Amsterdam, The Netherlands) equipped with an 8-channel head coil using a magnetization-prepared rapid-acquisition gradient-echo sequence (repetition/echo/inversion time 9/4/780 ms, field-of-view 240 × 240mm^2, 170 slices, voxel size 1 × 1 × 1mm^3, scan time 6min).

2.3. Voxel-based morphometry (VBM) analysis

Morphometric analysis was performed with the CAT12 toolbox (http://dbm.neuro.uni-jena.de/cat/) for SPM12b (http://www.fil.ion.ucl.ac.uk/spm/) and Matlab16b (The MathWorks Inc., Natick, USA) using standard parameters. After denoising, inhomogeneity correction and affine registration, the skull-stripped anatomical scans were tissue-segmented followed by diffeomorphic anatomical registration using lie algebra (DARTEL) to the default DARTEL_IXI555 Montreal Neurological Institute (MNI) space template with a final voxel size of 1 mm^3. Modulation of GM segments was performed by multiplication with the Jacobian determinant. Normalized data were smoothed with a 10 mm full-width-at-half-maximum (FWHM) Gaussian kernel. Between-group comparison was performed by implementing a full factorial random effects model adjusted for sex, age and TIV with absolute threshold masking of 0.1. Results of the whole-brain analysis at a cluster-forming (peak-level) threshold of $p < 0.001$ were family-wise error (FWE)-corrected for multiple comparisons at the cluster level ($p_{FWEc} < 0.05$).

2.4. Voxel-based asymmetry (VBA) analysis

Asymmetry analysis was performed based on a voxel-wise approach outlined by Kurth and colleagues [11]. To achieve the required accurate correspondence for voxel-wise comparisons (as the same brain structures can differ in spatial location between hemispheres), the structural MRI scans were first segmented and affine registered to a symmetric tissue probability map provided by Kurth and coworkers [11]. The resulting grey and white matter segments were then flipped at the midline. Subsequently, both flipped and non-flipped (original) segments were nonlinearly warped to a custom symmetric DARTEL_IXI555 MNI space template (previously created from segmented, flipped and non-flipped grey and white matter segments from 555 subjects of the publicly available IXI dataset (https://brain-development.org) using CAT12 default parameters) using DARTEL. Normalized data were modulated by multiplication with the Jacobian determinant. Next, voxel-wise asymmetry indices (AIs) were calculated from each subject's flipped and non-flipped modulated normalized GM segments ($AI = \frac{(original - flipped)}{0.5\,x\,(original + flipped)}$) so that in the right hemisphere positive AI values indicated rightward, and negative values indicate leftward asymmetry (in the left hemisphere vice versa). To eliminate redundant information, the left hemisphere was discarded through multiplication with a right-hemispheric mask. AI maps were smoothed with a 10 mm FWHM Gaussian kernel. Between-group comparisons were performed with a full factorial random effects model adjusted for sex and age at voxels with a mean GM value > 0.1 [11]. Results were corrected for multiple comparisons at the cluster level ($p_{FWEc} < 0.05$) at a peak-level threshold of $p < 0.001$ uncorrected. As results from voxel-wise group

Table 1
Clinical and demographic data.

	brass musicians with ED		healthy brass musicians	healthy non-musicians
Age, y (mean, SD)	43.5, 11.2		42.4, 11.2	42.7, 11.9
Sex (m/f)	23/3		22/1	18/6
TIV, cm^3 (mean, SD)	1602.6, 126.1		1582.4, 135.2	1527.9, 156.0
instrument (horn/trumpet/trombone)	9/7/8		12/5/6	NA
Age at start of play, y (mean, SD)	10.5, 2.5		10.7, 3.8	NA
Daily play, h (median, IQR)	before ED	with ED	2.5, 1.13	NA
	3.8, 1.3	1.0, 2.0		
ED score (median, IQR)[a]	3, 1.25		1, 1.0	NA

SD = standard deviation; IQR = interquartile range; y = years; h = hours; TIV = total intracranial volume; m = male; f = female; NA = not applicable.
1 = normal play, 2 = nearly normal play, not distinctly dystonic; 3–5 = abnormal playing with evidence of dystonic orofacial movements (minor/medium/severe degree).
[a] Embouchure dystonia score (dystonic symptom rating during performance of standardized sequences).

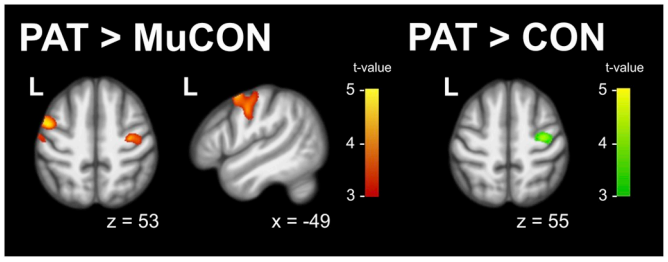

Fig. 1. Areas with significant increase in GM volume in PAT compared to MuCON (in red) and CON (in green), projected on the averaged anatomical scan from all 71 participants. Overlaid statistical parametric maps were thresholded at the cluster level ($p_{FWEc} < 0.05$). Slice position is given in MNI space in millimeters relative to the anterior commissure. PAT, patients with embouchure dystonia, MuCON, healthy brass players, CON, healthy nonmusicians. (For interpretation of the references to colour in this figure legend, the reader is referred to the Web version of this article.)

analysis cannot directly be interpreted unequivocally (e.g. a significant cluster in a positive contrast can indicate less negative or more positive AI values), the cluster-specific i) mean AIs and ii) mean left- and right-hemispheric GM volumes (GMVs) were extracted for significant clusters in each subject for post-hoc evaluation to determine i) the directionality of asymmetry, and ii) if the altered (a)symmetry was driven by focal GM changes in one hemisphere. To exclude bias by global hemispheric asymmetry, the hemispheric GMVs were calculated and compared between groups.

2.5. Atlas-based volumetry (ABV) analysis

To compensate possible method-related sensitivity/spatial specificity limitations of VBM, we additionally analyzed the mean GMV in macroanatomical atlas-defined regions of interest (ROIs) with putative role in idiopathic FD. To ensure unbiased ROI selection, respective brain areas were identified through activation likelihood estimation meta-analysis of existing VBM studies in FD (selection criteria see supplement) using the revised algorithm by Turkeltaub and colleagues (GingerALEv2.3.6, http://brainmap.org/ale/) [12]. This approach models entered activation foci from the literature as centroids of 3D Gaussian probability distributions, accounting for spatial uncertainty of neuroimaging data. The null distribution of cluster excursions for cluster threshold generation was established by calculating 5000 permutations of random distributions of activation foci throughout the brain using the toolbox-implemented nonparametric Monte Carlo method. Correction was performed at the cluster-level ($p_{FWEc} < 0.05$) at a cluster-forming threshold of $p < 0.001$ uncorrected [13]. Based on the meta-analysis results, we selected anatomical bilateral ROIs from the Harvard Oxford atlas (who showed good fit in all investigated regions verified by visual inspection; figure s-2) for brain regions within ± 9 mm (average smoothing kernel of all included studies) of the meta-analysis clusters' peak location to take the spatial uncertainty induced by smoothing into account. Next, mean GMV in each ROI were extracted from each subjects' unsmoothed segmented, normalized modulated GM images and statistically compared between-groups in SPSS25 in an analysis of variance adjusted for age, sex and TIV ($p < 0.05$) with a Bonferroni-adjusted post-hoc analysis.

2.6. Regression analyses

Possible linear correlations of "dystonia severity defined by ED score" and "disease duration (years)" with voxel-wise GM values (VBM analysis), volumetry-based mean GMVs (ABV analysis) and voxel-wise AI values (VBA analysis) in PAT were investigated using regression analyses in SPM12b and SPSS25 respectively. Nuisance regressors/correction for multiple comparisons were set as for between-group analyses, with additional Bonferroni-correction for two investigated covariates of interest. For voxel-wise analyses, voxels showing a significant main effect in the between-group comparisons were a-priori defined as volume of interest and small volume correction was applied.

3. Results

Statistical analysis did not show significant difference in brain volumes/demographic characteristics between-groups (ps > 0.05). There was no significant difference in average daily instrument play between MuCON and PAT before disease onset. After disease onset, daily practice abated ($z = -3.83$, $p < 0.001$), also compared to their healthy colleagues ($W_s = 411.5$, $z = -3.52$, $p < 0.001$). Mean disease duration was 7.2 ± 6.7 years and was not associated with years of musical practice ($r = -0.04$, $p = 0.84$). PAT screening by ADDS showed no signs of hand dystonia (99.6 ± 1.4%). PAT video ED rating scores were significantly higher than in MuCON ($W_s = 338.5$, $z = -4.87$, $p < 0.001$). A rating of three in one single healthy player was attributed to the setting of videotaped scoring, as the subject did not suffer from dystonic symptoms/impairment in clinical exam and history.

3.1. VBM analysis

Between-group contrasts revealed significantly increased GMV in the precentral gyrus (PreCG) and sulcus and the postcentral gyrus (PoCG) in the left, and the PreCG in the right hemisphere in PAT compared to MuCON. Compared to CON, GMV in PAT was increased in

Table 2
A. Changes of local grey matter volume between groups. B. Changes of local grey matter asymmetry between groups.

A.					
Effect of group					
	peak coordinate				
Region	**x**	**y**	**z**	**extent (voxel)**	**F score**
R precental gyrus (BA4)	36	−14	56	2485	14.88
R precentral gyrus (BA4)	40	−18	60		12.89
PAT > MuCON					
Region	**x**	**y**	**z**	**extent (voxel)**	**t score**
L precentral sulcus (BA6)	−44	0	54	5063	4.86
L precentral gyrus (BA4)	−52	−8	40		4.33
L postcentral gyrus (BA1)	−52	−14	54		3.45
R precentral gyrus (BA4)	36	−14	56	3427	4.97
PAT > CON					
Region	**x**	**y**	**z**	**extent (voxel)**	**t score**
R precentral gyrus (BA6)	34	−12	56	3974	4.42
R precentral gyrus (BA6)	32	−8	64		4.09
R postcentral gyrus (BA3)	18	−34	62		4.01
B.					
Effect of group					
	peak coordinate				
Region	**x**	**y**	**z**	**extent (voxel)**	**F score**
Thalamus	16	−21	13	5390	25.46
Putamen	31	−6	1		12.20
PAT vs. CON					
Region	**x**	**y**	**z**	**extent (voxel)**	**t score**
Thalamus	16	−21	13	9431	7.13
Putamen	31	−5	1		4.91
Insula	43	−9	2		3.71
MuCON vs. CON					
Region	**x**	**y**	**z**	**extent (voxel)**	**t score**
Thalamus	23	−15	13	2196	5.03

Coordinates (mm) in the Montreal Neurological Institute space. Displayed grey matter volume/asymmetry index differences significant at $p_{FWEc} < 0.05$. PAT = brass players with ED; MuCON = healthy brass players; CON = healthy non-musicians. R = right hemisphere; L = left hemisphere.

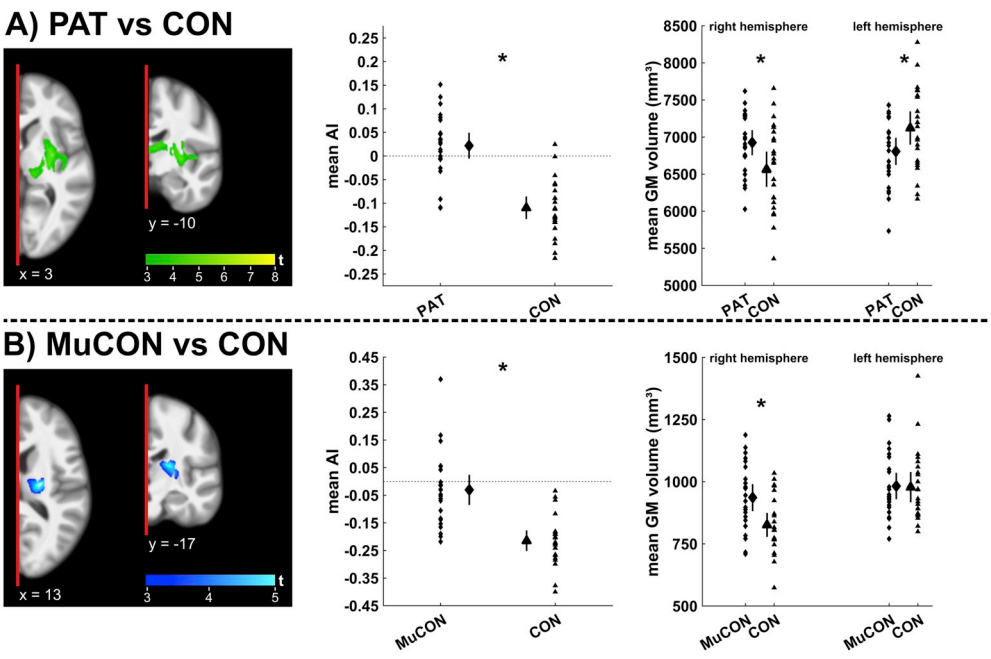

Fig. 2. Areas with significantly altered grey matter asymmetry in (A) PAT and (B) MuCON compared to CON. Left column: Areas with significantly higher asymmetry indices in patients (in green)/healthy brass players (in blue) projected on the right hemisphere of the averaged anatomical scan of all participants. Overlaid statistical parametric maps were thresholded at the cluster level $p_{FWEc} < 0.05$. Slice position is given in MNI space in millimeters relative to the anterior commissure. Middle column: Dot plot of cluster-specific mean AIs in each group. Right column: Dot plot of cluster-specific grey matter volumes in the right and left hemisphere in both groups. Error bars depict the double standard error of mean. Asterisks depict significant differences ($p < 0.05$) during exploratory analysis. AI, asymmetry index, GM, grey matter; CON, healthy nonmusicians (triangles); MuCON, healthy brass players (diamonds); PAT, patients with embouchure dystonia (circles). (For interpretation of the references to colour in this figure legend, the reader is referred to the Web version of this article.)

the right PreCG and PoCG (Fig. 1, Table 2). There was no significant difference between MuCON and CON.

3.2. VBA analysis

Compared with CON, MuCON showed significantly different (more positive) AI values in the thalamus, and PAT showed significantly different (more positive) AI values in a cluster encompassing the thalamus, putamen and insula (Fig. 2). There was no significant difference between PAT and MuCON.

Exploratory analysis of the cluster's mean AIs revealed that this was due to reduced leftward lateralization (= increasing symmetry) in the thalamus in MuCON compared to CON ($t_{46} = 7.24$, $p < 0.001$, $r = 0.73$). In PAT compared to CON, loss of left-hemispheric lateralization extended beyond the thalamus to the putamen and the insula and was more pronounced (a slight rightward lateralization was seen ($t_{45} = 4.81$, $p < 0.001$, $r = 0.58$)). Exploratory analysis of cluster mean GMVs indicated that this effect was on one side owed to a significantly increased right-hemispheric cluster-specific GMV in both PAT ($t_{46} = 2.45$, $p = 0.018$, $r = 0.34$) and MuCON ($t_{45} = 2.53$, $p = 0.015$, $r = 0.35$) compared to CON, but in PAT left-hemispheric cluster-specific GMV was additionally significantly reduced compared to CON ($t_{46} = -2.17$, $p = 0.035$, $r = 0.31$).

3.3. ABV analysis

Literature search identified 17 studies comprising in total 19 experiments and 93 experimental foci fulfilling the inclusion criteria (table s-1). GingerALE meta-analysis revealed significant clusters extending over the left primary sensorimotor cortex and at the border between putamen and pallidum in both hemispheres (figure s-1). Based on these results, we investigated the mean GMV in the PreCG, PoCG, putamen and pallidum in each hemisphere. Both hemispheres were investigated, as lateralization effects in the meta-analysis may be owed to the focus on the right hand in focal hand dystonia studies.

ABV revealed a significant main effect of group for each the right and left PreCG (R/L $F_{2,68} = 5.69/5.28$, $p = 0.005/0.008$, $\eta_p^2 = 0.15/0.14$) and each the right and left PoCG (R/L $F_{2,68} = 5.41/3.66$, $p = 0.007/0.031$, $\eta_p^2 = 0.10/0.14$; figure s-3). Bonferroni-corrected post-hoc analysis revealed a significantly increased mean GMV again in both the left and right PreCG in PAT compared to both MuCON (R/L $p = 0.021/0.015$) and CON (R/L $p = 0.011/0.027$). For the right PoCG, post-hoc contrasts indicated an increased GMV in PAT compared to CON ($p = 0.008$). For the left-hemispheric PoCG, no significant differences in the post-hoc between-group comparisons were seen after correction for multiple comparisons.

3.4. Regression analysis

ABV analysis: Multiple regression was significant for each the left and right putaminal ROI (R/L $F_{4,19} = 8.41/9.67$, $p < 0.001$; $R^2 = 0.64/0.67$), with disease duration being significantly explanatory of relatively lower mean putaminal GMV (R/L $\beta = -0.49/-0.42$, $p = 0.006/0.013$).

VBA analysis: Regression analysis with voxel-wise AI indices showed a significant association of GM asymmetry in the volume of interest with disease duration in the putamen (x|y|z = 29|-10|1, $t = 5.52$, $k = 368$, $p_{FWEsvc} = 0.003$), extending to the lateral pallidum (x|y|z = 24|-12|3, $t = 4.13$, $p_{FWEsvc} = 0.035$; figure s-4). Exploration of cluster-specific mean AI showed increasing disease duration significantly explaining rightward (loss of leftward) asymmetry ($\beta = 0.74$, $p < 0.001$; $R^2 = 0.55$). Evaluation of the cluster-specific GMV indicated that while volume decreased in both hemispheres with increasing disease duration, the change in brain symmetry was rather explained by a significant loss of left-hemispheric GMV ($\beta = -0.43$, $p = 0.013$) in the cluster.

There were no significant associations of disease duration with VBM data, and no associations with ED score in any analysis.

4. Discussion

4.1. Primary sensorimotor cortices

Increased primary sensorimotor cortex GMV was complementarily observed in hypothesis-supported ROI-based and assumption-free voxel-wise approaches, in the latter localizing to the face/lip representation. While earlier work in hand musician's dystonia did not report primary sensorimotor changes [14], studies of hand TSFD made such observations with conflicting directionality [5], for which methodological aspects, inter-study differences (e.g. mixed focal hand TSFD

collectives) or (partly) small sample sizes may be discussed [15]. The somatotopic character of changes in this first orofacial musician's TSFD study amends observations in hand TSFD. Studies at cellular level suggest that morphometric GM changes may be interpreted as correlate of altered (trans)neuronal organization (i.e. plasticity) [16], and healthy volunteers have accordingly shown such changes after motor training/repetitive transcranial magnetic stimulation [16]. In monkeys, dystonia-like symptoms induced by repetitive motor training were accompanied by disorganized primary somatosensory cortex somatotopy as a sign of dysfunctional neuronal plasticity [17]. Deranged right-hemispheric functional primary somatosensory somatotopy demonstrated in ED during task and somatosensory stimulation [3,18] may be mirrored by some cranial shift of right-compared to left-hemispheric findings. Electrophysiological studies in FD made corresponding observations for the motor cortex including nonsymptomatic muscle representations, pointing to accompanying failure of inhibitory mechanisms [19]. Consistent with loss of inhibition, task-related fMRI has shown primary sensorimotor overactivity in ED [2].

Though mean GMV of the pre-/postcentral gyrus in healthy brass players was in between the magnitudes in ED patients and nonmusicians (figure s-3), direct comparison to nonmusicians did not show significant differences. While the overall literature, performed almost exclusively in pianists/string players, provides evidence for primary sensorimotor changes in instrumentalists, describing (among others) greater topographic representations, altered central sulcus length and correlation with increasing professionalism [8], the extent and character of the primary sensorimotor VBM findings has been varying. Among others positive GM density correlations with musical professionalism, reduced GMV, or no abnormalities have been observed [8,20,21]. The only study looking into structural changes in wind players analyzing cortical thickness observed concurrently a thickness increase in the anterior, and a reduction in the posterior right postcentral gyrus and no change in the precentral cortex [9]. It is hence conceivable that methodological constraints (e.g. reduced sensitivity due to limited localization accuracy and fine facial sensorimotor representations) and methodological differences to previous studies (e.g. statistical control for brain size, modulation) might have played a role [22]. Giving special consideration to a certain sex frequency variation across groups, we did not see significant GMV sex effects, and no sex-associated voxel-level trends in sensorimotor cortices at uncorrected peak-level.

4.2. Abnormal symmetry in thalamus and basal ganglia

Healthy and diseased brass players both showed increased thalamic symmetry compared to nonmusicians, that showed left-hemispheric thalamic lateralization in line with previous data in the healthy [23]. As observed in both, this may mostly be attributable to musical practice. Prompt integration of multimodal sensorimotor information requires conjunct activity in a fronto-parieto-temporal network involving the pre- and supplementary motor, inferior frontal, superior temporal and supramarginal cortex [24], and the thalamus herein has been suggested an important relay, with (cortico-)thalamo-cortical loops guiding multimodal sensory processing (e.g. tone, rhythm) [25], and (cortico)-thalamo-basal-ganglia- and cerebello-cortical loops involved in motor learning/sensorimotor integration (e.g. motor sequencing, adaption) [6]. Increased thalamic symmetry may thus mirror an adaption to intensive, bilateral orofacial (and bimanual) coordinative sensorimotor training in brass playing, in which a musician's nondominant hemisphere seems to undergo stronger plastic reorganization [8]. This is the first description of voxel-wise thalamic changes in healthy brass musicians. Earlier studies investigating cerebral asymmetry in musicians focused on the absolute pitch subgroup, describing mainly leftward planum temporale asymmetry [7,8]. Seminal work in a mixed keyboard/string player group described left-hemispheric thalamic lateralization within-group, but did not conduct a comparison against nonmusicians [7].

The subcortical increase in symmetry/rightward tendency compared to nonmusicians was more pronounced in ED, comprising putaminal peaks not seen in the comparison involving healthy players, and was driven not only by locally increased right-hemispheric but also diminished left-hemispheric GMV. Thalamo-cerebellar and -basal ganglia loops described in the musical context seem also important in FD pathogenesis [5]. Interestingly, abnormal cerebellar structure has been reported quite regularly in nonmusician TSFDs, while BG structure change alone is reported more frequently in non-TSFDs compared to TSFDs [5], a discrepancy whose origins remains yet unknown. The BG's assumed important role in dystonia is deduced from their key position in motor learning by filtering relevant sensory input to the motor system, movement selection and cortical plasticity/excitability modulation [19]. In already highly-trained individuals, sensorimotor processes are greatly automized and seem to require less BG involvement [26], mirrored by abating BG volume in high motor-proficiency professionals [27] (contrasting cortical-level findings [16]). Granert and colleagues observed increased putaminal GMV in dystonic vs. healthy pianists, but at the same time an overall association of lower BG volumes with higher temporal piano key stroke precision (a measure of motor skill) [14]. Nonsymptomatic DYT1 mutation carriers show higher BG volume than diseased individuals [28]. Hence, alternatively to a correlate of symptom production in FD, increased BG volume has been discussed as possible correlate of compensatory effort. Our regression analyses suggested that i) the mean putaminal volume was negatively correlated with disease duration and ii) that this affected the left putamen more relative to the right in the voxel-wise approach. This is in line with findings in writer's cramp, where relative reduction of increased striatal GMV and abating somatosensory BG overactivity during tactile stimulation have been shown with increasing disease duration [29,30]. Considering the outline above, one might speculate if relative putaminal GMV reduction with disease duration in ED might be a correlate of adaptive processes leading to altered BG involvement, or sign of degradation of compensatory efforts with time [29,30] (as symptom severity increase/spread to other activities are seen in some in the first years [1]). As morphometry does not allow inferring if our observations are primary or compensatory, longitudinal research, yet sparse in FD, may be needed to further elucidate this phenomenon.

5. Conclusion

The present study provides robust first-time evidence for cortical and subcortical GM abnormalities in ED, investigating the largest patient sample in this rare disease to date. Further, the study provides evidence for brain (a)symmetry changes in healthy brass players and points to a possible role of such changes not only in musical professionalism [8] but also in dystonia. The good concordance of ROI- and voxel-based results underlines the relevance of meta-analyses for characterization of central disease-related changes.

Acknowledgements

We cordially thank all musicians and nonmusicians for their participation in the study.

Appendix A. Supplementary data

Supplementary data to this article can be found online at https://doi.org/10.1016/j.parkreldis.2019.05.008.

Funding

This study was supported by the Deutsche Forschungsgemeinschaft (DFG HA3370/5-1) Bonn, Germany, and the Kommission für Klinische Forschung (KKF H-05).

Full financial disclosures for the previous 12 months

T. Mantel receives research support from the KKF and has received travel grants from AbbVie Deutschland GmbH and Bayer Vital GmbH. E. Altenmüller serves in the editorial board of the Journal of Interdisciplinary Music Studies, Medical Problems of Performing Artists, Musicae Scientiae, Music and Medicine, BMC Movement Disorders, Neural Plasticity. He receives research-support from the DFG. He receives royalties from the publication of books from Oxford University Press and Cambridge University Press. T. Meindl has received travel grants from Pharm-Allergan-GmbH, Ipsen Pharma GmbH, Merz Pharma GmbH & Co. KGaA and Boston Scientific Medizintechnik GmbH. A. Jochim has received travel grants by Bayer Vital GmbH and Merz Pharmaceuticals GmbH as well as speaker honoraria by Pharm-Allergan GmbH and Merz Pharmaceuticals GmbH.C. Zimmer has served on scientific advisory boards for Philips and Bayer Schering. He serves as co-editor on the Advisory Board of Clinical Neuroradiology. He has received speaker honoraria from Bayer-Schering and Philips and has received research support and investigator fees for clinical studies from Biogen Idec, Quintiles, MSD Sharp & Dome, Boehringer Ingelheim, Inventive Health Clinical UK Ltd., Advance Cor, Brainsgate, Pfizer, Bayer Schering, Novartis, Roche, Servier, Penumbra, WCT GmbH, Syngis, SSS Internartional Clinical Research, PPD Germany GmbH, Worldwide Clinical Trials Ltd., Phenox, Covidien, Actelion, Medivation, Medtronic, Harrison Clinical Research, Concentric, Penumbra, Pharmtrace, Reverse Medical Corp., Premier Research Germany Ltd., Surpass Medical Ltd. and GlaxoSmithKline. B. Haslinger receives research support from Ipsen Pharma GmbH and the DFG, has received speaker honoraria from Pharm-Allergan GmbH, Bayer Health Care Pharmaceuticals and Ipsen Pharma GmbH and has received travel grants from Ipsen Pharma GmbH and Merz Pharmaceuticals GmbH. He has received royalties for book chapters from Cambridge University Press and Springer Medizin. The other authors report no disclosures.

References

[1] S.J. Frucht, S. Fahn, P.E. Greene, C. O'Brien, M. Gelb, D.D. Truong, J. Welsh, S. Factor, B. Ford, The natural history of embouchure dystonia, Mov. Disord. 16 (5) (2001) 899–906.

[2] B. Haslinger, E. Altenmuller, F. Castrop, C. Zimmer, C. Dresel, Sensorimotor overactivity as a pathophysiologic trait of embouchure dystonia, Neurology 74 (22) (2010) 1790–1797.

[3] T. Mantel, C. Dresel, E. Altenmuller, C. Zimmer, J. Noe, B. Haslinger, Activity and topographic changes in the somatosensory system in embouchure dystonia, Mov. Disord. 31 (11) (2016) 1640–1648.

[4] B. Haslinger, J. Noe, E. Altenmuller, V. Riedl, C. Zimmer, T. Mantel, C. Dresel, Changes in resting-state connectivity in musicians with embouchure dystonia, Mov. Disord. 32 (3) (2017) 450–458.

[5] V.K. Neychev, R.E. Gross, S. Lehericy, E.J. Hess, H.A. Jinnah, The functional neuroanatomy of dystonia, Neurobiol. Dis. 42 (2) (2011) 185–201.

[6] S.C. Herholz, R.J. Zatorre, Musical training as a framework for brain plasticity: behavior, function, and structure, Neuron 76 (3) (2012) 486–502.

[7] E. Luders, C. Gaser, L. Jancke, G. Schlaug, A voxel-based approach to gray matter asymmetries, Neuroimage 22 (2) (2004) 656–664.

[8] G. Schlaug, Musicians and music making as a model for the study of brain plasticity, Prog. Brain Res. 217 (2015) 37–55.

[9] U.S. Choi, Y.W. Sung, S. Hong, J.Y. Chung, S. Ogawa, Structural and functional plasticity specific to musical training with wind instruments, Front. Hum. Neurosci. 9 (2015) 597.

[10] D.A. Peterson, P. Berque, H.C. Jabusch, E. Altenmuller, S.J. Frucht, Rating scales for musician's dystonia: the state of the art, Neurology 81 (6) (2013) 589–598.

[11] F. Kurth, C. Gaser, E. Luders, A 12-step user guide for analyzing voxel-wise gray matter asymmetries in statistical parametric mapping (SPM), Nat. Protoc. 10 (2) (2015) 293–304.

[12] P.E. Turkeltaub, S.B. Eickhoff, A.R. Laird, M. Fox, M. Wiener, P. Fox, Minimizing within-experiment and within-group effects in activation likelihood estimation meta-analyses, Hum. Brain Mapp. 33 (1) (2012) 1–13.

[13] S.B. Eickhoff, T.E. Nichols, A.R. Laird, F. Hoffstaedter, K. Amunts, P.T. Fox, D. Bzdok, C.R. Eickhoff, Behavior, sensitivity, and power of activation likelihood estimation characterized by massive empirical simulation, Neuroimage 137 (2016) 70–85.

[14] O. Granert, M. Peller, H.C. Jabusch, E. Altenmuller, H.R. Siebner, Sensorimotor skills and focal dystonia are linked to putaminal grey-matter volume in pianists, J. Neurol. Neurosurg. Psychiatry 82 (11) (2011) 1225–1231.

[15] C. Delmaire, M. Vidailhet, A. Elbaz, F. Bourdain, J.P. Bleton, S. Sangla, S. Meunier, A. Terrier, S. Lehericy, Structural abnormalities in the cerebellum and sensorimotor circuit in writer's cramp, Neurology 69 (4) (2007) 376–380.

[16] B. Draganski, A. May, Training-induced structural changes in the adult human brain, Behav. Brain Res. 192 (1) (2008) 137–142.

[17] N.N. Byl, M.M. Merzenich, W.M. Jenkins, A primate genesis model of focal dystonia and repetitive strain injury: I. Learning-induced dedifferentiation of the representation of the hand in the primary somatosensory cortex in adult monkeys, Neurology 47 (2) (1996) 508–520.

[18] K. Uehara, S. Furuya, H. Numazawa, K. Kita, T. Sakamoto, T. Hanakawa, Distinct roles of brain activity and somatotopic representation in pathophysiology of focal dystonia, Hum. Brain Mapp. (**40** (6), 2019, 1738– 1749).

[19] A. Quartarone, M. Hallett, Emerging concepts in the physiological basis of dystonia, Mov. Disord. 28 (7) (2013) 958–967.

[20] P. Bermudez, J.P. Lerch, A.C. Evans, R.J. Zatorre, Neuroanatomical correlates of musicianship as revealed by cortical thickness and voxel-based morphometry, Cerebr. Cortex 19 (7) (2009) 1583–1596.

[21] L. Vaquero, K. Hartmann, P. Ripolles, N. Rojo, J. Sierpowska, C. Francois, E. Camara, F.T. van Vugt, B. Mohammadi, A. Samii, T.F. Munte, A. Rodriguez-Fornells, E. Altenmuller, Structural neuroplasticity in expert pianists depends on the age of musical training onset, Neuroimage 126 (2016) 106–119.

[22] C. Scarpazza, S. Tognin, S. Frisciata, G. Sartori, A. Mechelli, False positive rates in Voxel-based Morphometry studies of the human brain: should we be worried? Neurosci. Biobehav. Rev. 52 (2015) 49–55.

[23] K.E. Watkins, T. Paus, J.P. Lerch, A. Zijdenbos, D.L. Collins, P. Neelin, J. Taylor, K.J. Worsley, A.C. Evans, Structural asymmetries in the human brain: a voxel-based statistical analysis of 142 MRI scans, Cerebr. Cortex 11 (9) (2001) 868–877.

[24] B. Haslinger, P. Erhard, E. Altenmuller, U. Schroeder, H. Boecker, A.O. Ceballos-Baumann, Transmodal sensorimotor networks during action observation in professional pianists, J. Cogn. Neurosci. 17 (2) (2005) 282–293.

[25] G. Musacchia, E.W. Large, C.E. Schroeder, Thalamocortical mechanisms for integrating musical tone and rhythm, Hear. Res. 308 (2014) 50–59.

[26] B. Haslinger, P. Erhard, E. Altenmuller, A. Hennenlotter, M. Schwaiger, H. Grafin von Einsiedel, E. Rummeny, B. Conrad, A.O. Ceballos-Baumann, Reduced recruitment of motor association areas during bimanual coordination in concert pianists, Hum. Brain Mapp. 22 (3) (2004) 206–215.

[27] C.E. James, M.S. Oechslin, D. Van De Ville, C.A. Hauert, C. Descloux, F. Lazeyras, Musical training intensity yields opposite effects on grey matter density in cognitive versus sensorimotor networks, Brain Struct. Funct. 219 (1) (2014) 353–366.

[28] B. Draganski, S.A. Schneider, M. Fiorio, S. Kloppel, M. Gambarin, M. Tinazzi, J. Ashburner, K.P. Bhatia, R.S. Frackowiak, Genotype-phenotype interactions in primary dystonias revealed by differential changes in brain structure, Neuroimage 47 (4) (2009) 1141–1147.

[29] K.E. Zeuner, A. Knutzen, O. Granert, J. Gotz, S. Wolff, O. Jansen, D. Dressler, H. Hefter, M. Hallett, G. Deuschl, T. van Eimeren, K. Witt, Increased volume and impaired function: the role of the basal ganglia in writer's cramp, Brain Behav. 5 (2) (2015) e00301.

[30] M. Peller, K.E. Zeuner, A. Munchau, A. Quartarone, M. Weiss, A. Knutzen, M. Hallett, G. Deuschl, H.R. Siebner, The basal ganglia are hyperactive during the discrimination of tactile stimuli in writer's cramp, Brain 129 (Pt 10) (2006) 2697–2708.

Supplement

Supplementary methods

Subject inclusion criteria

All subjects were of European descent, right-handed[1], < 65 years old, did not suffer from major internal, neurologic or psychiatric comorbidity and showed no relevant macroscopic abnormalities in structural MRI. No subject had received botulinum toxin treatment within the last three months or was on anticholinergic medication at the time of the study; no subject had received neuroleptics prior to or after disease onset. Diagnosis of ED had been made by a movement disorders specialist experienced with ED based on extensive evaluation of history, clinical examination and evaluation of instrument play. Except for two ED patients who had given up regular practice, all healthy/diseased brass musicians played their instrument regularly.

Meta-analysis study selection criteria

Relevant publications were identified by searches in PubMed and GoogleScholar using the keywords “dystonia” plus “morphometry”, “VBM”, and “grey/gray matter volume/density” as well as by exploring additional publication from the reference list of those articles. Studies were included in the analysis if they (i) used voxel-based morphometry as described by Ashburner and Friston or Good and colleagues [2,3], (ii) reported between-group results of GM density or volume between idiopathic FD patients and controls, (iii) made available stereotactic space coordinates for all significant clusters (Talairach or MNI) or provided them on request, and (iv) applied correction for multiple comparisons in their statistical analysis beyond the default uncorrected cluster defining threshold of the respective software package (e.g. $p<0.001$ uncorrected for SPM, 0.01 uncorrected in FSL) and beyond a mere extent

threshold at an arbitrarily chosen voxel size (e.g. 80-100 voxels). The latter criterion was set to minimize a possible influence of published results at an increased risk for false positives[4].

Supplementary tables

Table s-1: Studies introduced into meta-analysis (17 studies, 19 experiments)		
Study	**focal dystonia type**	**subjects (patients/controls)**
Bono et al. 2015 [5]	cervical dystonia	25/25
Delmaire et al. 2007 [6]	focal hand dystonia	30/30
Delnooz et al. 2015 [7]	cervical dystonia	23/22
Draganski et al. 2003 [8]	cervical dystonia	10/10
Egger et al. 2007 [9]	focal hand dystonia	11/31
Etgen et al. 2006 [10]	blepharospasm	16/16
Filip et al. 2017 [11]	cervical dystonia	30/25
Garraux et al. 2004 [12]	focal hand dystonia	36/36
Granert et al. 2011 [13]	focal hand dystonia	11/11
Mantel et al. 2018 [14]	focal hand dystonia	26/27
Martino et al. 2011 [15]	blepharospasm	25/24
Obermann et al. 2007 [16]	blepharospasm	11/11
	cervical dystonia	09/09
Pantano et al. 2011 [17]	cervical dystonia	19/28
Ramdhani et al. 2014 [18]	mixed non-TSFD	24/24
	mixed TSFD	21/24
Simonyan et al. 2012 [19]	laryngeal dystonia	40/40
Suzuki et al. 2011 [20]	blepharospasm	32/48
Zeuner et al. 2015 [21]	focal hand dystonia	25/31

Supplementary figures

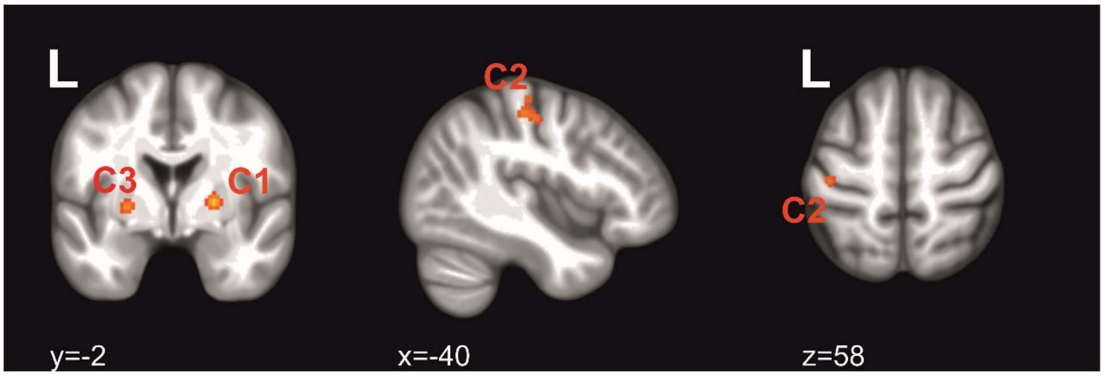

Cluster	Volume (mm^3)	weighted center of mass (x|y|z)			maximum ALE value	maximum ALE peak (x|y|z)		
Cluster 1 (C1)	1280	24.8	-6	2.1	0.0192	26	-8	2
Cluster 2 (C2)	1208	-43.4	-23.6	51	0.0187	-44	-26	50
Cluster 3 (C3)	1016	-22.2	-0.5	-4.2	0.0124	-24	-4	-2

Figure s-1. Significant clusters identified by activation likelihood estimation (ALE) projected on the averaged anatomical scan from all 71 study participants. Slice position is given in MNI space in millimeters relative to the anterior commissure.

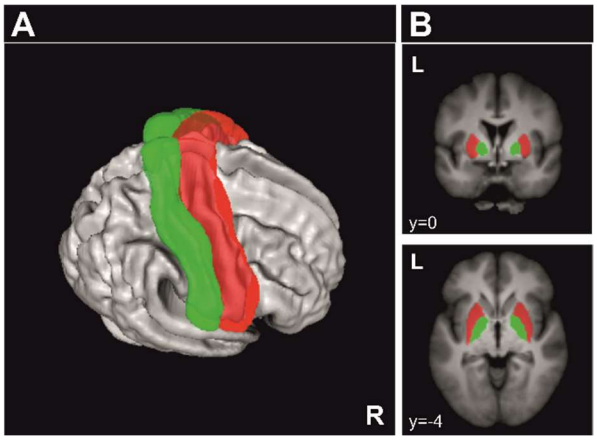

Figure s-2. Cortical (A) and subcortical (B) regions of interest selected from the Harvard Oxford anatomical atlas projected on the averaged anatomical scan from all 71 study participants. Slice position is given in MNI space in millimeters relative to the anterior commissure. A: red = precentral gyrus, green = postcentral gyrus; B: red = putamen, green = pallidum. R/L = right/left hemisphere.

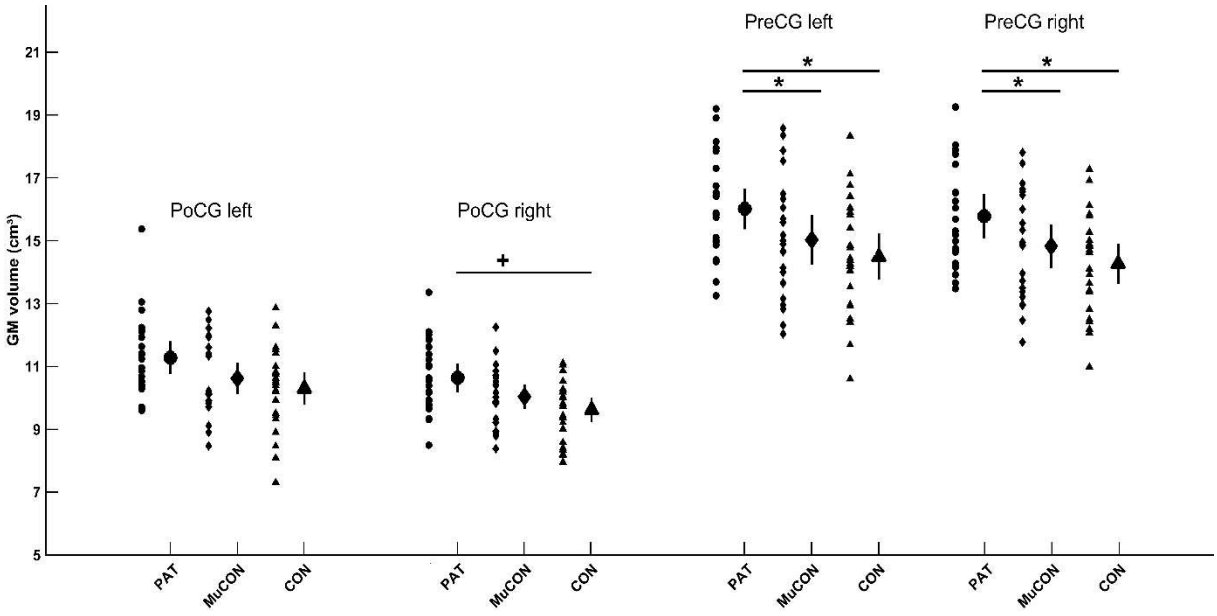

Figure s-3. GM volumes of the precentral and postcentral gyrus by ROI-based volumetry. Dots represent the GM volumes for each subject. Error bars depict the double standard error of mean. Asterisks depict significant ($p<0.05$, corrected) between-group differences, the "plus" analyses with a significant effect of group without significant results in the post-hoc analysis after Bonferroni-correction. CON, healthy nonmusicians (triangles); GM, grey matter; MuCON, healthy brass players (diamonds); PAT, patients with embouchure dystonia (circles); PoCG, postcentral gyrus; PreCG, precentral gyrus.

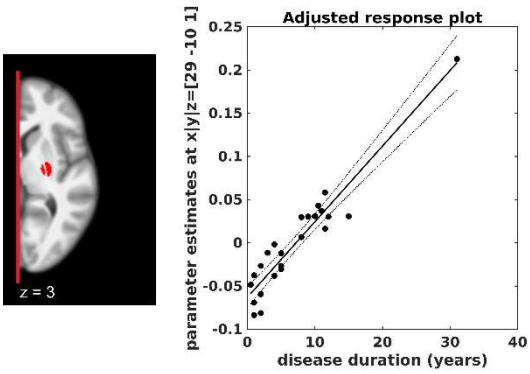

Figure s-4. Results of the voxel-wise regression analysis with disease duration showing increasingly positive AI values in the putamen with increasing disease duration in patients with embouchure dystonia. Slice position is given in MNI space in millimeters relative to the anterior commissure. The graph plot shows the age- and sex-adjusted individual effect sizes (y-axis) against disease duration (x-axis) in the putamen mirroring an increasing loss in leftward/growing rightward asymmetry with increasing disease duration. Bold line = regression line; dotted line = 95% confidence interval.

Supplementary References

[1] R.C. Oldfield, The assessment and analysis of handedness: the Edinburgh inventory, Neuropsychologia 9(1) (1971) 97-113.

[2] C.D. Good, I.S. Johnsrude, J. Ashburner, R.N. Henson, K.J. Friston, R.S. Frackowiak, A voxel-based morphometric study of ageing in 465 normal adult human brains, Neuroimage 14(1 Pt 1) (2001) 21-36.

[3] J. Ashburner, K.J. Friston, Voxel-based morphometry--the methods, Neuroimage 11(6 Pt 1) (2000) 805-21.

[4] A. Eklund, T.E. Nichols, H. Knutsson, Cluster failure: Why fMRI inferences for spatial extent have inflated false-positive rates, Proc. Natl. Acad. Sci. U. S. A. 113(28) (2016) 7900-5.

[5] F. Bono, D. Salvino, A. Cerasa, B. Vescio, S. Nigro, A. Quattrone, Electrophysiological and structural MRI correlates of dystonic head rotation in drug-naive patients with torticollis, Parkinsonism Relat. Disord. 21(12) (2015) 1415-20.

[6] C. Delmaire, M. Vidailhet, A. Elbaz, F. Bourdain, J.P. Bleton, S. Sangla, S. Meunier, A. Terrier, S. Lehericy, Structural abnormalities in the cerebellum and sensorimotor circuit in writer's cramp, Neurology 69(4) (2007) 376-80.

[7] C.C. Delnooz, J.W. Pasman, B.P. van de Warrenburg, Dynamic cortical gray matter volume changes after botulinum toxin in cervical dystonia, Neurobiol. Dis. 73 (2015) 327-33.

[8] B. Draganski, C. Thun-Hohenstein, U. Bogdahn, J. Winkler, A. May, "Motor circuit" gray matter changes in idiopathic cervical dystonia, Neurology 61(9) (2003) 1228-31.

[9] K. Egger, J. Mueller, M. Schocke, C. Brenneis, M. Rinnerthaler, K. Seppi, T. Trieb, G.K. Wenning, M. Hallett, W. Poewe, Voxel based morphometry reveals specific gray matter changes in primary dystonia, Mov. Disord. 22(11) (2007) 1538-42.

[10] T. Etgen, M. Muhlau, C. Gaser, D. Sander, Bilateral grey-matter increase in the putamen in primary blepharospasm, J. Neurol. Neurosurg. Psychiatry 77(9) (2006) 1017-20.

[11] P. Filip, C. Gallea, S. Lehericy, E. Bertasi, T. Popa, R. Marecek, O.V. Lungu, T. Kasparek, J. Vanicek, M. Bares, Disruption in cerebellar and basal ganglia networks during a visuospatial task in cervical dystonia, Mov. Disord. 32(5) (2017) 757-768.

[12] G. Garraux, A. Bauer, T. Hanakawa, T. Wu, K. Kansaku, M. Hallett, Changes in brain anatomy in focal hand dystonia, Ann. Neurol. 55(5) (2004) 736-9.

[13] O. Granert, M. Peller, H.C. Jabusch, E. Altenmuller, H.R. Siebner, Sensorimotor skills and focal dystonia are linked to putaminal grey-matter volume in pianists, J. Neurol. Neurosurg. Psychiatry 82(11) (2011) 1225-31.

[14] T. Mantel, T. Meindl, Y. Li, A. Jochim, G. Gora-Stahlberg, J. Kraenbring, M. Berndt, C. Dresel, B. Haslinger, Network-specific resting-state connectivity changes in the premotor-parietal axis in writer's cramp, Neuroimage Clin 17 (2018) 137-144.

[15] D. Martino, A. Di Giorgio, E. D'Ambrosio, T. Popolizio, A. Macerollo, P. Livrea, A. Bertolino, G. Defazio, Cortical gray matter changes in primary blepharospasm: a voxel-based morphometry study, Mov. Disord. 26(10) (2011) 1907-12.

[16] M. Obermann, O. Yaldizli, A. De Greiff, M.L. Lachenmayer, A.R. Buhl, F. Tumczak, E.R. Gizewski, H.C. Diener, M. Maschke, Morphometric changes of sensorimotor structures in focal dystonia, Mov. Disord. 22(8) (2007) 1117-23.

[17] P. Pantano, P. Totaro, G. Fabbrini, E. Raz, G.M. Contessa, F. Tona, C. Colosimo, A. Berardelli, A transverse and longitudinal MR imaging voxel-based morphometry study in patients with primary cervical dystonia, AJNR Am. J. Neuroradiol. 32(1) (2011) 81-4.

[18] R.A. Ramdhani, V. Kumar, M. Velickovic, S.J. Frucht, M. Tagliati, K. Simonyan, What's special about task in dystonia? A voxel-based morphometry and diffusion weighted imaging study, Mov. Disord. 29(9) (2014) 1141-50.

[19] K. Simonyan, C.L. Ludlow, Abnormal structure-function relationship in spasmodic dysphonia, Cereb. Cortex 22(2) (2012) 417-25.

[20] Y. Suzuki, M. Kiyosawa, M. Wakakura, M. Mochizuki, K. Ishii, Gray matter density increase in the primary sensorimotor cortex in long-term essential blepharospasm, Neuroimage 56(1) (2011) 1-7.

[21] K.E. Zeuner, A. Knutzen, O. Granert, J. Gotz, S. Wolff, O. Jansen, D. Dressler, H. Hefter, M. Hallett, G. Deuschl, T. van Eimeren, K. Witt, Increased volume and impaired function: the role of the basal ganglia in writer's cramp, Brain Behav 5(2) (2015) e00301.

SCIENTIFIC REPORTS
nature research

Check for updates

OPEN

Altered sensory system activity and connectivity patterns in adductor spasmodic dysphonia

Tobias Mantel[1], Christian Dresel[1,2], Michael Welte[1], Tobias Meindl[1], Angela Jochim[1], Claus Zimmer[3] & Bernhard Haslinger[1] ✉

Adductor-type spasmodic dysphonia (ADSD) manifests in effortful speech temporarily relievable by botulinum neurotoxin type A (BoNT-A). Previously, abnormal structure, phonation-related and resting-state sensorimotor abnormalities as well as peripheral tactile thresholds in ADSD were described. This study aimed at assessing abnormal central tactile processing patterns, their spatial relation with dysfunctional resting-state connectivity, and their BoNT-A responsiveness. Functional MRI in 14/12 ADSD patients before/under BoNT-A effect and 15 controls was performed (i) during automatized tactile stimulus application to face/hand, and (ii) at rest. Between-group differential stimulation-induced activation and resting-state connectivity (regional homogeneity, connectivity strength within selected sensory(motor) networks), as well as within-patient BoNT-A effects on these differences were investigated. Contralateral-to-stimulation overactivity in ADSD before BoNT-A involved primary and secondary somatosensory representations, along with abnormalities in higher-order parietal, insular, temporal or premotor cortices. Dysphonic impairment in ADSD positively associated with left-hemispheric temporal activity. Connectivity was increased within right premotor (sensorimotor network), left primary auditory cortex (auditory network), and regionally reduced at the temporoparietal junction. Activation/connectivity before/after BoNT-A within-patients did not significantly differ. Abnormal ADSD central somatosensory processing supports its significance as common pathophysiologic focal dystonia trait. Abnormal temporal cortex tactile processing and resting-state connectivity might hint at abnormal cross-modal sensory interactions.

Focal laryngeal dystonia (FLD) is a debilitating task-specific focal dystonia (TSFD) affecting the laryngeal muscles, resulting in phonation impairment that can be classified into a number of overlapping clinical phenotypes[1]. In the most frequent phenotype, adductor-FLD (adductor-type spasmodic dysphonia, ADSD), laryngeal muscle spasms during vocalisation lead to effortful, jerky speech patterns[2]. Previous studies have outlined several functional and structural cortical abnormalities in the disease involving cortices of the phonation network[3], including altered phonation-related activity using functional MRI (fMRI)[4–6] or transcranial magnetic stimulation[7], resting-state connectivity[8] and grey matter structure[9] in primary and higher-order (mostly inferior parietal, pre-/supplementary motor) sensorimotor cortices in ADSD. Subcortically, abnormal putaminal structure and connectivity[8,9] as well as thalamic and cerebellar structure and phonation-related activity[9,10] have been shown.

Phonation and speech production in the healthy rely on both somatosensory and auditory feedback mechanisms[11,12]. Botulinum neurotoxin type A (BoNT-A) injection into the vocal cords yields temporary symptomatic relief in ADSD by attenuating the symptom-producing muscle spasms (primarily of the thyroarytenoid muscles), yet its possible central role is not well understood[13]. Reduction of phonation-induced electromyographic activity in the bilateral thyroarytenoid muscles in ADSD after unilateral injection with BoNT-A hinted at a possible role of altered sensory feedback from the treated muscle, leading to adapted motor drive also to the non-treated muscle[14]. If one postulates that this represents a central modulation due to peripheral BoNT-A application, it remains to date unresolved if this is guided by modulation of sensory feedback following BoNT-A-induced changes of muscle activity in the injected muscle during phonation, or if there is a direct central BoNT-A effect also present in

[1]Department of Neurology, Klinikum rechts der Isar, Technische Universität München, Ismaningerstrasse, 22, Munich, Germany. [2]Department of Neurology, Johannes Gutenberg University, Langenbeckstrasse, 1, Mainz, Germany. [3]Department of Neuroradiology, Klinikum rechts der Isar, Technische Universität München, Ismaningerstrasse, 22, Munich, Germany. ✉e-mail: bernhard.haslinger@tum.de

absence of phonatory activity[13]. BoNT-A-associated alterations of cortical activity have been reported in orofacial non-TSFD during both motor task and somatosensory processing[15,16], but conflicting observations have been made during phonation in spasmodic dysphonia[4,5]. Further clarification of the relationship of BoNT-A injections and sensory processing in ADSD may inform the development of sensory (e.g. somatosensory, auditory) modulation strategies to complementarily enhance benefit gained from BoNT-A treatment.

Abnormal somatosensory processing and dysfunctional interaction with the motor system is one central aspect in pathophysiologic theories in focal dystonia (FD)[17]. Yet the central patterns of somatosensory stimulus processing abnormalities in the absence of motor task have not been investigated in ADSD, complicated by anatomic constraints in this TSFD. While the principle feasibility of direct laryngeal stimulation was described during magnetencephalography (MEG) in a small group of healthy subjects, several challenges such as its moderate reproducibility, sensitivity to noise/artefacts and considerable efforts regarding both technique and subject training have not yet been sufficiently addressed[18]. Findings in other types of FD suggest that abnormal somatosensory processing may constitute a form of endophenotypic trait[19]. This provides the opportunity to investigate the somatosensory system in ADSD through somatosensory stimulation to more accessible asymptomatic body regions.

This work aimed at characterizing (i) patterns of abnormal central tactile stimulus processing in ADSD, (ii) possible spatial relations between areas of altered stimulation-related activity and dysfunctional (long-range and regional) connectivity at rest, and (iii) possible effects of BoNT-A treatment on the above findings, avoiding confounds by motor execution, BoNT-A-modulated muscle function, or acute compensation mechanisms.

Methods

Participants. Fourteen right-handed patients with idiopathic isolated ADSD (PATpre, m/f = 7/7, age 48.0 ± 14.9y; disease duration 6.7 ± 5.6y) were recruited from the hospital movement disorders outpatient clinic in cooperation with a specialized outpatient phoniatric center and compared to a control group of fifteen age- and sex-matched healthy volunteers (CONTR, m/f = 7/8, 46.5 ± 12.3y). Diagnosis of ADSD was established by an experienced phoniatrist, with additional clinical neurological evaluation by a movement disorders-specialised neurologist. Procedures included evaluation of the medical history, phoniatric voice analysis for typical auditive voice/speech abnormalities (e.g. during vocalisations, conversation, standardised text readings), voice acoustic analysis and electroglottography (involving evaluation of jitter, shimmer, and normalized noise energy), microlaryngoscopy and microstroboscopy. We limited our study to ADSD, as it is far more common than the abductor type[2]. Twelve patients (m/f = 7/5, 48.0 ± 13.2y) received regular abobotulinumtoxin injections (total dosage 15.3 ± 5.9 units) in 3–9-month intervals (depending on individual effect duration) with good clinical benefit (as certified by patients' subjective reports and the expert impression of the treating phoniatrist), two were BoNT-A-naïve (i.e. have never recieved BoNT-A treatment). Except for the BoNT-A-naïve patients that were only scanned once, patients were scanned twice in pseudo-randomized order: 34.9 ± 7.3d after BoNT-A treatment (PATpost) when their voice was at its best and post-injection breathiness had recovered, and prior to the next BoNT-A treatment (individually, ≥3 months after the last BoNT-A injection) when the BoNT-A effect had clinically waned. The voice handicap index (VHI) was collected at both timepoints to ascertain subjective impairment by dysphonia. The institutional ethics board (Ethikkommission der Technischen Universität München, https://www.ek-med-muenchen.de) approved of the study and all participants gave written informed consent according to the Declaration of Helsinki. All methods were carried out in accordance with relevant guidelines and regulations. All participants had a normal structural MRI scan and, as certified by medical history and a detailed clinical examination by a senior neurologist and movement disorders specialist (C.D.), no additional neuropsychiatric disorders (including no other movement disorders), no sensory deficits, and no neuroleptic drug use; patients had no dystonic symptoms in body regions other than the laryngeal muscles and did not receive voice therapy or medication for dystonia beyond BoNT-A.

Data acquisition and analysis. MRI acquisition parameters and software for data analysis are detailed in the supplement.

Tactile stimulation experiment. The tactile stimulation experiment was performed as previously outlined[15,20]. In brief, trains of punctate tactile stimuli (stimulus duration 2 s, jittered inter-stimulus interval of 7–15 s, intensity adapted to local skin sensitivity) were pseudo-randomly applied to forehead (V1, intensity 32 mN), upper lip (V2, 22 mN) and hand (Ha, 45 mN) on either side by von Frey-monofilaments during three fMRI runs using an automated MR-compatible simulation device. A stimulation-induced painless feeling of touch was additionally ensured by mechanical and pain threshold testing in all participants[21]. Preprocessing was performed as in earlier studies employing this stimulation paradigm[15,20], with an additional inclusion of six head motion parameters as regressors in the first-level general linear model contrasting the individual regressors (stimulation onsets * canonical hemodynamic response function) for the six stimulation conditions (V1, V2, Ha on either side) to the implicit baseline (rest) separately for each condition. One patient was excluded due to suspicion of corrupted stimulation paradigm. Population-based inferences were drawn by introducing the first-level individual contrast images to a second-level flexible factorial model with factors *subject*, *condition* (see above) and *group* (PATpre, PATpost, CONTR) accounting for possible non-sphericity of the error term, with post-hoc planned longitudinal contrasts (PATpre vs. PATpost) applied in case of a significant difference to healthy subjects pre-BoNT-A. A comparison of healthy subjects with patients post-BoNT-A was not primarily performed as no ancillary information was expected compared to the direct within patient group longitudinal analysis. Considering the subtlety of short-time punctate tactile stimuli and the interindividual anatomical variability of sensory representations, significance was determined at a cluster-forming (peak-level) threshold of $p < 0.001$ with cluster-level multiple comparison-correction at $p_{FWEc} < 0.05$ (FWE, family-wise error), adjusted for the six conditions ($p < 0.0083$ (0.05/6)).

Resting-state experiment. Spatial independent component analysis (sICA) and regional homogeneity (ReHo) analysis were performed on resting-state data to investigate both changes in (i) long-range and (ii) regional functional connectivity (FC). Basic preprocessing of resting-state fMRI (rs-fMRI) scans involved realignment, slice-timing correction, normalization to Montreal Neurological Institute (MNI) space after coregistration with the anatomical scan, followed by linear detrending, regression of six head motion parameters and despiking using AFNI's (analysis of functional neuroimages) *3dDespike*[22]. One control was excluded from further analysis due to high frame-to-frame motion. The sICA approach reliably separates non-grey matter signal and noise from physiologically meaningful components[23]. For short-range FC analysis, we removed five white matter and cerebrospinal fluid signal principal components in an additional step using the CompCor (component-based noise correction) method, and bandpass filtering (0.01–0.08 Hz) was applied. Image smoothing for regional FC analysis was performed after connectivity measure calculation as recommended[24].

Long-range FC analysis. sICA extracts maximally independent spatial resting-state networks comprising distributed, functionally related (temporally coherent) brain regions by decomposing their linearly mixed signals contained in the spatiotemporal fMRI dataset[25]. Data across participants and conditions were concatenated and stepwise principal component analysis data reduction was performed guided by a prior dimensionality estimation using the minimum description length algorithm, retaining 39 subject-level and 28 group-level components. Data were variance-normalized and z-transformed. The Infomax algorithm was run 100 times in ICASSO[26] and cluster quality quantified using the index I_q mirroring the difference between intra- and extracluster similarity (range 0–1). Direct data back-reconstruction from the aggregate spatiotemporal dataset was performed using GICA I, which is robust for lower model orders[25]. Following the study goal, we then selected three robust ($I_q > 0.95$) lower-model order cortical resting-state networks of interest guided by the spatial pattern of tactile stimulation-induced cerebral activity (figure s-1) for further analysis: the sensorimotor network (SMN), the auditory network (AN) and the task-positive network (central executive network, CEN; figure s-1). Between-group differences were investigated as above using a flexible factorial random effects model (factors *subject*, *group)*. To ensure that only highly connected network regions were analysed, a combined binary mask representing the effect of the within-group analysis ($p_{FWE} < 0.05$) was applied. Results were peak-level-corrected for multiple comparisons at $p_{FWE} < 0.05$, adjusted for three investigated networks ($p < 0.017$ (0.05/3)).

Regional FC analysis. ReHo characterizes the local temporal coherence/synchronization of the regional blood oxygen-level dependent signal. The similarity of the time series of each voxel with those of its 26 nearest neighbours (voxels) was calculated in a whole-brain approach, using Kendall's coefficient of concordance[24]. After z-transformation to increase normality and data smoothing, between-group analysis was performed as above using a flexible factorial random effects model (factors *subject*, *group)*. Following the aim of the study, the statistical analysis was constrained to a combined binary mask of voxels with a robust within-group response to tactile stimulation ($p_{FWE} < 0.05$) across conditions. Results were peak-level-corrected for multiple comparisons at $p_{FWE} < 0.05$.

Regression analyses. Significant associations of severity by VHI and duration of dysphonia with functional activity/connectivity changes were investigated within PAT post-hoc by multiple regression analysis for those analyses showing significant differential between-group activity/connectivity patterns. FWE-multiple comparison corrections were applied as for the respective between-group task/rest analyses and the significance level adjusted for the number of regressors ($p < 0.025$ (0.05/2)).

Results

All patients reported a subjective voice improvement after BoNT-A treatment. Accordingly, the VHI improved significantly post BoNT-A (PATpre $72.6 \pm 12.4/67.3 \pm 19.4$ with/without BoNT-A-naïve patients; PATpost 32.3 ± 18.3; Wilcoxon signed-ranks, $z = -2.93$, $p = 0.003$). Mechanical detection and pain thresholds and mean perceived intensities did not significantly differ between groups (repeated-measures analyses of variance (rmANOVAs) [*group* × *condition*], $ps > 0.05$). Average frame-to-frame motion (rotation and translation) across analysed subject scanning sessions during rest/task fMRI was 0.12 ± 0.046 mm/0.12 ± 0.054 mm and not significantly different between groups (rest: ANOVA, $F_{2,37} = 0.94$, $p = 0.40$/task: rmANOVA [*group* × *session*], $ps > 0.05$).

Tactile stimulation experiment. Tactile stimulation in patients (pre-/post-BoNT-A) and controls yielded activity in a network involving primary somatosensory cortex (S1), secondary somatosensory cortex (S2), superior parietal cortex, precuneus, intraparietal sulcus, supramarginal gyrus, supplementary motor area, dorsal and ventral premotor cortex, inferior and middle frontal gyrus, insular cortex, superior and middle temporal cortex, anterior cingulate cortices, and thalamus (figure s-1).

Between-group analysis of PATpre against CONTR revealed significantly increased functional activity in the contralateral S1 during left hand/face (V2, Ha) and right face (V1, V2) stimulation, and in the contralateral S2 during right face (V1, V2) stimulation (Table 1, Fig. 1). Further areas of increased contralateral parietal activity in these conditions encompassed the intraparietal sulcus, supramarginal gyrus or superior parietal lobe. Besides enhanced S2 activation, right face stimulation (V1, V2) induced increased temporal activity in the left-hemispheric superior temporal gyrus (STG). Enhanced contralateral insular activity was observed after both left- (V2) and right-sided (V1) stimulus application to the face. Within the frontal lobe, enhanced right ventral (pre)motor (M1/PMv) was seen during left face stimulation (V2), and was visible as trend also in the other

L-sided stimulation						R-sided stimulation					
V1						**V1**					
Area	x	y	z	t	V	Area	x	y	z	t	V
–	–					L primary somatosensory, face (BA2)	−54	−20	32	4.78	760
						L supramarginal (BA40)	−60	−34	24	4.58	
						L superior parietal (BA7)	−54	−38	46	4.20	
						L superior temporal (BA22)	−58	−42	16	3.80	
						L secondary somatosensory (OP1)	−64	−20	22	3.63	
						L intraparietal sulcus	−42	−50	58	3.59	
						L superior parietal (BA5)	−32	−52	56	3.21	
						L dorsal insula (BA13)	−32	28	2	4.39	348
						L ventral insula (BA13)	−38	18	−10	4.23	
V2						**V2**					
Area	x	y	z	t	V	Area	x	y	z	t	V
R primary somatosensory, face (BA3b)	54	−8	44	4.98	364	L primary somatosensory, face (BA1)	−58	−14	42	4.34	411
R primary motor/ ventral premotor (BA4/6)	42	−4	58	3.79		L primary somatosensory, face (BA2)	−50	−20	36	3.63	
R inferior frontal (BA44)	36	26	0	4.37	346	L intraparietal sulcus (BA40)	−26	−48	42	4.00	
R ventral premotor (BA6)	46	4	10	3.61		L secondary somatosensory (OP4)	−64	−16	20	4.51	396
R dorsal insula	40	2	6	3.67		L superior temporal (BA22)	−64	−44	14	4.41	
						L supramarginal (BA40)	−64	−32	22	4.28	
Ha						**Ha**					
Area	x	y	z	t	V	Area	x	y	z	t	V
R primary somatosensory, hand (BA2)	30	−36	66	4.46	1135	–	–				
R primary somatosensory, face (BA1)	56	−18	44	4.03							
R intraparietal sulcus (BA7)	28	−58	60	3.91							
R superior parietal (BA5/7)	18	−54	64	3.73							
R secondary somatosensory (OP4)	58	−16	18	3.51							
R supramarginal (BA40)	36	−36	42	3.32							

Table 1. Areas with stronger activation in patients with ADSD before BoNT-A treatment when compared to healthy controls. Coordinates (in mm) in the Montreal Neurological Institute space. All differences are significant at $p_{FWEc} < 0.0083$ at a cluster-forming threshold of $p < 0.001$ uncorrected. BA, Brodmann area; OP, operculum parietale; R, right; L, left; t, t-score; V, cluster volume (voxels).

conditions in the hemisphere contralateral to stimulation where it did not survive adjustment for the number of conditions (see table s-1 for trends). Post-hoc evaluation of functional activity changes in these conditions before and after BoNT-A within patients did not yield significant differences.

Resting state experiment. During rest, we observed increased FC in the right medial dorsal premotor cortex (PMd; x | y | z = 24 | −2 | 56; t = 5.26, p = 0.012) within the SMN in PATpre compared to CONTR, increased FC in the left primary auditory cortex (A1; x | y | z = −44 | −14 | 2; t = 5.47, p = 0.004) within the AN in PATpre compared to CONTR and no significant abnormalities in the CEN. We further observed significantly reduced regional homogeneity at the right parieto-temporal junction (TPJ; x | y | z = 60 | −50 | 8; t = 4.97, p = 0.039; Fig. 2) in PATpre compared to CONTR, with a corresponding left-hemispheric trend at $k > 50$ voxels (x | y | z = −48 | −58 | 14; t = 5.26, k = 86). Post-hoc evaluation of FC changes in these analyses before and after BoNT-A within patients did not yield significant differences.

Regression analyses. There was a significant positive association of disease severity by voice handicap index with stimulation-induced activation in the left posterior STG (BA41/42; x | y | z = −52 | −30 | 10; t = 6.01, p = 0.009) caudal to A1 during right face (V1) stimulation in PATpre (Fig. 3). All other regression analyses did not yield significant results.

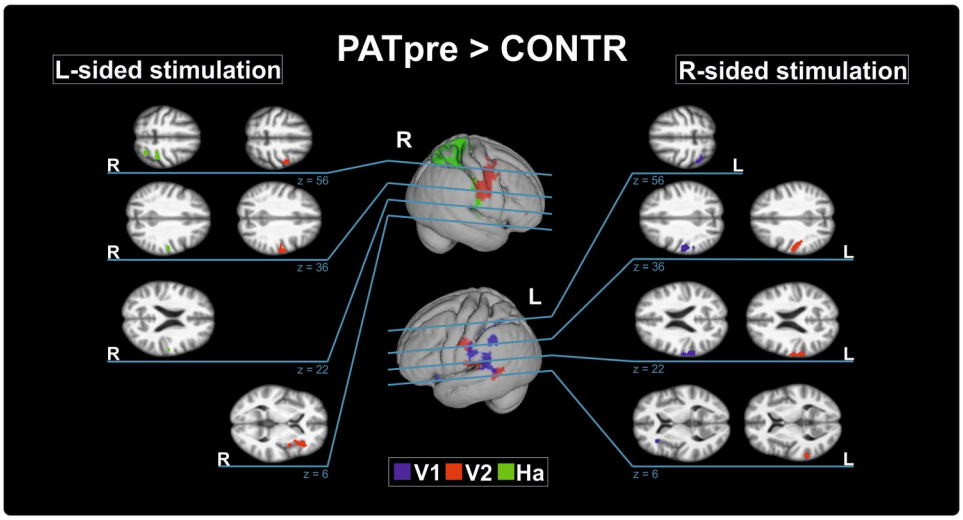

Figure 1. Areas with significantly increased activity in patients with ADSD. The middle column shows differential activation (color coded for each body region) projected on the respective contralateral hemisphere of the participants' 3D-reconstructed average brain. In the lateral columns, increased activity in in selected areas (top to bottom: S1/superior parietal lobe, S2, insular/temporal cortex) is projected on axial slices of the averaged brain. The overlaid statistical parametric maps were thresholded at $p_{FWEc} < 0.0083$ and a cluster-forming threshold of $p < 0.001$ uncorrected. Slice position in MNI space in mm is given relative to the anterior commissure (above +; below −). CONTR, healthy control participants; PATpre, ADSD patients before botulinum toxin A treatment; Ha, dorsal hand; V1, forehead; V2, upper lip, L/R, left/right hemisphere.

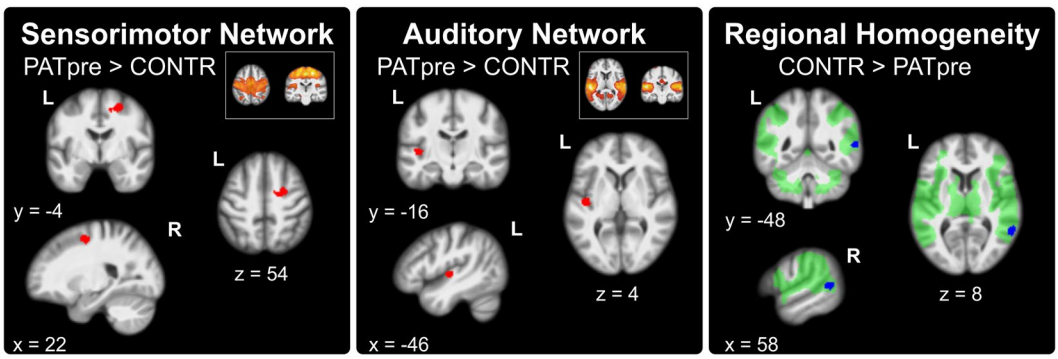

Figure 2. From left to right: Significant increases ($p_{FWE} < 0.017$) of long-range FC within the sensorimotor and the auditory network (in red) as well as significant reduction of short-range FC by regional homogeneity ($p_{FWE} < 0.05$; in blue) overlaid onto the participants' averaged structural images (clusters displayed at $p < 0.001$ uncorrected); areas with robust within-group response to tactile stimulation across conditions and participants are underlaid in light green. Slice positions in MNI space in mm are given relative to the anterior commissure (right/anterior/above +; left/posterior/below −). CONTR, healthy controls; PATpre, ADSD patients before botulinum toxin A treatment; L/R, left/right hemisphere.

Discussion

Abnormal primary somatosensory processing. This work provides evidence for abnormal primary and higher-order somatosensory input processing in ADSD in absence of motor tasks, amending observations in other cranial FDs[15,20,27]. Among studies investigating cranial dystonia, reduced activity during cutaneous somatosensory stimulation was seen in non-task-specific subtypes[15,27], and increased activity was reported in task-specific forms including the present work[20]. While there is some homogeneity of methodology among those cranial dystonia studies[15,20], considerable variation of both methodology and directionality of findings is seen in studies in focal dystonias affecting other body parts[28], and the investigation of cranial cutaneous tactile processing as surrogate to the laryngeal mucosa is a limiting factor regarding the present work. It hence remains uncertain if those variations in directionality might indeed mirror a pathophysiologic difference between dystonia subtypes. In S1, increased activity was observed in the present study during stimulation of both cortically proximate (face) and distant (hand) non-dystonic S1 representations and in both hemispheres, fitting the concept of an underlying endophenotype. Demonstration of such endophenotypic abnormality in cutaneous surrogate areas in ADSD may encourage further research in sensory modulation strategies in the disease. Modulation of sensory input

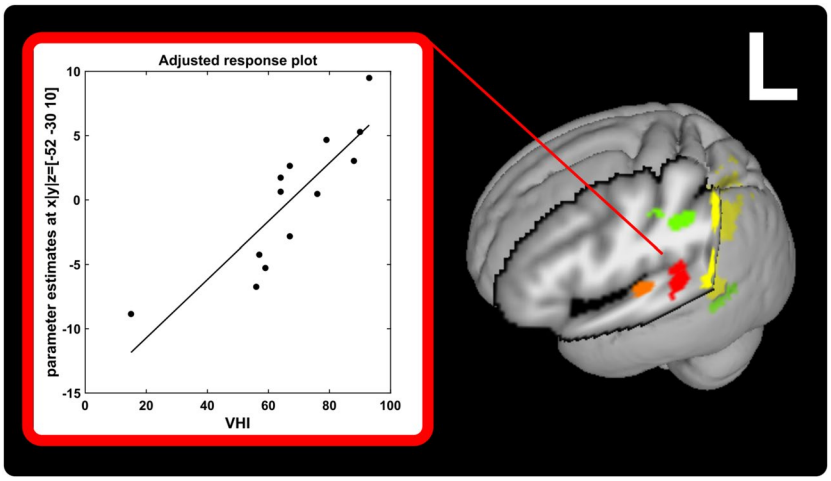

Figure 3. Left-hemispheric temporal cortices showing spatial pattern of abnormal tactile stimulation-induced changes or abnormal resting connectivity. Clusters with a significant positive relation to symptom severity by VHI during right face (V1) stimulation (in red), are displayed together with primary auditory FC-changes within the auditory network (orange) at rest and left-hemispheric temporal (and parietal) activity changes induced by right-hemispheric tactile stimulation of the face (V1/V2, in yellow/green) at a cluster-forming threshold of $p < 0.001$ uncorrected.

from mostly proximate body regions (i.e. sensory tricks) is known to ameliorate dystonic symptoms in some FD patients, and sensory retraining was able to improve motor function in TSFD of the hand in the past[29]. Quite recent work in FLD already made steps in this direction, indicating positive modulatory effects on voice function through ventral cervical cutaneous vibration[30], hence the investigation of effects of sensory retraining strategies applied to nondystonic/surrogate sensory areas might be of interest for future work.

Altered cortical activity during left hand stimulation spread lateral into the somatotopic face representations, while increased activity during face stimulation was rather limited to its expected somatotopic representation located superior and posterior to the putative S1 larynx representation reported for the healthy[18]. Increase and spread of somatosensory activation affecting symptomatic and non-symptomatic body parts have been pathophysiologically attributed to deficient intracortical inhibition and dysfunctional plasticity resulting in dedifferentiation and topographic shifts of otherwise concise cortical activation[31–33]. Such cortex-level dedifferentiation in FDs has been suggested to manifest peripherally in altered tactile discrimination thresholds[29], and altered somatosensory temporal discrimination has also been reported for ADSD[34]. In patients with cervical dystonia, peripheral temporal discrimination thresholds and central correlates of intracortical inhibition were abnormally reduced and further deteriorated by high-frequency somatosensory stimulation of a non-dystonic body part, whereas the opposite effect was seen in healthy controls[35]. As observed for a body part not affected by dystonic posturing, this observation had been discussed in support of a primary rather than adaptive nature of abnormal somatosensory processing and underlines the vulnerability of such predisposing abnormality to intensive somatosensory input as it occurs during high-proficiency motor tasks, as are affected in TSFDs like ADSD.

Abnormal higher-order sensory processing. Beyond S1, higher-order somatosensory cortices encompassing the left-hemispheric S2 as well as left- and right-hemispheric superior and inferior parietal cortex showed increased tactile-stimulation induced activity in ADSD. Further, right-hemispheric PMv activity was enhanced during left face stimulation (with respective contrahemispheric trends observed during stimulation of other body parts), and medial PMd connectivity was increased at rest. Other rs-fMRI studies in spasmodic dysphonia described reduced connectivity in either the supplementary motor area or the PMd within the SMN. Yet, cluster locations differed compared to the present study, and the lack of dimensionality information in previous studies impairs comparability[8,36]. Disordered information transfer from the sensory to the motor cortices (i.e sensorimotor integration) is discussed as a possible mechanism of dystonic posturing[17], occurring either at the cortico-cortical or subcortico-cortical level involving the basal ganglia or cerebellum[37,38]. In support of a possible top-down process (from those cortices to primary/subcortical areas), recent work in spasmodic dysphonia suggested abnormal premotor-parietal-putaminal circuitry with abnormal excitatory left inferior parietal projections to the putamen and interhemispheric information transfer from the right to left premotor cortex[36]. Yet, the lack of differentiability of primary and adaptive changes by fMRI ultimately limited the interpretation of the findings' origins. Past studies in other FDs have attempted to modulate sensorimotor higher-order axis processing through transcranial stimulation paradigms (mostly of the premotor cortex), showing mixed and mostly short-term results on motor function; yet such studies are to date lacking in FLD[39].

Temporoparietal interface. An interesting aspect of this study was the observation of temporal cortex and temporoparietal junction abnormalities in absence of phonation. Cortical activity after right-sided face stimulation was increased in the left posterior STG. In parts of the left posterior STG, the impairment (by VHI) further

predicted the degree of right face stimulation-induced activity in patients, amending a prior structural analysis that observed a positive relationship of left superior temporal cortical thickness with the mean number of voice breaks in sporadic spasmodic dysphonia[40]. Given that patients in the present study did not undergo a complementary external rating of their disease-related voice impairment (e.g. based on a Likert scale or scorings such as the Unified Spasmodic Dysphonia Rating Scale), this association warrants confirmation in future studies. Additionally, FC of the left A1 cortex within the auditory network was increased at rest, and regional FC in the parieto-temporal junction at rest was disturbed in the right hemisphere with a trend for the left hemisphere (possibly owed to right-hemispheric dominance of processing at the TPJ[11]). Associations of disease duration with functional connectivity, hinted at by previous work in FLD reporting inverse correlation of disease duration with SMN parietal connectivity[41], were not observed in this work. The above primary/associative (superior) temporal regions have been suggested to be part of primary areas within the phonation network besides the larynx motor cortex, associated PMv, supplementary motor area and cerebellum[3], that guides speech processing modulated by somatosensory/auditory feedback loops[12] which have been shown to interact e.g. during stabilisation of the fundamental frequency[42]. Cross-modal interplays within the sensory system have recently gained increasing attention in the healthy. Multisensory processing may occur at different hierarchical levels of the respective sensory system and/or may modulate the sensory processing in classical (primary) stimulus-specific areas via feedback mechanisms[43,44]. Especially a role of regions in and around (posterior to) the auditory cortex has been suggested of relevance in this regard using event-related potentials in humans and intracranial recording in macaques[43,44]. With regard to audiotactile processing, fMRI studies have shown considerable spatial overlap of tactile and auditory stimulation-induced cortical networks with possible frequency-specific components[45,46]. A MEG study described modulation of somatosensory processing speed in the healthy in the presence of auditory stimuli[47]. Cross-modal convergence may occur at the cortico-cortical or subcortical (e.g. superior colliculi) level[43]. Disturbed neuronal synchrony by regional homogeneity in the TPJ may hint at disturbed intracortical processing in this multimodal area. Impaired sensory processing beyond the somatosensory system is yet little researched in FD. Nevertheless, impaired visuo-cerebellar (seed-based/ between-network) connectivity profiles have been described in cranial FDs, and for musician's embouchure dystonia auditory network abnormalities at rest have previously been shown[48], hinting at a possible subtype-associated component. Elucidating the effects of possible cross-modal dysfunctional interactions may hence be of interest in future studies aiming at further elucidating FD pathophysiology or between-subtype differences. Further, in analogy to somatosensory retraining approaches, this might incent the development of auditory (re)training approaches to ameliorate FLD symptoms, e.g. based on auditory perceptual observations such as an abnormal Lombard effect previously observed in ADSD patients[49].

Absence of overlapping differential activity and connectivity profiles. While both connectivity and stimulation-induced activation abnormalities affected the premotor cortex and upper parts of the temporal cortex, we did not observe spatial overlap. Premotor cortices were abnormally active in the ventral domain during tactile processing, while task-free connectivity was altered dorsally. In the upper temporal cortex, changes differed in their anterior-posterior location (Fig. 3). While some resting state networks seem to display a degree of task/event-related co-activation[50], the degree to which (parts of) certain intrinsic connectivity networks are recruited for[50,51] and during[52] a task or intervention may be varying and undergo dynamic change. Hence, beyond methodological aspects (e.g. sample size, network dimensionality) these observations may point to potential context-related dynamics in the disease whose relevance needs to be better understood to gain further insights into the complex focal dystonia pathophysiology, and may warrant cautious study design in interventional studies aiming at focal non-invasive (transcranial) modulation of cortical activity to ameliorate motor function as discussed above.

Absence of cortical BoNT-A-related change. In the present study we did not find evidence for BoNT-A-induced modulation of abnormal cortical processing. Methodological aspects such as small sample size, small applied average doses (Ø 15 units Abobotulinumtoxin) and the fact that the larynx representation was not directly tested may have resulted in reduced sensitivity to detect those changes. Alternatively, the probably endophenotypic changes in non-symptomatic representations might mirror underlying predisposing pathophysiology and hence not be responsive to BoNT-A, indicating that modulation of sensory input through BoNT-A observed in earlier clinical work[14] might indeed rather be closely linked to its modulation of muscle activity. Prior investigations of BoNT-A effects on phonation-induced brain activity were equivocal in spasmodic dysphonia[4,5]. Other studies investigating BoNT-A effects focused on craniocervical non-TSFDs and reported varying sensorimotor system effects[13].

Conclusion

The present study provides evidence for abnormally organized somatosensory processing in ADSD amending previous observations of abnormal peripheral tactile discrimination thresholds in the disease. Beyond supporting the notion of dysfunctional sensory processing as common pathophysiologic trait across FD subtypes, evidence of abnormal central somatosensory processing in cutaneous surrogate areas may serve as working point regarding sensory modulation strategies in the disease. Temporal cortex abnormalities during rest and tactile stimulus processing might hint at abnormal cross-modal sensory interactions warranting further research.

Received: 21 November 2019; Accepted: 26 May 2020;
Published online: 23 June 2020

References

1. Jinnah, H. A. *et al.* The focal dystonias: current views and challenges for future research. *Movement disorders: official journal of the Movement Disorder Society* **28**, 926–943, https://doi.org/10.1002/mds.25567 (2013).
2. Ludlow, C. L. Spasmodic dysphonia: a laryngeal control disorder specific to speech. *J Neurosci* **31**, 793–797, https://doi.org/10.1523/JNEUROSCI.2758-10.2011 (2011).
3. Brown, S. *et al.* The somatotopy of speech: phonation and articulation in the human motor cortex. *Brain Cogn* **70**, 31–41, https://doi.org/10.1016/j.bandc.2008.12.006 (2009).
4. Ali, S. O. *et al.* Alterations in CNS activity induced by botulinum toxin treatment in spasmodic dysphonia: an H215O PET study. *J Speech Lang Hear Res* **49**, 1127–1146, https://doi.org/10.1044/1092-4388(2006/081) (2006).
5. Haslinger, B. *et al.* "Silent event-related" fMRI reveals reduced sensorimotor activation in laryngeal dystonia. *Neurology* **65**, 1562–1569, https://doi.org/10.1212/01.wnl.0000184478.59063.db (2005).
6. Simonyan, K. & Ludlow, C. L. Abnormal activation of the primary somatosensory cortex in spasmodic dysphonia: an fMRI study. *Cerebral cortex* **20**, 2749–2759, https://doi.org/10.1093/cercor/bhq023 (2010).
7. Suppa, A. *et al.* Abnormal motor cortex excitability during linguistic tasks in adductor-type spasmodic dysphonia. *The European journal of neuroscience* **42**, 2051–2060, https://doi.org/10.1111/ejn.12977 (2015).
8. Battistella, G., Fuertinger, S., Fleysher, L., Ozelius, L. J. & Simonyan, K. Cortical sensorimotor alterations classify clinical phenotype and putative genotype of spasmodic dysphonia. *Eur J Neurol* **23**, 1517–1527, https://doi.org/10.1111/ene.13067 (2016).
9. Simonyan, K. & Ludlow, C. L. Abnormal structure-function relationship in spasmodic dysphonia. *Cerebral cortex* **22**, 417–425, https://doi.org/10.1093/cercor/bhr120 (2012).
10. Simonyan, K. *et al.* Focal white matter changes in spasmodic dysphonia: a combined diffusion tensor imaging and neuropathological study. *Brain: a journal of neurology* **131**, 447–459, https://doi.org/10.1093/brain/awm303 (2008).
11. Rauschecker, J. P. & Scott, S. K. Maps and streams in the auditory cortex: nonhuman primates illuminate human speech processing. *Nature neuroscience* **12**, 718–724, https://doi.org/10.1038/nn.2331 (2009).
12. Hickok, G. The cortical organization of speech processing: feedback control and predictive coding the context of a dual-stream model. *J Commun Disord* **45**, 393–402, https://doi.org/10.1016/j.jcomdis.2012.06.004 (2012).
13. Weise, D., Weise, C. M. & Naumann, M. Central Effects of Botulinum Neurotoxin-Evidence from Human Studies. *Toxins (Basel)* **11**, https://doi.org/10.3390/toxins11010021 (2019).
14. Bielamowicz, S. & Ludlow, C. L. Effects of botulinum toxin on pathophysiology in spasmodic dysphonia. *Ann Otol Rhinol Laryngol* **109**, 194–203, https://doi.org/10.1177/000348940010900215 (2000).
15. Dresel, C. *et al.* Botulinum toxin modulates basal ganglia but not deficient somatosensory activation in orofacial dystonia. *Movement disorders: official journal of the Movement Disorder Society* **26**, 1496–1502, https://doi.org/10.1002/mds.23497 (2011).
16. Dresel, C., Haslinger, B., Castrop, F., Wohlschlaeger, A. M. & Ceballos-Baumann, A. O. Silent event-related fMRI reveals deficient motor and enhanced somatosensory activation in orofacial dystonia. *Brain: a journal of neurology* **129**, 36–46, https://doi.org/10.1093/brain/awh665 (2006).
17. Quartarone, A. & Hallett, M. Emerging concepts in the physiological basis of dystonia. *Movement disorders: official journal of the Movement Disorder Society* **28**, 958–967, https://doi.org/10.1002/mds.25532 (2013).
18. Miyaji, H. *et al.* Neuromagnetic detection of the laryngeal area: Sensory-evoked fields to air-puff stimulation. *Neuroimage* **88**, 162–169, https://doi.org/10.1016/j.neuroimage.2013.11.008 (2014).
19. Meunier, S. *et al.* Human brain mapping in dystonia reveals both endophenotypic traits and adaptive reorganization. *Annals of neurology* **50**, 521–527 (2001).
20. Mantel, T. *et al.* Activity and topographic changes in the somatosensory system in embouchure dystonia. *Mov Disord* **31**, 1640–1648, https://doi.org/10.1002/mds.26664 (2016).
21. Dresel, C. *et al.* A new device for tactile stimulation during fMRI. *Neuroimage* **39**, 1094–1103, https://doi.org/10.1016/j.neuroimage.2007.09.033 (2008).
22. Vergara, V. M., Mayer, A. R., Damaraju, E., Hutchison, K. & Calhoun, V. D. The effect of preprocessing pipelines in subject classification and detection of abnormal resting state functional network connectivity using group ICA. *Neuroimage* **145**, 365–376, https://doi.org/10.1016/j.neuroimage.2016.03.038 (2017).
23. Murphy, K., Birn, R. M. & Bandettini, P. A. Resting-state fMRI confounds and cleanup. *Neuroimage* **80**, 349–359, https://doi.org/10.1016/j.neuroimage.2013.04.001 (2013).
24. Zuo, X. N. *et al.* Toward reliable characterization of functional homogeneity in the human brain: preprocessing, scan duration, imaging resolution and computational space. *Neuroimage* **65**, 374–386, https://doi.org/10.1016/j.neuroimage.2012.10.017 (2013).
25. Calhoun, V. D., Adali, T., Pearlson, G. D. & Pekar, J. J. A method for making group inferences from functional MRI data using independent component analysis. *Hum Brain Mapp* **14**, 140–151 (2001).
26. Himberg, J., Hyvarinen, A. & Esposito, F. Validating the independent components of neuroimaging time series via clustering and visualization. *Neuroimage* **22**, 1214–1222, https://doi.org/10.1016/j.neuroimage.2004.03.027 (2004).
27. Feiwell, R. J. *et al.* Diminished regional cerebral blood flow response to vibration in patients with blepharospasm. *Neurology* **52**, 291–297 (1999).
28. Neychev, V. K., Gross, R. E., Lehericy, S., Hess, E. J. & Jinnah, H. A. The functional neuroanatomy of dystonia. *Neurobiology of disease* **42**, 185–201, https://doi.org/10.1016/j.nbd.2011.01.026 (2011).
29. Stamelou, M., Edwards, M. J., Hallett, M. & Bhatia, K. P. The non-motor syndrome of primary dystonia: clinical and pathophysiological implications. *Brain* **135**, 1668–1681, https://doi.org/10.1093/brain/awr224 (2012).
30. Khosravani, S. *et al.* Laryngeal vibration as a non-invasive neuromodulation therapy for spasmodic dysphonia. *Sci Rep* **9**, 17955, https://doi.org/10.1038/s41598-019-54396-4 (2019).
31. Tamura, Y. *et al.* Impaired intracortical inhibition in the primary somatosensory cortex in focal hand dystonia. *Movement disorders: official journal of the Movement Disorder Society* **23**, 558–565, https://doi.org/10.1002/mds.21870 (2008).
32. Tinazzi, M. *et al.* Abnormal central integration of a dual somatosensory input in dystonia. Evidence for sensory overflow. *Brain: a journal of neurology* **123**(Pt 1), 42–50 (2000).
33. Nelson, A. J., Blake, D. T. & Chen, R. Digit-specific aberrations in the primary somatosensory cortex in Writer's cramp. *Annals of neurology* **66**, 146–154, https://doi.org/10.1002/ana.21626 (2009).
34. Termsarasab, P. *et al.* Neural correlates of abnormal sensory discrimination in laryngeal dystonia. *NeuroImage. Clinical* **10**, 18–26, https://doi.org/10.1016/j.nicl.2015.10.016 (2016).
35. Erro, R. *et al.* High frequency somatosensory stimulation in dystonia: Evidence fordefective inhibitory plasticity. *Movement disorders: official journal of the Movement Disorder Society* **33**, 1902–1909, https://doi.org/10.1002/mds.27470 (2018).
36. Battistella, G. & Simonyan, K. Top-down alteration of functional connectivity within the sensorimotor network in focal dystonia. *Neurology* **92**, e1843–e1851, https://doi.org/10.1212/WNL.0000000000007317 (2019).
37. Nowak, D. A. & Hermsdorfer, J. Predictive and reactive control of grasping forces: on the role of the basal ganglia and sensory feedback. *Exp Brain Res* **173**, 650–660, https://doi.org/10.1007/s00221-006-0409-7 (2006).
38. Popa, T. *et al.* Abnormal cerebellar processing of the neck proprioceptive information drives dysfunctions in cervical dystonia. *Sci Rep* **8**, 2263, https://doi.org/10.1038/s41598-018-20510-1 (2018).
39. Quartarone, A. *et al.* Therapeutic Use of Non-invasive Brain Stimulation in Dystonia. *Front Neurosci* **11**, 423, https://doi.org/10.3389/fnins.2017.00423 (2017).

40. Bianchi, S. *et al*. Phenotype- and genotype-specific structural alterations in spasmodic dysphonia. *Movement disorders: official journal of the Movement Disorder Society* **32**, 560–568, https://doi.org/10.1002/mds.26920 (2017).
41. Putzel, G. G. *et al*. Polygenic Risk of Spasmodic Dysphonia is Associated With Vulnerable Sensorimotor Connectivity. *Cerebral cortex* **28**, 158–166, https://doi.org/10.1093/cercor/bhw363 (2018).
42. Larson, C. R., Altman, K. W., Liu, H. & Hain, T. C. Interactions between auditory and somatosensory feedback for voice F0 control. *Exp Brain Res* **187**, 613–621, https://doi.org/10.1007/s00221-008-1330-z (2008).
43. Driver, J. & Noesselt, T. Multisensory interplay reveals crossmodal influences on 'sensory-specific' brain regions, neural responses, and judgments. *Neuron* **57**, 11–23, https://doi.org/10.1016/j.neuron.2007.12.013 (2008).
44. Schroeder, C. E. & Foxe, J. Multisensory contributions to low-level, 'unisensory' processing. *Curr Opin Neurobiol* **15**, 454–458, https://doi.org/10.1016/j.conb.2005.06.008 (2005).
45. Perez-Bellido, A., Anne Barnes, K., Crommett, L. E. & Yau, J. M. Auditory Frequency Representations in Human Somatosensory Cortex. *Cerebral cortex* **28**, 3908–3921, https://doi.org/10.1093/cercor/bhx255 (2018).
46. Schurmann, M., Caetano, G., Hlushchuk, Y., Jousmaki, V. & Hari, R. Touch activates human auditory cortex. *Neuroimage* **30**, 1325–1331, https://doi.org/10.1016/j.neuroimage.2005.11.020 (2006).
47. Sugiyama, S., Takeuchi, N., Inui, K., Nishihara, M. & Shioiri, T. Effect of acceleration of auditory inputs on the primary somatosensory cortex in humans. *Sci Rep* **8**, 12883, https://doi.org/10.1038/s41598-018-31319-3 (2018).
48. Haslinger, B. *et al*. Changes in resting-state connectivity in musicians with embouchure dystonia. *Movement disorders: official journal of the Movement Disorder Society* **32**, 450–458, https://doi.org/10.1002/mds.26893 (2017).
49. McColl, D. & McCaffrey, P. Perception of spasmodic dysphonia speech in background noise. *Percept Mot Skills* **103**, 629–635, https://doi.org/10.2466/pms.103.2.629-635 (2006).
50. Laird, A. R. *et al*. Networks of task co-activations. *Neuroimage* **80**, 505–514, https://doi.org/10.1016/j.neuroimage.2013.04.073 (2013).
51. Mennes, M., Kelly, C., Colcombe, S., Castellanos, F. X. & Milham, M. P. The extrinsic and intrinsic functional architectures of the human brain are not equivalent. *Cerebral cortex* **23**, 223–229, https://doi.org/10.1093/cercor/bhs010 (2013).
52. Deco, G., Jirsa, V. K. & McIntosh, A. R. Emerging concepts for the dynamical organization of resting-state activity in the brain. *Nat Rev Neurosci* **12**, 43–56, https://doi.org/10.1038/nrn2961 (2011).

Acknowledgements

We cordially thank Dr. Hulin for patient recruitment and all patients/healthy controls for their participation in the study. This study was supported by the Deutsche Forschungsgemeinschaft (DFG HA3370/5-1) Bonn, Germany and the Kommission für Klinische Forschung, Technical University of Munich School of Medicine (KKF H-05).

Author contributions

B.H. and C.D. conceived the study. C.D. and M.W. organized the study and acquired the data. T.M. (the first author) and M.W. analyzed the data. T.M. (the first author) wrote the manuscript and prepared tables and figures. C.Z. provided technical equipment and support. B.H., T.M. (the co-author) and A.J. reviewed the analysis and statistical design. All authors reviewed the manuscript.

Competing interests

T. Mantel receives research support from the KKF (H-05). T. Meindl has received travel grants from Pharm-Allergan GmbH, Ipsen Pharma GmbH, Merz Pharma GmbH & Co. KGaA. A. Jochim has received travel grants by Merz Pharma GmbH & Co. KGaA as well as speaker honoraria by Pharm-Allergan GmbH and Merz Pharma GmbH & Co. KGaA.C. Zimmer has served on scientific advisory boards for Philips. He has received speaker honoraria from Philips. He serves as co-editor on the Advisory Board of Clinical Neuroradiology. C. Dresel received research support from the DFG (DFG HA3370/3-1). B. Haslinger received research support from Ipsen Pharma GmbH and the DFG (DFG HA3370/5-1), has received speaker honoraria from Pharm-Allergan GmbH and Ipsen Pharma GmbH and has received travel grants from Ipsen Pharma GmbH and Merz Pharmaceuticals GmbH. He has received royalties for book chapters from Cambridge University Press and Springer Medizin. The other authors report no disclosures.

Additional information

Supplementary information is available for this paper at https://doi.org/10.1038/s41598-020-67295-w.

Correspondence and requests for materials should be addressed to B.H.

Reprints and permissions information is available at www.nature.com/reprints.

Publisher's note Springer Nature remains neutral with regard to jurisdictional claims in published maps and institutional affiliations.

Supplementary material

Altered sensory system activity and connectivity patterns in adductor spasmodic dysphonia

Tobias Mantel, MD[1]; Christian Dresel, MD[1,2]; Michael Welte, MD[1]; Tobias Meindl, MD[1]; Angela Jochim, MD[1]; Claus Zimmer, MD[3] and Bernhard Haslinger, MD[1]*

[1]Department of Neurology, Klinikum rechts der Isar, Technische Universität München, Ismaningerstrasse 22, Munich, Germany

[2]Department of Neurology, Johannes Gutenberg University, Langenbeckstrasse 1, Mainz, Germany

[3]Department of Neuroradiology, Klinikum rechts der Isar, Technische Universität München, Ismaningerstrasse 22, Munich, Germany

***Correspondence to:** Prof. Dr. Bernhard Haslinger, Klinik und Poliklinik für Neurologie, Klinikum rechts der Isar, Technische Universität München, Ismaninger Strasse 22, D - 81675 München, Germany; E-Mail (corresponding author): bernhard.haslinger@tum.de; Tel 0049-89-4140-4672)

Supplementary methods: data acquisition and software

Data were acquired on a 3T Achieva scanner (Philips N.V., the Netherlands) using an 8-channel head coil. Participants were instructed to keep their eyes closed during the whole experiment, concentrate on the tactile stimuli during the task runs (encouraged by announcing a post-fMRI questionnaire[1,2]) and the head was fixed with foam pads to minimize the risk of motion artefacts. One resting-state run, and subsequently three runs of experimental tactile stimulation at each 303 T2*-weighted echo planar scans (repetition time/echo time (TR/TE) 2200/30ms, field of view (FoV) 216x216 mm^2, 36 slices, slice gap 0.5mm, voxel size 3x3x3mm^3) were collected. Additionally, a high-resolution 3D T1-weighted scan was acquired as anatomical reference (TR/TE/TI=9/4/780ms, FoV=240x240mm^2, voxel size 1x1x1mm^3, 170 slices).

Functional data were analysed using SPM12 (https://www.fil.ion.ucl.ac.uk/spm), DPABI routines (v3.0, http://rfmri.org/DPARSF) and GIFT (v3.0a; http://mialab.mrn.org/software/gift) for Matlab2016a (MathWorks Inc., USA). Deformation parameters for normalization of functional data were calculated from structural data following coregistration using CAT12 (http://dbm.neuro.uni-jena.de/cat/).

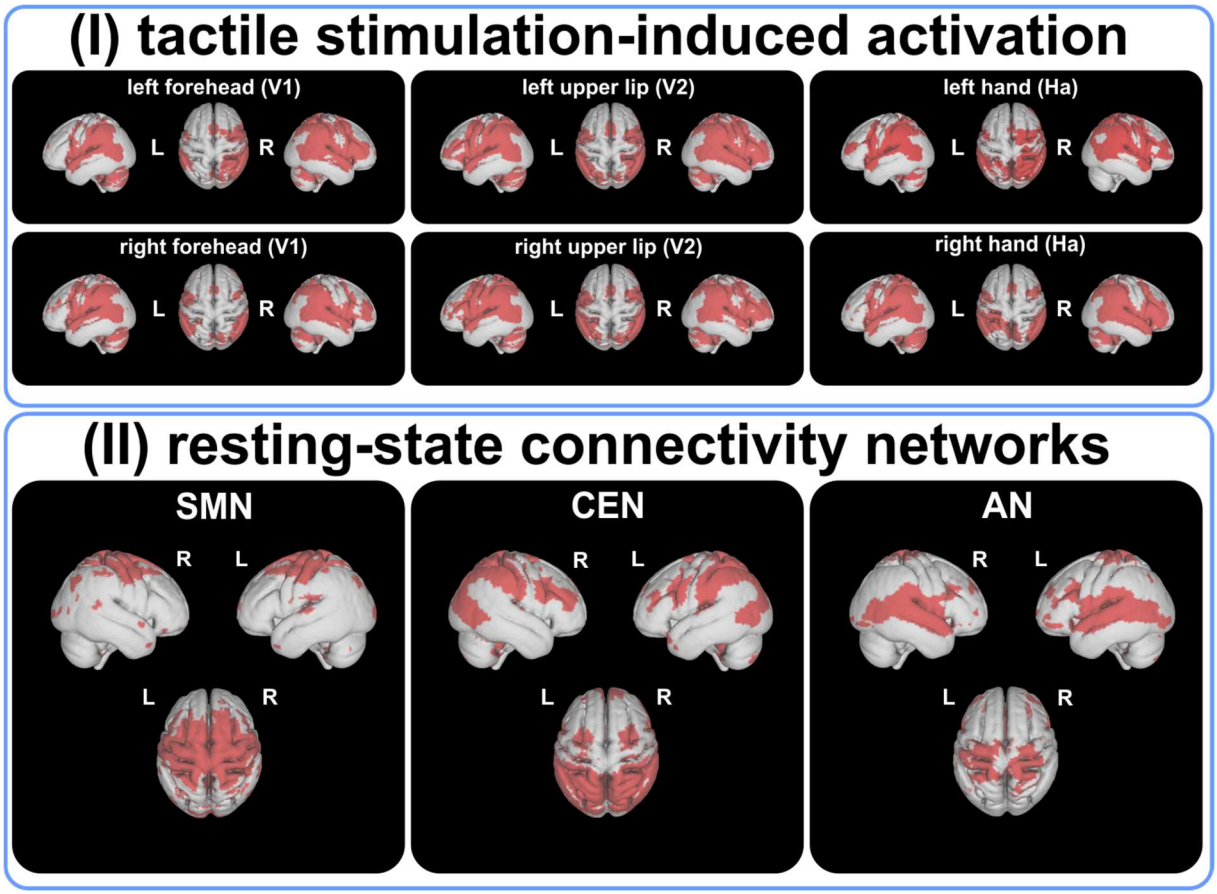

Figure s-1. Tactile stimulation-induced cortical activity networks (I) and resting-state connectivity networks (II) across all study participants, tresholded at p<.001 uncorrected, projected on the 3D reconstructed anatomical scan of all participants in MNI space. SMN, sensorimotor network; CEN, central executive network; AN, auditory network; L/R, left/right hemisphere.

Table s-1. Areas with trends (k>50 voxels) towards stronger activation in patients with ADSD before BoNT treatment when compared to healthy controls

L-sided stimulation						R-sided stimulation					
V1						**V1**					
Area	**x**	**y**	**z**	**t**	**V**	**Area**	**x**	**y**	**z**	**T**	**V**
–			–			**R primary motor, face (BA4)**	**-40**	**-8**	**56**	**4.24**	**267**
						R dorsal premotor (BA6)	**-32**	**-4**	**50**	**3.68**	
						R dorsal insula (BA13)	**36**	**12**	**0**	**4.08**	**223**
						R dorsal insula	**38**	**28**	**-2**	**3.68**	
						L inferior frontal (BA44/45)	**-50**	**12**	**24**	**4.07**	**319**
						R caudate nucleus	16	6	6	5.01	92
						L inferior parietal sulcus (BA5)	-32	-40	40	4.71	176
						L caudate nucleus	-14	2	14	3.97	107
						L thalamus	-10	-12	18	3.85	
						L inferior frontal sulcus (A45/46)	-50	38	18	3.91	50
						R middle frontal (BA10)	38	-8	48	3.81	75
						L primary motor (BA4)	-26	-22	66	3.78	56
						R inferior parietal (BA40)	64	-40	22	3.72	55
						R inferior frontal (BA44)	44	14	28	3.40	51
						R ventral premotor (BA6)	42	8	36	3.31	
V2						**V2**					
Area	**x**	**y**	**z**	**t**	**V**	**Area**	**x**	**y**	**z**	**T**	**V**
R ventral premotor/ inferior frontal (BA6/44)	**60**	**8**	**18**	**4.10**	**215**	L primary motor, face (BA4)	-40	-8	54	4.13	168
R ventral premotor (BA6)	46	8	44	4.22	78	L ventral premotor (BA6)	-30	-2	54	3.55	
L secondary somatosensory (OP4)	-62	-18	20	4.03	68	R primary somatosensory, face (BA1/2)	56	-16	40	3.77	81
L primary somatosensory, face (BA1)	-58	-20	38	3.96	130	L ventral premotor/ inferior frontal (BA6/44)	-50	12	24	3.69	54
L superior temporal (BA22)	-52	0	0	3.61	56	L primary somatosensory (BA1/2)	-26	-38	66	3.64	70
L inferior frontal (BA44)	-50	2	10	3.40		L superior parietal (BA5)	-22	-44	74	3.19	
						L inferior parietal (BA39)	-48	-74	20	3.51	81
						L parietotemporal junction (BA37/39)	-50	-64	12	3.23	
Ha						**Ha**					
Area	**x**	**y**	**z**	**t**	**V**	**Area**	**x**	**y**	**z**	**T**	**V**
R ventral premotor (BA6/44)	**48**	**8**	**28**	**4.16**	**288**	**L ventral premotor (BA6/44)**	**-54**	**12**	**26**	**3.99**	**290**
R inferior frontal junction (BA6/8/44)	**44**	**8**	**42**	**3.20**		**L inferior frontal junction (BA6/8/44)**	**-42**	**4**	**48**	**3.45**	
R dorsal premotor (BA6)	32	-2	58	4.18	138	**R primary motor (BA4)**	**-40**	**-8**	**54**	**3.25**	
L secondary somatosensory (OP4)	-60	-18	22	4.08	84	L intraparietal sulcus (BA7)	-30	-54	42	3.99	115
L superior parietal (BA5)	-30	-38	48	3.95	147	L ventral insula (BA13)	-30	22	-6	3.87	65
L primary motor (BA4/6)	-56	8	32	3.66	200	L primary somatosensory, hand (BA2)	-26	-38	54	3.80	64
L ventral premotor (BA6/44)	-44	8	34	3.65		L superior temporal (BA22)	-60	-42	12	3.79	87

Trends are depicted k>50 voxels at a cluster-forming threshold of p<.001 uncorrected. Clusters that were significant at p_{FWEc}<.05 but did not survive correction for the number of conditions are highlighted in bold.
Coordinates (in mm) in the Montreal Neurological Institute space. BA, Brodmann area; OP, operculum parietale; R, right; L, left; t, t-score; V, cluster volume (voxels).

References (supplement)

1 Dresel, C., Haslinger, B., Castrop, F., Wohlschlaeger, A. M. & Ceballos-Baumann, A. O. Silent event-related fMRI reveals deficient motor and enhanced somatosensory activation in orofacial dystonia. *Brain : a journal of neurology* **129**, 36-46, doi:10.1093/brain/awh665 (2006).

2 Mantel, T. *et al.* Activity and topographic changes in the somatosensory system in embouchure dystonia. *Movement disorders : official journal of the Movement Disorder Society* **31**, 1640-1648, doi:10.1002/mds.26664 (2016).

NeuroImage: Clinical 28 (2020) 102410

Contents lists available at ScienceDirect

NeuroImage: Clinical

journal homepage: www.elsevier.com/locate/ynicl

Structure-function abnormalities in cortical sensory projections in embouchure dystonia

Tobias Mantel[a], Eckart Altenmüller[b], Yong Li[a], André Lee[a,b], Tobias Meindl[a], Angela Jochim[a], Claus Zimmer[c], Bernhard Haslinger[a,*]

[a] Department of Neurology, Klinikum rechts der Isar, Technische Universität München, Ismaningerstrasse 22, Munich, Germany
[b] Hochschule für Musik, Theater und Medien Hannover, Emmichplatz 1, Hanover, Germany
[c] Department of Neuroradiology, Klinikum rechts der Isar, Technische Universität München, Ismaningerstrasse 22, Munich, Germany

ARTICLE INFO

Keywords:
Musician's Dystonia
Dystonia, Focal, Task-Specific
Diffusion Tractography
Sensorimotor Cortex
Basal Ganglia

ABSTRACT

Background: Embouchure dystonia (ED) is a task-specific focal dystonia in professional brass players leading to abnormal orofacial muscle posturing/spasms during performance. Previous studies have outlined abnormal cortical sensorimotor function during sensory/motor tasks and in the resting state as well as abnormal cortical sensorimotor structure. Yet, potentially underlying white-matter tract abnormalities in this network disease are unknown.
Objective: To delineate structure-function abnormalities within cerebral sensorimotor trajectories in ED.
Method: Probabilistic tractography and seed-based functional connectivity analysis were performed in 16/16 ED patients/healthy brass players within a simple literature-informed network model of cortical sensorimotor processing encompassing supplementary motor, superior parietal, primary somatosensory and motor cortex as well as the putamen. Post-hoc grey matter volumetry was performed within cortices of abnormal trajectories.
Results: ED patients showed average axial diffusivity reduction within projections between the primary somatosensory cortex and putamen, with converse increases within projections between supplementary motor and superior parietal cortex in both hemispheres. Increase in the mode of anisotropy in patients was accompanying the latter left-hemispheric projection, as well as in the supplementary motor area's projection to the left primary motor cortex. Patient's left primary somatosensory functional connectivity with the putamen was abnormally reduced and significantly associated with the axial diffusivity reduction. Left primary somatosensory grey matter volume was increased in patients.
Conclusion: Correlates of abnormal tract integrity within primary somatosensory cortico-subcortical projections and higher-order sensorimotor projections support the key role of dysfunctional sensory information propagation in ED pathophysiology. Differential directionality of cortico-cortical and cortico-subcortical abnormalities hints at non-uniform sensory system changes.

1. Introduction

Embouchure dystonia (ED) is a task-specific focal dystonia (TSFD) manifesting in highly-trained brass players during musical performance. In the otherwise asymptomatic patients, playing the instrument evokes abnormal posturing, tremor, and spasms in the (peri)oral muscles that control the airflow through the mouthpiece, severely disabling musical performance (Frucht, 2009). Abnormal sensorimotor information integration has been postulated a central feature with regard to the manifestation of dystonic postures. Observations during both task and rest in ED suggest that this dysfunctional integration may encompass primary and higher-order sensorimotor cortices (Haslinger et al., 2010, 2017). Maladaptive plasticity, abnormal intracortical/basal ganglia inhibition, and abnormal processing of sensory information are assumed the most relevant pathophysiologic mechanisms leading to sensorimotor dysfunction in the disease (Quartarone and Hallett, 2013). Yet, the exact nature of their interplay eventually resulting in the cortical frontoparietal (e.g. sensorimotor) network abnormalities observable using functional

Abbreviations: AD, axial diffusivity; ADDS, arm dystonia disability scale; CON, healthy musicians; dMRI, diffusion MRI; DTI, diffusion tensor image; ED, embouchure dystonia, FA, fractional anisotropy; FD, focal dystonia; FDR, false discovery rate; FWE, family-wise error; GM, grey matter; M1, primary motor cortex; MO, mode of anisotropy; PAT, brass players with embouchure dystonia; Put, Putamen; RD, radial diffusivity; ROI, region of interest; rsfMRI, resting state functional MRI; S1, primary somatosensory cortex; SLF, superior longitudinal fascicle; SMA, supplementary motor area; SPL, superior parietal lobe; TE/TR, echo/repetition time; TSFD, task-specific focal dystonia

* Corresponding author.
E-mail address: bernhard.haslinger@tum.de (B. Haslinger).

https://doi.org/10.1016/j.nicl.2020.102410
Received 7 May 2020; Received in revised form 29 July 2020; Accepted 30 August 2020
Available online 02 September 2020

neuroimaging is unclear (Haslinger et al., 2017). Previous findings in musician's dystonia favour an emphasized role of abnormal (somato) sensory processing in orderly predisposed individuals in the emergence of this form of TSFD (Lim et al., 2003; Rosenkranz et al., 2005). Sensory dysfunction in ED has been observed both in presence and in absence of tasks (Haslinger et al., 2010, 2017; Mantel et al., 2016), accompanied by reports of abnormal somatosensory topography and grey matter (GM) volume hinting at maladaptive plasticity in such cortices (Mantel et al., 2019, 2016; Uehara et al., 2019). Subcortically, findings in ED during task paradigms and in structural analysis both in embouchure and pianist's musician's dystonia point to particular relevance of the striatum (Granert et al., 2011; Haslinger et al., 2010; Mantel et al., 2019). This is in line with recent observations in non-musician TSFD suggesting an abnormal dopamine receptor expression in both motor and nonmotor sections of the striatum, which may in turn result in a reduced inhibition/increased excitation in the cortex due to an imbalance in basal-ganglia outflow pathways (Fujita and Eidelberg, 2017; Simonyan et al., 2017).

Based on the evidence outlined above, this work aimed at further structuro-functional characterization of abnormal cerebral sensorimotor interaction patterns in ED focusing on projections of cortical origin. Following the previously reported abnormalities in ED, a simple model mirroring basic cerebral sensorimotor interaction involving primary and higher-order sensory and motor cortices and the putamen (due to its role as main entry point of cortical input to the basal ganglia) was set up. This allowed to sensitively investigate the integrity of structural and functional sensory and motor trajectories with regard to their inter- and subcortical relations, focusing on trajectories within which we hypothesized abnormalities in tract integrity (and concomitant functional changes) to be most likely to occur based on the existing evidence.

2. Methods

2.1. Participants

The study included 16 professional brass musicians with ED (44.2 ± 12.4 years, 14 males, 2 females; PAT) recruited from the Institute for Music Physiology and Musicians Medicine in Hanover, and 16 healthy professional brass players recruited from local conservatories/orchestras (44.1 ± 12.1 years, 16 males; CON). All were right-handed (Oldfield, 1971) musical professionals with no (other) neuro(psychiatric) deficits or symptoms (including no other movement disorders), no major internal disease and no abnormal brain structure on MRI (table 1 for details). No patient was treated with botulinum neurotoxin (15 patients were never treated; one patient had received one injection 20 months prior to participation) or under the effect of oral medication for dystonia at the time of the study. The study was approved by the institutional ethics board (Ethikkommission der Technischen Universität München, https://www.ek-med-muenchen.de). All participants gave written informed consent according to the Declaration of Helsinki. In addition to MRI acquisition, each participant's lower face and neck were videotaped during musical performance of predefined sequences (ascending/descending scales, fourths, tones). Given insensitivity of established focal dystonia (FD) rating scales (e.g. Burke-Fahn-Marsden, Tubiana-Chamagne score) to ED-specific symptoms such as deterioration of sound or attack of the tongue, video performances were blindly rated by an ED expert (E.A.) according to a previously employed customized score (Haslinger et al., 2010, 2017; Mantel et al., 2019, 2016). Further, the Arm Dystonia Disability Scale (ADDS) was collected to screen for possible co-incident symptoms of hand TSFD.

2.2. Data acquisition

Data were acquired on a 3T Achieva MRI scanner (Philips, the Netherlands) with an 8-channel head coil. First, 64-gradient direction diffusion tensor MR images (dMRI) were acquired using a cardiac-gated single-shot spin-echo echo-planar imaging sequence (echo time (TE) = 92 ms, repetition time (TR) = 11–22 bpm (heart-rate dependent), b-value = 1400 s/mm^2, α = 90°; field-of-view = 232 × 232 mm; voxel size = 1.81 × 1.81 × 2 mm^3; 66 axial slices without gap). Participants' heads were fixed with foam pads to minimize the risk of motion artefacts. To further reduce motion risk in view of relatively long dMRI scan durations owed to cardiac gating, image acquisition was divided into two separate runs of 32 diffusion-weighted images each. Second, 303 echo-planar resting-state functional MR images (rsfMRIs) were collected (TR/TE = 2200/30 ms, field-of-view = 216 × 216 mm^2, voxel size 3 × 3 × 3 mm^3, 36 axial slices, gap 0.5 mm). Participants were instructed to keep their eyes closed during the whole measurement. Third, a 3D high-resolution gradient echo T1-weighted reference image was acquired (TR/TE/inversion time = 9/4/780 ms; α = 8°; field-of-view = 240 × 240 mm, voxel size 1 × 1 × 1 mm^3, 170 axial slices without gap).

2.3. Software

dMRI data were preprocessed using ExploreDTIv4.8.6 (www.exploredti.com) and analysed in FSLv5.0.10 (https://fsl.fmrib.ox.ac.uk/fsl/). RsfMRI data were analysed in SPM12br6906 (https://www.fil.ion.ucl.ac.uk/spm/) and DPABIv3.0. Anatomical scans were processed in CAT12r1152 (http://www.neuro.uni-jena.de/cat/). Statistical analysis was performed using PALMα112 (https://fsl.fmrib.ox.ac.uk/fsl/fslwiki/PALM), MatlabR2016b (the MathWorks Inc., Natick, USA), and SPSS25 (IBM, New York, USA).

2.4. Diffusion data analysis

2.4.1. Preprocessing

dMRI data from the two runs were concatenated, corrected for motion/eddy current-induced geometrical distortions (Leemans and Jones, 2009) and for susceptibility-induced distortion aided by information from the aligned anatomical scan (Irfanoglu et al., 2012) with upsampling to a voxel size of 1 mm isotropic. Registration and data quality were visually checked. *BEDPOSTx* was applied to fit a probabilistic diffusion model on the corrected data, modelling two fibres per voxel. Scalar images were calculated from the diffusion tensor images (DTI) based on a linear tensor model using *DTIFIT*.

2.4.2. Probabilistic tractography

Following the study's objective, we set up a simple model mirroring potentially abnormal intracerebral trajectories of sensorimotor integration originating from the cortical level: probabilistic tractography was performed to reconstruct connections between (i) the superior parietal lobe (SPL) and supplementary motor area (SMA) within the superior longitudinal fascicle (SLF) (Bozkurt et al., 2017; Makris et al., 2005), (ii) the facial primary somatosensory ($S1_{FACE}$) and facial primary motor cortex ($M1_{FACE}$), (iii) the SMA and $M1_{FACE,}$ and (iv) these cortical areas and the putamen (Put). All regions fulfilled our internal reliability requirement of having been reported abnormal in musician's or embouchure dystonia in more than one study and more than one neuroimaging approach (Granert et al., 2011; Haslinger et al., 2010, 2017; Kita et al., 2018; Mantel et al., 2019, 2016). The cortical regions of interest (ROIs) were derived from the Brainnetome atlas (https://atlas.brainnetome.org/) (Fan et al., 2016), whose detailed connectivity-based cortical parcellation makes it advantageous for analyses using corresponding modality. The subcortical putamen ROIs (serving as target only, see below) were derived from the Harvard-Oxford subcortical atlas (https://fsl.fmrib.ox.ac.uk/fsl/), achieving good overlay with the subject basal ganglia macroanatomy with reliable exclusion of neighbouring white matter of the capsule (table s-1A). Tract reconstruction was performed in native space pursuing a previously described two-pass procedure that allows for reliable reconstruction of trajectories with small structural connectivity probabilities (Schulz et al., 2015). Tracking was performed from the juxtacortical white

Table 1
Demographic and clinical characteristics.

	brass musicians with ED		healthy brass musicians	p-value
Age, y (mean, SD)	44.2, 12.4		44.1, 12.1	0.98[1)]
Sex (m/f)	14/2		16/0	0.10[2)]
TIV, cm^3 (mean, SD)	1604.8		1593.5	0.79[1)]
age at start of play, y (mean, SD)	11.2, 2.5		11.0, 3.8	0.82[1)]
main instrument (trumpet/trombone/horn)	4/8/4		3/3/10	
Disease duration, mo	65.8, 50.7			
Daily training, h (median, IQR)[a]	before ED	4.0, 1.8	2.5, 1.3	0.005[2)] / 0.002[3)](between/within-group)
	with ED	0.9, 2.0		
ED score (median, IQR)[b]	4.0, 1.8		1.0, 0	< 0.001[2)]
ADDS (mean, SD)	99.4, 1.7			

Demographic and clinical characteristics of healthy and diseased brass musicians. To further account for potential nuisance effects of age, sex and total intracranial volume (TIV), these variables were additionally included as nuisance covariates in statistical analyses where appropriate (see section 'Statistical analyses'). Statistical between-group comparisons applied [1)]t-tests, [2)]Wilcoxon rank-sum or [3)]signed-ranks tests. Evaluation by both ADDS and neurologic exam did not reveal signs of signs of concomitant hand dystonia in patients. SD = standard deviation; IQR = interquartile range; y = years; h = hours; TIV = total intracranial volume; m = male; f = female; NA = not applicable.

[a]Based on retrospective reports. For daily training at the time of the study, the average for the last four weeks was indicated. Given the nature of the disease, daily training was reduced after disease onset compared to healthy brass players.

[b]Embouchure dystonia score (dystonic symptom rating during performance of standardized sequences): 1 = normal play, 2 = nearly normal play, not distinctly dystonic; 3–5 = abnormal playing with evidence of dystonic orofacial movements (minor/medium/severe degree).

matter: following atlas registration to the individuals' native space applying the warping parameters generated during segmentation and Montreal Neurological Imaging (MNI) space normalisation of the aligned anatomical scan, the final native-space tractography seeds for each participant were generated by multiplication of the atlas-derived ROIs with a Ø 2 mm white matter surface margin generated by respective erosion of the aligned anatomical native space white matter segment (figure s-1). For cortico-cortical connections 50,000 streamlines were sent reciprocally from the seeds and combined (Jeurissen et al., 2019; Schulz et al., 2015), and for cortico-putaminal connections 25,000 streamlines were sent unidirectionally form the cortical seeds (curvature threshold 0.2, step length 0.5 mm) in native space. Tracking was constrained to voxels with FA > 0.15 which reliably prevented tracking through non-white matter tissue. For initial tract reconstruction, anatomy-informed standardized exclusion masks created on literature-based knowledge on tract courses (Kamali et al., 2014; Lehericy et al., 2004) were applied to guide tractography (table s-1B). Notably, these encompassed subcortical nuclei of no interest, passages to the brainstem/through the internal capsule, GM, cerebrospinal fluid, and neighbouring juxtacortical white matter to exclude erroneous tract propagation through U-fibres. In a second step, refined exclusion masks were generated by mean dilation of the initial trajectory volume four times at a common 5% threshold and further addition of specific exclusion masks (if necessary) to eliminate erroneous fibre courses. After refinement in this second pass, resulting individual tracts were thresholded at connection probabilities of 2%, 5%, 10%, and 20%. Mean values of fractional anisotropy (FA), the (orthogonal) mode-of-anisotropy (MO), axial (AD) and radial diffusivity (RD) were extracted from the individual tract volumes in native space for evaluation of tract integrity. As there is no objective standard for thresholding in probabilistic tractography we chose not to investigate a single threshold but calculated the mean across the above thresholds (Schulz et al., 2015). Given that cortico-(sub)cortical $M1/S1_{FACE}$-seeded probable tracts run in close proximity, we calculated Jaccard's coefficients (range 0–1; 0 = full dissimilarity, 1 = full similarity) for each participant to detect relevant overlays.

2.5. Functional data analysis

2.5.1. Preprocessing

Data preparation included discarding of the first five scans, realignment, slice-timing correction (to first slice), coregistration with the anatomical scan, and normalization to MNI space applying anatomical scan-derived warping parameters. This was followed by linear detrending, regression of six motion parameters, scrubbing of scans with framewise displacement > 0.5 mm (including the preceding and two following scans) (Jenkinson et al., 2002), removal of five white matter and cerebrospinal fluid signal principal components (CompCor), and bandpass-filtering (0.01–0.08 Hz). Scans were smoothed with a 6 mm full-width-at-half-maximum Gaussian kernel.

2.5.2. Seed-based correlation analysis

ROI-based functional connectivity (FC) analysis was conducted for all eight cortical ROIs in MNI space. Following ROI intersection with the individual GM, seed-to-voxel correlations in each subject were calculated through Pearson correlation of voxel-averaged time courses within each ROI with all other voxels in the brain (figure s-1). Correlation coefficients were Fisher-z-transformed. Given the study objective, subsequent statistical analysis was constrained to voxels within the combined volume of each ROIs respective target areas investigated during tractography.

2.6. Post-hoc analysis of grey matter volume

We were further interested if abnormal trajectories might originate from areas of abnormal GM structure. Yet, the sample size in the present study was not suitable for a comprehensive evaluation of GM structure. We hence conducted a planned post-hoc volumetric analysis in cortices previously reported structurally abnormal in ED (Mantel et al., 2019), in case consistent structure–function abnormalities in trajectories involving this cortex were found. Volumetry of absolute GM volumes was performed applying the same cortical ROI as during the respective FC analysis to the subjects' DARTEL (Diffeomorphic Anatomical Registration Through Exponentiated Lie Algebra)-normalized, modulated, nonsmoothed GM.

2.7. Statistical analyses

Between-group differences in tract integrity measures, FC and GM volume were analysed applying two-tailed permutation testing according to the Freedman-Lane approach (Winkler et al., 2014, 2016), calculating 10,000 permutations for image and 100,000 permutations for non-image data. Voxel-wise FC analysis results were voxel-level family-wise error (FWE)-corrected. The significance level in all analyses was set at $\alpha = 0.05$, with estimated p-values in each analysis false discovery-rate (FDR)-adjusted for multiple comparisons (i.e. 14

investigated tracts, 8 FC analyses, and the number of GM volumes analysed *post-hoc*). All statistical analyses were adjusted for potential effects of age and sex; for analyses involving GM, the total intracranial volume was additionally included. Beyond exploration of structuro-functional associations in case of coincident differences in a trajectory, adjunct linear regression analyses with clinical parameters (disease duration, severity by ED score) within patients were added for significant between-group differences.

2.8. Control analyses

(i) In order to assess whether potential significant structural/functional abnormalities in the primary somatosensory or motor cortex were also present in clinically non-affected areas of those cortices, control analyses for tractography/functional connectivity/grey matter volumetry results were performed for a medial Brainnetome atlas parcel most likely comprising the trunk/neck area within the respective primary cortices, provided that the results in the main analysis was significant. (ii) To control for the possibility of local FC potentially affecting remote FC abnormalities (Jiang and Zuo, 2016) we additionally tested for abnormalities of regional homogeneity between groups. For this assessment, we calculated Kendall's coefficient of concordance on the normalized, nuisance signal-regressed, bandpass-filtered (0.01–0.08 Hz) functional data. Data were then Fisher-z-transformed, and smoothed with a 6 mm full-width-at-half-maximum Gaussian kernel. (iii) To assess whether potential structure–function associations were specific to ED, the respective regression analyses were repeated for the healthy control group in case of significant results.

3. Results

3.1. Probabilistic tractography of sensorimotor trajectories

Tractography yielded probable trajectories connecting the primary/higher-order sensorimotor cortices and the putamen in all subjects. Probable tracts connecting sensory and motor cortices were reconstructable in all subjects for primary $S1_{FACE}$ -$M1_{FACE}$ connections, and in > 90% of participants for the higher-order SPL-SMA connection. Trajectories connecting parietal and frontal lobes ran distinct courses either in the SLF1 (SPL-SMA) or the lateral portion of the SLF2/the U-fibres ($S1_{FACE}$-$M1_{FACE}$). The intercortical trajectory between SMA and $M1_{FACE}$ showed lesser reconstructability (left hemisphere 78%, right hemisphere 84% of participants). Beyond technical aspects given the abundance crossing fibres in the frontal central white matter, the reason for this difficulty remained unclear. Subcortical tract terminations followed the putaminal topography (Tziortzi et al., 2014) (Fig. 1). In comparable trajectories, spatial variability of tract courses mirrored by reduced spatial overlay of tract volumes with increasing probability thresholds was higher in trajectories of sensory than of motor cortical origin, and rather elevated in trajectories involving higher-order compared to primary cortices, probably attributable to the higher cortical variability in such areas (figure s-2 for details of the descriptive evaluation) (Schulz et al., 2015). Reconstruction of cortico-subcortical and cortico-cortical tracts involving the primary sensorimotor cortices was possible without relevant overlay between the different tracts across analysed thresholds (table s-2).

3.2. Analyses of tract-related white matter integrity

Between-group analysis revealed significantly reduced AD in the left- and right-hemispheric trajectories between $S1_{FACE}$ and the putamen in ED patients compared to healthy brass players. Conversely, AD was significantly increased in ED patients compared to healthy brass players in the projections between SPL and SMA in both hemispheres. In the left hemisphere, this was accompanied by a significant increase in MO in ED patients compared to healthy brass players. Furthermore, ED patients showed significantly increased MO in the left-hemispheric trajectory connecting $M1_{FACE}$ and SMA compared to controls (table 2 for details, table s-3 for other DTI scalars and trends).

3.3. Analyses of related functional connectivity profiles

FC analysis revealed significantly reduced connectivity of the left $S1_{FACE}$ with the sensorimotor area in the left putamen ($x|y|z = -24|-8|7$; $p_{FWE} = 0.015$, FDR-adjusted) in ED patients compared to controls, the cluster being located inferior to the termination of the white matter tract between $S1_{FACE}$ and the putamen (Fig. 2A). Other analyses did not yield significant results.

3.4. Post-hoc structural analyses

Based on the above results, between-group volumetric GM analysis was performed for the left putamen and $S1_{FACE}$. This revealed increased GM volume in ED patients in left $S1_{FACE}$ ($p_{FDR} = 0.039$; Fig. 2B) and no significant differences in the left putamen ($p_{FDR} = 0.20$).

3.5. Regression analyses

Linear regression did not reveal significant associations of disease duration or ED score in patients with tract integrity measures. Further exploration of structure–function abnormalities in the trajectory $S1_{FACE}$-to-putamen in patients revealed that the change in structural tract integrity by AD showed significant association with average FC ($\beta = 0.60$, $p = 0.013$, $R^2 = 0.36$; Fig. 2B). GM volume in $S1_{FACE}$ was found neither a significant explaining variable of AD nor FC change (adjusted for total intracranial volume; AD: $\beta = 0.10$, $p = 0.74$; FC: $\beta = 0.40$, $p = 0.14$).

3.6. Control analyses

Control analyses evaluating tractography, functional connectivity and grey matter volume in the medial S1 / its projection to the putamen did not observe significant abnormalities in both hemispheres (all $p \geq 0.05$; see table s-4/figure s-3 for details). A control analysis for abnormalities in local functional connectivity (regional homogeneity) between-groups did not reveal significant results ($p_{FWE} > 0.05$). A control analysis for group specificity of the association between AD and FC in the trajectory $S1_{FACE}$-putamen conducted within the group of healthy brass players indicated that this association was specific to the patient group ($R^2 = 0.01$, $\beta = -0.10$, $p = 0.71$).

4. Discussion

We observed bihemispheric AD reduction within projections between $S1_{FACE}$ and the putamen, and converse bihemispheric AD increases within projections between supplementary motor and superior parietal cortex in the patient group. Further, patient's left $S1_{FACE}$ grey matter volume was increased, and left $S1_{FACE}$ FC with the putamen was abnormally reduced; the latter was significantly associated with the AD reduction within the patient group. Increase in MO in patients accompanied the left-hemispheric diffusion abnormalities within the SLF1, and were additionally observed in the supplementary motor area's projection to $M1_{FACE}$.

In the present study, ED patients displayed significantly reduced axial diffusivity in the trajectory connecting the left and right S1 with the respective ipsilateral putamen. At the same time no significant differences in the mode of anisotropy, a measure sensitive to changes in fibre orientation predominance (Douaud et al., 2011), were seen. Axial diffusivity describes linear diffusion of water molecules along aligned fibres in a trajectory. The reduction of such directed diffusion may mirror reduction of equal fibre alignment and has in some animal studies been associated with loss of axonal integrity (Winklewski et al., 2018), though

the inference of a distinct underlying microstructural abnormality from a certain DTI scalar in humans has to date proven difficult. In the left hemisphere, this finding was accompanied by a significant reduction of $S1_{FACE}$-to-putamen functional connectivity, and a significant moderate linear positive relationship between the two abnormalities was seen that was not observed in the patient group. Significant reduction of S1 functional connectivity with the striatum is consistent with a previous observation in (non-task-induced) orofacial dystonia in the resting state

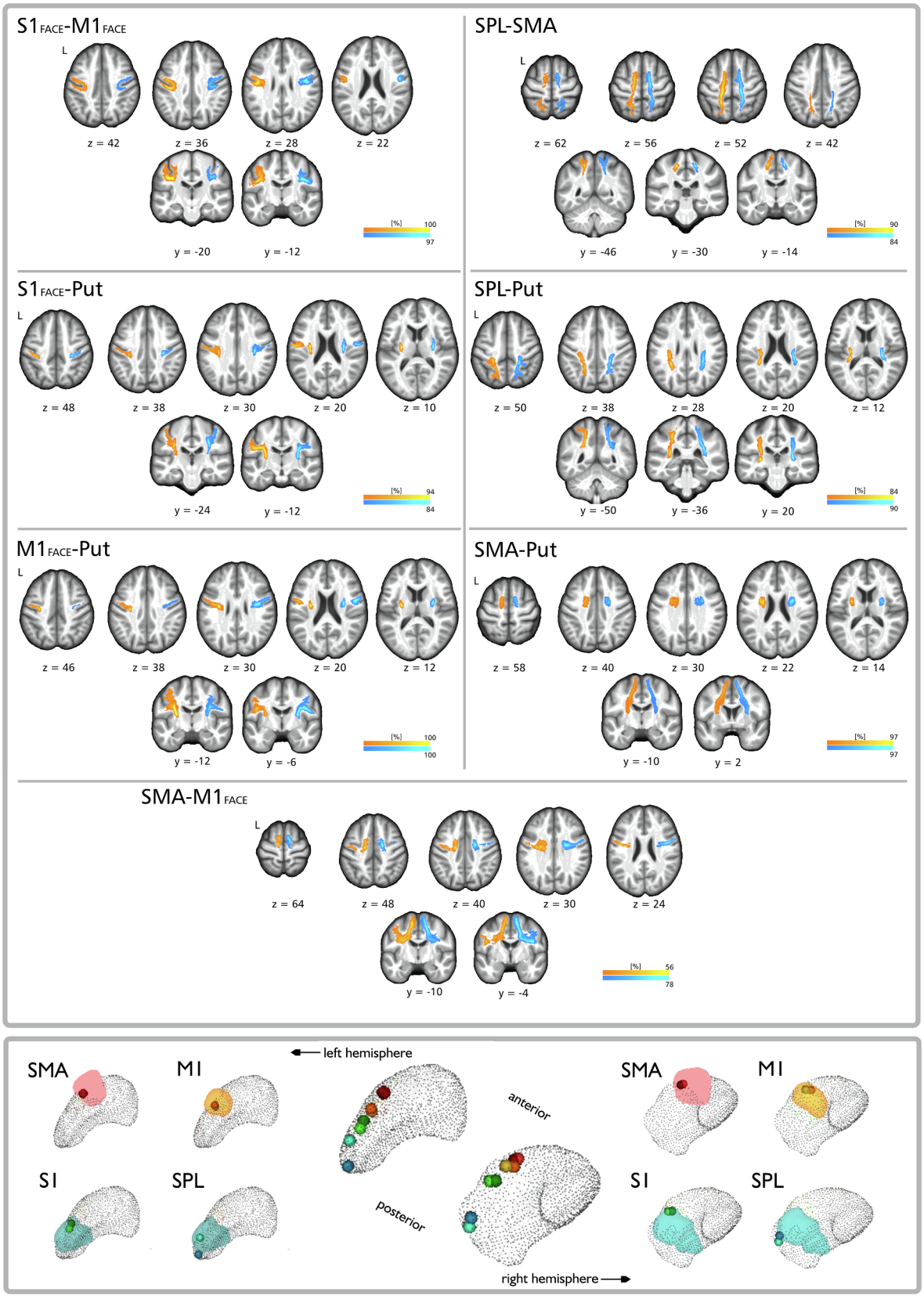

(caption on next page)

Fig. 1. *Upper panel:* Averaged probable trajectories from all participants and for all investigated projections shown in neurological display convention. Probable trajectories involving primary cortices are shown on the left, and trajectories involving higher-order cortices are shown on the right side of the panel. All probable trajectories are displayed at a tract probability threshold of 5%, allowing for visualisation of trajectory-associated variability, with intensities illustrating the percentage of subject overlay at the given threshold (group-wise overlay across probability thresholds is detailed in figure s-2). Warm colors represent tracts in the left, and cold colors represent tracts in the right hemisphere. *Lower panel:* Centroids representing the spatially most likely tract termination in the putamen in each group. Tract terminations followed the known topographic anterior-posterior distribution in the putamen (central column), patients being shown in dark and controls in light colors (centroid coordinates given in table s-5). Tract terminations were further in line with their respective topographic label in the striatal connectivity atlas (Tziortzi et al., 2014) visualized in the lateral columns (centroids projected on the 25% probability maps of striatal connectivity atlas labels: red = rostral motor; orange = caudal motor; blue = parietal). (For interpretation of the references to colour in this figure legend, the reader is referred to the web version of this article.)

(Jochim et al., 2018). Similarly in the task setting, reduced connectivity with S1 was described in writer's cramp patients during dystonic writing using the sensorimotor putamen as seed region (Gallea et al., 2016). The basal ganglia have long been implicated in FD pathophysiology due to their role in the adaptive selection of appropriate motor programs for a desired movement, processing information originating from cortically interconnected areas within functionally (yet not rigidly spatially) segregated cortico-basal-ganglia-cortical loops (Mink, 1996; Wilson, 2014). Particularly the basal ganglia's (somato)sensory circuits have recently gained growing attention for their potential involvement in context-related predictions of sensory outcomes that may modulate action selection during movement(Robbe, 2018; Wilson, 2014). Early work in writer's cramp pointed to a basal ganglia role in the abnormal somatosensory processing in the disease by demonstrating abnormal premovement somatosensory information gating (Murase et al., 2000). Recent positron emission tomography data suggested a hyperfunctionality of the direct basal ganglia output pathway potentially driven by a D1/2 dopamine receptor imbalance encompassing also nonmotor areas of the striatum (Simonyan et al., 2017). In contrast, other previous (mainly electrophysiological) studies favoured disordered inhibitory circuits and homeostatic plasticity within the cortex as basis of the disordered somatosensory processing in FD (Erro et al., 2018; Hallett, 2011). Neuroimaging techniques are limited regarding the differentiation of causative and compensatory changes. It is hence not possible to infer if our new findings of an abnormal link between the sensory cortex and the basal ganglia may be the result of a primary neuronal dysfunction of the primary somatosensory cortex leading to abnormal afferent integration at the striatal level (Conn et al., 2005; Kreitzer and Malenka, 2008; Wall et al., 2013), or the result of a primary (somato)sensory striatal neuronal abnormality facilitating a disinhibition/dysplasticity at the cortical level that subsequently leads to a secondary impairment of its link with the striatum (Quartarone and Hallett, 2013; Simonyan et al., 2017). Brain γ-aminobutyric acid reductions as a potential correlate of impaired inhibitory projections have been observed both in the lentiform nucleus and in the primary sensorimotor cortex of the affected hemisphere in focal hand dystonia patients using magnetic resonance spectroscopy (Levy and Hallett, 2002). While the significant cortico-subcortical tract abnormality reported in this work was confined to sensory trajectories, data in writer's cramp similarly showed a reduction in axial diffusivity in the trajectory connecting the middle frontal gyrus and the putamen (together with fractional anisotropy) (Berndt et al., 2018). This may indicate that other non-sensory cortices undergo comparable changes, though potential FD subtype-associated differences cannot be excluded (Bianchi et al., 2019; Ramdhani et al., 2014). A control analysis of the medial S1 did not reveal similar abnormalities in structural and functional parameters, which might speak against a general underlying character of the above findings within the cortex. Yet, primary somatosensory somatotopy is complex and variable, and establishing reliable somatotopic specificity would require the combination of a functional mapping of such cortices with diffusion imaging, hence warranting confirmation in a accordingly designed event-related fMRI study.

The additionally observed significant increase in left $S1_{FACE}$ GM volume in ED patients fitted a previous observation in the disease using a whole-brain approach (located at a similar level as the ROI used in the present work) and is compatible with findings in other TSFDs (Mantel et al., 2019; Neychev et al., 2011). Yet, there were no significant associations of left $S1_{FACE}$ GM volume with the structure-functional correlates of an impaired link of the area with the putamen. The potential pathophysiologic relation between cortical grey matter volume changes and measures relating to the integrity of related functional or structural projections in FD remains unresolved (Bianchi et al., 2019), complicated by the complex embedding of areas such as S1 within brain connectivity networks (Sepulcre et al., 2012).

Beyond cortico-subcortical abnormalities our findings hinted at altered tract integrity in ED patients within the SLF1, linking the SMA and the SPL. Both cortices have early been identified as important relays for fine motor control during musical performance in the healthy. The SPL is essential for multimodal sensory and spatial processing, and the SMA is a key structure for the execution of internally stored complex movements (e.g. through bihemispheric, top-down and sequential coordination) (Altenmuller, 2003). We observed a significant increase in axial diffusivity in this trajectory in both hemispheres, in the left hemisphere accompanied by a significant mode of anisotropy increase (with a respective right-hemispheric trend that did not survive correction for multiple comparisons). Taken together, this might suggest that (relatively) increased alignment or packing of fibres in this tract could have driven the observed abnormalities through increased diffusion along the fibre's trajectory. The SLF has been proposed to mediate synchronisation of frontoparietal neuronal oscillations implicated in the selective gating of top-down control processes (D'Andrea et al., 2019; Marshall et al., 2015). Our observations might thus hint at a possible facilitation between the two cortices of either compensatory or causative nature. In this regard, interestingly the SMA and SPL have recently both been implicated in premovement sensory facilitation in the presence of reduced/abnormal afferent input (Lhomond et al., 2018). Such dysfunctional afferent input processing both at the central level (also indicated by our above-described finding of sensory cortico-striatal dysconnectivity), and in the periphery (mirrored by abnormal peripheral sensory thresholds) are considered key features in FD (Conte et al., 2019; Stamelou et al., 2012). Moreover, recent work using dynamic causal modelling in laryngeal dystonia (a cranial non-musician TSFD) demonstrated a top-down disruption in sensorimotor network integrity involving the parietal cortex (Battistella and Simonyan, 2019). While the present study focused on a constrained literature-guided sensorimotor model given the expected subtlety of findings in this highly specific disease, parcellating the different components of the SLF to characterize a potential specificity of diffusion abnormalities to certain projections within the fascicle (as far as the technical limitations of diffusion imaging allow) may be of interest for follow-up studies in light of the present findings. Further, while we observed significant diffusion abnormalities in the link between the SMA and M1, a trajectory that is also assumed to mediate top-down motor control, the lack of significant abnormality in other DTI scalars accompanying this change in fibre orientation predominance prevents further interpretation. While unfortunately being beyond the scope of the present study, associating diffusion imaging findings with detailed task fMRI-established mappings of higher-order cortices such as the SMA may be of interest for future work in light of the present results.

In view of the above-described significant abnormalities in the mode of anisotropy within the left SLF1 trajectory and the nature of the measure, it may alternatively be conceivable that a relative reduction in a SLF1-crossing fibre population may have induced or contributed to the observed changes in the predominant fibre orientation and the axial

Table 2
Tract-related white-matter integrity in embouchure-dystonia patients and healthy brass musician controls.

		M1–Put		S1–Put		SMA–Put		SPL–Put
		LH	RH	LH	RH	LH	RH	RH
AD	PAT	0.938 ± 0.007	0.980 ± 0.009	0.974 ± 0.007	0.999 ± 0.005	1.011 ± 0.006	1.022 ± 0.007	1.057 ± 0.007
	CON	0.950 ± 0.006	0.998 ± 0.005	0.998 ± 0.008	1.022 ± 0.008	1.002 ± 0.010	1.016 ± 0.011	1.048 ± 0.010
	t	1.755	2.189	2.635	2.680	−0.426	0.100	−0.967
	P_{unc}	0.091	0.038	0.014	0.011	0.683	0.922	0.343
	P_{FDR}	0.181	0.106	**0.049**	**0.049**	0.922	0.922	0.601
MO	PAT	0.396 ± 0.031	0.438 ± 0.022	0.307 ± 0.030	0.46 ± 0.028	0.548 ± 0.018	0.585 ± 0.017	0.494 ± 0.025
	CON	0.448 ± 0.023	0.479 ± 0.018	0.38 ± 0.033	0.534 ± 0.026	0.472 ± 0.040	0.546 ± 0.030	0.464 ± 0.032
	t	1.700	1.055	1.585	1.706	−1.671	−0.986	−0.926
	P_{unc}	0.096	0.297	0.126	0.100	0.090	0.334	0.372
	P_{FDR}	0.200	0.461	0.22	0.200	0.200	0.467	0.473

	SPL–Put	M1–S1		SMA–M1		SMA–SPL	
	RH	LH	RH	LH	RH	LH	RH
AD	1.086 ± 0.01	0.944 ± 0.005	0.943 ± 0.007	0.985 ± 0.012	1.005 ± 0.010	1.048 ± 0.012	1.05 ± 0.013
	1.082 ± 0.009	0.947 ± 0.004	0.953 ± 0.007	0.979 ± 0.008	0.998 ± 0.013	0.997 ± 0.014	0.999 ± 0.012
	−0.295	0.447	1.821	0.227	−0.176	−2.647	−2.758
	0.770	0.656	0.078	0.822	0.865	0.014	0.012
	0.922	0.922	0.181	0.922	0.922	**0.049**	**0.049**
MO	0.524 ± 0.028	0.275 ± 0.023	0.252 ± 0.032	0.427 ± 0.017	0.416 ± 0.026	0.372 ± 0.035	0.351 ± 0.036
	0.528 ± 0.021	0.207 ± 0.020	0.217 ± 0.024	0.316 ± 0.031	0.434 ± 0.024	0.163 ± 0.042	0.243 ± 0.046
	0.122	−2.158	−0.490	−3.697	−2.181	−3.190	0.1109
	0.905	0.040	0.628	0.009	0.038	0.003	0.914
	0.914	0.140	0.732	**0.018**	0.914	**0.013**	0.914

Average axial diffusivity AD (given in $10^{-3}mm^2s^{-1}$) and mode of anisotropy MO within the seven investigated tracts in the left and right hemisphere in patients (PAT) and musician controls (CON). Results are displayed as mean ± standard error of the mean. P-value estimates of the two-tailed between-group comparisons were based on 100,000 permutations. All p-values were FDR-corrected for 14 analysed tracts. Results for other DTI scalars FA, RD are given in the supplement.

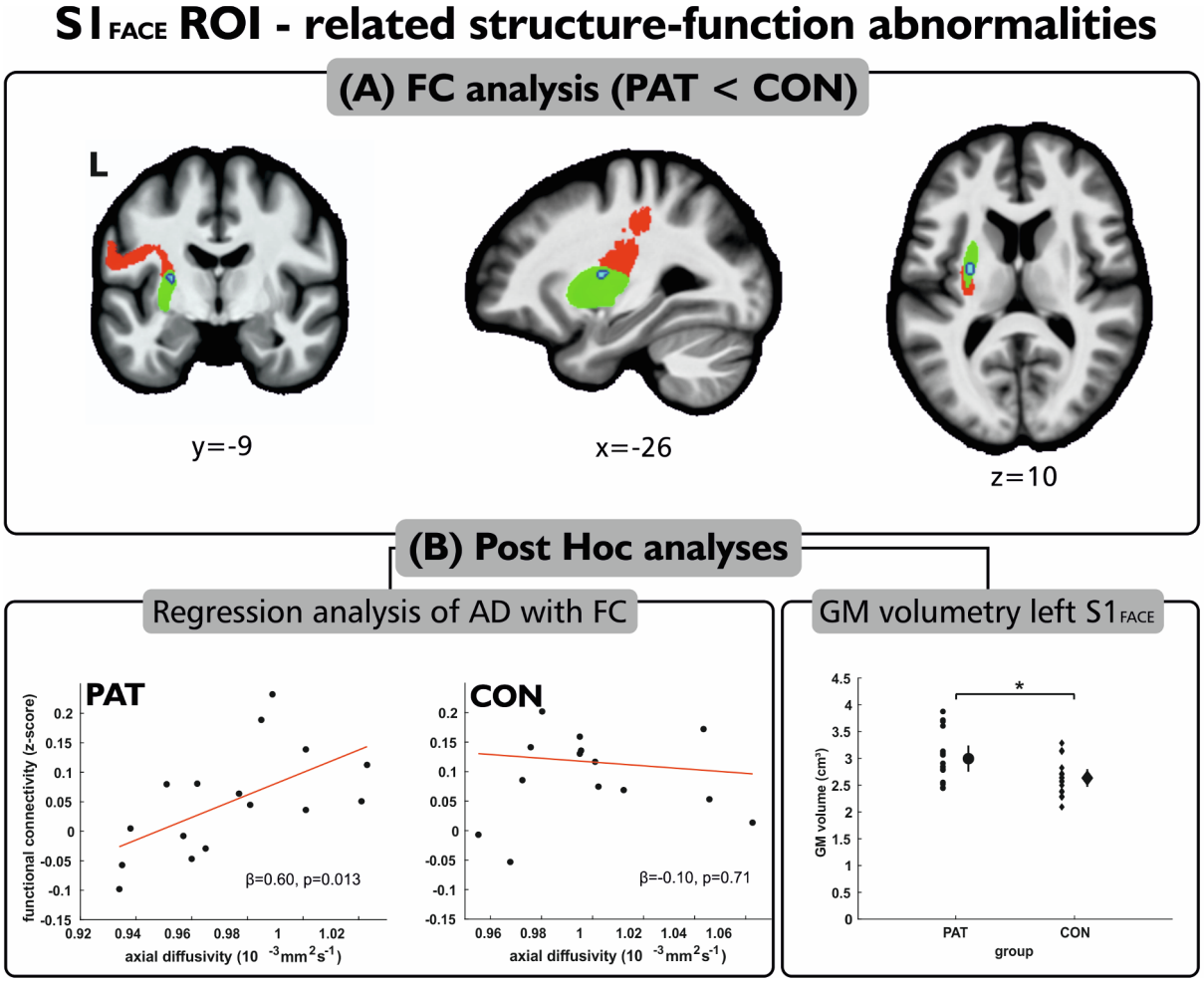

Fig. 2. (A) Results of the FC analysis showing reduced left $S1_{FACE}$ FC (in blue) with the putamen (highlighted in green). The area of altered FC within the putamen was spatially located beneath the terminations of the cortico-subcortical tract from S1 to the putamen (visualized through the overlaid averaged tract from Fig. 1, shown in red). (B) Results of post hoc analyses. The left panels depict the results of the regression analysis for both groups showing moderate significant positive association of the average axial diffusivity in the trajectory between $S1_{FACE}$ and the putamen with the average FC with the putamen (extracted from a 10 mm sphere around the significant cluster's peak coordinate). The right panel illustrated the result of the post-hoc GM volume analysis in the S1 ROI in patients (filled circles) and controls (filled diamonds). Error bars depict the double standard error of mean. (For interpretation of the references to colour in this figure legend, the reader is referred to the web version of this article.)

diffusivity. Yet in this area, the trunk or foot somatotopic sensorimotor representations would be origin or destination of the main crossing trajectories. While a spread of task-specific dystonic symptoms to the hand (i.e. writer's cramp) in ED along the disease course has been described in some patients and discussed within the concept of an endophenotype potentially mirrored by functional MRI abnormalities in the respective primary somatosensory somatotopic representation, a dystonic involvement of the trunk or foot is unlikely in consideration of previous observations in ED (Frucht, 2009; Haslinger et al., 2010, 2017; Mantel et al., 2019, 2016), and we did not observe abnormalities in a control analyses of the projection from the medial S1 to the putamen. Functionally, we did not observe abnormal SMA or SPL resting FC. The reason for this beyond general methodological constraints of seed-based resting-state FC analyses remains unresolved. Studies focusing on differential characterization of higher-order parieto-premotor connectivity are unfortunately sparse in TSFD. One study in writer's cramp observed reduced resting connectivity in the SPL seeding from the dorsal premotor cortex, but did not investigate the SMA (Delnooz et al., 2012).

Our description of abnormal white matter integrity in sensory trajectories in patients supports the key role of the sensory system in ED, although the lack of abnormal fractional anisotropy as a more common measure of tract integrity is a limitation of this work. The reasons remain ultimately unclear, yet method-associated aspects owed to the focus on tract-averaged measures cannot be excluded. For instance, tract-averaged measures may make focal abnormalities potentially less influential compared to voxel-based or tract segment-focused statistics given the long course of the investigated tracts.

The overall majority of previous diffusion imaging studies comparing white matter integrity in TSFD against healthy controls did not conduct evaluations based on whole-tract measures but focused on the voxel level, and findings at the cortical level were rarely reported (Neychev et al., 2011): A recent study found an isolated focal reduction of fractional anisotropy beneath the precuneus comparing a mixed TSFD collective against healthy controls using tract-based spatial statistics (Bianchi et al., 2019). One study in writer's cramp investigating voxel-wise differences within the normalized across-group primary sensorimotor corticospinal tract volume described abnormal subcortical (internal capsule and below) fractional anisotropy (Delmaire et al., 2009). Other diffusion imaging investigations in TSFD mainly relied on selected ROI analyses without reconstruction of distinct trajectories and reported mostly abnormalities below the cortical level: in the internal capsule, cerebral and middle cerebellar peduncle in laryngeal dystonia, and the internal capsule in focal hand dystonia (Neychev et al., 2011). Overall, this sparsity of diffusion imaging studies in TSFD (especially

with regard to tract-level analyses) as well as the technical heterogeneity of previous investigations underlines the necessity of further work to characterize the abnormal structural connectome in the disease. In this regard, our observation of abnormalities in the mode of anisotropy may be of particular interest, as to our knowledge, measures sensitive to changes in fibre orientation predominance have not yet been employed in previous diffusion imaging studies in FD.

5. Conclusion

The first-time observation of correlates of reduced structural (-functional) integrity in the primary somatosensory cortico-putaminal trajectory might point to an impairment of afferent sensory input to the putamen in the context of abnormal somatosensory processing in ED. Abnormalities within the higher-order cortico-cortical sensorimotor projections of the superior longitudinal fascicle might hint at cortical sensorimotor facilitation processes of either dysfunctional or compensatory nature.

Ethics approval

The study has been approved by the local ethics review board and written informed consent was obtained from all subjects.

Funding

This study was supported by the Deutsche Forschungsgemeinschaft (DFG HA3370/5-1) Bonn, Germany and the Kommission für Klinische Forschung, Technical University of Munich School of Medicine (KKF H-05).

CRediT authorship contribution statement

Tobias Mantel: Investigation, Formal analysis, Methodology, Visualization, Writing - original draft, Writing - review & editing. **Eckart Altenmüller:** Investigation, Resources, Writing - review & editing. **Yong Li:** Investigation, Validation, Data curation. **Tobias Meindl:** Writing - review & editing. **Angela Jochim:** Writing - review & editing. **André Lee:** Validation, Writing - review & editing. **Claus Zimmer:** Resources, Writing - review & editing. **Bernhard Haslinger:** Conceptualization, Funding acquisition, Resources, Project administration, Supervision, Writing - review & editing.

Acknowledgments

We cordially thank all musicians for their participation in the study.

Appendix A. Supplementary data

Supplementary data to this article can be found online at https://doi.org/10.1016/j.nicl.2020.102410.

References

Altenmuller, E., 2003. Focal dystonia: advances in brain imaging and understanding of fine motor control in musicians. Hand. Clin. 19 (523–538), xi.
Battistella, G., Simonyan, K., 2019. Top-down alteration of functional connectivity within the sensorimotor network in focal dystonia. Neurology 92, e1843–e1851.
Berndt, M., Li, Y., Gora-Stahlberg, G., Jochim, A., Haslinger, B., 2018. Impaired white matter integrity between premotor cortex and basal ganglia in writer's cramp. Brain Behav. 8, e01111.
Bianchi, S., Fuertinger, S., Huddleston, H., Frucht, S.J., Simonyan, K., 2019. Functional and structural neural bases of task specificity in isolated focal dystonia. Mov. Disord. 34, 555–563.
Bozkurt, B., Yagmurlu, K., Middlebrooks, E.H., Cayci, Z., Cevik, O.M., Karadag, A., Moen, S., Tanriover, N., Grande, A.W., 2017. Fiber connections of the supplementary motor area revisited: methodology of fiber dissection, DTI, and three dimensional documentation. J. Vis. Exp.
Conn, P.J., Battaglia, G., Marino, M.J., Nicoletti, F., 2005. Metabotropic glutamate receptors in the basal ganglia motor circuit. Nat. Rev. Neurosci. 6, 787–798.
Conte, A., Defazio, G., Hallett, M., Fabbrini, G., Berardelli, A., 2019. The role of sensory information in the pathophysiology of focal dystonias. Nat. Rev. Neurol. 15, 224–233.
D'Andrea, A., Chella, F., Marshall, T.R., Pizzella, V., Romani, G.L., Jensen, O., Marzetti, L., 2019. Alpha and alpha-beta phase synchronization mediate the recruitment of the visuospatial attention network through the Superior Longitudinal Fasciculus. Neuroimage 188, 722–732.
Delmaire, C., Vidailhet, M., Wassermann, D., Descoteaux, M., Valabregue, R., Bourdain, F., Lenglet, C., Sangla, S., Terrier, A., Deriche, R., Lehericy, S., 2009. Diffusion abnormalities in the primary sensorimotor pathways in writer's cramp. Arch. Neurol. 66, 502–508.
Delnooz, C.C., Helmich, R.C., Toni, I., van de Warrenburg, B.P., 2012. Reduced parietal connectivity with a premotor writing area in writer's cramp. Mov. Disord. 27, 1425–1431.
Douaud, G., Jbabdi, S., Behrens, T.E., Menke, R.A., Gass, A., Monsch, A.U., Rao, A., Whitcher, B., Kindlmann, G., Matthews, P.M., Smith, S., 2011. DTI measures in crossing-fibre areas: increased diffusion anisotropy reveals early white matter alteration in MCI and mild Alzheimer's disease. Neuroimage 55, 880–890.
Erro, R., Rocchi, L., Antelmi, E., Liguori, R., Tinazzi, M., Berardelli, A., Rothwell, J., Bhatia, K.P., 2018. High frequency somatosensory stimulation in dystonia: Evidence fordefective inhibitory plasticity. Mov. Disord. 33, 1902–1909.
Fan, L., Li, H., Zhuo, J., Zhang, Y., Wang, J., Chen, L., Yang, Z., Chu, C., Xie, S., Laird, A.R., Fox, P.T., Eickhoff, S.B., Yu, C., Jiang, T., 2016. The human Brainnetome atlas: a new brain atlas based on connectional architecture. Cereb. Cortex 26, 3508–3526.
Frucht, S.J., 2009. Embouchure dystonia–Portrait of a task-specific cranial dystonia. Mov. Disord. 24, 1752–1762.
Fujita, K., Eidelberg, D., 2017. Imbalance of the direct and indirect pathways in focal dystonia: a balanced view. Brain 140, 3075–3077.
Gallea, C., Horovitz, S.G., Najee-Ullah, M., Hallett, M., 2016. Impairment of a parieto-premotor network specialized for handwriting in writer's cramp. Hum. Brain Mapp. 37, 4363–4375.
Granert, O., Peller, M., Jabusch, H.C., Altenmuller, E., Siebner, H.R., 2011. Sensorimotor skills and focal dystonia are linked to putaminal grey-matter volume in pianists. J. Neurol. Neurosurg. Psychiatry 82, 1225–1231.
Hallett, M., 2011. Neurophysiology of dystonia: the role of inhibition. Neurobiol. Dis. 42, 177–184.
Haslinger, B., Altenmuller, E., Castrop, F., Zimmer, C., Dresel, C., 2010. Sensorimotor overactivity as a pathophysiologic trait of embouchure dystonia. Neurology 74, 1790–1797.
Haslinger, B., Noe, J., Altenmuller, E., Riedl, V., Zimmer, C., Mantel, T., Dresel, C., 2017. Changes in resting-state connectivity in musicians with embouchure dystonia. Mov. Disord. 32, 450–458.
Irfanoglu, M.O., Walker, L., Sarlls, J., Marenco, S., Pierpaoli, C., 2012. Effects of image distortions originating from susceptibility variations and concomitant fields on diffusion MRI tractography results. Neuroimage 61, 275–288.
Jenkinson, M., Bannister, P., Brady, M., Smith, S., 2002. Improved optimization for the robust and accurate linear registration and motion correction of brain images. Neuroimage 17, 825–841.
Jeurissen, B., Descoteaux, M., Mori, S., Leemans, A., 2019. Diffusion MRI fiber tractography of the brain. NMR Biomed. 32, e3785.
Jiang, L., Zuo, X.N., 2016. Regional homogeneity: a multimodal, multiscale neuroimaging marker of the human connectome. Neuroscientist 22, 486–505.
Jochim, A., Li, Y., Gora-Stahlberg, G., Mantel, T., Berndt, M., Castrop, F., Dresel, C., Haslinger, B., 2018. Altered functional connectivity in blepharospasm/orofacial dystonia. Brain Behav. 8, e00894.
Kamali, A., Flanders, A.E., Brody, J., Hunter, J.V., Hasan, K.M., 2014. Tracing superior longitudinal fasciculus connectivity in the human brain using high resolution diffusion tensor tractography. Brain Struct. Funct. 219, 269–281.
Kita, K., Rokicki, J., Furuya, S., Sakamoto, T., Hanakawa, T., 2018. Resting-state basal ganglia network codes a motor musical skill and its disruption from dystonia. Mov. Disord. 33, 1472–1480.
Kreitzer, A.C., Malenka, R.C., 2008. Striatal plasticity and basal ganglia circuit function. Neuron 60, 543–554.
Leemans, A., Jones, D.K., 2009. The B-matrix must be rotated when correcting for subject motion in DTI data. Magn. Reson. Med. 61, 1336–1349.
Lehericy, S., Ducros, M., Van de Moortele, P.F., Francois, C., Thivard, L., Poupon, C., Swindale, N., Ugurbil, K., Kim, D.S., 2004. Diffusion tensor fiber tracking shows distinct corticostriatal circuits in humans. Ann. Neurol. 55, 522–529.
Levy, L.M., Hallett, M., 2002. Impaired brain GABA in focal dystonia. Ann. Neurol. 51, 93–101.
Lhomond, O., Teasdale, N., Simoneau, M., Mouchnino, L., 2018. Supplementary motor area and superior parietal lobule restore sensory facilitation prior to stepping when a decrease of afferent inputs occurs. Front. Neurol. 9, 1132.
Lim, V.K., Bradshaw, J.L., Nicholls, M.E., Altenmuller, E., 2003. Perceptual differences in sequential stimuli across patients with musician's and writer's cramp. Mov. Disord. 18, 1286–1293.
Makris, N., Kennedy, D.N., McInerney, S., Sorensen, A.G., Wang, R., Caviness Jr., V.S., Pandya, D.N., 2005. Segmentation of subcomponents within the superior longitudinal fascicle in humans: a quantitative, in vivo, DT-MRI study. Cereb. Cortex 15, 854–869.
Mantel, T., Altenmuller, E., Li, Y., Meindl, T., Jochim, A., Lee, A., Zimmer, C., Dresel, C., Haslinger, B., 2019. Abnormalities in grey matter structure in embouchure dystonia. Parkinsonism Relat. Disord. 65, 111–116.
Mantel, T., Dresel, C., Altenmuller, E., Zimmer, C., Noe, J., Haslinger, B., 2016. Activity and topographic changes in the somatosensory system in embouchure dystonia. Mov. Disord. 31, 1640–1648.

Marshall, T.R., Bergmann, T.O., Jensen, O., 2015. Frontoparietal structural connectivity mediates the top-down control of neuronal synchronization associated with selective attention. PLoS Biol. 13, e1002272.
Mink, J.W., 1996. The basal ganglia: focused selection and inhibition of competing motor programs. Prog. Neurobiol. 50, 381–425.
Murase, N., Kaji, R., Shimazu, H., Katayama-Hirota, M., Ikeda, A., Kohara, N., Kimura, J., Shibasaki, H., Rothwell, J.C., 2000. Abnormal premovement gating of somatosensory input in writer's cramp. Brain 123 (Pt 9), 1813–1829.
Neychev, V.K., Gross, R.E., Lehericy, S., Hess, E.J., Jinnah, H.A., 2011. The functional neuroanatomy of dystonia. Neurobiol Dis 42, 185–201.
Oldfield, R.C., 1971. The assessment and analysis of handedness: the Edinburgh inventory. Neuropsychologia 9, 97–113.
Quartarone, A., Hallett, M., 2013. Emerging concepts in the physiological basis of dystonia. Mov. Disord. 28, 958–967.
Ramdhani, R.A., Kumar, V., Velickovic, M., Frucht, S.J., Tagliati, M., Simonyan, K., 2014. What's special about task in dystonia? A voxel-based morphometry and diffusion weighted imaging study. Mov. Disord. 29, 1141–1150.
Robbe, D., 2018. To move or to sense? Incorporating somatosensory representation into striatal functions. Curr. Opin. Neurobiol. 52, 123–130.
Rosenkranz, K., Williamon, A., Butler, K., Cordivari, C., Lees, A.J., Rothwell, J.C., 2005. Pathophysiological differences between musician's dystonia and writer's cramp. Brain 128, 918–931.
Schulz, R., Koch, P., Zimerman, M., Wessel, M., Bonstrup, M., Thomalla, G., Cheng, B., Gerloff, C., Hummel, F.C., 2015. Parietofrontal motor pathways and their association with motor function after stroke. Brain 138, 1949–1960.
Sepulcre, J., Sabuncu, M.R., Yeo, T.B., Liu, H., Johnson, K.A., 2012. Stepwise connectivity of the modal cortex reveals the multimodal organization of the human brain. J. Neurosci. 32, 10649–10661.
Simonyan, K., Cho, H., Hamzehei Sichani, A., Rubien-Thomas, E., Hallett, M., 2017. The direct basal ganglia pathway is hyperfunctional in focal dystonia. Brain 140, 3179–3190.
Stamelou, M., Edwards, M.J., Hallett, M., Bhatia, K.P., 2012. The non-motor syndrome of primary dystonia: clinical and pathophysiological implications. Brain 135, 1668–1681.
Tziortzi, A.C., Haber, S.N., Searle, G.E., Tsoumpas, C., Long, C.J., Shotbolt, P., Douaud, G., Jbabdi, S., Behrens, T.E., Rabiner, E.A., Jenkinson, M., Gunn, R.N., 2014. Connectivity-based functional analysis of dopamine release in the striatum using diffusion-weighted MRI and positron emission tomography. Cereb. Cortex 24, 1165–1177.
Uehara, K., Furuya, S., Numazawa, H., Kita, K., Sakamoto, T., Hanakawa, T., 2019. Distinct roles of brain activity and somatotopic representation in pathophysiology of focal dystonia. Hum. Brain Mapp. 40, 1738–1749.
Wall, N.R., De La Parra, M., Callaway, E.M., Kreitzer, A.C., 2013. Differential innervation of direct- and indirect-pathway striatal projection neurons. Neuron 79, 347–360.
Wilson, C.J., 2014. The sensory striatum. Neuron 83, 999–1001.
Winkler, A.M., Ridgway, G.R., Webster, M.A., Smith, S.M., Nichols, T.E., 2014. Permutation inference for the general linear model. Neuroimage 92, 381–397.
Winkler, A.M., Webster, M.A., Brooks, J.C., Tracey, I., Smith, S.M., Nichols, T.E., 2016. Non-parametric combination and related permutation tests for neuroimaging. Hum. Brain Mapp. 37, 1486–1511.
Winklewski, P.J., Sabisz, A., Naumczyk, P., Jodzio, K., Szurowska, E., Szarmach, A., 2018. Understanding the physiopathology behind axial and radial diffusivity changes-what do we know? Front. Neurol. 9, 92.

Supplemental Material

Structure-function abnormalities in cortical sensory projections in embouchure dystonia

Tobias Mantel, MD,[1] E. Altenmüller, MD,[2] Yong Li, PhD,[1] André Lee, MD,[1,2] Tobias Meindl, MD,[1] Angela Jochim, MD,[1] Claus Zimmer, MD,[3] and Bernhard Haslinger, MD[1]

Table s-1. Seeds and composition of basic standardized exclusion masks applied during tractography

A. Regions of interest

Seed	Brainnetome atlas label(s)	HVO atlas label
left/right SMA	A6m	
left/right SPL	A7r,c,pc; A5l	
left/right $M1_{FACE}$	A4hf	
left/right $S1_{FACE}$	A123uhf	
Putamen L/R		putamen

B. Basic exclusion masks

Tract	exclusion mask components
Upper interlobar Cortico-cortical (SMA-SPL)	Grey matter, cerebrospinal fluid; subcortical white matter surface adjacent the seed; sagittal midplane (medial); sagittal plane guided by the depth of the superior frontal sulcus and intraparietal sulcus (lateral); axial plane defined by the upper surface of the corpus callosum (inferior).
Lower interlobar cortico-cortical ($M1_{FACE}$-$S1_{FACE}$)	Grey matter, cerebrospinal fluid; subcorical white matter edge not part of the seed; coronar plane at the level of the anterior and posterior commissure (rostral/caudal), axial plane at the level of the depth of the lateral fissure (= superior border of the insular cortex), not including the operculum (inferior); sagittal plane lateral to lateral ventricles (medial).
Intralobar cortico-cortical (SMA-$M1_{FACE}$)	Grey matter, cerebrospinal fluid; subcorical white matter edge not part of the seed; sagittal midplane (medial); coronar plane along the depth of the central sulcus and the rostral end of the lateral vetnricles (rostral/caudal); axial plane at the level of the depth of the lateral fissure (= superior border of the insular cortex), not including the operculum (inferior).
Cortico-subcortical (cortical seeds to Put)	Grey matter, cerebrospinal fluid; subcorical white matter edge not part of the seed; caudate nucleus, pallidum, thalamus, internal capsule; sagittal midplane (medial), axial plane inferior to the putamen (inferior), coronar plane at the level of the anterior (rostral; for sensory seeds) or posterior commissure (caudal; for motor seeds).

A. Composition of region of interests from the parcellation provided by the Harvard Oxford subcortical atlas and the Brainnetome atlas.

B.: Composition of standardized exclusion masks applied for tracking (in addition to FA restrictions). Standardized ROIs were drawn based on expected tract courses given in the literature, guided by macro-anatomical landmarks and applied to all subjects; the main spatial direction restricted by the respective component is given in brackets. Components of the cortico-cortical sensorimotor tracts excluded trajectories to subcortical nuclei. For cortico-subcortical tracts, subcortical trajectories as well as nuclei of no interest (i.e. except the putamen) were specifically excluded (for the latter using masks from the subcortical atlas).

Table s-2. Jaccard coefficients of primary sensorimotor cortex-derived trajectories.

		PAT	CON	p-value
$JC_{S1\text{-}Put\|M1\text{-}Put}$	left hemisphere	0.030 (±0.007)	0.033 (±0.007)	0.71
	right hemisphere	0.039 (±0.009)	0.033 (±0.010)	0.66
$JC_{S1\text{-}Put\|S1\text{-}M1}$	left hemisphere	0.013 (±0.003)	0.016 (±0.004)	0.68
	right hemisphere	0.027 (±0.006)	0.026 (±0.004)	0.29
$JC_{M1\text{-}Put\|S1\text{-}M1}$	left hemisphere	0.027 (±0.008)	0.026 (±0.005)	0.89
	right hemisphere	0.029 (±0.008)	0.033 (±0.008)	0.70

Jaccard coefficients of probable tracts seeded from the primary somatosensory and motor cortex given as mean ± standard error of the mean. A value of 0 of the Jaccard coefficient indicates full spatial dissimilarity (no shared voxels) and 1 equals full spatial similarity of the respective trajectories. The exploratory statistical comparison (t-test) did not reveal significant between-group differences. P-values are given uncorrected for multiple comparisons. JC, Jaccard coefficient; M1, primary motor cortex; Put, putamen; S1, primary somatosensory cortex; PAT, embouchure dystonia patients; CON, healthy brass players.

Table s-3. Tract-related white-matter integrity in embouchure-dystonia patients and healthy brass musician controls.

		M1−Put		S1−Put		SMA−Put		SPL−Put		M1−S1		SMA−M1		SMA−SPL	
		LH	RH	LH	RH	LH	LH	RH	RH	LH	RH	LH	RH	LH	RH
FA	PAT	0.425 ±0.008	0.430 ±0.006	0.453 ±0.007	0.461 ±0.008	0.468 ±0.008	0.467 ±0.008	0.455 ±0.008	0.466 ±0.008	0.434 ±0.008	0.413 ±0.007	0.452 ±0.009	0.460 ±0.008	0.521 ±0.011	0.494 ±0.012
	CON	0.429 ±0.005	0.444 ±0.007	0.457 ±0.006	0.469 ±0.008	0.463 ±0.008	0.460 ±0.008	0.454 ±0.008	0.467 ±0.007	0.429 ±0.008	0.415 ±0.010	0.451 ±0.007	0.454 ±0.008	0.483 ±0.015	0.465 ±0.012
	P_{FDR}	0.943	0.943	0.943	0.943	0.943	0.943	0.943	0.943	0.943	0.943	0.943	0.943	0.200†	0.200†
MO	PAT	0.396 ±0.031	0.438 ±0.022	0.307 ±0.030	0.46 ±0.028	0.548 ±0.018	0.585 ±0.017	0.494 ±0.025	0.524 ±0.028	0.275 ±0.023	0.252 ±0.032	0.427 ±0.017	0.416 ±0.026	0.372 ±0.035	0.351 ±0.036
	CON	0.448 ±0.023	0.479 ±0.018	0.38 ±0.033	0.534 ±0.026	0.472 ±0.040	0.546 ±0.030	0.464 ±0.032	0.528 ±0.021	0.207 ±0.020	0.217 ±0.024	0.316 ±0.031	0.434 ±0.024	0.163 ±0.042	0.243 ±0.046
	P_{FDR}	0.200	0.461	0.22	0.200	0.200	0.467	0.473	0.914	0.140†	0.732	**0.018**	0.914	**0.013**	0.140†
AD	PAT	0.938 ±0.007	0.980 ±0.009	0.974 ±0.007	0.999 ±0.005	1.011 ±0.006	1.022 ±0.007	1.057 ±0.007	1.086 ±0.01	0.944 ±0.005	0.943 ±0.007	0.985 ±0.012	1.005 ±0.010	1.048 ±0.012	1.05 ±0.013
	CON	0.950 ±0.006	0.998 ±0.005	0.998 ±0.008	1.022 ±0.008	1.002 ±0.010	1.016 ±0.011	1.048 ±0.010	1.082 ±0.009	0.947 ±0.004	0.953 ±0.007	0.979 ±0.008	0.998 ±0.013	0.997 ±0.014	0.999 ±0.012
	P_{FDR}	0.181	0.106†	**0.049**	**0.049**	0.922	0.922	0.601	0.922	0.922	0.181	0.922	0.922	**0.049**	**0.049**
RD	PAT	0.473 ±0.008	0.49 ±0.009	0.471 ±0.006	0.467 ±0.007	0.466 ±0.008	0.469 ±0.008	0.499 ±0.009	0.503 ±0.010	0.470 ±0.009	0.475 ±0.009	0.448 ±0.009	0.472 ±0.010	0.479 ±0.007	0.497 ±0.007
	CON	0.472 ±0.004	0.483 ±0.008	0.475 ±0.006	0.465 ±0.007	0.468 ±0.007	0.472 ±0.006	0.495 ±0.008	0.498 ±0.007	0.474 ±0.008	0.474 ±0.006	0.468 ±0.011	0.483 ±0.010	0.487 ±0.008	0.502 ±0.007
	P_{FDR}	0.900	0.931	0.900	0.931	0.900	0.900	0.931	0.931	0.805	0.900	0.900	0.900	0.805	0.805

Averaged tract integrity measures in the groups and results of the statistical analysis. Fractional anisotropy (FA), the mode of anisotropy (MO), axial diffusivity (AD, given in $10^{-3}mm^2s^{-1}$) and radial diffusivity (RD, given in $10^{-3}mm^2s^{-1}$) within the seven investigated tracts in the left and right hemisphere in patients (PAT) and musician controls (CON). Results are displayed as mean ± standard error of the mean. P-value estimates of the two-tailed between-group comparisons were based on 100,000 permutations. All p-values were false discovery-rate (FDR)-corrected for 14 analysed tracts. Significant results are highlighted in bold. Differences significant at $p<0.05$ uncorrected that did not survive FDR-correction for multiple comparisons are marked with a cross (†).

Table s-4. Control analyses of the medial S1 ($S1_{TR}$).

analysis		hemisphere	PAT	CON	t-value	p-value
Tractography $S1_{TR}$-Put	FA	LH	0.505 (±0.009)	0.500 (±0.008)	-0.695	0.495[a]
		RH	0.505 (±0.008)	0.501 (±0.008)	-0.468	0.645[a]
	MO	LH	0.632 (±0.026)	0.632 (±0.022)	-0.349	0.731[a]
		RH	0.650 (±0.018)	0.633 (±0.023)	-0.626	0.534[a]
	AD	LH	1.050 (±0.007)	1.053 (±0.009)	-0.200	0.843[a]
		RH	1.056 (±0.006)	1.057 (±0.011)	0.364	0.719[a]
	RD	LH	0.440 (±0.008)	0.442 (±0.006)	0.684	0.504[a]
		RH	0.443 (±0.007)	0.446 (±0.006)	0.724	0.479[a]
FC $S1_{TR}$-Put		LH		–	2.583	0.889[b]
		RH		–	2.489	0.883[b]
GM $S1_{TR}$		LH	2.290 (±0.400)	2.272 (±0.36)	-0.186	0.852[a]

Between-group results of control analyses conducted for a medial primary somatosensory cortex area comprising clinically non-effected representations ($S1_{TR}$, Brainnetome atlas label A123tru). Averaged tract integrity measures (FA, MO, AD in $10^{-3}mm^2s^{-1}$ and RD AD in $10^{-3}mm^2s^{-1}$) for the probable tracts between $S1_{TR}$ and the putamen, and grey matter volume of the left-hemispheric $S1_{TR}$ in cm^3 (as control evaluation of post-hoc analysis results) are displayed as mean ± standard error of the mean for patients (PAT) and musician controls (CON). P-values are given [a]uncorrected/[b]voxel-level FWE-corrected. P-value estimates of the two-tailed between-group comparisons were based on 100,000 permutations for non-image and 10,000 permutations for image (voxel-wise) data.

Table s-5. Centroid coordinates of cortico-putaminal tract terminations

ROI	group	MNI coordinates left hemsiphere			MNI coordinates right hemisphere		
		x	y	z	x	y	z
SMA	CON	-26.0	-3.9	12.5	26.5	-2.5	12.1
	PAT	-26.3	-3.7	12.7	26.6	-3.4	12.2
$M1_{FACE}$	CON	-26.9	-9.2	12.0	27.1	-6.5	12.2
	PAT	-26.8	-9.6	12.0	27.7	-4.9	12.0
$S1_{FACE}$	CON	-27.8	-14.3	9.9	27.9	-11.3	10.8
	PAT	-27.6	-12.0	10.8	28.3	-10.2	10.6
SPL	CON	-28.3	-18.3	8.4	29.5	-20.5	2.5
	PAT	-29.6	-21.7	0.9	29.8	-19.7	4.9

Centroids representing the spatially most likely tract termination in the putamen in each group. Coordinate position is given in the Montreal Neurologic Imaging (MNI) in mm relative to the anterior commissure (above/anterior/right +; below/posterior/left −).

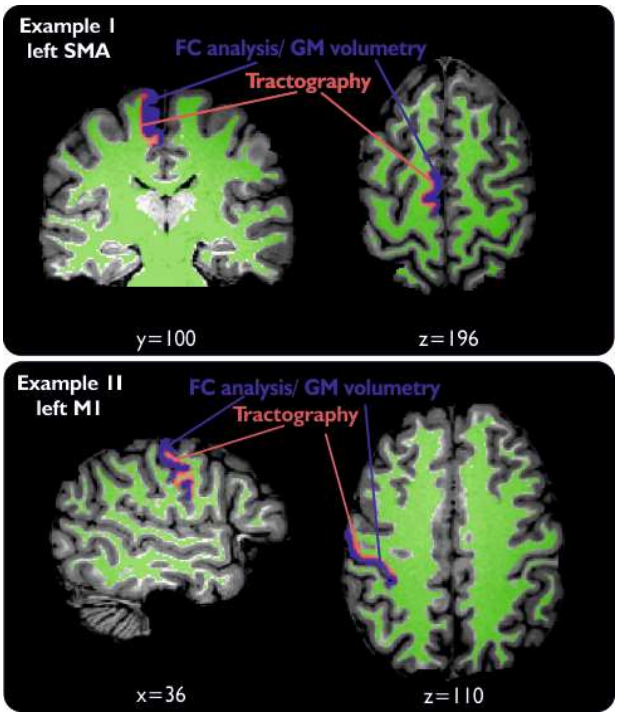

Figure s-1. Exemplary illustration of seed application for different analysis in one example participant shown in native space for $M1_{FACE}$ and SMA in the left hemisphere. Tractography was performed from a Ø 2mm surface margin of white matter at the grey matter border in native space (juxtacortical white matter; shown in red). Functional connectivity analysis and grey matter volume extraction were performed from the grey matter-intersected cortical part of the atlas ROIs (shown in blue) in MNI space. Green shows white matter voxels included for probabilistic tractography analysis. Coordinates give the position in native space ($240x240x170mm^3$).

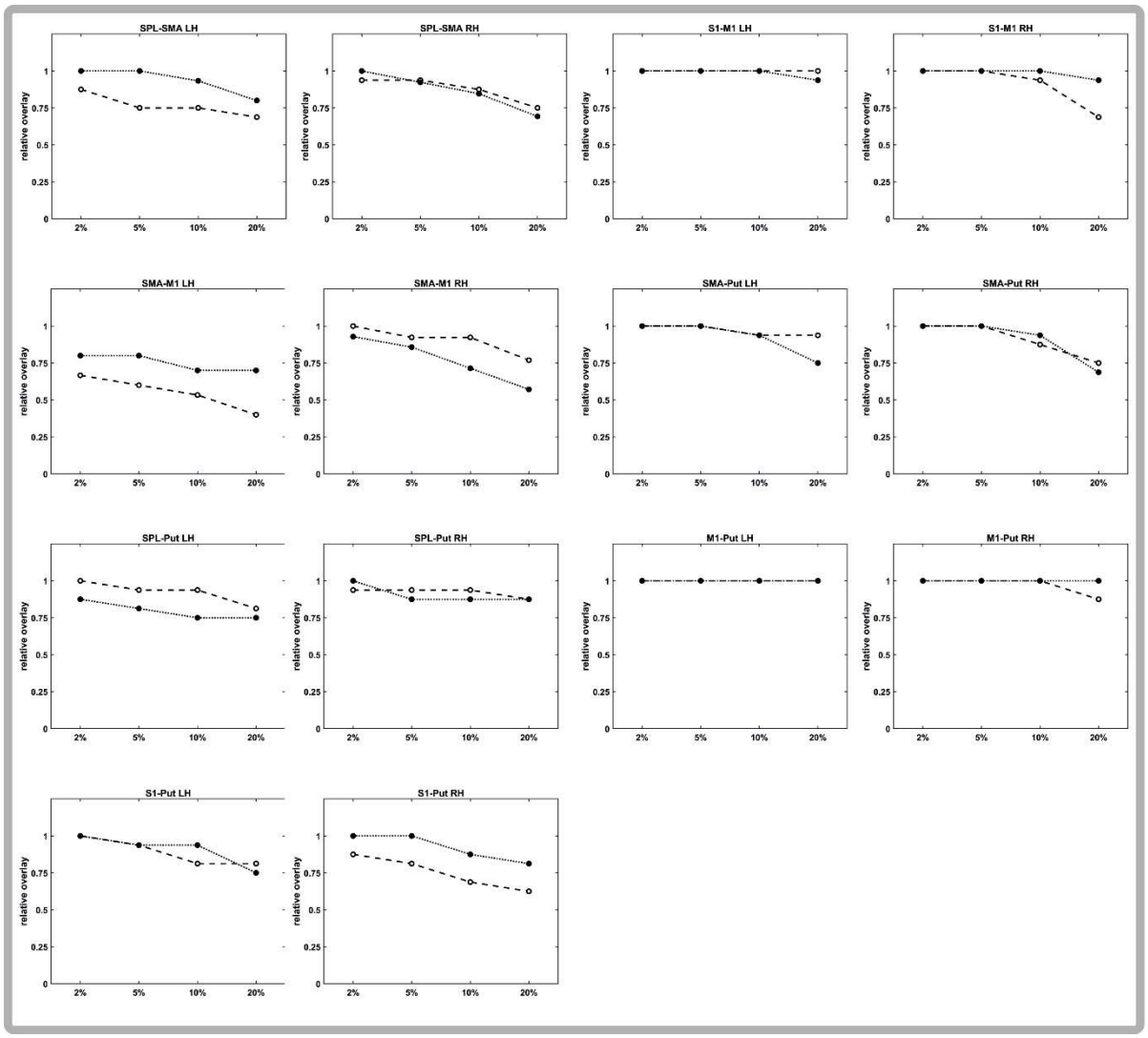

Figure s-2. Spatial variability of tract courses in each group, mirrored in reduced overlay of tract volumes after normalization to MNI space at increasing connection probability thresholds. Circles represent the relative overlay of tracts at the different probability thresholds across the participants in each group (empty circles = patients; filled circles = controls; lines visualisation of tendencies across probability thresholds). In trajectories that were suitable for comparative evaluation (e.g. primary vs. higher cortico-cortical sensorimotor, primary/higher-order sensory vs. motor cortico-subcortical projections), variability by visual inspection seemed higher in trajectories of sensory than of motor cortical origin, and rather elevated in trajectories involving higher-order compared to primary cortices (esp. cortico-cortical), probably attributable to the higher cortical variability in respective areas. No broader systematic patterns of difference between groups across tracts were visible in this strictly descriptive evaluation.

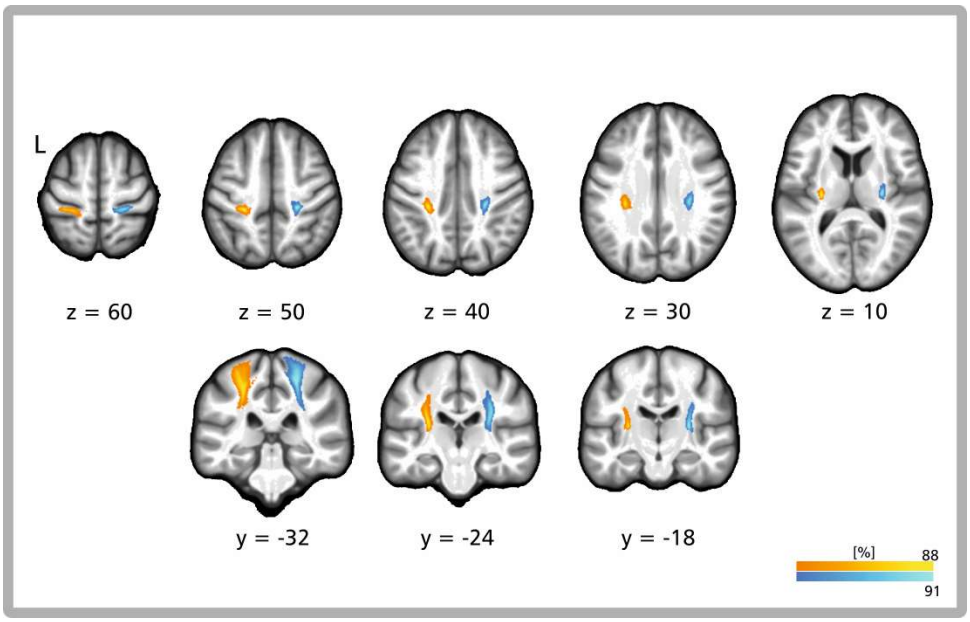

Figure s-3. Averaged probable trajectories from all participants for the projections from the medial S1 ($S1_{TR}$) to the putamen (data is given in table s-4). Probable trajectories are displayed at a tract probability threshold of 5%, allowing for visualisation of trajectory-associated variability, with intensities illustrating the percentage of subject overlay at the given threshold. Warm colors represent tracts in the left, and cold colors represent tracts in the right hemisphere.

NeuroImage: Clinical 34 (2022) 103013

Contents lists available at ScienceDirect

NeuroImage: Clinical

journal homepage: www.elsevier.com/locate/ynicl

Thalamic structural connectivity profiles in blepharospam/ Meige's syndrome

Tobias Mantel [a,1], Angela Jochim [a,1], Tobias Meindl [a], Jonas Deppe [a], Claus Zimmer [b], Yong Li [a], Bernhard Haslinger [a,*]

[a] Department of Neurology, Klinikum rechts der Isar, Technische Universität München, Ismaninger Strasse 22, Munich, Germany
[b] Department of Neuroradiology, Klinikum rechts der Isar, Technische Universität München, Ismaninger Strasse 22, Munich, Germany

ARTICLE INFO

Keywords:
Focal dystonia
Diffusion tractography
Thalamus connectivity mapping
Blepharospasm

ABSTRACT

Background: Blepharospasm is a debilitating focal dystonia characterized by involuntary eyelid spasms that can be accompanied by oromandibular muscle involvement (Meige's syndrome). Frequently observed abnormality in functional neuroimaging hints at an important position of the thalamus, that relays involved cortico-basal ganglia-cortical and cortico-cerebello-cortical circuits, within the abnormal network in blepharospasm.
Objective: To characterize abnormal cortico-thalamic structural/streamline connectivity (SC) patterns in the disease, as well as their potential co-occurrence with abnormal subcortico-thalamo-cortical projections using diffusion tractography.
Methods: Diffusion imaging was obtained in 17 patients with blepharospasm (5 with mild lower facial involvement) and 17 healthy controls. Probabilistic tractography was used for quantification of SC between six cortical regions and thalamus, and voxel-level thalamic SC mapping as well as evaluation of the thalamic SC distributions' topography by center-of-gravity analysis was performed. *Post-hoc*, correlations of SC with clinical parameters were evaluated. Further, white matter integrity was investigated within representative segments of the dentato-thalamo-cortical and pallido-thalamo-cortical tract.
Results: Connectivity mapping showed significant reduction of right (pre)motor- and left occipital-thalamic SC, as well as a topographic shift of the left occipital-thalamic SC distribution in patients. Significant positive correlation of occipital-thalamic SC with disease severity was found. *Post-hoc* analysis revealed significantly reduced mean fractional anisotropy in patients within the dentato-thalamo-cortical trajectory connecting to right (pre) motor and left occipital cortex.
Conclusion: Abnormal occipital/motor SC provides evidence for dysfunction of the thalamus-relayed visual and motor network as a key aspect in the disease. Concurrent impairment of microstructural integrity within the dentato-thalamic trajectories targeting those cortices hints at cerebellar contribution.

1. Introduction

Blepharospasm is a frequent focal dystonia characterized by disabling involuntary blinking and eyelid spasms leading to functional blindness in its most severe form (Valls-Sole and Defazio, 2016). In up to 50% of cases additional involvement of contiguous muscles mainly in the oromandibular region may occur, then labeled Meige's syndrome (Berman et al., 2020; Pandey and Sharma, 2017). First-choice symptomatic treatment is regular local botulinum toxin A (BoNT-A) injection into overactive muscles (Colosimo et al., 2010). While dystonia has traditionally been described as a disorder mainly caused by altered basal ganglia function, the common view of the pathophysiology has shifted in recent years towards the interpretation as a network disease. Beyond the basal ganglia, such network concept includes sensory and motor cortical areas, thalamus, cerebellum and brainstem (Mascia et al., 2020). Clinical dystonia is thought to result from dysfunctional

Abbreviations: BDS, blepharospasm disability scale; BoNT-A, botulinum toxin A; CoG, center of gravity; CON, healthy controls; JRS, Jankovic rating scale; PAT, blepharospasm/Meige's syndrome patients; SC, streamline/structural connectivity; TFCE, threshold-free cluster enhancement.

* Corresponding author at: Klinik und Poliklinik für Neurologie, Klinikum rechts der Isar, Technische Universität München, München, Germany.
E-mail address: bernhard.haslinger@tum.de (B. Haslinger).

[1] These authors contributed equally.

https://doi.org/10.1016/j.nicl.2022.103013
Received 19 December 2021; Received in revised form 18 April 2022; Accepted 19 April 2022
Available online 22 April 2022

interaction of the networks' brain regions, possibly with weighted type-associated involvement (Jinnah et al., 2017). In blepharospasm, retrospective studies/case summaries on its acquired form report lesions with thalamic involvement with considerable frequency, followed by basal ganglia, brainstem, and other lesions within the above network (Khooshnoodi et al., 2013; Mascia et al., 2020). Past functional neuroimaging studies conducted in the idiopathic form frequently and consistently observed abnormal thalamic activation (Baker et al., 2003; Emoto et al., 2010; Murai et al., 2011; Obermann et al., 2008; Suzuki et al., 2019; Suzuki et al., 2007). Accordingly, supported by its role in relaying (among others) the cortico-basal ganglia-cortical and cortico-cerebello-cortical circuits (Conte et al., 2020; Jinnah et al., 2017) that display abnormal functional connectivity (FC) profiles in blepharospasm (Jochim et al., 2018a; Ni et al., 2017), the thalamus has been proposed as a potential key hub in the blepharospasm network (Mascia et al., 2020). Yet, it remains to date ultimately unknown if the projections between thalamus and cortex within such proposed network are abnormal in idiopathic blepharospasm. The present study therefore aimed at elucidating the structural connectivity pattern between thalamus and cortex in the disease. We hypothesized to observe bilateral alterations of thalamic connectivity in projections involved in sensorimotor and/or visuomotor processing (i.e. (pre)motor, somatosensory, posterior parietal, occipital) that are discussed dysfunctional in the disease, without assumptions regarding directionality. We were further interested if potential findings were accompanied by impaired white matter integrity in ascending projections from basal ganglia and cerebellum that are relayed via the thalamus.

2. Materials and methods

2.1. Participants

Seventeen patients (PAT; age 62.2 ± 10.7 years, male/female 10/7) and 17 age- and sex-matched healthy controls (CON; age 62.4 ± 10.2 years, male/female 10/7) were investigated. Twelve patients suffered from isolated blepharospasm. Five had mild additional involvement of the lower face mimic/orbicularis oculi muscles not requiring treatment (i.e. Meige's syndrome). PAT were recruited from the movement disorders outpatient clinic of the Department of Neurology, Klinikum rechts der Isar, Technical University of Munich. Diagnosis had previously been made by a movement disorders expert neurologist. All participants were right-handed (Oldfield, 1971), with no relevant structural abnormalities on MRI by neuroradiologic evaluation (see supplement for further inclusion/exclusion details). All patients received regional periorbital BoNT-A injections in regular intervals (Table 1); MRI measurements were performed prior to the next planned BoNT-A injection after the effect had waned. The study protocol was approved by the local ethics committee (https://www.ek-med-muenchen.de). Written informed consent according to the Declaration of Helsinki was obtained from all participants. Patients were videotaped to assess disease-related impairment using the Jankovic Rating Scale (JRS), an external rating of symptom severity and frequency, calculated as sum score from ratings between "0″ (no symptoms) to "4" (severe or very frequent eyelid spasms) (Jankovic and Orman, 1987). The rater (B.H.) was blinded to neuroimaging analysis results and treatment status. Further, patients' subjective impairment was evaluated using the Blepharospasm Disability Scale (BDS). In this questionnaire, the patient is asked to rate the functional impairment in eight specific situations of daily life, resulting in a sum score of 100% (no impairment) or lower (Lindeboom et al., 1995). Thirteen of the 17 PAT had been previously examined using resting state fMRI reported elsewhere (Jochim et al., 2018a).

Table 1
Demographic and clinical characteristics.

	Dystonia patients (n = 17)	Healthy controls (n = 17)	p-value
Age, years (mean, SD)	62.2, 10.7	62.4, 10.2	0.95[1)]
Sex (male/female)	10/7	10/7	1.0[2)]
TIV, cm^3 (mean, SD)	1421.2, 105.5	1478.9, 110.3	0.13[1)]
Disease duration, years (mean, SD)	9.24, 6.51	–	
Light sensitivity (yes/no)	14/3		
Treatment duration, years (mean, SD)	6.74, 6.72	–	
Interval since last treatment, weeks (mean, SD)	12.4, 1.79	–	
Treatment doses, MU (mean, SD)			
-Onoabotulinumtoxin (Botox®, 7 patients)	43.00, 13.88	–	
-Incoboutlinumtoxin (Xeomin®, 3 patients)	66.5, 9.97		
-Abobotulinumtoxin (Dysport®, 7 patients)	162.86, 31.94		
Blepharospasm Disability Scale (median, IQR / mean, SD)[b]	0.48, 0.24 / 0.51, 0.23	–	
Jankovic Rating Scale (median, IQR / mean, SD)	5, 3 / 4.35, 2.74	–	

Demographic and clinical characteristics of orofacial dystonia patients and healthy controls. Statistical between-group comparisons of demographic characteristics were conducted using [1)]t-tests and [2)]Wilcoxon-Mann-Whitney tests. SD = standard deviation; IQR = interquartile range; MU, mouse units; y = years; h = hours; TIV = total intracranial volume; m = male; f = female.

2.2. MRI data acquisition and preparation

Acquisition. Data were acquired on a 3 T Achieva MRI scanner (Philips, the Netherlands) with an 8-channel head coil. Software for data analysis is detailed in supplemental table s-1. 64-gradient direction diffusion tensor MR images were acquired using a cardiac-gated single-shot spin-echo echo-planar imaging sequence (echo time = 92 ms, (heart rate-dependent) repetition time = 11–22 bpm, b-value = 1400 s/mm^2, α = 90°; field-of-view = 232 × 232 mm; voxel size = 1.81 × 1.81 × 2 mm^3; 66 axial slices without gap, 2 b0 total, (heart rate-dependent) overall scan time 30–36 min). Participants' heads were fixed with foam pads to minimize risk of motion artefacts. To further reduce motion risk in view of relatively long scan durations owed to cardiac gating, image acquisition was divided into two separate runs of 32 diffusion-weighted images each. Additionally, a high-resolution 3D gradient-echo T1 for anatomical reference, and a 2D FLAIR (for neuroradiological evaluation) were acquired.

Preparation. Diffusion MRI data from both sessions were concatenated, corrected for motion/eddy current-induced geometrical distortions, and for susceptibility-induced distortion aided by information from the aligned anatomical scan with upsampling to a voxel size of 1 mm isotropic (Irfanoglu et al., 2012; Leemans and Jones, 2009). Proper alignment of diffusion and anatomical scan was visually checked independently by two experienced neuroscientists (A.J./T.M.). Data quality control included visual checks of structural data integrity and of fitting residuals, evaluation of motion, and of voxel outliers of the diffusion tensor fit (table s-2). For probabilistic tractography preparation, FSL's *bedpostx* was applied to model two crossing fibers/voxel after automatic voxel-wise determination of the number of crossing fibers (Behrens et al., 2007; Jbabdi et al., 2012; Jenkinson et al., 2012). T1 scans were tissue-segmented using CAT12 for use in tractography and morphometric control analyses (see supplement for details) (Gaser and Dahnke, 2016).

2.3. Seed-based probabilistic tractography mapping of thalamic connectivity profiles

Probabilistic tractography (henceforth 'tractography') was performed as implemented in the FSL probabilistic fiber tracking tool (*probtrackx2*) to reconstruct the probable diffusion trajectories between the prefrontal, motor/premotor, (somato)sensory, posterior-parietal, occipital, temporal cortices and the thalamus separately for each

hemisphere in the native space of each participant (Behrens et al., 2007; Behrens et al., 2003a; Behrens et al., 2003b). All regions of interest (ROIs, figure s-1) were derived from the Brainnetome atlas parcellation (Fan et al., 2016), that provides detailed structural/streamline (SC)-based brain segmentation making it suitable for this purpose. Cortical ROIs were defined in accordance with previous similarly conceived studies in line with known connectional anatomy (Jones, 2007; Nair et al., 2013; Zhang et al., 2010). Some of those studies had investigated connectivity profiles of the posterior-parietal and occipital lobe either separately (Behrens et al., 2003a; Giraldo-Chica et al., 2018) or in combination (Nair et al., 2013; Zhang et al., 2010). We opted for the separate approach to discriminate potential parietal and occipital findings in light of previous functional neuroimaging observations of both abnormal connectivity profiles of occipital cortices at rest (Jochim et al., 2018a), and abnormal occipital activity in task activation studies related to blinking (Baker et al., 2003; Nguyen et al., 2020) or visual processing (Suzuki et al., 2019). The thalamic target ROI comprised the entire thalamus including the corpus geniculatum mediale et laterale. Tractography was performed in the respective participant's native space and all required ROIs/masks registered accordingly applying the inverse transformation parameters derived from (linear and nonlinear) registration of the anatomical scan to Montreal Neurologic Institute (MNI) standard space (Behrens et al., 2003b). Trajectories were seeded from the grey-matter-white-matter interface (5,000 streamlines/voxel) of each cortical seed ROI and separately for each hemisphere as done in other work (Nair et al., 2013), anatomically-constrained to the ipsihemispheric white matter. Exclusion masks were set to eliminate potential fiber propagation through brainstem/cerebellum/basal ganglia. Tractography was performed using standard parameters and loopcheck (curvature threshold 0.2, maximum number of steps 2000, step length 0.5 mm, subsidiary fiber volume threshold 0.01). Distance correction was applied to account for the fact that connectivity distribution drops with distance from the seed mask.

The above tractography procedure generates voxel-wise probabilities of an existing path between the cortical seed ROIs and the thalamus (used as waypoint target ROI) in each hemisphere in each subject as a surrogate measure of white matter connectivity (Behrens et al., 2007; Jbabdi and Johansen-Berg, 2011; Zhang et al., 2010). To enable inter-subject comparability, those voxel-wise connection probabilities in the individual streamline density maps were normalized by the total number of valid streamlines in each individual tractography ("*waytotal*"), taking into account inter-subject variabilities including differing ROI-sizes and the use of exclusion masks (Zhang et al., 2010). Then, these voxel maps containing the information about the normalized connection probability (structural/streamline connectivity) for each cortical seed ROI were registered to standard space for identification of thalamic areas exhibiting group differences, and for correlation analyses.

2.4. Topographic evaluation of thalamic connectivity profiles

To additionally evaluate for potential topographic differences in thalamic SC distribution patterns, we extracted the distribution's center of gravity (CoG) as a surrogate marker for each cortical thalamic SC profile (prefrontal, motor/premotor, (somato)sensory, posterior-parietal, occipital, temporal) in each subject. The CoG (with SC values substituted for mass in this situation) for a given thalamic SC distribution is a 3D space coordinate that is calculated as the weighted average of the coordinates of all voxels in that thalamic SC distribution (Behrens et al., 2003a). The CoG therefore is (by contrast to the maximum coordinate) representative of the overall intra-thalamic spatial connection pattern with the underlying cytoarchitecture. The measure has been demonstrated to relate both to underlying histology and to function in SC-based analyses, and has been applied as in previous tractography-based analyses of subcortical/cortical SC patterns (Anwander et al., 2007; Bertino et al., 2020; Devlin et al., 2006; Johansen-Berg et al., 2004).

2.5. Post-hoc evaluation of cerebello- and pallido-thalamic fiber integrity

For cortices with abnormal group thalamic SC profiles, we evaluated the microstructural integrity within the efferent sections of cortico-basal ganglia-cortical and cortico-cerebellar circuits that are relayed via the thalamus. Details are outlined in the supplementary methods. In brief, we applied a previously employed anatomically-constrained tractography approach to reconstruct the dentato-thalamo-cortical tract (DTCT) and the pallido-thalamo-cortical tract (PTCT) in each participant, respectively seeding from either the contralateral dentate area in the cerebellum or the ipsilateral pallidum to the grey matter-white matter interface of the respective cortex of interest. Resulting projections were thresholded across a number of commonly used connection probability thresholds. Tracking through bottleneck sections and/or fibre crossings along the tracts' courses in the narrow brainstem may technically bias SC values and affect spatial accuracy of subsequent tract reconstruction (Jones, 2010; Mangin et al., 1996). We therefore focused on the analysis of FA as reliable measure of white matter integrity as sensitive and (especially in the subcortical domain (Luque Laguna et al., 2020)) reliable measure of fiber integrity in a representative tract segment. Accordingly, mean FA was extracted in the native space from the tract segments across thresholds (see figure s-3), averaged, and screened for potential group differences.

2.6. Statistical design and control analyses

The primary statistical analysis focused on the detection of local (i.e. voxel-level) between-group differences in thalamic SC. Statistical analysis was performed applying nonparametric permutation testing according to the Freedman-Lane approach (5,000 permutations) with threshold-free cluster enhancement (TFCE) (Salimi-Khorshidi et al., 2011; Smith and Nichols, 2009), family-wise error (FWE) corrected for multiple comparisons at the voxel level (Holmes et al., 1996; Winkler et al., 2016; Winkler et al., 2014). Beyond avoiding assumptions on data distribution, TFCE is robust to non-stationarity requiring only minimal pre-smoothing, and avoids arbitrary cluster-forming thresholds (Eklund et al., 2016). To maximize statistical power, the corresponding left and right-hemispheric normalized connectivity maps for a given cortical ROI were analyzed in combination. Analyses were masked to include only voxels with an average relative connection probability greater than 10% for a given projection (Giraldo-Chica et al., 2018). Probability maps were slightly pre-smoothed (4 mm Gaussian kernel) to minimize noise. Results were deemed significant surviving Bonferroni-adjustment for the total number of analyses performed ($p_{FWE(TFCE)} < 0.05/6$). To aid interpretation of results from a descriptive standpoint, we additionally characterized the ipsihemispheric cortical SC profile of those thalamic voxels showing significant between-group difference across all study participants (see supplement/figure s-2 for details). Further, abnormalities in topography mirrored by differences in the centers of gravity of the thalamic connectivity distributions as surrogate marker were tested for significant GROUP × COORDINATE interaction effects using multivariate ANOVAs (factors: GROUP, COORDINATE; variates: CoG coordinates for a given cortical ROI in each hemisphere) at a corresponding Bonferroni-corrected significance-level of $p < 0.05/6$. Significant results were followed by separate two-way ANOVAs for each hemisphere ($p < 0.05/2$) with planned simple effects analyses to look into differences at the coordinate level, adjusted for the 3D space ($p < 0.05/3$) (Fisher, 1992). Co-occurrence of significant topographic shifts with local SC abnormalities in the primary analysis were followed up with a between-group comparisons of the average SC within the thalamic ROI for further characterization (Wilcoxon-Mann-Whitney test, $p < 0.05$) (Mann and Whitney, 1947).

Second, *post-hoc* secondary exploratory analyses were conducted for further characterization of significant results in the primary analysis. (i) Potential group differences in microstructural integrity by FA within representative segments of the probable trajectories of the DTCT and

PTCT were investigated (Wilcoxon-Mann-Whitney test, $p < 0.05$). (ii) Correlations with three clinical parameters (disease severity by JRS and BDS, age at onset) were calculated (Spearman's ρ, $p < 0.05/3$) (Spearman, 1904).

3. Results

3.1. Thalamic structural connectivity mapping

SC mapping (Fig. 1) revealed a significantly reduced left occipital-thalamic SC in PAT (x|y|z = -16|-30|8, $t_{TFCE} = 102.04$, $p_{FWE(TFCE)} = 0.001$, cluster size = 192 mm^3). Further, right motor/premotor-thalamic SC was reduced (x|y|z = 14|-12|8, $t_{TFCE} = 88.79$, $p_{FWE(TFCE)} = 0.007$, cluster size = 8 mm^3). The descriptive reverse tracking control analysis

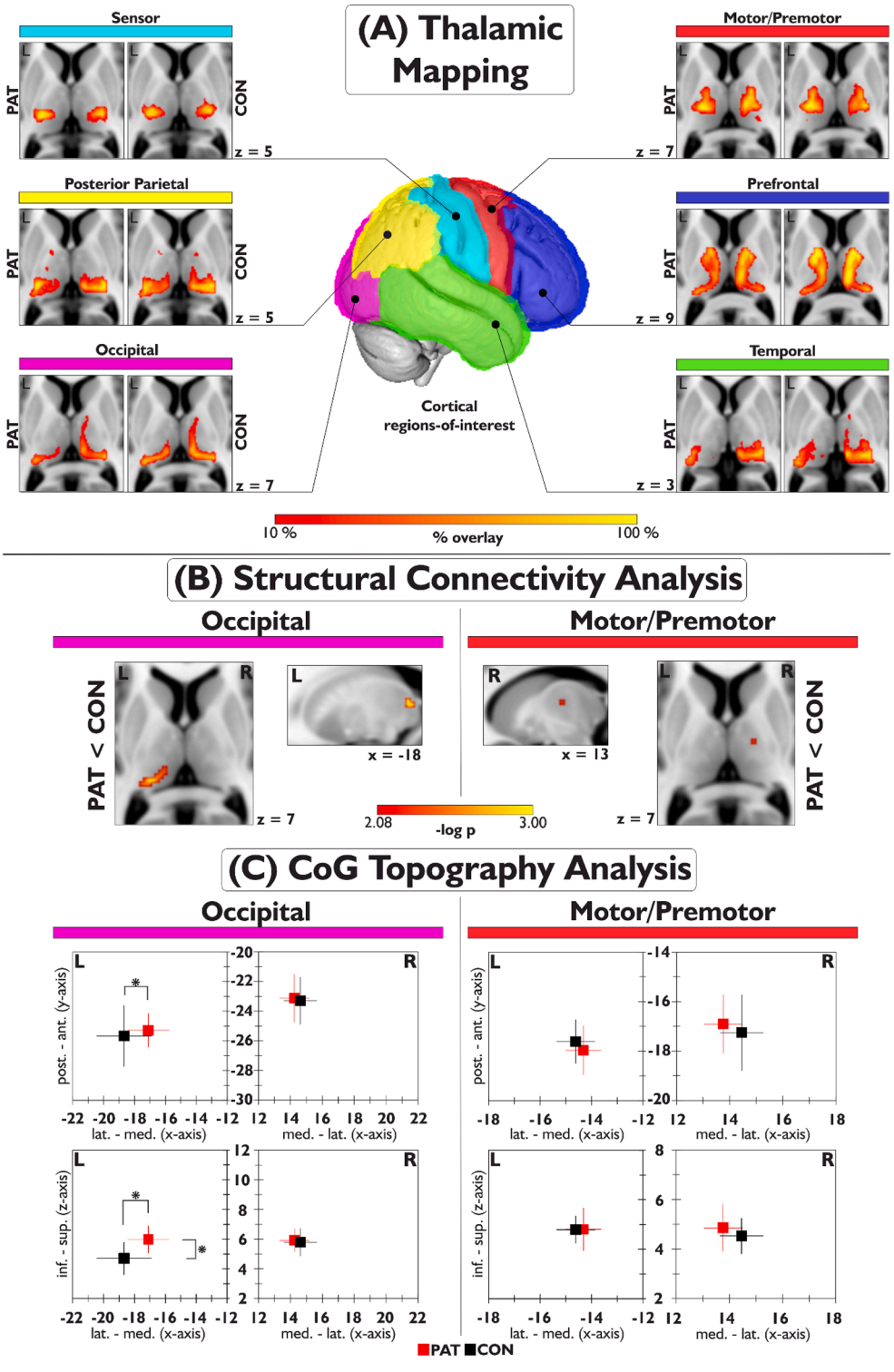

Fig. 1. Results of the thalamic SC mapping analysis in blepharospasm/Meige's syndrome patients and healthy controls, displayed in neurological convention in standard (MNI) space. *Section A:* Individual group results of the thalamic connectivity mapping for each of the six investigated cortical regions of interest in each hemisphere. Colorbar indicates percent overlay of trajectories across participants in each group at an average connection probability threshold of 10%. *Section B:* Significant local SC group differences found for the motor/premotor and occipital SC distributions ($p_{FWE(TFCE)} < 0.0083$ (0.05/6). *Section C*: the corresponding results of the topographic analysis calculated from the unthresholded thalamic SC distribution's centers of gravity (CoGs) as surrogate marker. Asterisks highlight significant differences. PAT, dystonia patients; CON, healthy controls; L, left hemisphere, R, right hemisphere.

from these significant voxels indicated that the (pre)motor thalamic cluster was mainly connected to the supplementary motor, dorsal premotor area and motor cingulum. The occipital thalamic cluster had rather distributed occipital connectivity profile with emphasis on cuneus, lateral/superior occipital cortex and the parieto-occipital sulcus area (fig. s-2). The amount of grey and white matter within the thalamic ROIs did not differ between groups (Wilcoxon-Mann-Whitney test, total intracranial volume (TIV)-normalized volumes; all $z<|0.98|$, all $p > 0.34$). Average thalamic SC values were not associated with the amount of thalamic grey and white matter (all $\rho<|0.12|$, all $p > 0.51$).

3.2. Topographic evaluation of thalamic SC profiles

Group comparison of CoGs revealed a significant GROUP × COORDINATE interaction effect for the occipital thalamic SC distribution ($F_{4,192} = 3.81$, $p = 0.005$) attributable to the left hemisphere ($F_{2,96} = 8.29$, $p < 0.001$, partial $\eta^2 = 0.15$), indicating a group topographic difference in the left occipital SC distribution (Fig. 1/table s-2). Simple effects analysis suggested this was owed to a medio-superior CoG shift in PAT (x/y/z-axis $p = 0.0021/0.43/0.012$; Fig. 1). Adjunct between-group analysis of mean left thalamic occipital lobe SC within the thalamic ROI - conducted in light of the co-occurrence of local SC and CoG abnormality - showed a significant mean SC reduction in PAT consistent with the voxel-wise main analysis ($z = -2.78$, $p = 0.0047$). This indicated that the local difference observed in the main analysis was not explained by the shift in CoGs. Otherwise, no significant differences were found.

3.3. Post-hoc exploratory evaluation of occipital/motor cerebello- and pallido-thalamic fiber integrity

Post-hoc evaluation of structural integrity in representative segments of the DTCT and PTCT revealed significantly reduced mean FA in PAT within the probable DTCT trajectories connecting to the right motor/premotor ($z = -2.29$, $p = 0.022$, effect size $r = 0.39$) and left occipital cortex ($z = -2.13$, $p = 0.033$; $r = 0.37$; Fig. 2), and no significant group differences for the PTCT (all $p > 0.16$, all $z<|1.43|$).

3.4. Post-hoc correlation of abnormal occipital/motor thalamic SC with clinical parameters

Average SC of voxels within the occipital thalamic SC cluster showed a significant moderate positive correlation with the JRS-based grading of disease severity by blinking frequency and spasm severity ($\rho = 0.58$; $p = 0.014$), but not with BDS-defined disease-related impairment ($\rho = -0.34$, $p = 0.18$). No significant correlation with age of disease onset, and no significant correlations for the motor/premotor thalamic SC cluster were observed (all $\rho<|0.33|$, all $p > 0.20$).

4. Discussion

The present study showed reductions of left occipital and right motor/premotor thalamic SC in patients with blepharospasm. Mapping of the thalamus according to its probable white matter connections has previously been applied in several neurologic/neuropsychiatric diseases with suspected thalamic involvement (Giraldo-Chica et al., 2018; Nair et al., 2013). Work in the healthy suggests that such diffusion imaging-based mappings of grey matter structures show spatial similarity to underlying histology (i.e. accordingly connected areas) (Jbabdi and Johansen-Berg, 2011), yet we emphasize thalamic mappings as performed here do not generate individual hard anatomical segmentations/labels of the single thalamic subnuclei (Clayden et al., 2019). The thalamic (pre)motor SC distribution in the present study was centered in the ventral (anterolateral) thalamus while the one generated from occipital projections was centered in the posterior thalamus. This is consistent both with previous studies (Behrens et al., 2003a; Giraldo-Chica et al., 2018; Nair et al., 2013; Zhang et al., 2010), and with the broader spatial distribution of thalamic nuclear areas accordingly involved in the processing of these modalities. Further, an additional reverse-tracking control analysis across participants confirmed a predominant link of significantly abnormal thalamic (pre)motor and

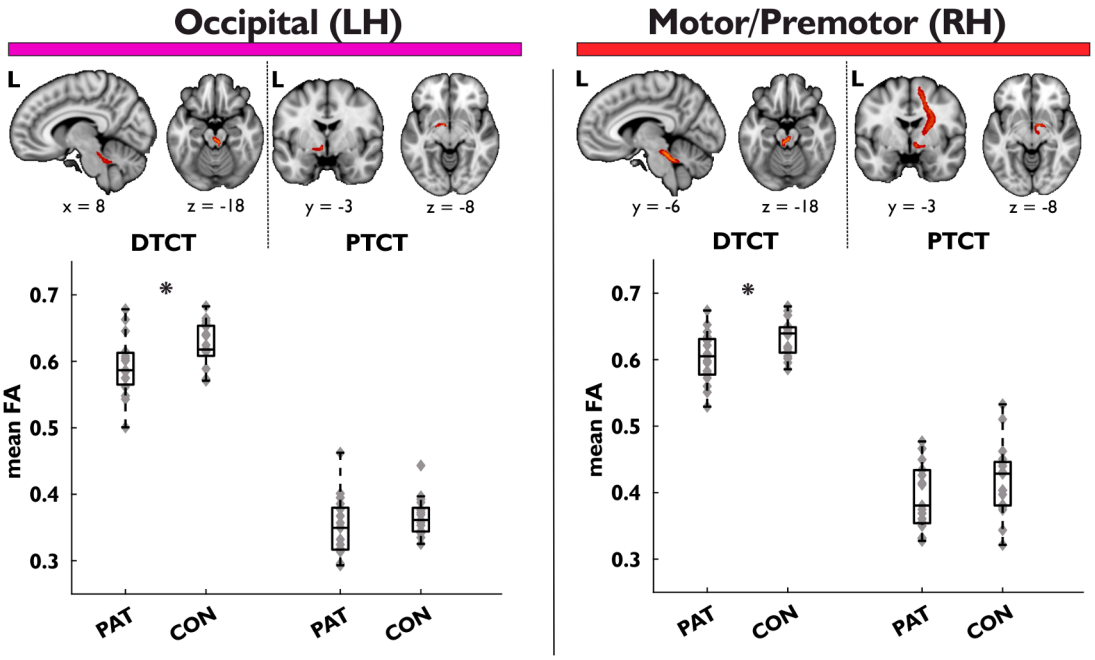

Fig. 2. Results of *post-hoc* reconstruction and group comparison of the probable trajectories of the dentato-thalamo-cortical tract (DTCT) and the pallido-thalamo-cortical tract (PTCT) targeting the left occipital and the right motor/premotor cortex respectively. *Upper panel:* Overview over subcortical sections of reconstructed projections (for more extensive depiction, see supplemental figure s-3). For visualization purpose, images were thresholded to show voxels shared among at least 4/34 participants at a connection probability threshold of 5%. *Lower panel*: Results of the group comparison of average FA in representative tract segments, visualized as box plots (maximum whisker length = 1.5*IQR), with grey diamonds indicating single values. Asterisks marks significant ($p < 0.05$) group differences in the nonparametric statistical analysis. PAT, dystonia patients; CON, healthy controls; FA, fractional anisotropy; L(H), left hemisphere; R(H), right hemisphere.

occipital voxels with the (pre)motor cortices (especially right supplementary motor, dorsal premotor area and motor cingulum), and occipital cortices respectively (with some emphasis on cuneus, lateral/superior occipital cortex and the area around the parieto-occipital sulcus).

Based on our information, a specific analysis of thalamic SC profiles using connectivity mapping has not been undertaken before in dystonia. In the healthy, the thalamus is a key integrative hub, gating both ascending pathways (from periphery, brainstem nuclei, basal ganglia, cerebellum) as well as distinct cortico-cortical projections (Guillery and Sherman, 2002; Hintzen et al., 2018; Hwang et al., 2017). In our work, (pre)motor SC was found reduced in the right thalamus. (Pre)motor thalamic projections mediate cerebellar and basal ganglia control of cortical excitability/surround inhibition and cortical plasticity that are considered defective in dystonia, ultimately leading to motor overflow (Quartarone and Hallett, 2013). Previous resting-state fMRI in a subset of participants of the present work hinted at potential modulation of FC between ipsilateral cingulate/supplemental motor area and right thalamus by BoNT-A, though directionality remains unclear (Jochim et al., 2018a). We further observed reduced left occipital thalamic SC. Regarding functional abnormality in occipital cortices, early event-related functional MRI studies hinted at abnormal involvement in primary/and or associative visual cortices within an abnormally activated visuomotor network related to simple blinking tasks (further including anterior cingulum, primary motor cortex, basal ganglia, and superior cerebellum) (Baker et al., 2003). Recently, increased activity in the occipital associative cortex (in addition to increased primary somatosensory, motor cortical and cerebellar activity) has additionally been demonstrated during reflexive blinking (Nguyen et al., 2020). While increases in visual input interruption in blepharospasm (mirrored by disease severity) and the resulting reduction in quantitative visual input are assumed to lead to reduced relative visual cortex glucose metabolism over time as secondary phenomenon (Suzuki et al., 2019), it remains to date unclear if quantitively comparable visual input is processed differently in the disease. The observation of anticorrelation of increased occipital cortex activity during reflexive blinking with disease severity may hint at a context-related dimension of functional abnormality in the occipital cortices. Further, seed-based FC in the eyes-closed resting state indicated decreased cerebellar and basal ganglia FC to the occipital association cortices that were equally not explained by disease-related impairment (Jochim et al., 2018a). Our observation of occipital-thalamic SC supports a role of thalamus-relayed projections with regard to these described functional occipital abnormalities seen in the disease.

Interestingly, occipital thalamic SC reduction in our study was relatively less pronounced in more severely affected patients. Previous functional neuroimaging studies indicated that thalamic activity increases with disease severity during various tasks (Murai et al., 2011; Suzuki et al., 2019). Yet, the multimodality (motor, multi-sensory) of processed information in these paradigms together with the fMRI techniques' limitation to identify the underlying process makes direct deductions regarding our present finding difficult. Information relayed via the thalamus to the occipital (or other) cortex undergoes modulatory influence from the cortex it is projected to, as well as from other higher-order brain areas and/or from thalamic nuclei/interneurons (Guillery and Sherman, 2002). This may indicate that our observation could reflect the presence of either a maladaptive, or a broken-down compensatory process. As diffusion imaging cannot discern functionally distinct fiber subpopulations within the occipital radiation, this warrants further research on thalamus-related network dynamics in the disease.

Altogether, the observation of structural occipital and motor cortical thalamic dysconnectivity supports a role also of the thalamocortical segment within the dystonia network. Such notion would fit well with observations in limb dystonia suggesting that abnormal microstructure within motor thalamocortical (and not corticostriatal) pathways may determine the limb phenotype (Vo et al., 2015). Given the limitations inherent to neuroimaging, we cannot discern if the observed thalamic abnormality is of causative or compensatory/adaptive nature. The thalamus functions as a hub that relays and converges, but is also modulated by its afferences (Aumann, 2002; Hintzen et al., 2018; Kaas, 1999; Silkis, 2001) making it subject to complex influences, and tractography cannot provide information on fiber directionality (Behrens et al., 2003a). Further, it remains to date unclear if altered connectivity as observed here is determined by a differing number of axons, affection of myelinization, axon spreading or other reasons.

An intriguing new observation was an additional topographic shift of the left occipital thalamic SC distribution in patients. While topographic shifts of functional body-part representations within somatosensory cortices have consistently been demonstrated across other forms of focal dystonia and discussed as an indirect correlate of maladaptive plasticity demonstrated in electrophysiological studies in focal dystonia (Neychev et al., 2011), this has to our knowledge to date not been the case for blepharospasm, the thalamus or the visual sensory modality using neuroimaging. The observation of abnormality in the visual sensory modality is conceptually congruent with early observations during thalamic micro-stimulation indicating reorganization of sensory thalamic maps in upper-limb dystonia as a potential contributor to overflow of muscle activation (Lenz et al., 1999); yet, the question may arise why thalamic SC abnormalities were not identified for somatosensory cortex connections in the present study. In light of a less prominent clinical involvement compared to the visual system in blepharospasm, a reduced sensitivity of our approach in detecting those changes compared to visual sensory abnormalities (e.g. possibly owed to a less pronounced structural aspect of thalamic reorganisation in the somatosensory domain) may be conceivable.

To explore the potential co-occurrence of our occipital/ (pre)motor thalamic findings with microstructural abnormality of major thalamic afferences originating from cerebellum and basal ganglia - both assumed to play a key role within the dystonia network concept (Jinnah et al., 2017) - we conducted a planned secondary analysis investigating the microstructural integrity of the thalamus-relayed dentato- (rubro)-thalamo-cortical and pallido-thalamo-cortical trajectories (Aumann, 2002; Hintzen et al., 2018; Kaas, 1999; Silkis, 2001). This secondary analysis indicated abnormal microstructural integrity mirrored by FA reduction within the DTCT connecting the dentate (via the thalamus) to the right (pre)motor and left occipital cortex, that had both displayed thalamic SC abnormalities in the primary analysis. Given the inherent limitations of neuroimaging, further experimental studies may be needed to clarify if such coherence indeed translates into interactions at the histological level. While work in hereditary dystonia with cranial involvement reported cerebello-thalamic tract abnormalities (Argyelan et al., 2009; Jochim et al., 2018b), tractography studies are to date sparse in idiopathic blepharospasm. One ROI-based diffusion study in blepharospasm found abnormal cerebellar FA but did not perform tractography (Yang et al., 2014). Though our observation is intriguing, confirmation in follow-up studies is warranted given this evaluation of DTCT and PTCT constituted a secondary analysis.

In our study, we did not observe bilateral abnormality of occipital and motor projections. The descriptive nature of neuroimaging studies limits direct inferences regarding the underlying causes of such lateralization, that are frequently observed also in clinically bilateral forms of dystonia including blepharospasm. We emphasize that our observations naturally do not preclude bilateral abnormality, as sensitivity for any neuroimaging finding may be influenced by factors on such as methodological aspects, varying magnitude of the underlying effect (also as consequence physiological or disease-related asymmetries), or other. From a methodological point of view, a comparatively small number of the subjects examined may have led to limited sensitivity and was owed to the fact that in addition to focal dystonia being a rare disease, the MRI study eligibility is even more narrowed down due to the increased age of onset in this form of dystonia compared to other types (accompanied by

an increased prevalence of relevant cerebral lesions and concomitant diseases). With regard to a potential relationship of structural lateralization with anomalies in lateralized functional networks, the inferences from structural imaging on their specific embedding in such functional networks are inherently limited. To provide some perspective regarding reported hemispheric lateralization in function networks of potential relevance in the disease, right motor lateralization has been observed in studies on cerebral lesions impairing eyelid function and neuroimaging studies in volitional and spontaneous blinking (Hanakawa et al., 2008; van Eimeren et al., 2001; Yoon et al., 2005). Left occipital lateralization is seen during left-lateralized complex task- and attention-dependent visual processing, and left lateralized functional occipital abnormality has been reported across previous fMRI studies in blepharospasm (Jiang et al., 2019; Kerrison et al., 2003; Nguyen et al., 2020).

5. Conclusion

Altogether, thalamic occipital and (pre)motor structural dysconnectivity with the cortex support the concept of abnormal sensory (visual) processing and dysfunctional ascending motor control via the thalamus within the pathologic network in blepharospasm. Secondary findings suggest concurrent microstructural abnormalities of the respective cerebellar afferent projections routed through the thalamic network node.

Funding

This study was supported by the Deutsche Forschungsgemeinschaft (DFG HA3370/5-1) Bonn, Germany.

CRediT authorship contribution statement

Tobias Mantel: Conceptualization, Methodology, Formal analysis, Visualization, Writing – original draft, Writing – review & editing. **Angela Jochim:** Conceptualization, Investigation, Formal analysis, Writing – original draft, Writing – review & editing. **Tobias Meindl:** Writing – review & editing. **Jonas Deppe:** Writing – review & editing. **Claus Zimmer:** Resources, Writing – review & editing. **Yong Li:** Investigation, Data curation, Writing – review & editing. **Bernhard Haslinger:** Conceptualization, Funding acquisition, Resources, Project administration, Supervision, Writing – review & editing.

Declaration of Competing Interest

The authors declare that they have no known competing financial interests or personal relationships that could have appeared to influence the work reported in this paper.

Acknowledgments

We thank with the German Dystonia Society for their support in patient and recruitment and all subjects for their participation and the study.

Appendix A. Supplementary data

Supplementary data to this article can be found online at https://doi.org/10.1016/j.nicl.2022.103013.

References

Anwander, A., Tittgemeyer, M., von Cramon, D.Y., Friederici, A.D., Knosche, T.R., 2007. Connectivity-based parcellation of Broca's area. Cereb. Cortex 17, 816–825.
Argyelan, M., Carbon, M., Niethammer, M., Ulug, A.M., Voss, H.U., Bressman, S.B., Dhawan, V., Eidelberg, D., 2009. Cerebellothalamocortical connectivity regulates penetrance in dystonia. J. Neurosci. 29 (31), 9740–9747.
Aumann, T.D., 2002. Cerebello-thalamic synapses and motor adaptation. Cerebellum 1 (1), 69–77.
Baker, R.S., Andersen, A.H., Morecraft, R.J., Smith, C.D., 2003. A functional magnetic resonance imaging study in patients with benign essential blepharospasm. J. Neuroophthalmol. 23 (1), 11–15.
Behrens, T.E.J., Berg, H.J., Jbabdi, S., Rushworth, M.F.S., Woolrich, M.W., 2007. Probabilistic diffusion tractography with multiple fibre orientations: What can we gain? Neuroimage 34 (1), 144–155.
Behrens, T.E.J., Johansen-Berg, H., Woolrich, M.W., Smith, S.M., Wheeler-Kingshott, C. A.M., Boulby, P.A., Barker, G.J., Sillery, E.L., Sheehan, K., Ciccarelli, O., Thompson, A.J., Brady, J.M., Matthews, P.M., 2003a. Non-invasive mapping of connections between human thalamus and cortex using diffusion imaging. Nat. Neurosci. 6 (7), 750–757.
Behrens, T.E.J., Woolrich, M.W., Jenkinson, M., Johansen-Berg, H., Nunes, R.G., Clare, S., Matthews, P.M., Brady, J.M., Smith, S.M., 2003b. Characterization and propagation of uncertainty in diffusion-weighted MR imaging. Magn. Reson. Med. 50 (5), 1077–1088.
Berman, B.D., Groth, C.L., Sillau, S.H., Pirio Richardson, S., Norris, S.A., Junker, J., Brüggemann, N., Agarwal, P., Barbano, R.L., Espay, A.J., Vizcarra, J.A., Klein, C., Bäumer, T., Loens, S., Reich, S.G., Vidailhet, M., Bonnet, C., Roze, E., Jinnah, H.A., Perlmutter, J.S., 2020. Risk of spread in adult-onset isolated focal dystonia: a prospective international cohort study. J. Neurol. Neurosurg. Psychiatry 91 (3), 314–320.
Bertino, S., Basile, G.A., Bramanti, A., Anastasi, G.P., Quartarone, A., Milardi, D., Cacciola, A., 2020. Spatially coherent and topographically organized pathways of the human globus pallidus. Hum. Brain Mapp. 41 (16), 4641–4661.
Clayden, J.D., Thomas, D.L., Kraskov, A., 2019. Tractography-based parcellation does not provide strong evidence of anatomical organisation within the thalamus. Neuroimage 199, 418–426.
Colosimo, C., Suppa, A., Fabbrini, G., Bologna, M., Berardelli, A., 2010. Craniocervical dystonia: clinical and pathophysiological features. Eur. J. Neurol. 17 (Suppl 1), 15–21.
Conte, A., Defazio, G., Mascia, M., Belvisi, D., Pantano, P., Berardelli, A., 2020. Advances in the pathophysiology of adult-onset focal dystonias: recent neurophysiological and neuroimaging evidence. F1000Res 9, 67.
Devlin, J.T., Sillery, E.L., Hall, D.A., Hobden, P., Behrens, T.E.J., Nunes, R.G., Clare, S., Matthews, P.M., Moore, D.R., Johansen-Berg, H., 2006. Reliable identification of the auditory thalamus using multi-modal structural analyses. Neuroimage 30 (4), 1112–1120.
Eklund, A., Nichols, T.E., Knutsson, H., 2016. Cluster failure: Why fMRI inferences for spatial extent have inflated false-positive rates. Proc. Natl. Acad. Sci. USA 113 (28), 7900–7905.
Emoto, H., Suzuki, Y., Wakakura, M., Horie, C., Kiyosawa, M., Mochizuki, M., Kawasaki, K., Oda, K., Ishiwata, K., Ishii, K., 2010. Photophobia in essential blepharospasm–a positron emission tomographic study. Mov. Disord. 25 (4), 433–439.
Fan, L., Li, H., Zhuo, J., Zhang, Y.u., Wang, J., Chen, L., Yang, Z., Chu, C., Xie, S., Laird, A.R., Fox, P.T., Eickhoff, S.B., Yu, C., Jiang, T., 2016. The Human Brainnetome Atlas: A New Brain Atlas Based on Connectional Architecture. Cereb. Cortex 26 (8), 3508–3526.
Fisher, R.A., 1992. Statistical methods for research workers. In: Kotz, S., Johnson, N.L. (Eds.), Breakthroughs in Statistics: Methodology and Distribution. Springer New York, New York, NY, pp. 66–70.
Gaser, C., Dahnke, R., 2016. CAT-a computational anatomy toolbox for the analysis of structural MRI data. Hbm 2016, 336–348.
Giraldo-Chica, M., Rogers, B.P., Damon, S.M., Landman, B.A., Woodward, N.D., 2018. Prefrontal-thalamic anatomical connectivity and executive cognitive function in schizophrenia. Biol. Psychiatry 83 (6), 509–517.
Guillery, R.W., Sherman, S.M., 2002. Thalamic relay functions and their role in corticocortical communication: generalizations from the visual system. Neuron 33 (2), 163–175.
Hanakawa, T., Dimyan, M.A., Hallett, M., 2008. The representation of blinking movement in cingulate motor areas: a functional magnetic resonance imaging study. Cereb. Cortex 18 (4), 930–937.
Hintzen, A., Pelzer, E.A., Tittgemeyer, M., 2018. Thalamic interactions of cerebellum and basal ganglia. Brain Struct. Funct. 223 (2), 569–587.
Holmes, A.P., Blair, R.C., Watson, J.D.G., Ford, I., 1996. Nonparametric analysis of statistic images from functional mapping experiments. J. Cereb. Blood Flow Metab. 16 (1), 7–22.
Hwang, K., Bertolero, M.A., Liu, W.B., D'Esposito, M., 2017. The Human Thalamus Is an Integrative Hub for Functional Brain Networks. J. Neurosci. 37 (23), 5594–5607.
Irfanoglu, M.O., Walker, L., Sarlls, J., Marenco, S., Pierpaoli, C., 2012. Effects of image distortions originating from susceptibility variations and concomitant fields on diffusion MRI tractography results. Neuroimage 61 (1), 275–288.
Jankovic, J., Orman, J., 1987. Botulinum A toxin for cranial-cervical dystonia: a double-blind, placebo-controlled study. Neurology 37, 616-623.
Jbabdi, S., Johansen-Berg, H., 2011. Tractography: where do we go from here? Brain Connect. 1 (3), 169–183.
Jbabdi, S., Sotiropoulos, S.N., Savio, A.M., Graña, M., Behrens, T.E.J., 2012. Model-based analysis of multishell diffusion MR data for tractography: how to get over fitting problems. Magn. Reson. Med. 68 (6), 1846–1855.
Jenkinson, M., Beckmann, C.F., Behrens, T.E.J., Woolrich, M.W., Smith, S.M., 2012. FSL. Fsl. Neuroimage 62 (2), 782–790.
Jiang, W., Lan, Y., Cen, C., Liu, Y., Feng, C., Lei, Y., Guo, W., Luo, S., 2019. Abnormal spontaneous neural activity of brain regions in patients with primary blepharospasm at rest. J. Neurol. Sci. 403, 44–49.

Jinnah, H.A., Neychev, V., Hess, E.J., 2017. The anatomical basis for dystonia: the motor network model. Tremor Other Hyperkinet. Mov. (N Y) 7, 506.
Jochim, A., Li, Y., Gora-Stahlberg, G., Mantel, T., Berndt, M., Castrop, F., Dresel, C., Haslinger, B., 2018a. Altered functional connectivity in blepharospasm/orofacial dystonia. Brain Behav. 8, e00894.
Jochim, A., Li, Y., Zech, M., Lam, D., Gross, N., Koch, K., Zimmer, C., Winkelmann, J., Haslinger, B., 2018b. Microstructural white matter abnormalities in patients with COL6A3 mutations (DYT27 dystonia). Parkinsonism Relat. Disord. 46, 74–78.
Johansen-Berg, H., Behrens, T.E.J., Robson, M.D., Drobnjak, I., Rushworth, M.F.S., Brady, J.M., Smith, S.M., Higham, D.J., Matthews, P.M., 2004. Changes in connectivity profiles define functionally distinct regions in human medial frontal cortex. Proc. Natl. Acad. Sci. USA 101 (36), 13335–13340.
Jones, D.K., 2010. Challenges and limitations of quantifying brain connectivity in vivo with diffusion MRI. Imaging Med. 2 (3), 341–355.
Jones, E.G., 2007. The Thalamus. University Press, Cambridge, UK.
Kaas, J.H., 1999. Is most of neural plasticity in the thalamus cortical? Proc. Natl. Acad. Sci. USA 96 (14), 7622–7623.
Kerrison, J.B., Lancaster, J.L., Zamarripa, F.E., Richardson, L.A., Morrison, J.C., Holck, D. E.E., Andreason, K.W., Blaydon, S.M., Fox, P.T., 2003. Positron emission tomography scanning in essential blepharospasm. Am. J. Ophthalmol. 136 (5), 846–852.
Khooshnoodi, M.A., Factor, S.A., Jinnah, H.A., 2013. Secondary blepharospasm associated with structural lesions of the brain. J. Neurol. Sci. 331 (1-2), 98–101.
Leemans, A., Jones, D.K., 2009. The B-matrix must be rotated when correcting for subject motion in DTI data. Magn. Reson. Med. 61 (6), 1336–1349.
Lenz, F.A., Jaeger, C.J., Seike, M.S., Lin, Y.C., Reich, S.G., DeLong, M.R., Vitek, J.L., 1999. Thalamic single neuron activity in patients with dystonia: dystonia-related activity and somatic sensory reorganization. J. Neurophysiol. 82 (5), 2372–2392.
Lindeboom, R., De Haan, R., Aramideh, M., Speelman, J.D., 1995. The blepharospasm disability scale: an instrument for the assessment of functional health in blepharospasm. Mov. Disord. 10 (4), 444–449.
Luque Laguna, P.A., Combes, A.J.E., Streffer, J., Einstein, S., Timmers, M., Williams, S.C. R., Dell'Acqua, F., 2020. Reproducibility, reliability and variability of FA and MD in the older healthy population: A test-retest multiparametric analysis. Neuroimage Clin. 26, 102168.
Mangin, J., Regis, J., Frouin, V., 1996. Shape Bottlenecks and Conservative Flow Systems. IEEE Workshop on Mathematical Methods in Biomedical Image Analysis. IEEE Computer Society, 1996, San Francisco, pp. 131-138.
Mann, H.B., Whitney, D.R., 1947. On a Test of Whether one of Two Random Variables is Stochastically Larger than the Other. Ann. Math. Stat. 18 (1), 50–60.
Mascia, M.M., Dagostino, S., Defazio, G., 2020. Does the network model fits neurophysiological abnormalities in blepharospasm? Neurol. Sci. 41 (8), 2067–2079.
Murai, H., Suzuki, Y., Kiyosawa, M., Wakakura, M., Mochizuki, M., Ishiwata, K., Ishii, K., 2011. Positive correlation between severity of blepharospasm and thalamic glucose metabolism. Case Rep. Ophthalmol. 2, 50–54.
Nair, A., Treiber, J.M., Shukla, D.K., Shih, P., Muller, R.A., 2013. Impaired thalamocortical connectivity in autism spectrum disorder: a study of functional and anatomical connectivity. Brain 136, 1942–1955.
Neychev, V.K., Gross, R.E., Lehéricy, S., Hess, E.J., Jinnah, H.A., 2011. The functional neuroanatomy of dystonia. Neurobiol. Dis. 42 (2), 185–201.
Nguyen, P., Kelly, D., Glickman, A., Argaw, S., Shelton, E., Peterson, D.A., Berman, B.D., 2020. Abnormal Neural Responses During Reflexive Blinking in Blepharospasm: An Event-Related Functional MRI Study. Mov. Disord. 35, 1173–1180.
Ni, M.F., Huang, X.F., Miao, Y.W., Liang, Z.H., 2017. Resting state fMRI observations of baseline brain functional activities and connectivities in primary blepharospasm. Neurosci. Lett. 660, 22–28.
Obermann, M., Yaldizli, O., de Greiff, A., Konczak, J., Lachenmayer, M.L., Tumczak, F., Buhl, A.R., Putzki, N., Vollmer-Haase, J., Gizewski, E.R., Diener, H.C., Maschke, M., 2008. Increased basal-ganglia activation performing a non-dystonia-related task in focal dystonia. Eur. J. Neurol. 15, 831–838.
Oldfield, R.C., 1971. The assessment and analysis of handedness: the Edinburgh inventory. Neuropsychologia 9 (1), 97–113.
Pandey, S., Sharma, S., 2017. Meige's syndrome: History, epidemiology, clinical features, pathogenesis and treatment. J. Neurol. Sci. 372, 162–170.
Quartarone, A., Hallett, M., 2013. Emerging concepts in the physiological basis of dystonia. Mov. Disord. 28 (7), 958–967.
Salimi-Khorshidi, G., Smith, S.M., Nichols, T.E., 2011. Adjusting the effect of nonstationarity in cluster-based and TFCE inference. Neuroimage 54 (3), 2006–2019.
Silkis, I., 2001. The cortico-basal ganglia-thalamocortical circuit with synaptic plasticity. II. Mechanism of synergistic modulation of thalamic activity via the direct and indirect pathways through the basal ganglia. Biosystems 59 (1), 7–14.
Smith, S., Nichols, T., 2009. Threshold-free cluster enhancement: addressing problems of smoothing, threshold dependence and localisation in cluster inference. Neuroimage 44 (1), 83–98.
Spearman, C., 1904. The proof and measurement of association between two things. Am. J. Psychol. 15, 72–101.
Suzuki, Y., Kiyosawa, M., Wakakura, M., Ishii, K., 2019. Glucose hypometabolism in the visual cortex proportional to disease severity in patients with essential blepharospasm. Neuroimage Clin 24, 101995.
Suzuki, Y., Mizoguchi, S., Kiyosawa, M., Mochizuki, M., Ishiwata, K., Wakakura, M., Ishii, K., 2007. Glucose hypermetabolism in the thalamus of patients with essential blepharospasm. J. Neurol. 254, 890–896.
Valls-Sole, J., Defazio, G., 2016. Blepharospasm: Update on Epidemiology, Clinical Aspects, and Pathophysiology. Front. Neurol. 7, 45.
van Eimeren, T., Boecker, H., Konkiewitz, E.C., Schwaiger, M., Conrad, B., Ceballos-Baumann, A.O., 2001. Right lateralized motor cortex activation during volitional blinking. Ann. Neurol. 49, 813–816.
Vo, A., Sako, W., Niethammer, M., Carbon, M., Bressman, S.B., Ulug, A.M., Eidelberg, D., 2015. Thalamocortical Connectivity Correlates with Phenotypic Variability in Dystonia. Cereb. Cortex 25, 3086–3094.
Winkler, A.M., Ridgway, G.R., Douaud, G., Nichols, T.E., Smith, S.M., 2016. Faster permutation inference in brain imaging. Neuroimage 141, 502–516.
Winkler, A.M., Ridgway, G.R., Webster, M.A., Smith, S.M., Nichols, T.E., 2014. Permutation inference for the general linear model. Neuroimage 92, 381–397.
Yang, J., Luo, C., Song, W., Guo, X., Zhao, B., Chen, X., Huang, X., Gong, Q., Shang, H.F., 2014. Diffusion tensor imaging in blepharospasm and blepharospasm-oromandibular dystonia. J. Neurol. 261, 1413–1424.
Yoon, H.W., Chung, J.Y., Song, M.S., Park, H., 2005. Neural correlates of eye blinking; improved by simultaneous fMRI and EOG measurement. Neurosci. Lett. 381, 26–30.
Zhang, D., Snyder, A.Z., Shimony, J.S., Fox, M.D., Raichle, M.E., 2010. Noninvasive functional and structural connectivity mapping of the human thalamocortical system. Cereb. Cortex 20, 1187–1194.

Supplementary Material

to

Thalamic Structural Connectivity Profiles in Blepharospam/Meige's Syndrome

Tobias Mantel, MD*[1], Angela Jochim, MD *[1], Tobias Meindl, MD [1], Jonas Deppe, MD [1], Claus Zimmer, MD [2], Yong Li, PhD [1], and Bernhard Haslinger, MD [1]

[1]Department of Neurology, Klinikum rechts der Isar, Technische Universität München, Ismaninger Strasse 22, Munich, Germany

[2]Department of Neuroradiology, Klinikum rechts der Isar, Technische Universität München, Ismaninger Strasse 22, Munich, Germany

1 Inclusion/exclusion criteria (extension)

Participants in the study did not suffer from major neuropsychiatric disease; any depression or cognitive impairment were defined as exclusion criteria. No participant was on serotonergic or GABAergic medication at the time of the study. Patients with a history of dystonia-inducing medication (e.g. neuroleptics, metoclopramide etc.), any surgical intervention for dystonia, cervical involvement, dystonia in other body parts, or tremor were not included. No patients had a positive dystonia/movement disorders family history or other phenotypic/demographic/clinical characteristics indicating potential genetic cause including by recently validated criteria(Zech et al., 2021; Zech et al., 2020).

Participants structural MRIs underwent thorough neuroradiological evaluation. Besides minor white matter hyperintensities in two controls and three patients (mainly small juxtaventricular 'caps' at the anterior horn of the lateral ventricle in the prefrontal cortex, no subcortical lesions or lacunes), no intracerebral abnormality was seen.

2 Supplementary Experimental Procedures

2.1 Structural image segmentation and extraction of thalamic grey and white matter volumes

After denoising, bias correction and affine registration, the skull-stripped anatomical scans were tissue-segmented followed by diffeomorphic anatomical registration using lie algebra (DARTEL) to the default DARTEL_IXI555 Montreal Neurological Institute (MNI) space template with a final voxel size of 1 mm^3. For the control analysis of thalamic tissue volumes, the left and right-hemispheric thalamic grey matter and white mater volumes were respectively extracted from the segmented grey and white matter images in native space applying the Brainnetome atlas -derived thalamic ROIs that was also applied during the diffusion tractography approach. Extracted thalamic grey matter and white matter volumes were normalized with the total intracranial volume (TIV) and statistically compared between groups using nonparametric statistics (Wilcoxon-Mann-Whitney test). Further, potential correlations of these volumes with average intra-thalamic SC values were explored calculating Spearman's rho.

2.2 Descriptive evaluation of cluster-related cortical connectivity profiles

To characterize the cortical connectivity profile of thalamic areas demonstrating significant between-group difference from an additional descriptive standpoint as control analysis, we

tracked the connectivity of significant clusters to the entire (i.e. not confined to a distinct lobe/cortex) ipsihemispheric cerebral cortex in the native space of each participant. This descriptive analysis comprehensively evaluated all participants and did not separately look into patients and controls to avoid circular group-related inference(Kriegeskorte et al., 2009). Significant clusters were warped back to each participant's native (diffusion) space applying the inverse transformation parameters derived from the (linear and nonlinear) registration of the anatomical T1 scan to the standard (MNI) space to serve as ROI. Probabilistic tractography was then seeded from these thalamic seed voxels to the entire ipsihemispheric grey matter – white matter interface serving as target ROI tractography (5,000 streamlines/voxel, curvature threshold 0.2, maximum number of steps 2000, step length 0.5 mm, subsidiary fibre volume threshold 0.01). Anatomical constraints using exclusion masks were set as in the main analysis. The streamline connectivity values were normalized by the 'waytotal' and registered to the MNI space. The subject-averaged result is displayed in figure s-2.

2.3 *Post-hoc* evaluation of the integrity of cerebello- and pallido-thalamo-cortical trajectories

Subcortico-cortical tracts were reconstructed applying a previously employed(Mantel et al., 2020; Schulz et al., 2015) anatomically-constrained two-pass probabilistic tractography approach allowing for reliable reconstruction of core trajectories even at low connection probabilities (parameters curvature threshold of 0.2, maximum number of steps 2000, step length 0.5 mm, subsidiary fiber volume threshold 0.01, fractional anisotropy threshold 0.15). Tractography was again performed in the native (diffusion) space. All required ROIs and masks were accordingly warped to the participant's native (diffusion) space applying the inverse transformation parameters derived from the (linear and nonlinear) registration of the anatomical T1 scan to the standard (MNI) space(Behrens et al., 2003). First, an initial tract reconstruction

was performed confined to the individual's segmented white matter(Gaser and Dahnke, 2016), that was guided by the literature-based knowledge on tract courses:

Dentato-thalamo-cortical tract (DTCT). The DTCT originates from the dentate nucleus, ascends through the superior cerebellar peduncle, then crosses the midline to pass through the nucleus ruber to the thalamus (i.e. the dentato-rubro-thalamic tract)(Afifi and Bergman, 2005; Kwon et al., 2011), where the trajectory is then relayed to the respective cortical area. For reconstruction of the probable trajectory of the DTCT targeting the respective cortex of interest, streamlines were seeded from the area of the contralateral dentate. The dentate area was defined as a cuboid based on data from topographic publications (coordinates: x|y|z= ±9 to ±23|-46 to -64|-28 to -42)(Diedrichsen et al., 2011; Dimitrova et al., 2002; Dimitrova et al., 2006). The contralateral thalamus served as a *waypoint*. Trajectories erroneously passing through the middle cerebral peduncle or through the hemisphere ipsilateral to the dentate were discarded, as were passages through subcortical structures of no interest (i.e. the basal ganglia).

Pallido-thalamo-cortical tract (PTCT). The majority of fibers pass from the anteroventral pallidum to the thalamus through the subthalamic area lateral to the fornix, rostral to the corticospinal and superior to the optic tract and subthalamic nucleus to reach the thalamus where they are then relayed to the cortex(Gallay et al., 2008; Rozanski et al., 2017). For reconstruction of the probable trajectory of the PTCT, streamlines were seeded from the area of the ipsilateral pallidum as defined in the Brainnetome atlas(Fan et al., 2016). The ipsilateral anterior subthalamic area (defined as a cuboid relatively to the adjacent subcortical anatomical structures) and the thalamus served as *waypoints*. Trajectories erroneously passing through contralateral hemisphere or through subcortical structures of no interest (i.e. the other basal ganglia) were discarded.

In a second step, refined exclusion masks were generated by mean dilation of the volume of the initial probable trajectory four times at a 5% connection probability threshold, and (if necessary) further addition of specific exclusion masks to eliminate erroneous fiber courses. Considering

that there are no objective standards for thresholding probabilistic tractography, the resulting final projections were thresholded across a number of commonly used connection probability thresholds (1%, 2%, 5%, and 10%). Representative sections of the DTCT and PTCT were defined as the segment between the dentate and the mesencephalic midline and the segment between the pallidum and thalamus respectively, given that tracking through complex/bottleneck fiber crossings along the tracts' further courses in the brainstem and the mixed tissue structure thalamus limit accuracy of further tract reconstruction(Maier-Hein et al., 2017; Schilling et al., 2018; Tuch et al., 2003). Further, as the above-outlined technical considerations in the brainstem may make quantitative evaluation of thalamic SC unreliable, we focused on evaluation of microstructural integrity within the representative tract segments only. For each tract segment, the mean fractional anisotropy (FA) values as a sensitive and (especially in subcortical areas) reliable(Luque Laguna et al., 2020) measure of white matter integrity were then extracted in the native space from a representative segment of each tract at each threshold, averaged across thresholds and then evaluated for potential between-group differences.

3 Supplementary Tables

Table s-1. Software tools for data processing and analysis.		
DWI processing, analysis	exploreDTI4.8.6, FSL5.0.8	www.exploredti.com https://fsl.fmrib.ox.ac.uk/fsl/
T1 processing, segmentation	CAT12r1152	http://www.neuro.uni-jena.de/cat/
Statistical analysis	SPSS27	IBM, New York, USA https://www.ibm.com/products/spss-statistics
	Matlab2018b (incl. Statistics and Machine Learning Toolbox)	https://www.mathworks.com/products/matlab the MathWorks Inc., Natick, USA
	PALMα116	https://fsl.fmrib.ox.ac.uk/fsl/fslwiki/PALM

Table s-2. Diffusion data quality metrics

	orofacial dystonia patients		**healthy controls**		**statistics**	
	median	**IQR**	**median**	**IQR**	**z-value**	**p-value**
x translation	0.07	± 0.05	0.07	± 0.03	1.601	0.11
y translation	0.07	± 0.03	0.07	± 0.02	0.465	0.64
z translation	0.80	± 0.06	0.81	± 0.04	-0.603	0.55
x rotation	0.08	± 0.05	0.08	± 0.01	-0.155	0.88
y rotation	0.13	± 0.08	0.15	± 0.04	-0.982	0.33
z rotation	0.05	± 0.04	0.06	± 0.02	1.120	0.26
DT fit outliers	0.0005	± 0.0008	0.0006	± 0.0003	0.052	0.96

Motion parameters represent the average gradient volume-to-volume motion, given in mm for translation, and in degree for rotation. Diffusion tensor fit outlier voxels as calculated by exploreDTI are given as the average portion of outlier voxels (in percent) across gradients volumes. Statistical analysis was performed using nonparametric Wilcoxon-Mann-Whitney tests with α=0.05 uncorrected. DT, diffusion tensor; IQR inter-quartile range.

Table s-3. Results of the centre of gravity (CoG) analysis.

Thalamic Connectivity Distribution	Hem	CoG PAT x	PAT y	PAT z	CON x	CON y	CON z	F-value	p-value
Motor/Premotor	**LH**	-14.3 (±0.7)	-18 (±1.0)	4.8 (±0.9)	-14.6 (±0.7)	-17.6 (±0.9)	4.8 (±0.6)	1.88	0.115
	RH	13.8 (±0.7)	-16.9 (±1.2)	4.9 (±1.0)	14.5 (±0.8)	-17.3 (±1.5)	4.5 (±0.8)		
Occipital	**LH**	-17.1 (±1.3)	-25.3 (±1.1)	6.0 (±0.9)	-18.7 (±1.8)	-25.7 (±2.1)	4.7 (±1.1)	3.81	0.005*
	RH	14.3 (±0.9)	-23.1 (±1.6)	5.9 (±0.8)	14.6 (±1.0)	-23.3 (±1.6)	5.8 (±0.9)		
Parietal	**LH**	-16.5 (±1.3)	-22.2 (±1.0)	6.4 (±0.9)	-17.4 (±1.4)	-22.5 (±1.7)	5.9 (±1.0)	1.56	0.186
	RH	15.2 (±0.7)	-21.5 (±1.2)	6.0 (±0.9)	15.6 (±0.7)	-21.8 (±0.9)	6.2 (±1.0)		
Prefrontal	**LH**	-12.2 (±0.6)	-15.4 (±1.5)	6.5 (±1.7)	-12.2 (±0.6)	-14 (±1.8)	5.7 (±1.5)	1.54	0.192
	RH	11.6 (±0.9)	-17.2 (±0.9)	6.5 (±1.0)	11.7 (±0.9)	-16.2 (±1.8)	5.8 (±1.3)		
Sensor	**LH**	-16.9 (±0.9)	-21.9 (±0.9)	4.9 (±1.0)	-17.3 (±0.9)	-22.1 (±1.8)	4.9 (±1.3)	0.25	0.910
	RH	16.2 (±0.7)	-20.8 (±0.8)	3.7 (±1.1)	16.9 (±0.9)	-21.3 (±0.7)	4.1 (±0.7)		
Temporal	**LH**	-17.0 (±0.7)	-23.2 (±0.9)	5.7 (±1.3)	-17.8 (±0.6)	-23.2 (±0.8)	4.8 (±1.0)	1.18	0.321
	RH	14.7 (±1.6)	-21.9 (±1.6)	5.5 (±1.4)	15.2 (±1.6)	-22.0 (±2.0)	5.5 (±1.3)		

Coordinates of the thalamic connectivity distributions' centers of gravity (CoGs) are given as mean (± standard deviation for each hemisphere (LH, left hemisphere; RH, right hemisphere) and for each group (PAT, orofacial dystonia patients; CON, healthy controls) in the Montreal Neurologic Imaging space relative to the anterior commissure in mm. Statistical significance for significant GROUP × COORDINATE interaction effects in the multivariate of analyses of variance was calculated using Pillais Trace. Asterisks highlight significant between-group differences after Bonferroni-correction for multiple comparisons ($p<0.05/6$).

Table s-4. Tract-related white-matter integrity in dystonia patients and healthy controls in the secondary analysis.

Target ROI	Occipital LH		Motor RH	
	DTCT	**PTCT**	**DTCT**	**PTCT**
PAT	0.592 ± 0.047	0.343 ± 0.037	0.607 ± 0.040	0.393 ± 0.046
CON	0.624 ± 0.034	0.366 ± 0.029	0.633 ± 0.027	0.420 ± 0.054
z-value	-2.134	-1.292	-2.290	-1.429
p-value	**0.033**	0.160	**0.022**	0.205

Averaged tract integrity by fractional anisotropy (FA) in the groups and results of the statistical analysis for the dentato-thalamo-cortical (DTCT) and pallido-thalamo-cortical tract (PTCT) to the left-hemispheric occipital and right-hemispheric motor/premotor cortex respectively. Results are display as mean ± standard deviation. Significant results of group comparisons (Wilcoxon-Mann-Withney tests) at $p<0.05$ are highlighted in bold. PAT, dystonia patients; CON, healthy controls; ROI, region of interest; LH, left hemisphere; RH, right hemisphere.

4 Supplementary Figures

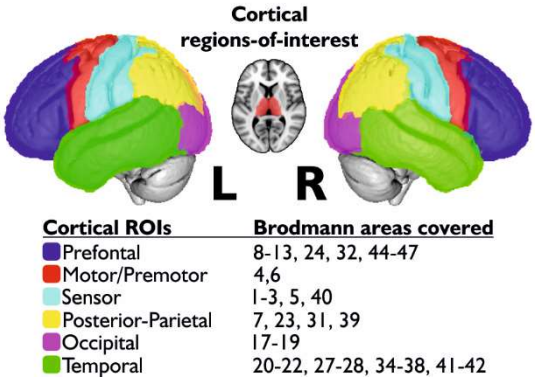

Figure s-1. Cortical regions-of-interest and thalamus. High-resolution structural connectivity-based cortical parcellation provided by the Brainnetome atlas(Fan et al., 2016) was used to create ROIs for the thalamus (middle), prefrontal cortex (blue), motor/premotor cortex (red), sensory cortex (cyan), temporal cortex (green), posterior parietal cortex (yellow), and occipital cortex (violet). ROIs were defined deduced from the thalamic connectomic neuroanatomy(Jones, 2007) in accordance with previous studies of similar objective(Fair et al., 2010; Nair et al., 2013; Zhang et al., 2010), with separation of posterior-parietal and occipital cortex(Behrens et al., 2003; Sheffield et al., 2020). The cortical ROIs and thalamus were used as seed and targets, respectively, to quantify thalamocortical streamline/structural connectivity using probabilistic tractography.

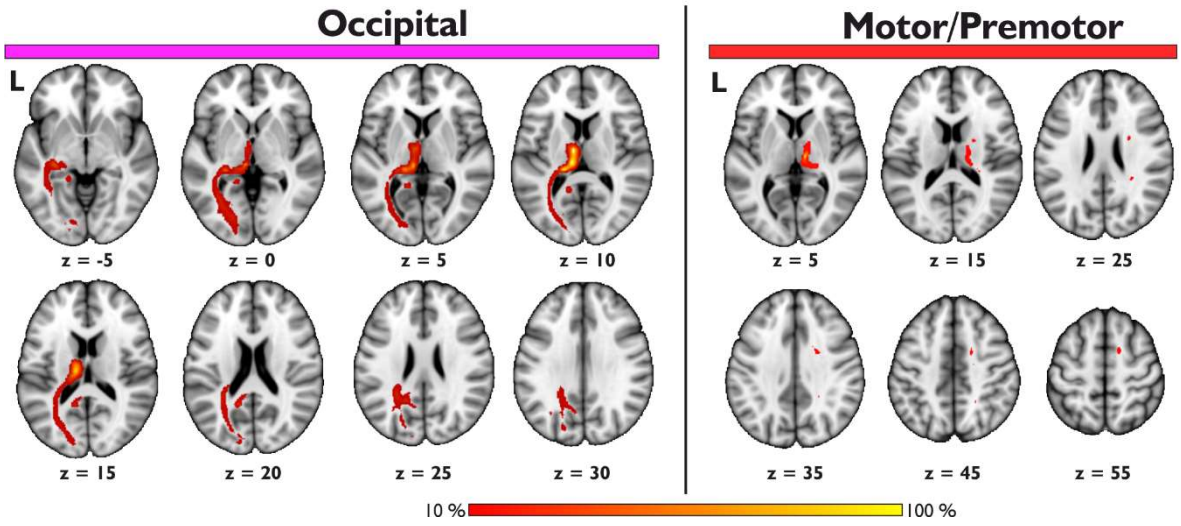

Figure s-2. Participant-averaged results of reverse tractography. Projections were seeded from the significant group cluster in the left thalamus (occipital) and right thalamus (motor/premotor) in each participant in the native space. For purpose of visualization of the most prominent connections, tract voxels shared among at least 4/34 participants at a connection probability threshold of 5% are displayed in standard (MNI) space in neurological convention.

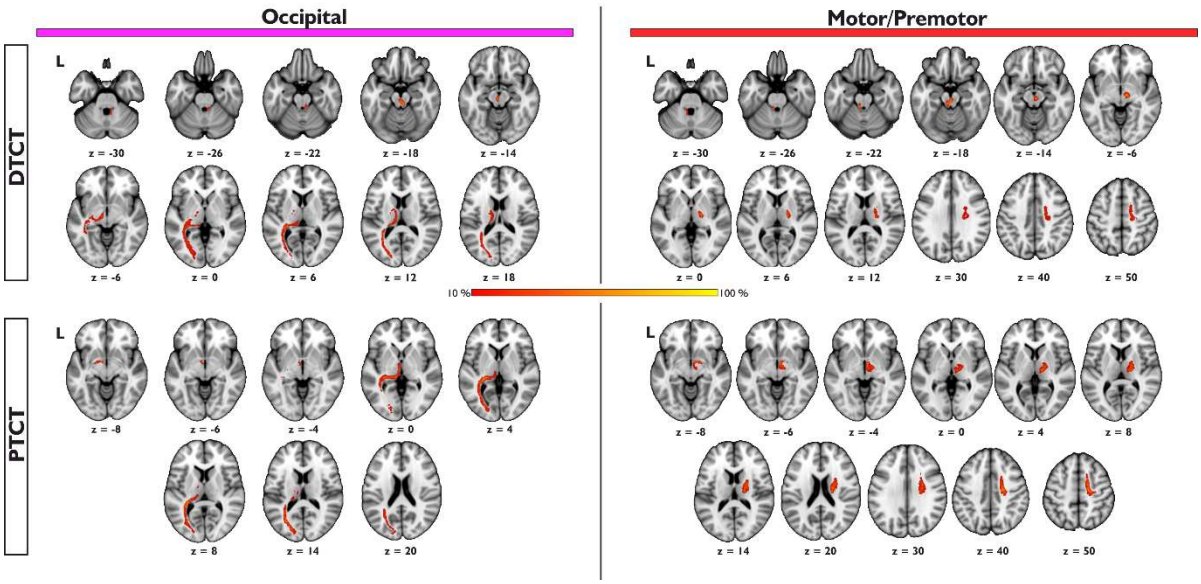

Figure s-3. Results of the reconstruction of the probable trajectories of the dentato-thalamo-cortical tract (DTCT) and the pallido-thalamo-cortical tract (PTCT) targeting the left occipital and the right motor/premotor cortex respectively. For visualization purposes, images were thresholded to show voxels shared among at least 4/34 participants at a connection probability threshold of 5% in standard (MNI) space in neurological convention. Colorbars represent the percent overlay across participants.

5 Supplementary References

Afifi, A.K., Bergman, R.A., 2005. Functional neuroanatomy: text and atlas, 2 ed. McGraw-Hill Education Ltd, New York.

Behrens, T.E., Johansen-Berg, H., Woolrich, M.W., Smith, S.M., Wheeler-Kingshott, C.A., Boulby, P.A., Barker, G.J., Sillery, E.L., Sheehan, K., Ciccarelli, O., Thompson, A.J., Brady, J.M., Matthews, P.M., 2003. Non-invasive mapping of connections between human thalamus and cortex using diffusion imaging. Nat Neurosci 6, 750-757.

Diedrichsen, J., Ridgway, G.R., Friston, K.J., Wiestler, T., 2011. Comparing the similarity and spatial structure of neural representations: a pattern-component model. Neuroimage 55, 1665-1678.

Dimitrova, A., Weber, J., Redies, C., Kindsvater, K., Maschke, M., Kolb, F.P., Forsting, M., Diener, H.C., Timmann, D., 2002. MRI atlas of the human cerebellar nuclei. Neuroimage 17, 240-255.

Dimitrova, A., Zeljko, D., Schwarze, F., Maschke, M., Gerwig, M., Frings, M., Beck, A., Aurich, V., Forsting, M., Timmann, D., 2006. Probabilistic 3D MRI atlas of the human cerebellar dentate/interposed nuclei. Neuroimage 30, 12-25.

Fair, D.A., Bathula, D., Mills, K.L., Dias, T.G., Blythe, M.S., Zhang, D., Snyder, A.Z., Raichle, M.E., Stevens, A.A., Nigg, J.T., Nagel, B.J., 2010. Maturing thalamocortical functional connectivity across development. Front Syst Neurosci 4, 10.

Fan, L., Li, H., Zhuo, J., Zhang, Y., Wang, J., Chen, L., Yang, Z., Chu, C., Xie, S., Laird, A.R., Fox, P.T., Eickhoff, S.B., Yu, C., Jiang, T., 2016. The Human Brainnetome Atlas: A New Brain Atlas Based on Connectional Architecture. Cereb Cortex 26, 3508-3526.

Gallay, M.N., Jeanmonod, D., Liu, J., Morel, A., 2008. Human pallidothalamic and cerebellothalamic tracts: anatomical basis for functional stereotactic neurosurgery. Brain Struct Funct 212, 443-463.

Gaser, C., Dahnke, R., 2016. CAT-a computational anatomy toolbox for the analysis of structural MRI data. Hbm 2016, 336-348.

Jones, E.G., 2007. The Thalamus. University Press, Cambridge, UK.

Kriegeskorte, N., Simmons, W.K., Bellgowan, P.S., Baker, C.I., 2009. Circular analysis in systems neuroscience: the dangers of double dipping. Nat Neurosci 12, 535-540.

Kwon, H.G., Hong, J.H., Hong, C.P., Lee, D.H., Ahn, S.H., Jang, S.H., 2011. Dentatorubrothalamic tract in human brain: diffusion tensor tractography study. Neuroradiology 53, 787-791.

Luque Laguna, P.A., Combes, A.J.E., Streffer, J., Einstein, S., Timmers, M., Williams, S.C.R., Dell'Acqua, F., 2020. Reproducibility, reliability and variability of FA and MD in the older healthy population: A test-retest multiparametric analysis. Neuroimage Clin 26, 102168.

Maier-Hein, K.H., Neher, P.F., Houde, J.C., Cote, M.A., Garyfallidis, E., Zhong, J., Chamberland, M., Yeh, F.C., Lin, Y.C., Ji, Q., Reddick, W.E., Glass, J.O., Chen, D.Q., Feng, Y., Gao, C., Wu, Y., Ma, J., He, R., Li, Q., Westin, C.F., Deslauriers-Gauthier, S., Gonzalez, J.O.O., Paquette, M., St-Jean, S., Girard, G., Rheault, F., Sidhu, J., Tax, C.M.W., Guo, F., Mesri, H.Y., David, S., Froeling, M., Heemskerk, A.M., Leemans, A., Bore, A., Pinsard, B., Bedetti, C., Desrosiers, M., Brambati, S., Doyon, J., Sarica, A., Vasta, R., Cerasa, A., Quattrone, A., Yeatman, J., Khan, A.R., Hodges, W., Alexander, S., Romascano, D., Barakovic, M., Auria, A., Esteban, O., Lemkaddem, A., Thiran, J.P., Cetingul, H.E., Odry, B.L., Mailhe, B., Nadar, M.S., Pizzagalli, F., Prasad, G., Villalon-Reina, J.E., Galvis, J., Thompson, P.M., Requejo, F.S., Laguna, P.L., Lacerda, L.M., Barrett, R., Dell'Acqua, F., Catani, M., Petit, L., Caruyer, E., Daducci, A., Dyrby, T.B., Holland-Letz, T., Hilgetag, C.C., Stieltjes, B., Descoteaux, M., 2017. The challenge of mapping the human connectome based on diffusion tractography. Nat Commun 8, 1349.

Mantel, T., Altenmuller, E., Li, Y., Lee, A., Meindl, T., Jochim, A., Zimmer, C., Haslinger, B., 2020. Structure-function abnormalities in cortical sensory projections in embouchure dystonia. Neuroimage Clin 28, 102410.

Nair, A., Treiber, J.M., Shukla, D.K., Shih, P., Muller, R.A., 2013. Impaired thalamocortical connectivity in autism spectrum disorder: a study of functional and anatomical connectivity. Brain 136, 1942-1955.

Rozanski, V.E., da Silva, N.M., Ahmadi, S.A., Mehrkens, J., da Silva Cunha, J., Houde, J.C., Vollmar, C., Botzel, K., Descoteaux, M., 2017. The role of the pallidothalamic fibre tracts in deep brain stimulation for dystonia: A diffusion MRI tractography study. Hum Brain Mapp 38, 1224-1232.

Schilling, K., Gao, Y., Janve, V., Stepniewska, I., Landman, B.A., Anderson, A.W., 2018. Confirmation of a gyral bias in diffusion MRI fiber tractography. Hum Brain Mapp 39, 1449-1466.

Schulz, R., Koch, P., Zimerman, M., Wessel, M., Bonstrup, M., Thomalla, G., Cheng, B., Gerloff, C., Hummel, F.C., 2015. Parietofrontal motor pathways and their association with motor function after stroke. Brain 138, 1949-1960.

Sheffield, J.M., Huang, A.S., Rogers, B.P., Giraldo-Chica, M., Landman, B.A., Blackford, J.U., Heckers, S., Woodward, N.D., 2020. Thalamocortical Anatomical Connectivity in Schizophrenia and Psychotic Bipolar Disorder. Schizophr Bull.

Tuch, D.S., Reese, T.G., Wiegell, M.R., Wedeen, V.J., 2003. Diffusion MRI of complex neural architecture. Neuron 40, 885-895.

Zech, M., Jech, R., Boesch, S., Skorvanek, M., Necpal, J., Svantnerova, J., Wagner, M., Sadr-Nabavi, A., Distelmaier, F., Krenn, M., Serranova, T., Rektorova, I., Havrankova, P., Mosejova, A., Prihodova, I., Sarlakova, J., Kulcsarova, K., Ulmanova, O., Bechyne, K., Ostrozovicova, M., Han, V., Ventosa, J.R., Brunet, T., Berutti, R., Shariati, M., Shoeibi, A., Schneider, S.A., Kuster, A., Baumann, M., Weise, D., Wilbert, F., Janzarik, W.G.,

Eckenweiler, M., Mall, V., Haslinger, B., Berweck, S., Winkelmann, J., Oexle, K., 2021. Scoring Algorithm-Based Genomic Testing in Dystonia: A Prospective Validation Study. Mov Disord 36, 1959-1964.

Zech, M., Jech, R., Boesch, S., Skorvanek, M., Weber, S., Wagner, M., Zhao, C., Jochim, A., Necpal, J., Dincer, Y., Vill, K., Distelmaier, F., Stoklosa, M., Krenn, M., Grunwald, S., Bock-Bierbaum, T., Fecikova, A., Havrankova, P., Roth, J., Prihodova, I., Adamovicova, M., Ulmanova, O., Bechyne, K., Danhofer, P., Vesely, B., Han, V., Pavelekova, P., Gdovinova, Z., Mantel, T., Meindl, T., Sitzberger, A., Schroder, S., Blaschek, A., Roser, T., Bonfert, M.V., Haberlandt, E., Plecko, B., Leineweber, B., Berweck, S., Herberhold, T., Langguth, B., Svantnerova, J., Minar, M., Ramos-Rivera, G.A., Wojcik, M.H., Pajusalu, S., Ounap, K., Schatz, U.A., Polsler, L., Milenkovic, I., Laccone, F., Pilshofer, V., Colombo, R., Patzer, S., Iuso, A., Vera, J., Troncoso, M., Fang, F., Prokisch, H., Wilbert, F., Eckenweiler, M., Graf, E., Westphal, D.S., Riedhammer, K.M., Brunet, T., Alhaddad, B., Berutti, R., Strom, T.M., Hecht, M., Baumann, M., Wolf, M., Telegrafi, A., Person, R.E., Zamora, F.M., Henderson, L.B., Weise, D., Musacchio, T., Volkmann, J., Szuto, A., Becker, J., Cremer, K., Sycha, T., Zimprich, F., Kraus, V., Makowski, C., Gonzalez-Alegre, P., Bardakjian, T.M., Ozelius, L.J., Vetro, A., Guerrini, R., Maier, E., Borggraefe, I., Kuster, A., Wortmann, S.B., Hackenberg, A., Steinfeld, R., Assmann, B., Staufner, C., Opladen, T., Ruzicka, E., Cohn, R.D., Dyment, D., Chung, W.K., Engels, H., Ceballos-Baumann, A., Ploski, R., Daumke, O., Haslinger, B., Mall, V., Oexle, K., Winkelmann, J., 2020. Monogenic variants in dystonia: an exome-wide sequencing study. Lancet Neurol 19, 908-918.

Zhang, D., Snyder, A.Z., Shimony, J.S., Fox, M.D., Raichle, M.E., 2010. Noninvasive functional and structural connectivity mapping of the human thalamocortical system. Cereb Cortex 20, 1187-1194.